The University of Sydney

Installation of Suction Caissons in Dense Sand and the Influence of Silt and Cemented Layers

By

Manh Ngoc Tran

B.E.
(UNSW, First Class Honours)

A thesis submitted for the degree of Doctor of Philosophy
at
The University of Sydney

Department of Civil Engineering

October 2005

Dedication

To my wife, Tường Vi, and my parents

Table of Contents

Chapter 3: **Soil Properties and Sample Preparation Techniques**

Chapter 4: **Installation Behaviour at Normal Gravity (1g)**

Chapter 5: **Centrifuge Modelling: Installation Behaviour in Homogenous Sand**

Chapter 6: **Centrifuge Modelling: Installation Behaviour in Layered Soils**

Chapter 7: **Numerical Investigation of Suction Installation Behaviour**

Chapter 8: **Conclusions**

Synopsis

Suction caissons have been used in the offshore industry in the last two decades as both temporary mooring anchorages and permanent foundation systems. Although there have been more than 500 suction caissons installed in various locations around the world, understanding of this concept is still limited. This thesis investigates the installation aspect of suction caissons, focusing on the installation in dense sand and layered soils, where sand is inter-bedded by silt and weakly cemented layers. The research was mainly experimental, at both normal gravity and elevated acceleration levels in a geotechnical centrifuge, with some numerical simulations to complement the experimental observations.

This study firstly explored the suction caisson installation response in the laboratory at 1g. The influence and effect of different design parameters, which include caisson size and wall thickness, and operational parameters including pumping rate and the use of surcharge were investigated in dense silica sand. The sand heave inside the caisson formed during these installations was also recorded and compared between tests. The 1g study also investigated the possibility of installing suction caissons in layered sand-silt soil, where caissons were installed by both slow and rapid pumping. The heave formation in this case is also discussed. The mechanism of heave formation in dense sand and deformation of the silt layer was further investigated using a half-caisson model and the particle image velocimetry (PIV) technique.

The installation response at prototype soil stress conditions was then investigated in a geotechnical centrifuge. The effects of caisson size, wall thickness, as well as surcharge were investigated in various types of sand, including silica sand, calcareous sand dredged from the North Rankin site in the North West Shelf (Australia), and mixed soil where silica sand was mixed with different contents of silica flour. Comparison with the 1g results was also made. The general trend for the suction pressure during installation in homogenous sand was identified.

The installation in layered soil was also investigated in the centrifuge. The installation tests were performed in various sand-silt profiles, where the silt layers were on the

surface and embedded within the sand. Comparison with the results in homogenous sand was made to explore the influence of the silt layer. Installations in calcareous sand with cemented layers were also conducted. The penetration mechanism through the cemented layer is discussed, and also compared with the penetration mechanism through the silt layer.

Finite element modelling was performed to simulate key installation behaviour. In particular, it was applied to simulate the sand deformation observed in the PIV tests. The likely loosening range of the internal sand plug during suction installation in silica sand was estimated. By investigating the development of hydraulic gradient along the inner wall, the principle underlying the suction response for different combinations of self-weight and wall thickness was identified. FE modelling was also performed to explore the influence of the hydraulic blockage by the silt layer.

This study found that the caissons could penetrate into all soils by suction installation. Among the key findings are the observations that the suction pressure increases with depth following a distinct pressure slope, corresponding to a critical hydraulic condition along the inner wall; and the installation was possible in both layered sand-silt and uncemented-cemented soils if sufficient pumping was available. While the caisson could penetrate the weakly cemented layers well with no notable adverse effects, problems were observed in the installation in layered sand-silt soil. These include piping failure in slow pumping rate installation at 1g, and the formation of extremely unstable soil heave during installation.

Preface

The candidate conducted the work reported in this thesis from March 2003 to October 2005. All the experimental work was conducted at the Centre for Offshore Foundation Systems (COFS), the University of Western Australia, with the exception of some suction installation tests at normal gravity, which were conducted at the University of Oxford, UK. The test analyses were conducted in both COFS and the Department of Civil Engineering at the University of Sydney, Australia. The candidate was supervised by **Professor Mark Randolph** and **Associate Professor David Airey**.

The By-Laws of the University of Sydney require that the original sections of a thesis submitted for the degree of Doctor of Philosophy be indicated. In accordance with the By-Laws, information obtained from other sources has been appropriately acknowledged and referenced in the text. The author claims originality for the following work:

- In Chapter 2: the design and development of all the test apparatus for both the PIV tests and the suction installation experiments, including the 1g models and the centrifuge models.
- In Chapter 3: all the soil tests reported, and the sample preparation techniques for layered sand-silt soil, and layered uncemented-cemented sand.
- In Chapter 4: all the PIV tests, and the suction installation tests in both homogenous sand and layered sand-silt soil, as well as interpretation of the experimental data that are not explicitly acknowledged.
- In Chapter 5: all the centrifuge suction installation tests in homogenous silica sand, in homogenous calcareous sand and in mixed soils, and interpretation of the data.
- In Chapter 6: all the centrifuge suction installation tests in layered sand-silt soil, and layered uncemented-cemented soils, and all the interpretations of the experimental data.
- In Chapter 7: all the numerical analyses conducted for the PIV tests and the suction installation tests; the simulation of the suction installation trend, and

the identification of the principles underlying the suction pressure trend in homogenous sand; the simulation of suction installation in layered sand-silt soil.

During the period of candidature, the author prepared several papers for publication. They are listed as follows:

1. Tran, M.N., Randolph, M.F. and Airey, D.W. (2005). "Installation of suction caissons in sand with silt layers". Submitted to *ASCE Journal of Geotechnical and Geoenvironmental Engineering*.

2. Tran, M.N. and Randolph, M.F. (2005). "Variation of suction pressure during caisson installation in sand". Submitted to *Géotechnique*.

3. Tran, M.N., Randolph, M.F. and Airey, D.W. (2005). "Study of sand heave formation in suction caissons using particle image velocimetry (PIV)", *Proc. International Symposium on Frontiers in Offshore Geotechnics - ISFOG*, Perth, Australia, 259-265.

4. Tran, M.N., Randolph, M.F. and Airey, D.W. (2005). "Study of seepage flow and plug loosening in installation of suction caissons in sand", *Proc. 15th International Offshore and Polar Engineering Conference - ISOPE*, Seoul, Korea, 2, 516-521.

5. Tran, M.N., Randolph, M.F. and Airey, D.W. (2004). "Experimental study of suction installation of caissons in dense sand", *Proc. 23rd International Conference on Offshore Mechanics and Artic Engineering - OMAE*, Vancouver, Canada. Paper: OMAE2004-51076.

Acknowledgements

This research would not have been possible without the help and contribution of the many individuals and organisations to whom I would like to express my thanks.

Firstly, I would like to thank my supervisors, **Professor Mark Randolph** and **Associate Professor David Airey**, for their support and guidance during the research. To **Mark**, I would like to express my sincerest thank for not only providing me with the opportunity to work on this project, but also always being patient, understanding and kind to me throughout the years. His insightful criticisms and advice have always been of great value to me. **Mark** cared not only about my research, but also about my future, and that is some thing that I will not forget. Very special thanks to **David**, who has always been kind, supportive, and never seemed to be short of valuable comments and suggestions (guarantee at least one full page for every submitted paper). It has been a pleasure and an advantage to work with both of them, from whom I have learned so much. My sincere thanks to them.

My research was funded by the International Postgraduate Research Scholarship and the International Postgraduate Award, provided by the University of Sydney. Additional financial support was provided by the Centre for Offshore Foundation Systems (COFS). These are gratefully acknowledged.

I would like to thank **Professor John Carter** and **Professor Martin Fahey** for their help during the initial stage of my candidature. I would also like to thank **Dr David White** for providing the GeoPIV software, and kindly hosting me (with nice lunch sandwiches) during my visit to Cambridge. I am extremely appreciative for the collaborative research experience at the University of Oxford, which would not have been possible without the support from **Professor Guy Houlsby**. I thank him for providing me with this opportunity, and his helpful discussions during my time at Oxford. **Dr Byron Byrne**'s help with the test set-up at Oxford is gratefully acknowledged.

Back at COFS, I would like to thank **Ms Monica Mackman** for her help with the administrative matters throughout the years. Also thanks to the COFS technicians for

their excellent support during my research. I am particularly grateful to UWA workshop technician **Mr John Bagrie**, who has patiently listened to my lengthy explanation, and tried so hard to work on my design. I wish him an enjoyable retirement in his Albany home. I am also thankful to UWA electronics technician **Mr John Breen**. He has always been of great help, and at times even stayed back long after 5 just to fix my broken transducers. I am very grateful to him. The appreciation is also extended to **Mr Don Herley**, **Mr Bart Thompson**, **Mr Wayne Galbraith**, **Mr Binaya Bhattarai**, **Ms Claire Bearman**, **Dr Wenge Liu**, and other workshop personnel and electronics technicians. Also many thanks to my UWA and USyd friends for enjoying discussions not only about work, but also life and the world, which have made my postgraduate time memorable and pleasant.

Finally but most importantly, I want to express my deepest gratitude to my wife, **Vi**, and my family. **Vi** has always been there for me during the ups and downs, sharing my excitement and frustration, listening patiently to my endless (and boring) stories about my research. Her love and understanding have allowed me to make it this far. I am deeply grateful to her. To my parents, brothers and sister, their continuing encouragement and support have been a great source of inspiration. Especially to my parents, without their unbounded love and care, I would not have been the person I am today. I am forever indebted to them.

Manh Ngoc Tran

October 2005

Chapter 1
Introduction

1.1 Overview

Suction caissons have become increasingly popular in the offshore industry, especially over the last decade. This chapter aims to provide a basic understanding of suction caissons by firstly giving a general introduction to this concept. It then looks through the history of their practical uses in the field and the potential for future applications. The chapter discusses the advantages and benefits of suction caissons, and explains the reasons behind their popularity, and also justifies why research is needed. The final parts of this chapter give a general review of what studies have been conducted on suction caissons, and later reveal the need for the research that is the focus of this thesis. In this study, the research reviews and aims will be addressed by examining the following key questions:

- *What* is a suction caisson ?
- *Why* are suction caissons used ?
- *When* can suction caissons be used ?
- *How* should suction caissons be used ?

The next sections in this chapter will address the first two questions, and part of the third. The rest of this thesis will explore the latter two, focusing on installation in homogenous and layered sandy soils.

1.2 Suction caissons: definition and terminology

Suction caissons are also known under a number of different names (Tjelta, 2001), such as suction piles, suction cans, suction anchors, bucket foundations etc. Despite the name differences, they all share the same installation principle, which will be described below. In this thesis, the term "suction caisson" will be used. A suction caisson is a hollow circular tube closed by a lid at the upper end. Literally, it resembles an upturned can. The caisson lid can be a stiffened flat plate, or a dome. The maximum wall length to diameter ratio is smaller than in a pipe pile, normally less than 10. Wall thickness to diameter ratio is also smaller, generally in the range of 0.3% - 0.6%. In long caissons, stiffeners are often added along the internal perimeter (ring stiffeners) or longitudinally to prevent them from buckling during installation. Stiffeners are common in suction caissons in clay, where the maximum wall length to diameter ratio can be as high as 9 (Tjelta, 2001), but generally less common in caissons in sand due to a much lower ratio, often smaller than 1. Illustrations of typical suction caissons can be seen in Figure 1.1.

Suction caissons are installed to the desired depth by first allowing them to penetrate into soil under their self-weight. Then water is pumped out of the caisson interior, which creates a net pressure difference across the lid that "sucks" (penetrates) the caisson into soil to the targeted depth (which also explains the "suction caisson" name). There are a number of terms associated with suction caissons and the installation process that will be used frequently in this study. To avoid confusion, these terms are defined below, and will imply these meanings throughout this thesis (these are further illustrated in Figure 1.2):

- *Suction pressure*, or *differential pressure*: the net pressure difference across the caisson lid, created as a result of pumping water out of the caisson compartment.
- *Maximum wall length*: the length of the caisson wall measured from the lower lid surface (i.e. the lid face inside the caisson) to the wall tip.
- *Aspect ratio*: ratio between maximum wall length to the caisson internal diameter.
- *Pumping rate*: total flow rate at which water is pumped out of the caisson interior.
- *Sand heave (plug)*: the difference between the soil surface level inside the caisson compartment and that of the surrounding soil outside the caisson.

1.3 History of suction caissons

1.3.1 History of field applications

Although suction caissons are still viewed as a relatively new concept in the offshore industry, their first use as a type of anchorage and foundation system dated back to the late 1950s. Since then, there have been numerous field applications of suction caissons around the world. To limit this section to manageable length, only milestone applications will be discussed.

Among the earliest reported use of this concept is probably the portable core sampler device by Mackereth (1958). The equipment was used to core samples in a lake bottom, where the sampling tube was lowered to the soil surface, and held in place during coring by a small (0.45 m diameter, 1.2 m long) suction embedded caisson. It was later retrieved by supplying compressed air into the compartment. In 1972, Shell developed a self-operating unit to conduct cone tests in the North Sea, where a suction caisson was used to resist the cone penetration force, and retrieved by reverse pumping, i.e. pumping water into the caisson interior (North Sea report, 1972). The similarity between these early uses of suction caissons is that they were both used as temporary anchorages to operate other soil testing equipment, and were invented because of difficulties in operating conventional devices in deep water. In 1980, suction caissons were first used commercially at large scale in the Gorm field, North Sea (Senpere and Auvergne, 1982). A total of 12 suction caissons, 3.5 m in diameter and 8.5 m to 9 m long, were installed and used for anchoring mooring buoys. The first field observations of installation problems, where excessive sand heave formed inside the caisson, were also recorded in this project.

The year 1989 saw the first time the suction concept was applied to a permanent foundation system in the Gullfaks C gravity platform (Tjelta et al., 1990). The foundation wall was able to penetrate to the final depth of 22 m with the assistance of suction pressure, created by pumping water out of the concrete cells. It was also observed that most of the platform submerged weight was carried by the wall tip and the wall skin friction. This observation, together with the successful suction-assisted installation of this very large gravity platform (a similar structure is illustrated in Figure 1.3a) created

significant confidence in the concept, and led to further application for the Snorre Tension Leg Platform (TLP) (Fines et al., 1991; Stove et al., 1992; Dyvik et al., 1993), and later the Draupner E (previously Europipe 16/11E) and Sleipner T platforms (Bye et al., 1995; Tjelta, 1995), all in the North Sea. It is worth noting here that the Draupner E and Sleipner T plaforms (Figure 1.3b) marked the first time that suction caissons alone were used as a permanent foundation in sand. They also demonstrated that with the use of suction, wall penetration in very dense sand was possible.

The success of the above projects has led to a rapid increase in the use of suction caissons in the offshore industry over the past decade. It is estimated that at present, there have been nearly 500 suction caissons installed in more than 50 locations around the world (Andersen et al., 2005[a]). This number may still be modest compared with traditional piled foundations, but it is a significant increase from the limited field applications prior to the early 1990s. Today, suction caissons are used virtually in all five continents (Europe, Africa, Asia, America, Australia), in water depths varying from shallow water (20-40 m) to ultra deep (over 1000 m). Evolved from the original anchorage intention, they are now used in different soil types for numerous purposes, from mooring anchorages to permanent foundations for platforms, support for ship salvage, means to deploy other anchorage systems such as the Suction Embedded Plate Anchors (SEPLA) etc. They have also been considered for military use (Bang et al., 1999), and as foundation systems for future offshore wind turbines (Feld et al., 1999; Houlsby and Byrne, 2000; Feld, 2001). The way suction caissons are put together in operation also varies, from a single unit as in most cases, to single units with multiple compartments (Masui et al., 2001) and cluster units, i.e. many caissons put together as a unit, such as those in the Hanze project (Aas et al., 2002; Sparrevik, 2002) shown in Figure 1.4. Significant projects using suction caissons and their references are listed in Table 1.1. The rapid increase in field applications for a wide range of water depths over the last decade, compiled from nearly 50 different projects, can be seen in Figure 1.5.

1.3.2 Advantages of suction caissons

The rapid increase in field applications discussed above is a direct indication of the many advantages of suction caissons over traditional methods. A significant advantage of

suction caissons is cost effectiveness, which is perhaps the most important factor in their consideration for offshore use (Tjelta, 2001; Bussemaker, 2005). This cost includes geotechnical investigation cost, steel and fabrication cost, and installation cost. The use of suction caissons does not appear to change the site investigation cost (Feld et al., 1999; Feld, 2001), and normally loses out to traditional piling in fabrication expense despite using less steel in most cases (Bussemaker, 2005). This is due to tight roundness tolerances, and extensive welding in caisson fabrication, which requires expensive welding materials and involves high labour costs. However, the suction installation process is often so cost effective that it offsets the greater fabrication costs and reduces the overall project expense to such an extent that suction caissons are a cost competitive option (Bussemaker, 2005). This significant installation saving is possible because of the use of simple installation equipment, much shorter installation times, normally within 24 hours compared with several days for a platform installation, and no requirement for expensive large crane barges because the structures can be "self-installed", as illustrated conceptually in Figure 1.6. In deep and ultra deep water, suction caissons become even more cost effective over traditional piling, where costly hammer modifications are required to extend their operational limit to greater depths (Colliat, 2002). It is worth noting here that the cost of installing the Draupner E platform suction caissons was similar to that of conventional pile alternatives, but this was largely because of the lack of previous experience, complicated and expensive monitoring systems, and the use of large crane barges (Rusaas et al., 1995).

The mobility and flexibility of suction caissons when in use are additional reasons for their attractiveness. They can be retrieved simply by reverse pumping for re-use, or during installation if obstructions such as boulders are encountered. This was one of the reasons that they were selected as the foundation choice in the Gorm field (Senpere and Auvergne, 1982). In some cases, the rapid installation and retrieval time, normally of just a few hours, and the flexibility during operation make them superior to other methods. An example is the Kursk submarine salvage project in the Barents sea, where suction caissons, used as supporting points for the sawing line, could be easily raised and lowered in soil to adjust this line during the hull cutting (Figure 1.7). The same operation would have been far more complicated if fixed anchoring systems, such as conventional piles, had been used (Bussemaker, 2005).

The ability to position the caissons to high accuracy, together with no embedment uncertainties also make suction caissons advantageous in congested seabeds, compared with, say, drag anchors (Andersen and Jostad, 1999; Tjelta, 2001). In these cases, interaction with other existing systems can be avoided, hence limiting potential damage to other structures. They also create less disturbance of the seabed, thus minimising the impact on the marine environment (i.e. being more environmentally friendly).

The discussion above has demonstrated the potential of suction caissons to provide a versatile anchoring system, which may soon see them gaining a larger share in the offshore foundation market (Riemers, 2005). However, future use and development of suction caissons will depend on the outcome of assessments of the performance of current installations and research to address some of the uncertainties still existing. These uncertainties and research being conducted to address them are considered in the next sections.

1.3.3 Research history

Planning and better design of suction caissons for field applications would not have been possible without the knowledge gained from research. To date, there have been many studies on various aspects of suction caissons in both clay and sand. This section will go through the history of research into suction caissons, highlighting key studies and findings.

In the early 1960s, Goodman et al. (1961), in a feasibility study that included perhaps some of the earliest published research results on suction caissons, proposed the wider use of the "vacuum" concept for marine anchoring purposes. During that time, it was common practice to use gravity anchors because their holding capacity could be easily calculated (Brown and Nacci, 1971). However, these soon showed their disadvantages. The low pullout force to weight ratio often meant large and heavy anchors were required, making them difficult to handle, inefficient and ineffective. To improve the anchorage capacity, systems that allowed for more soil-structure interaction needed to be developed. Although the "vacuum" anchor is a simple concept, it appears to be a brilliant idea as a foundation system. By allowing the conventional footing block (the caisson lid in this case) to extend some depth into soil to promote more soil-structure interaction, while at

the same time making use of the "vacuum" effect using a sealed lid, this system promised improvement in holding capacity. Goodman et al.'s study was motivated by the military demand for anchorage systems that allow for high mobility and rapid field deployment. In their research, which focused on holding capacity, vertical pullout tests in various types of soil with different moisture contents were conducted using transparent "vacuum cups" (suction caissons). The key observations were that the system worked very well in clayey soils. However, in more permeable soil such as sand, localised piping occurred, causing the loss of vacuum, or fluidisation resulting in increased soil permeability.

Following these initial results, there have been a number of other studies to investigate the behaviour of suction caissons in soil. Brown and Nacci (1971) explored the caisson pullout performance in granular soil, and reported high force to weight ratio and a conical failure surface. Wang et al. (1975, 1977) investigated the holding capacity in a wider range of soils, including sand, silt and clay, and developed a breakout capacity equation using Mohr-Coulomb failure theory. They also suggested that suction caissons could be particularly useful for short-term anchorages, and had potential in many other applications. A similar study was conducted for caissons in sand by Helfrich et al. (1976), which showed that a Mohr-Coulomb criterion could predict failure loads to within 13% of the measured values. The required caisson size in a field application was also predicted by extrapolating their model test data. Wilson and Sohota (1980), Sohota and Wilson (1982) presented studies using modified suction anchors, which were installed by water jetting, and buried at some depth below the surface.

Most research work during this early period was focused on simple monotonic pullout (short-term), with little investigation and discussion of the installation process, and the caisson long-term behaviour under cyclic loading. Since the late 1980s, research work on suction caissons has increased significantly. Apart from continuing studies on monotonic breakout capacity (e.g. Steensen-Bach, 1992), initial investigations on the caisson cyclic behaviour (Larsen, 1989) and computer modelling (Christensen and Haahr, 1992) were also conducted. This increase is due to the recognition of their potential, and thus increasing interest from the offshore industry, coupled with advances in technology, especially computer technology, that has allowed more sophisticated modelling.

Recently, especially over the past few years, caisson studies have been reported in much greater number and detail. They have ranged from numerical modelling to physical testing at normal gravity (1g) and at elevated gravity levels in geotechnical centrifuges. These studies may be divided into two main groups based on their research focus: installation related studies and in-place capacity and performance studies. For the latter, behaviour under both monotonic and cyclic loading has been considered. The soil types considered by the studies were diverse, including sand (Byrne, 2000; Iskander et al. 2002; Byrne and Houlsby, 2002; Byrne and Houlsby, 2004), clay (Fuglsang and Stensen-Bach, 1991; Andersen and Jostad, 1999; House, 2002; Iskander et al. 2002; Clukey et al., 2004), layered sand-clay (Allersma et al., 2001[a]), and calcareous soils (Watson and Randolph, 1997; Randolph et al., 1998; Watson, 1999). Along with experimental modelling, numerical studies of suction caissons have also been reported (Deng and Carter, 2000; Zdravkovic et al., 2001; Cao et al., 2002; Deng and Carter, 2002; Supachawarote et al., 2004). In addition to small-scaled model testing and computer modelling, research on this innovative foundation concept was also conducted through large scale field trials. These included systematic field tests of suction caissons from as early as the 1970s (Hogervorst, 1980) until recently (Stevenson, 2003; Fakharian and Rismanchian, 2004). It may be noted that research activities into suction caissons have mostly been conducted in the last decade, and are related to the rapid increase in field applications noted previously in Figure 1.5.

An important consideration when using suction caissons is the ability to install them successfully into the soil. Understanding of the installation process is also important, as the suction and other effects in the soil can affect the subsequent caisson performance. At present, there have been a number of research studies to investigate caisson installation in both clay and sand. Among different installation studies in clay were the investigations of limiting caisson aspect ratio to prevent plug upheaval (House et al., 1999), variations in soil stress along the caisson wall and set-up effects (Rauch et al., 2003; Andersen et al. 2004; Masui et al., 2004; Chen and Randolph, 2004), penetration and upheaval in soft clay (El-Gharbawy et al., 1999; Andersen et al., 2005[b]), and penetration prediction (Andersen and Jostad, 1999; Houlsby and Byrne, 2005[a]). Generally speaking, the installation in clay is fairly straightforward without notable problems, as long as the

caisson aspect ratio is smaller than the limit at which soil plug failure (i.e. where the internal clay plug is pulled up by the suction) may occur.

In sand the installation is, however, more complex due to the seepage flow in the soil, which may create excessive sand heave inside the caisson and piping failure. This was observed in the caisson installation in the Gorm field (Senpere and Auvergne, 1982). In this project, although the caissons were finally installed to the desired depth, excessive sand heave was observed inside the caissons during penetration in sand, which had to be removed by water jetting before the caissons could reach the intended embedment level. This experience created a subsequent negative impact on suction caisson use in the field (Tjelta, 2001). There have been a few subsequent research attempts to explore caisson installation behaviour in sand, but the number is still rather modest, and many field data are not available in the public domain. Hence, understanding is still limited, and more research is required to investigate the associated issues. These are discussed in greater detail in the next section.

1.4 Previous installation studies in sand

1.4.1 General mechanism of suction installation in sand

The general caisson installation mechanism in sand has been widely known and reported in previous studies (e.g. Hogervorst, 1980; Tjelta, 1995; Erbrich and Tjelta, 1999), and is summarised in this section. The mechanism is also illustrated schematically here in Figure 1.8. In suction installation in granular materials, such as sands which have high permeabilities, the suction pressure, while helps install the caisson by means of the differential force, also induces seepage flow through the soil around the caisson tip into the caisson interior. Depending on the flow direction (Figure 1.8), the seepage can have different impacts on the soil. On the external caisson wall, the downward seepage gradient resulting from the suction application leads to an increase in effective stress in the soil, and hence the external skin friction. On the other hand, the upward flow gradient inside the caisson reduces the soil effective stress at the caisson tip and along the inner wall, thus reducing the tip resistance and internal skin friction. This reduction, especially of the tip resistance, is normally large enough to easily offset the increased friction due to

the external downward flow, resulting in significant reduction in total driving force (the penetration force degradation effect) which assists the installation. However, the upward seepage can also create some sand loosening (reduced density) inside the caisson, leading to the creation of internal sand heave, thus preventing the caisson penetrating to the intended depth. The excessive heave observed in the Gorm field installation (Senpere & Auvergne, 1982) mentioned above is a good example. Furthermore, sand liquefaction, or "quick sand", may occur, leading to the formation of piping channels and the loss of the hydraulic seal in the soil. In this case, further pumping will create excessive water flow into the caisson compartment without any notable penetration (installation failure).

1.4.2 Review of previous installation in sand studies

Various research programs investigating installation in sand have been reported by a number of researchers around the world. Hogervorst (1980) described a series of field installation tests of small suction caissons in a shallow lake in 1976. The promising results from these initial tests led to more trials of larger caisson sizes (3.8 m diameter, 5 to 10 m long) in the following two years. The study found that small obstacles and caisson tilting did not significantly affect the installation. It was observed that the sand plug inside the caisson could become liquefied, hence reducing the internal skin friction. A significant reduction in penetration resistance due to groundwater flow was recorded. This was also observed in a large scale penetration test of an instrumented concrete panel, which was attached in the middle of two 6.5 m diameter suction caissons, and pushed into the soil by suction-installing these two caissons (Tjelta et al., 1986). Although the general mechanism of suction caisson installation in sand was identified and described in these early studies, no actual installation data were presented. The influence of caisson geometry, surcharge, as well as the heave formation for different installation conditions were not discussed.

Iskander et al. (1993) and Iskander et al. (2002) reported a 1g test program in sand, where 3 pressure transducers were fitted inside the caisson (along the wall) at different heights. The installations were conducted using both least possible suction to cause penetration, and full available suction. The tests found that although the penetration force (or suction pressure) was lower in the installation with least possible suction than in the maximum

suction case, the measured pore pressures inside the caisson during penetration were very similar for the two cases. They both indicated that a quick condition (liquefaction) in the sand inside the caisson occurred, which was also reflected in the unavoidable formation of excess sand heave and the reduction of suction penetration force compared with jacking (nearly one order of magnitude smaller). These results agree well with the field observations reported by Hogervorst (1980) and Tjelta et al. (1986) presented previously, and experimental results in earlier 1g tests by Larsen (1989). While Iskander et al.'s study could further support the observed mechanism of suction caisson installation in sand with some pore pressure measurements, the published data in this study were however still limited, with little information provided on the suction pressures for different installations. The effect of the key factors such as caisson geometry and surcharge on the suction installation behaviour (e.g. penetration resistance force, sand heave etc) was again not reported.

Tjelta (1995), Erbrich and Tjelta (1999) described a test series using a highly instrumented caisson model undertaken by the Norwegian Geotechnical Institute (NGI) as part of the preparation program for the Draupner E and Sleipner T platform installations. It was found that suction pressure could be applied at very shallow initial wall embedment depth, and piping failure was hard to induce if the caisson was free to move, even when the caisson was slightly tilted. This result is consistent with the previous field observation by Hogervorst (1980). However, these studies also showed that if the caisson was restrained, piping channels would form, but the caisson could always continue to penetrate once the restraining force was removed. The effect of surcharge (i.e. increase in dead weight) was investigated, and found to reduce the required suction pressure to install the caisson. Sand heave, averaging at about 4% of the penetrated wall depth, was recorded in the tests. A "safety mechanism", where the hydraulic gradient in the internal sand plug tends to drop due to sand loosening, was also discussed. In this study, installation data for several cases including measurements of suction pressures and pore pressures were presented. However, since only one caisson geometry was tested, the influence of absolute caisson size and wall thickness on the installation process and sand heave formation was still not known. Furthermore, the effect of different pumping rates was not discussed.

Installations in sand at 1g were also investigated by Bang et al. (1999) and Cho et al. (2002), who used minimum suction to penetrate the caissons. The studies found that plug loosening and sand heave were formed during penetration despite the use of minimum suction, which is similar to results from the studies discussed above. To quantify the reduction in frictional capacity due to sand loosening, the study introduced a "mobilised effective soil friction angle ratio" α, defined as follows:

$$\alpha = \frac{\tan \phi'_m}{\tan \phi'} \tag{1.1}$$

where ϕ'_m = the mobilised effective soil friction angle required for the equilibrium between the external force and the caisson bearing capacity (the first being measured from the experiments; the latter being calculated using conventional pile design for end bearing and skin friction);

ϕ' = the full available effective soil friction angle.

The study later proposed an empirical relationship between this α ratio and the normalised "equivalent external pressure" X (or suction pressure), which was defined as:

$$X = \frac{p_s + \frac{F_b}{A}}{\gamma_b L_p} \frac{D}{L_m} \tag{1.2}$$

where p_s = applied suction pressure;

F_b = submerged weight of the caisson;

A = area of the internal plug;

γ_b = soil buoyant unit weight;

D = caisson diameter;

L_p = wall embedment depth;

L_m = maximum wall embedment depth, at which further penetration by suction is not possible and causes piping failure.

However, the reliability of the α-X relationship is debatable due to the normalisation against uncertain quantities such as the maximum penetrated wall depth L_m.

Installation studies under equivalent prototype stress conditions in a geotechnical centrifuge have also been reported. Allersma et al. (1997), Allersma et al. (2001)[b] and Allersma (2003) reported suction caisson installation tests in a centrifuge, where the caisson was installed by both continuous pumping and by a percussion technique (with the suction pressure applied in pulses). Jacked installation, where no penetration resistance degradation due to seepage occurred, was also conducted at different soil stress levels, showing the stress dependent behaviour of the soil. It was also found that much less force, about 8 times less in one case, was required to penetrate the caisson during suction installation compared with jacking. This is consistent with both field observations by Hogervorst (1980) (at high soil stresses) and results at 1g, e.g. Iskander et al. (1993, 2002) (at much lower soil stresses), confirming the force degradation effect. Installation of caissons with aspect ratios of up to 4 was found to be possible. Installation in soils with varying densities was also conducted. The study found that the required suction pressure was lower for less dense sand, but increased linearly with wall penetration depth with quite similar gradient for all tested soil densities. Installation in steps, where the suction was stopped and re-started at different wall embedment depths during penetration, did not cause any significant difference in the recorded suction pressure when compared with continuous installation. It was also reported that a large amount of water, up to twice the caisson volume in one case, was collected at the end the installation due to seepage through the soil.

The observed sand heave was around 8-10 % of the penetrated wall depth, and appeared to be larger for thicker-walled caissons. The study also investigated the normalised suction pressures $\Delta pD/\gamma_{sat}Lt$ for various cases (γ_{sat} is the soil saturated unit weight, other parameters are defined in Figure 1.2), and found that they were quite similar. It was concluded, based on this result, that the suction caisson dimensions did not have any special influence on the penetration force. Considering the dependence of the suction pressure on the surcharge used, as reported by Erbrich and Tjelta (1999) (mentioned earlier), this conclusion appears premature as the observed similarity in the normalised suction pressures could be coincidental for the tested caisson weights. Since the effect of different caisson weights (or surcharge) was not investigated in this study, further verification could not be conducted. Although the study programme included tests with various caisson sizes and wall thicknesses, the presented data are still limited. Full

suction data (e.g. suction pressure against penetration depth) were only available for one caisson geometry. Also, no direct comparison of the suction pressure response with other test results, such as those at 1g, was made, hence the parameters influencing the generic caisson responses could not be fully determined from this study.

Attempts to predict the suction pressure during installation in sand have also been reported in several studies. From the field test observations, Hogervorst (1980) proposed a caisson penetration calculation (prediction) based on in-situ cone penetration test (CPT) results as follows:

$$R = \pi D(k_p q_c t + 2k_f \int_0^L f dz) \tag{1.3}$$

where R = penetration resistance;
D = caisson diameter;
L = penetrated wall depth;
t = wall thickness;
f, q_c = local friction and average cone resistance respectively;
k_f, k_p = empirical coefficients relating cone and caisson friction and end resistance respectively.

The above approach, although simple, is limited in its capability to model the suction installation mechanism in sand. For example, the difference between inside and outside wall friction due to seepage is not reflected in Equation (1.3).

Based on this empirical approach, Feld (2001) proposed a modified method, which included an expression for suction effects on the inside and outside wall friction, and the tip resistance as below:

$$\tau_{in} = r \tan\phi \sigma'_v (1 - r_i \frac{\Delta p}{\Delta p_{crit}}) \tag{1.4}$$

$$\tau_{out} = r \tan\phi \sigma'_v (1 + r_o \frac{\Delta p}{\Delta p_{crit}}) \tag{1.5}$$

$$\sigma_{tip} = k_p q_c (1 - r_p \frac{\Delta p}{\Delta p_{crit}}) \tag{1.6}$$

where τ_{in}, τ_{out}, σ_{tip} = unit stresses on outer wall, inner wall and caisson rim respectively;

Δp = applied suction pressure;

Δp_{crit} = critical suction (suction that creates a critical hydraulic gradient in the sand) = $\gamma'L/[1-0.68/(1.46L/D+1)]$ (derived from numerical steady state flow solution with L/D less than 0.5);

r = caisson wall roughness coefficient;

r_i, r_p = coefficients representing the maximum reduction in the inside skin friction and tip resistance respectively;

r_o = $0.1(L/D)^{0.25}$ (derived from the assumption that the outside wall friction increases by 13% when Δp equals Δp_{crit}, which was observed from Sleipner T installation);

q_c, k_p = cone resistance and coefficient relating this to caisson tip resistance.

The required suction Δp at any stage could then be calculated using:

$$W + \Delta p A_{caisson} = \tau_{in} A_{inner\ wall} + \tau_{out} A_{outer\ wall} + \sigma_{tip} A_{tip} \quad (1.7)$$

where W = caisson submerged weight;

τ_{in}, τ_{out}, σ_{tip} = defined above.

The advantage of the above method is that it provides a relatively simple means to estimate the suction pressure. However, calibration against test measurements is required to determine the likely range of the empirical coefficients.

Houlsby and Byrne (2005)[b] suggested an analytical method to calculate the required suction pressure. The analysis adopted conventional pile design for skin friction and assumed strip footing calculations for the caisson tip (with modifications). The study also introduced a pore pressure factor *a* to take into account the different suction effects (due to different pore pressures generated) on the inside and outside wall friction, and the caisson tip resistance. Seepage flow during suction penetration was also estimated using a flow factor *F*. A potential advantage of this approach when compared with previous

methods is that it does not require cone penetration test results to calculate the suction pressure. However, some key factors used in the analysis (e.g. the pore pressure factor *a*, the flow factor *F*) were derived from theoretical analyses, and may need further validation with experimental results. Care should also be taken when choosing the ratio of the permeability of the loosened sand plug inside the caisson k_{in} and that of the outside sand k_{out} (i.e. the k_{in}/k_{out} ratio, of which both factors *a* and *F* are a function), because the actual permeability range corresponding to minimum and maximum void ratio in some (non-liquefied) sands may be quite small.

A summary of the research on suction caisson installation in sand is shown in Table 1.2. Although the review of these research studies has been presented above, discussion of the published data available from some of the above studies is delayed until the main part of this thesis. These data will be introduced and compared where applicable to supplement the results of the present research and to help draw conclusions from the work.

1.4.3 Remaining issues

While the general installation mechanism was well recognised in the above studies, there are still many issues remaining to be resolved to fully understand the suction installation in sand. The effects of variation in pumping rate, which is perhaps the only controllable parameter during installation, have not been thoroughly studied in previous research. The influence of the caisson geometry, including sizes and wall thickness, on suction pressure and other installation behaviour is still not clearly understood. Also, it is known that seepage flow plays a very important role in installation in sand, but it has so far not been adequately addressed. Few seepage measurements have been reported, hence the seepage trend during wall penetration is not known. Another important aspect is the mechanism of sand heave formation inside the caisson and its development during the wall penetration. Whether the heave formed is caused by sand expansion, displaced sand volume by the caisson wall, or the inflow of the surrounding sand under the influence of the inwards seepage is not understood, and has not been fully investigated.

It is not uncommon to have layered soil conditions in the field, where sand is inter-bedded with bands of silt, or layers of cemented sand. These are of particular concern because they may obstruct the caisson installation. In layered sand-silt, the much less

permeable silt layers can block the seepage flow, hence may eliminate the beneficial penetration force degradation effect (discussed above in Section 1.4.1). The seepage blockage may not be as complete as the case for clay, since silt is still subjected to scouring, i.e. erosion of silt particles (these particles may also flow into and through the sand if the silt layer is overlain by the sand). This, as a result, may allow some seepage flow to pass through. However, substantially larger tip resistances are expected in silt than in clay, and this means higher driving pressures may be required to penetrate the caisson. This high pressure, combined with the possibility of scouring could lead to piping failure. Furthermore, under the influence of suction, a net differential force may be created across the silt layer due to its low permeability. This may cause the uplift of the silt layer, similar to the plug upheaval observed in clay, which as a result obstructs further penetration and creates plug instability. In sand where weakly cemented layers are present, the concern is mainly whether the caisson wall will "punch through" these layers. Until now, there have been no reported studies to investigate suction installation in these soils.

The above issues, together with the limited installation data in the literature for sand, and the confidentiality of most field installations, were the motivation for the research described in this thesis.

1.5 Objectives of this study and thesis outline

This study has investigated suction caisson installation in sand through the experimental programmes at both 1g and in a geotechnical centrifuge. Numerical studies were also conducted to simulate the test results. The objectives have been to extend the current experimental database, which is small and limited, and hence to provide better understanding of various aspects of the installation, including the effects of changing pumping rate, the influence of caisson geometry and surcharge on the suction pressure and other installation behaviour, and the likely sand heave formation mechanism. It also aimed to identify the principles underlying the suction response in homogenous sand, and to increase understanding of installation in layered soil, by providing some knowledge of how silt and cemented layers can influence the installation behaviour.

This thesis is organised into 8 chapters. A brief description of each chapter is outlined as follows:

- *Chapter 2*: summaries the test apparatus developed for the installation study, and the experimental procedures for both 1g and centrifuge tests. It also includes a discussion of the merits and limitations of small-scale model testing. The physical modelling approach of this research is also presented.
- *Chapter 3*: describes the properties of the different soils used in the suction installation tests. Details of various soil laboratory tests, and preparation of cemented sand are presented. Different sample preparation techniques are discussed for both homogenous and layered sands.
- *Chapter 4*: discusses the installation results for small-scale model tests at normal gravity (1g). These include a study of internal heave and soil deformation using the Particle Image Velocimetry (PIV) technique. Suction installation results in both homogenous silica sand and layered sand-silt profiles are also presented. The significance of these 1g results is discussed.
- *Chapter 5*: presents the caisson installation behaviour in homogenous sand for both silica and calcareous (uncemented) sands in the centrifuge. Installations in "artificially" mixed soil, where different proportions of silica flour were mixed with sand, are presented. The results are compared with other installations, including field data. The general suction pressure trends in sand are also identified.
- *Chapter 6*: presents the results from centrifuge installations in layered sand-silt, and layered cemented-uncemented calcareous soil. Comparisons are made with the 1g results. Comparisons with installation in homogenous soils are also made to explore the influence of the silt and cemented layers. Installation issues in these heterogenous soils are identified.
- *Chapter 7*: presents numerical investigations of the suction installation process. A numerical model is proposed and validated against experimental data. It is then used to simulate the PIV results, as well as predict the likely sand response during suction installation. The suction pressure trend in

homogenous sand is investigated, and the principles behind this trend are identified. Simulation results in layered sand-silt are also presented.

- *Chapter 8*: summarises the significant findings of this research. Suggestions and recommendation for further research are discussed.

Chapter **2**

Test Apparatus and Experimental Procedures

2.1 Overview

This chapter describes all the experiment-related developments in this research. It starts first by discussing the merits of conducting physical modelling, as well as some limitations of small-scale testing. This is followed by the introduction of the physical modelling proposed for this study, which includes 3 different test programmes. Normalisation of the quantities investigated in this study is discussed. The chapter then describes the test equipment and caisson models used in the research. These include models for the suction installation experiments at both normal gravity (1g) and elevated levels in a geotechnical centrifuge. For the latter, the general scaling rule and the effects of variation in radial length and relative sand-caisson size are discussed. A half-caisson model used to study the mechanism of sand deformation inside the caisson under the influence of suction is also described. The later part of this chapter describes the experimental procedure for each test programme. The theoretical seepage restriction due to the test chamber boundaries is discussed. Details of all the tests conducted in this research, including suction installation at 1g, at elevated g-levels in the centrifuge, and the half-caisson model test, are then presented.

2.2 Merits and limitations of small-scale model testing

Soil-structure interaction can be best investigated by conducting similar scale field tests. However, in most cases, especially where the tested structure is very large, it is practically difficult to do so. This is because of the high cost involved, and also the potential danger to human life (e.g. simulation of a slope failure). In the context of suction caisson installation studies, field installation tests can become very expensive due to high offshore operation costs, and hence are not financially viable in most cases.

The above issues can be accommodated by conducting small-scale model tests. They are not only considerably cheaper, but also more flexible, which allows changes in test conditions to be made easily. As a result, this allows more thorough investigation of the response of the structure at a much lower cost. However, a significant challenge of small-scale model testing is how to extrapolate the results for prototype cases. The differences in a number of aspects such as the soil stress and the relative soil-structure size can create variations in soil-structure interaction and response, and hence often invalidate simple extrapolation of the 1g data to large-scale cases. However, small-scale model tests can reveal the general trend of the response of the structure under a specific condition. In other words, they are useful in providing information on generic behaviour that can be expected in the prototype structure. This, when incorporated with other field data and numerical investigations, can be used to establish a design framework, which is also the aim of the small-scale model testing presented in this thesis.

2.3 Physical modelling in this study

Physical modelling of the suction caisson installation using small-scale models can be conducted at both 1g and in a centrifuge. Each of the test series, i.e. 1g or centrifuge tests, has its benefits and disadvantages. For the 1g tests, their flexibility provides more control of the experiments, allowing better investigation of many parameters such as the pumping rate during penetration, or observation of internal sand heave developed during the test. However, the soil stress in these 1g tests is much smaller than that in the field. The centrifuge tests, on the other hand, achieved higher soil stress levels similar to those in the field. However, with the current centrifuge set-up (presented later in this chapter),

less control over the tests compared with 1g was available, making them less flexible. As a result, the tests in this study were conducted at both 1g and in the centrifuge. The purpose was that by investigating the installation under both conditions, the disadvantages of each test series could be negated by the other. Hence, understanding of the caisson response under different conditions is maximised.

In this research, the suction caisson installation was investigated in 3 different test programmes:

- a half-caisson model test at 1g using the Particle Image Velocimetry (PIV) technique;
- suction installation tests at 1g;
- suction installation tests in the centrifuge.

Details of the apparatus and experimental programmes for the above the tests will be presented in the later sections of this chapter.

2.4 Normalisation of studied quantities

In the presentation of test results, normalisation of the measured quantities is generally adopted to enable simple allowance for the effects of differences in these parameters, and to reduce the number of variables involved. This was discussed in detail by Butterfield (1999).

In this thesis, the suction pressure has been normalised using a combination of the following group of parameters: the caisson penetrated wall depth L, the caisson diameter D, and the soil submerged unit weight γ'. The suction pressure against the penetrated wall depth relationship can be presented in a normalised form as either $p/\gamma'D$ or $p/\gamma'L$ against L/D. Figure 2.1 shows a typical suction recorded during a centrifuge installation and the normalised results. Figure 2.1a shows the data as recorded from the test in equivalent prototype units, Figure 2.1b shows the pressure normalised as $p/\gamma'D$, and Figure 2.1c shows the pressure normalised as $p/\gamma'L$. It can be seen that normalisation as $p/\gamma'D$ not only incorporates the importance of the overall foundation size on the resulting p, but also retains the original suction pressure trend. This normalisation will hence be used in

this thesis for the presentation of the suction results in the installation tests. The added surcharge amount will also be discussed using the same normalisation, i.e. $\Delta p/\gamma'D$, to allow comparisons between different cases. However, normalisation as $p/\gamma'L$ will be presented in this thesis when discussing matters relating to the hydraulic gradients developed in the sand, as the flow path is more related to L than to D.

There is also a need for normalisation of the seepage flow rate $Q_{seepage}$. The same absolute seepage can mean different groundwater flow conditions for caissons of different geometry. Furthermore, $Q_{seepage}$ is directly influenced by the suction pressure head applied H (or p/γ_w), and the soil permeability, especially permeability of the internal soil plug k_{plug} as this tends to change during suction installation. In order to take into account these two components, whilst still being able to reflect the effect of different caisson sizes, the seepage flow results $Q_{seepage}$ will be normalised against the caisson diameter D, the plug permeability k_{plug} and suction head H (i.e. $Q/k_{plug}HD$). Similarly, the total pumping rate will also be normalised to allow for comparisons of different installations. The same absolute pumping rate Q_{pump} can create different penetration rate and seepage effects when applied to caissons of different geometry. For slow installation, Q_{pump} comprises a very significant amount of seepage flow $Q_{seepage}$, which is highly influenced by soil permeability k. In order to take into account the effect of different caisson sizes, whilst still being able to reflect the seepage component, Q_{pump} results will be normalised against the caisson internal cross sectional area A, and permeability k. Normalised seepage and pumping rate will be shown later in this thesis.

2.5 The PIV test development

2.5.1 Background on PIV technique

Particle Image Velocimetry (PIV) technique is a non-intrusive, image-based technique, originally used in fluid mechanics to track the movement of objects. Details about the PIV technique and its application in geotechnics were described by White et al. (2003).

In this study, the PIV technique was applied to study how the heave occurs inside the caisson, and the soil deformation pattern under the influence of suction. For each test,

soil movement was captured by a digital camera and subsequently analysed using GeoPIV software, developed at Cambridge University Engineering Department, UK (White & Take, 2002).

Although offering high resolution measurements, there are a number of factors that can affect and reduce the performance in tests using PIV. These are caused by the PIV analysis itself and by optical effects that cause image distortion, including non-coplanarity of the CCD and object planes, camera lens distortion, and refraction through viewing windows (White et al., 2003). It is therefore important to evaluate the accuracy of deduced movements in each experimental set-up. In theory, with the current equipment and the parameters used in subsequent PIV analyses, as described in detail in the following section, a precision better than 1/100000th of the field of view (FOV) could be easily reached. Noting that a typical FOV was around 150 mm, this corresponds to an error of less than 1.5 μm.

2.5.2 Test apparatus and set-up

A half-caisson model, as shown in Figure 2.2, was developed to investigate the formation of sand heave during the application of pumping. The caisson was 100 mm in both diameter D and wall length L, and had a wall thickness t of 1.2 mm. A continuous rubber seal (cut 'O-ring'), 1 mm in diameter, was fitted along the caisson wall and top to prevent leakage during pumping. A water evacuation valve, which was left open during pushed-in penetration, was also available. It may be noted that the model caisson has a wall thickness-to-diameter ratio t/D of 1.2%, which is higher than typical prototype values of around 0.3%-0.5%. However this was necessary because the 1.2 mm thickness was the smallest width that allowed the rubber seal (the cut 'O-ring') to be fitted on.

Tests were conducted in a chamber of 370 × 220 × 400 mm (width × thickness × height). A transparent Perspex window was fitted in the front face to allow observations to be made. The sample depth was 200 mm and water depth was 170 mm. The caisson was held in place by a guide system, consisting of 3 arms with wheels. Each arm could independently move inward and outward in the radial direction. Details can be seen in Figure 2.3.

The caisson was connected to a hose to allow water to be pumped out. Flow was achieved using the water head difference between the test chamber and the hose outlet, with the mass recorded continuously using an electronic balance. Taking the water density as 1 g/cm^3, the water volume in cm^3 could be evaluated from the weight in grams, and hence the flow rate determined.

Differential pressure was measured using a differential pressure gauge. Since it could not be submerged, pressure was measured by connecting the gauge to 2 soft plastic tubes. With one tube embedded inside the caisson, and the other positioned on the caisson top, the differential pressure could be measured.

During each test, sand movement was captured by close-range photography using a 4-megapixel (2272 × 1704) digital still camera. It was set up at 0.3-0.5 m from the test chamber's Perspex window. Consecutive images were recorded at the rate of around 2 frames/second. The time between frames was determined from a watch (measuring down to 1/100th of a second) positioned in front of the Perspex window. To capture the fast movement of the soil skeleton, the camera shutter speed was set at 1/150th of a second. Since the flash was disabled to prevent reflection from the test chamber window, additional lighting was provided using a halogen light. Changes in lighting condition between frames can affect the result in from the PIV analyses. Using a halogen light helped avoid this as it gave constant lighting.

During the photo-taking period, continuous pressing of the camera "start" button was required. At the same time, no camera movement was allowed. To perform the task, an automatic device was developed. Details of this device, as well as the test set-up can be seen in Figure 2.4.

The PIV investigation presented here is limited to fixed tests, where the half-caisson was restrained from movement. The tests were, however, conducted at different wall embedment. The philosophy behind these PIV tests, and the application of these results to continuous suction caisson installations will be discussed in Chapter 4.

2.5.3 Test procedure

All tests followed the procedure given below:

a) The soil sample was prepared and the surface was levelled.
b) The half-caisson model was slowly pushed to penetrate to the desired embedment depth, with the evacuation valve left open.
c) The valve was then closed. Guide arms were adjusted to press the caisson against the Perspex window, hence locking it in place. Care was taken not to apply excessive force as it could result in caisson deformation.
d) The camera and light were then set up to capture the zone of interest. The camera was then started, followed by the application of pumping by opening the butterfly valve.

It was observed that immediately after commencing pumping, the suction quickly increased to a peak, and soil deformations were recorded, but with no immediate sign of piping channel formation. However, if pumping was maintained (for ~4-6 seconds), a piping channel was seen to form, which was also evident from a rapid drop in suction, and led to localised piping failure. If continuous caisson installation may be considered as a series of discrete movements (self-balancing between the driving force and soil resistance), the incremental sand heave that occurs at any given wall embedment depth can be represented in this restrained test by results taken immediately after starting pumping, i.e. when first sand movements were recorded.

PIV analyses were hence conducted on the results taken immediately after pumping, using a patch size of 40 × 40 pixels. In real object-space, this was roughly equivalent to 2.5 × 2.5 mm. The centre-to-centre distance of the patches varied from 20 to 40 pixels depending on the detail required.

2.6 1g installation test development

2.6.1 Test apparatus and set-up

Figure 2.5 shows a schematic diagram of the test apparatus used. It consists of a cylindrical soil chamber 400 mm in diameter and 420 mm high, filled with sand to a depth of 220 mm. The caisson model was positioned in the middle of the chamber, and could move freely in the vertical direction via a guide system. This comprised a straight

hollow rod attached to the caisson base allowing it to slide up and down freely, but preventing the caisson from any lateral movement. The rod also served as a pumping flow outlet.

As in the PIV tests, pumping could be easily simulated by making use of the water head difference between the soil chamber and the pipe outlet. The resulting flow, also known as gravity flow, is well described by Bernoulli's equation. Different pumping rates could be simply achieved by varying the degree of opening of the ball valve connected to the pipe. The technique proved to be very effective and versatile with fast and slow pumping being applied at ease by a simple twist of the outlet valve. This allowed for complicated installation procedures to be followed, where pumping flow could be increased or decreased in any manner and at any time during penetration.

Flow rates during each test were derived from the weight of water extracted, which was measured continuously by an electronic scale. As before, the water density is taken as $1g/cm^3$, hence the scale reading over a unit of time in gram/s is equivalent to the flow rate in cm^3/s. Caisson penetration depth and rate were also known from the displacement transducer (LVDT) positioned on top as shown in Figure 2.5. The differential pressure or suction pressure, i.e. pressure difference between the outside and inside of the caisson, was recorded using a differential pressure gauge as in the PIV tests. The gauge itself was connected by two plastic tubes: one embedded inside the caisson, and the other attached on top. The tubes were soft and small in size to minimise any potential impact on the caisson during testing. They were also cleared trapped water, if any, before the test.

Figure 2.6 shows a general illustration of the caisson used in the experiment. Models with various configurations were developed, with different total skirt length-to-diameter L_{max}/D ratios ranging from 1 to 2, as well as different wall thicknesses and diameters. Different levels of surcharge could also be applied in the tests by adding lead balls to a bucket attached to the caisson rod. A summary of all caissons used and their geometries is shown in Table 2.1.

The soil chamber and all caisson models, whose skirts were marked with 1 mm divisions for estimation of the inside sand column height, were fabricated from transparent material to assist observation of sand heave formation during installation. Each of the

tests was recorded using a digital video camera, allowing the heave to be estimated at any time during the penetration.

2.6.2 Test procedure

The tests were carried out in the same way as they are normally conducted in the field. This typically consists of two phases: a self-weight installation phase, followed by suction installation. During self-weight installation, the caisson penetrates into the soil using its own weight and any additional surcharge as the driving force. Once the caisson settles down under its self-weight, the suction installation phase is started by pumping water out of the caisson compartment. The net downward force created as a result provides the main driving force (other than the caisson's self-weight and surcharge) that penetrates the caisson to the desired depth.

All experiments were conducted in a way that resembles the above principle, following the procedure described below:

a) Before each test was conducted, sand was levelled and densified by vibration to obtain a flat surface.

b) The caisson, with water evacuation valve open, was lowered until its wall was in contact with the sand surface. This touchdown position was recorded for later determination of penetration depth.

c) The caisson was then slowly released to penetrate into the soil under self-weight, with care being taken not to disturb the surrounding soil. Once penetration under self-weight had ceased, the evacuation valve on the caisson base was closed manually, and pumping was started and continued until installation was complete, i.e. the caisson lid contacted the internal sand surface.

2.6.3 Effect of movement on the differential pressure gauge reading

As mentioned before, the differential pressure gauge could not be submerged. Hence the suction pressure across the caisson lid was measured indirectly via two soft plastic tubes. The changes in the levels of compression of the air inside these two tubes may affect the gauge reading. Such changes may be induced by variations in the speed of movement of

the tubes, as the rate of penetration of the caisson may vary in an installation test. To check the potential effect of movement speed on the gauge reading, a series of tests was conducted, where the tubes were moved at various speeds in the water. The gauge readings in these cases were then compared, and the results are shown in Figure 2.7. It can be seen that within the tested range, which covers the range of caisson penetration speeds in suction installation tests presented later in this thesis, the pressure readings (via the two plastic tubes) were essentially the same. The results suggest that indirect measurement of the suction pressure via the two tubes is not affected by the movement speed of tubes, and hence the caisson, within the investigated range.

2.7 Centrifuge installation test development

2.7.1 The geotechnical beam centrifuge and general scaling rules

The suction installation tests reported in this study were conducted in a geotechnical beam centrifuge at the University of Western Australia, illustrated here in Figure 2.8. The centrifuge is an Acutronic Model 661, with a maximum payload of 200 kg at the maximum acceleration level of 200 g. It has a swinging platform with a radius of 1.8 m. Further details were described by Randolph et al. (1991). In centrifuge tests, allowance must be made for the elevated acceleration *ng* in evaluating the results. Many publications have discussed the appropriate scaling laws, e.g. Taylor (1995). Table 2.2 presents a list of scaling factors for a number of common quantities.

2.7.2 Test apparatus and set-up

All installation tests were conducted in a standard centrifuge test box, or strongbox, which has internal dimensions of 390 mm × 650 mm × 325 mm (width × length × height). However, the strongbox was modified by adding an extension, 100 mm deep, to increase the overall height to 425 mm. The purpose was to increase the water depth to ensure all caissons, especially the longer ones, were fully submerged at the start of installation. The greater water depth also increased the pumping capacity, which was simulated by gravity flow (discussed previously). Furthermore, the extended box height allowed deeper soil samples to be tested, hence minimising boundary effects.

The caissons were installed using the apparatus shown in Figure 2.9. This included a guide system to ensure penetration of the caissons without tilting, and a weight control to adjust the caisson self-weight and surcharge. The guide system comprised a rigid straight rod screwed onto the caisson top. The rod could not move laterally, but could slide up and down inside a guide tube, which was fitted with linear bearings to eliminate the friction caused by the sliding motion. Any lateral effects on the motion, caused by the fittings and hoses on the caissons, were hence eliminated. The guide rod was also connected to a counter-balance bucket through a pulley system. By changing the amount of lead balls in the bucket, it was possible to control the caisson self-weight (and surcharge). However, this weight can change during caisson penetration due to the variations in the distance from the centrifuge axis. This will be investigated and discussed further in the next sections.

Two separate pore pressure transducers (PPTs) positioned on the caisson lid were used to measure the suction pressure during installation, one inside the caisson and the other outside the lid. The difference between the two PPT readings during installation, after correction for the initial offset due to the difference in their elevations, gave the net suction pressure across the caisson lid. Vertical caisson movement was recorded using a displacement transducer (LVDT) as shown in Figure 2.9. The caisson top was fitted with a pneumatically operated valve, which could be opened and closed in-flight. The valve acted as a water evacuation outlet during self-weight penetration of the caisson. A pipe fitting, connected to the pumping hose, was also located on the caisson lid. Details may be seen in Figure 2.10.

The caissons were installed by continuously pumping water out of the caisson compartment. Although a syringe pump is fitted within the base of the centrifuge swinging platform and has been used for suction caisson installation in clay (e.g. Chen and Randolph, 2004), its pumping capacity was insufficient to install the caissons in sand. Therefore, pumping was achieved by gravity flow, as in the 1g tests, and was created by the difference in water levels between the strongbox and the pumping hose outlet. The hosing had an internal diameter of 10 mm. In each test, the water pumped out of the caisson compartment was collected in a series of cylindrical reservoirs, connected to each other by overflow pipes. Each of the reservoirs was fitted with a pressure

transducer at the bottom, hence allowing the amount of water in the reservoir to be determined continuously during the test. These pressure transducers were calibrated against the height of the water column in the reservoirs in flight. A typical result is shown in Figure 2.11.

Pumping was started and stopped in each test by opening and closing an in-line valve in the pumping hose. This valve, referred to here as the pumping valve (to distinguish it from the water evacuation valve mentioned before), was also operated pneumatically, allowing it to be controlled in-flight.

Aluminium caissons with different sizes were used, with details given in Table 2.3. Note that most of the caisson configurations are similar to those used in the field. In particular, the aspect ratio, i.e. maximum wall length to diameter ratio L_{max}/D, was 1 for all caissons, and the wall thickness to diameter ratio t/D was 0.5 %, apart from a thick-walled caisson made deliberately to investigate the effect of the wall thickness. These ratios compare well with typical prototype caisson dimensions used in sand, which normally have L/D of 1 or less, and t/D in the region of 0.3 % to 0.4 %, but with internal stiffeners that increase the effective wall thickness.

2.7.3 Test procedure

The centrifuge installations reported in this thesis, apart from those where the caissons were deliberately jacked to a certain depth, were conducted in a way that resembles the field installation principle mentioned before. In particular, the following test procedure was adopted:

a) The caisson was lowered until the wall started to touch the previously levelled soil surface. This position was recorded as the touchdown position.

b) It was then gently released, and allowed to penetrate freely under its own weight. The water evacuation valve was left open.

c) The caisson was allowed to continue to penetrate under self-weight during centrifuge spinning. Once it settled down and no further significant movement

was recorded, the water evacuation valve was closed, and suction installation was started by opening the pumping valve.

In each test, the caisson was fully submerged before being lowered to the soil surface. Inspection was carried out to make sure that there was no air trapped inside the caisson, as this could affect its submerged weight.

2.7.4 Effect of variations in centrifuge radial length

Different points along the centrifuge arm experience different gravitational force, hence different g-levels. In this study, the effective centrifuge radius was set at 1/3 of the sample depth below its surface. This value was suggested by Schofield (1980) to best average the "under-stressed" and "over-stressed" regions within the sample due to differences in the radial length.

The variation in the radial length can also affect the caisson effective weight during the tests. As the caisson penetrates into the sample, it moves away from the centrifuge axis. The effective radial length hence increases, leading to increase in the caisson weight. Furthermore, with the current test apparatus, the counter-weight bucket will move in the opposite direction to the caisson, i.e. towards the centrifuge axis, hence its weight decreases. The combination of these opposite movements leads to the overall increase in the caisson effective weight. This increase may, however, be offset by the weight reduction due to the increasing submerged length of both the caisson guide rod and the LVDT rod rested on the caisson lid. To investigate this, a load cell was attached, and the caisson was moved along the centrifuge radial axis. The caisson was submerged at all time. The starting position was similar to that in the suction tests. Figure 2.12 shows the load cell reading when the caisson was moved over a distance of 25 mm. The result shows that the change in the tested caisson weight over that distance is negligible. In the suction installation tests presented in this thesis, the caissons travelled around 60-70 mm in most cases. From the results in Figure 2.12, it can be inferred that the changes in the caisson effective weight over this 60-70 mm distance are probably within only a few percent, and hence can be reasonably assumed to be negligible.

2.7.5 Effect of relative model-soil size

As previously discussed, the caisson wall thickness to diameter ratio t/D was kept similar to that in prototype case. This results in the absolute caisson wall thickness being much smaller, leading to a significant reduction in the wall thickness - average sand size ratio (i.e. t/d_{50} ratio) for a given sand. To investigate whether this compromise significantly affects the test results, a number of suction installation tests were performed on two caissons of the same t/D ratio, but different absolute wall thickness. This was achieved by comparing the centrifuge installations of these caissons, each at an appropriate g-level so that they both represent a single prototype installation. Hence, variations in the results, if any, are attributed to the effect of the absolute wall thickness (i.e. changing t/d_{50} ratio), as this is the only difference between them.

Figure 2.13a shows the results of the installations of a 100 mm diameter, 0.5 mm wall thickness caisson at 60g, and a 60 mm diameter, 0.3 mm wall thickness caisson at 100g (note that the caissons have the same t/D of 0.5%). Essentially, both cases simulate only one prototype installation, that is the installation of a 6 m diameter, 30 mm wall thickness caisson. Similarly, Figure 2.13b shows the results of the installations of these two caissons but at different g-levels of 72 and 120 respectively, representing a prototype caisson of 7.2 m diameter in this case. For each case in Figure 2.13a and Figure 2.13b, the caisson weights were chosen so that they represented the same prototype weight. It can be seen that excellent agreements are recorded in each figure, suggesting that variations in the absolute wall thickness (within the range here) are not likely to affect the installation response significantly. However, further research may be required if the results are to be extended to caissons with larger absolute wall thickness.

2.8 Experimental programmes

2.8.1 Seepage restriction due to test chamber boundaries

As mentioned before, seepage flow is a key factor in installation of suction caissons in sand, because it helps reduce the effective stress in the sand near the caisson tip, hence reducing the soil resistance. This makes installation possible even in very dense sand,

such as where cone resistances exceeding 60 MPa have been recorded (Bye et al., 1995). Upward seepage within the caisson will also tend to loosen the sand, and this can be an important consideration in the operating conditions for the caisson. Any restriction of seepage flow, whether due to valve malfunction or the presence of low permeability soil layers, may therefore affect the installation response.

In model testing, the seepage may be influenced if the caisson is too close to the sides or base of the test box. Figure 2.14 shows the theoretical effects of test chamber boundaries on the overall seepage flow. Two different sets of results are shown, illustrating the effect of varying the distance from the caisson wall to the chamber sides and bottom. The theoretical seepage was calculated assuming steady ground water flow. It can be seen from the results that the side clearance, i.e. the distance from the caisson centre to the side boundary, has significantly higher effect on the reduction in seepage flow, $Q_{seepage}$, than the distance to the base. This suggests that most of the seepage flow will emanate from the sand surface (near the caisson) around the wall into the caisson interior, rather than upwards from the soil below the caisson. A distance of at least 4 times the caisson radius from the chamber sides will allow almost unrestricted seepage (more than 97 % of the unrestricted case) to flow inside the caisson. For the bottom boundary, a smaller depth, of about 1.6 times the caisson embedment depth, will give a similar result. Hence the restriction of seepage flow is minimal if the distance from the conducted test sites to the strongbox boundaries is larger than these values.

2.8.2 Experimental programmes

This section describes the detail of the experimental programmes for each of the 3 sets of experiments conducted: the PIV tests at 1g, the suction installation tests at 1g, and the suction installation tests in the centrifuge. These tests were considered in 3 different soil profiles: homogenous sand, layered silica sand-silica flour (i.e. layered sand-silt) soil, and calcareous sand inter-bedded with weakly cemented soil layers. For homogenous sand, various types of sands, including silica sand, calcareous sand and mixed soils, were tested to help draw more general conclusions. These sands will be described in more detail in Chapter 3. The tests were conducted in dense sand with relative density of around 91%, unless indicated otherwise.

Ideally, installation tests should be conducted in all soil types at both 1g and higher g-levels in the centrifuge, so that a comparison between them could be made. However, due to the lack of the calcareous sand (which was not available commercially), tests in this sand type were only conducted in the centrifuge. It is also worth noting here that each calcareous sand sample was only tested once, i.e. was not re-used after each test due to concerns of breakage of the sand particles, which could lead to changes in particle size distribution, and hence density and permeability complicating test interpretation.

In all cases, the distances from the test sites to the chamber sides were always equal or larger than 4 times the caisson radii, and the sample depth was always larger than 1.6 times the wall embedment level. Hence the seepage restriction was minimised. Details of the soil profiles, as well as the test plan, will be presented in the following sections.

The PIV test programme

The PIV tests were conducted in homogenous silica sand and in layered sand-silt soil. For the first case, tests at 3 different wall embedment levels L/D of 0.1, 0.2 and 0.3 were conducted. Testing at larger L/Ds was not achieved due to leakage problems. However, it will be shown later in Chapter 4 that this does not appear to significantly affect the general conclusion made on the heave formation mechanism.

In layered sand-silt soil, 3 different tests were carried out, including tests when the caisson wall tip was above, within and below the silt layer. The purpose was to explore the influence of suction on the silt and sand deformation pattern.

The details of each tested soil profile are shown in Figure 2.15a and b. All the PIV tests conducted are listed in Table 2.4a.

The 1g suction installation test programme

Similarly to the PIV tests, the suction installation tests at 1g were conducted in both homogenous silica sand and layered sand-silt soils.

In homogenous silica sand, the tested profile is shown in Figure 2.16. All tests were conducted in one sand sample, which was re-densified by vibration after each test. The

suction tests were conducted for different installation scenarios, including:

- Variation in pumping rate: includes slow pumping installation, fast pumping installation, gradual change and sudden change in pumping rate during installation.
- Variation in caisson geometry: includes changes in absolute size and changes in wall thickness ratio t/D.
- Variation in the caisson effective weight.

For layered sand-silt soil, soil profiles where the silt layer was either on the surface, or embedded in the sand were both tested. For the latter case, the thickness and the depth of the silt layer below the surface was also varied. The tested soil profiles are shown in Figures 2.17a, b and c. Due to the small size of the soil chamber, only one complete test could be done in each layered sample. The disturbed sand-silt was removed after each test, and a new sample was prepared using the technique and procedure described later in Section 3.7. Details of all the suction installation tests at 1g are listed in Table 2.4b.

The centrifuge suction installation test programme

Suction installation tests in the centrifuge were conducted in the following soils:

- Homogenous sand: including silica sand, calcareous sand and mixed soils, where silica sand was mixed with silica flour to create soils with 10%, 20% and 40% fines contents.
- Layered sand-silt soils.
- Layered cemented-uncemented soils.

Variations in installation condition including caisson geometry, effective weight and initial penetration depths were considered. For the layered sand-silt soil, installations in profiles with the silt layer on the surface and below the surface were both investigated. The thickness of the silt layer and its depth below the surface were varied (i.e. similar to the 1g tests). Installations in soil with 2 bands of silt were also conducted. For layered cemented-uncemented soils, installations were conducted in calcareous sand inter-bedded by layers of weakly cemented soils. Two levels of cementation were tested: “weaker” cemented soil with unconfined compressive strength (UCS) of 80 kPa, and the “stronger”

soil with UCS of 120 kPa. Further details of these soils will be presented in Chapter 3. Different arrangements of these cemented layers in the sand were also tested.

In all centrifuge tests, water was used as the pore fluid. This has some potential limitations and can result in: (a) high seepage velocities compared with similar size model testing at 1g (and thus higher ratio of seepage volume to evacuated volume); (b) rapid consolidation. Specific results regarding these will be shown and discussed in further detail in Chapter 5.

All the tested soil profiles are shown in Figures 2.18 to 2.20. Figure 2.18 shows the profile for tests in homogenous sand. Figure 2.19 shows the tested profiles for layered sand-silt soil. Figure 2.20 shows all profiles of the cemented-uncemented soils in which the suction tests were conducted.

Figure 2.21a and b shows the plan of the test sites within the strongbox. The plan in Figure 2.21a was generally used for the larger caisson (i.e. the 100 mm diameter one) to ensure the test sites were at least 4 caisson radii from the strongbox sides to avoid seepage restriction.

All the centrifuge suction installation tests conducted are listed in Table 2.4c.

Chapter 3

Soil Properties and Sample Preparation Techniques

3.1 Overview

All the soils used in this study will be described in this chapter, which starts by giving a general description of the soils. This includes the description of the soil origins and their particle size distributions. Then the result of a number of laboratory tests conducted to characterise the soils are discussed. The soil permeability tests are first discussed; these were conducted using both constant head and falling head test methods. Direct shear tests against aluminium plates, similar to the tested caisson wall, are then presented. These are followed by the results from a series of triaxial compression tests. Some of the triaxial test results are also compared with those from other studies. This chapter then discusses the preparation of cemented samples, which were used to create soil layers of various strength levels in the suction installation tests. This section includes a detailed description of the preparation technique, as well as the results from the unconfined compressive tests (UCS). The last part of this chapter presents the sample preparation technique used to create homogenous sand and layered soil for the model installation tests. The latter includes layered sand-silt soil, and layered uncemented-cemented soils.

3.2 General soil description

4 different types of soils were used in this study. They are as follows:

- fine silica sand;
- silica flour;
- North Rankin calcareous sand (uncemented and cemented);
- mixed silica sand-silica flour soils.

Both the silica sand and silica flour, which is crushed silica sand, are commercially available. The silica sand has rounded particles, its specific gravity G_s was measured at 2.67 (which was also the value for silica flour). The silica flour was used in this study to simulate silt, and to create "silty" sands, which will be discussed below. The measured maximum and minimum void ratio and density for the silica sand are listed in Table 3.1. No measurement of maximum and minimum void ratio was conducted for silica flour because, practically, it was difficult to do so. The saturated unit weight for silica flour for "dense" conditions (similar to those in all suction test samples) was measured and found to be around 20 kN/m^3.

The North Rankin calcareous sand, on the other hand, was not commercially available. It was dredged from the sea bed in the vicinity of the North Rankin site on the North West Shelf of Western Australia. The soil contains flaky particles, and traces of coral fragments and fish bones. In this study, sand particles larger than 0.3 mm were sieved out. The specific gravity G_s of the sand was measured at 2.73. The soil void ratio and density are also listed in Table 3.1. It is noted that this North Rankin sand has very high void ratio, as is quite common in calcareous sand.

The mixed soils were created by mixing silica sand with different proportions of silica flour. In this study, silica sand was mixed with silica flour to create soils with 10%, 20% and 40% fines content (particle size < 0.075 mm), giving 3 different "silty" sands. Previous studies of similar mixtures (Salgado et al., 2000; Cubrinovski and Ishihara, 2002) suggest that increasing fines up to a certain content, the minimum void ratio will decrease to its lowest value because the voids between sand grains are occupied by these fines. However, the minimum void ratio will increase again if more fines are added. As for silica flour, the maximum and minimum void ratios were not measured for these soils

because of difficulties in the measurements, especially for soils with high silica flour contents. This difficulty was also acknowledged by Salgado et al. (2000) and Cubrinovski and Ishihara (2002). The saturated unit weight γ_{sat} for vibrated dense samples, similar to those in the suction tests, was found quite similar for all 3 mixed soils, slightly above 20 kN/m^3. For practical purpose, it has been rounded to 20 kN/m^3 in this study.

Figure 3.1 shows the particle size distribution for all soils. The particle size distribution below 0.075 mm was determined using a laser sizing technique, described previously by Bruno (1999). It can be seen that the silica sand is poorly graded, with most particle sizes in the range of 0.07-0.3 mm. The sand has very low fines content (particle size < 0.075 mm), typically less than 5%. The North Rankin calcareous sand, on the other hand, has quite significant amount fines content at around 15%. For silica flour, it can be seen that all particle sizes are below 0.075 mm (i.e. the soil comprises 100% fines).

3.3 Permeability test

3.3.1 Test description

Two types of permeability tests were conducted: constant head and falling head tests. For silica sand and loose North Rankin calcareous sand, the permeability for various soil densities was determined from a constant head test. For dense North Rankin sand, because the permeability was much lower, a falling head test was used to determine its permeability. This method, however, could not be used to measure the permeability of the silica flour, mainly because the filter at the bottom of the test apparatus could not block silt particles. Instead, the permeability of this soil was obtained in a modified constant head apparatus, which allows application of large pressure. The permeability for silica flour (silt) was measured only for one density, similar to the density obtained from the suction installation test sample.

3.3.2 Test results

Figures 3.2 a and b show the permeability k of the sands as a function of the soil void

ratio and relative density D_r, for silica sand and for the North Rankin calcareous sand respectively. It can be seen consistently from these results that, as expected, the soil permeability decreases when the sand becomes denser. For D_r of around 91%, which is the sand density obtained in the suction installation test samples, the permeability of silica sand is around 1.0×10^{-4} m/s, and that of North Rankin calcareous sand is about 1.5×10^{-5} m/s, roughly about 7 times less.

The permeability of silica flour for γ_{sat} of 20 kN/m^3 was found to be around 1.3×10^{-6} m/s, which is nearly two orders of magnitude lower than that of the silica sand. The permeabilities of mixed soils with 10%, 20% and 40% fines content were not measured and have been interpolated from those of silica sand and silica flour. Since the soil d_{10} is likely to be an important parameter affecting its permeability (as suggested by the Hazen formula: $k = cd_{10}^2$), the interpolation of the permeabilities of the mixed soils was based on this parameter. The results gave the permeability values of around 8×10^{-5} m/s, 2×10^{-5} m/s and 6×10^{-6} m/s for soils with 10%, 20% and 40% fines respectively.

3.4 Interface friction: direct shear test

3.4.1 Test description

The direct shear test apparatus used is shown in Figure 3.3a. The shear box, as seen in Figure 3.3b, has an internal dimension of 100 × 60 mm. The shear tests were conducted over a normal stress range of 50-200 kPa. This is slightly higher than the soil effective stress range experienced by the caisson wall in the centrifuge tests, which was typically less than 100 kPa, or less than 10 m soil depth at prototype scale. However, range was chosen because shear test results at lower normal stresses are likely to be affected by the system friction. The shearing rate was 0.2 mm/min.

All soil samples were prepared to densities similar to those in the suction installation tests. The soil was sheared against an aluminium plate (the same material as the centrifuge caissons). The surface roughness of the plate was similar to that of the caisson, measured at around 0.3 μm for both cases.

3.4.2 Test results

Figures 3.4a shows the direct shear results obtained from the tests for silica sand. Figure 3.4b plots the measured peak interface shear stresses against the normal stress. Figures 3.5 and 3.6 show similar results for the calcareous sand and the silica flour, respectively. It can be seen from the results that the shear stresses at lower normal stresses, e.g. the 50 kPa normal stress case for silica flour, is slightly above the common trend, represented by the straight line through the origin. This is probably because of the friction introduced from the test apparatus. Furthermore, particle jamming, especially for the silt case, was observed, resulting in additional friction. Nonetheless, it can be deduced from the results that the peak interface friction angles for calcareous sand, silica sand and silica flour are 19^0, 22^0 and 30^0 respectively. These fitted well with the peak interface friction angle-surface roughness relationship proposed by Kishida and Uesugi (1987).

Similarly, the residual friction angles can also be deduced from the results, and found to be around 15^0, 19^0 and 27^0 for calcareous sand, silica sand and silica flour respectively. The residual interface friction angles for mixed soils were assumed from the interpolation of those for silica sand and silica flour, which led to values of around 20^0, 21^0 and 22^0 for soils with 10%, 20% and 40% fines respectively.

3.5 Triaxial compression test

3.5.1 Test description

The soil densities in the triaxial compression tests, as in the shear tests, were kept similar to those in the suction installation tests. The triaxial samples were prepared by compacting dry soil in 4 layers in a 72 mm diameter mould. The typical sample length was around 150 mm. It was saturated by first flushing them with CO_2 to facilitate the saturation process. Water was then flushed through the soil using a small pressure head (10 kPa) over a 45-minute period. The confining stress during this saturation period was around 20 kPa. The sample saturation was checked before shearing. The "B-values" for all samples were found to be 0.95 and above, indicating that a good degree of saturation was achieved.

The shearing rate was 0.1 mm/min, or ~ 0.067% axial strain/min. The effective confining stress σ_3' during shearing was 100 kPa. All the tests conducted were isotropically consolidated drained tests (CID).

3.5.2 Test results

Figure 3.7 shows the triaxial compression test results for different soils. The result for soil with 40% silt may not be reliable, since post-test inspection of this sample showed a very soft base, with apparently less fines particles. This was probably caused by the accidental application of very large pressure during CO_2 flushing (which could blow the silt particles from the soil base). Also, no data were available for the volumetric change of that sample (due to problematic GDS readings). For the mixed soil with 10% silt, the strange response at 10% axial strain may be due to local non-uniformity of the sample. Nonetheless, the trend is clear from the result. It was observed from the test that for silica soils, especially for soil mixed with the non-plastic silt, very stiff response was recorded during shearing. This is consistent with the observation that, physically, the saturated mixed soil was very hard. The stiff responses observed here are consistent with other triaxial tests of similar mixed soils, reported by Salgado et al. (2000).

For calcareous sand, very different response was observed. Very high compressibility was recorded, and no stress peak was observed for the sand. The volumetric measurement in Figure 3.7 indicates that the soil volume decreased continuously during the test. This is consistent with the post-test inspection of the sample, showing that it bulged out significantly, with no visible shear plane. The behaviour is very different from those for silica sand and mixed soils, where a clear shear plane was always seen (see Figure 3.8). The calcareous sand behaviour is in fact similar to that of loose silica sand, although the tested sample was very dense. The response may be due to the very high void ratio and brittle nature of the particles, resulting in high compressibility.

The friction angles were calculated for the soils, giving peak values of 49^0 for soils with 10% and 20% silt, 43^0 for silica sand, and 40^0 for North Rankin sand. The residual friction angles for mixed soils were quite similar, at around 38^0. The corresponding values for silica sand and calcareous sand were 36^0 and 40^0 respectively.

3.6 Cemented North Rankin calcareous sand

3.6.1 Preparation of cemented samples

Gypsum was added to the North Rankin calcareous sand to produce cemented samples. The gypsum used in this study was commercially available hard wall plaster. The amount of gypsum was varied to create different levels of cementation in the soil. In the tests presented here, different cemented soils were created by mixing the calcareous North Rankin sand with 5%, 10% and 15% gypsum (by dry weight).

The cemented samples were prepared by first mixing dry sand with the required gypsum content. The mixture was then poured into a 72 mm diameter mould. For loose samples (γ_{sat} ~ 14 kN/m^3), no vibration was applied. However, for dense ones (γ_{sat} ~ 16 kN/m^3), the soil was prepared in 4 layers, with vibration being applied to each layer. In all cases, the sample length was around 150-160 mm. Saturation was then achieved by slowly flushing water from the bottom of the sample. The process was continued for at least two hours before all samples were submerged and left to cure overnight before testing. This procedure closely resembles that used to create the cemented samples in the centrifuge, which will be described later in this chapter. The water contents for loose and dense samples (after saturation and curing) were measured after the test, and found consistently to be 63% and 47%.

Unconfined compressive strength (UCS) tests were conducted to determine the strength of the cementation. The loading rate was 0.2 mm/min.

3.6.2 Unconfined compressive strength

Figures 3.9 to 3.11 show the UCS tests results for sand with 5%, 10% and 15% gypsum content respectively. It can be seen that a clear peak and drop in strength were only observed in the cemented soil with 15% gypsum content (the "strongest" cementation). In other cases, no clear drop in strength was recorded. This indicates that the cementation in these soils was very weak, which was also confirmed by the low peak values and their failure modes. Figure 3.12a and b show the post-test dense samples with 5% and 15% gypsum respectively. It can be seen that for the first case, the soil column tended to bulge out during loading, indicating low strength. For the latter case, crack formation in the

tested sample can be clearly observed, suggesting that higher strength and a more brittle response has been obtained.

Figure 3.13 plots the highest load applied to each sample (including the self-weight of the cap). The trend is clear from the results: the strength of the cemented soils increases with higher gypsum content used. It is also higher for denser soil. The results in Figure 3.13 also suggest that the rate of increment in the cemented strength (for the same added amount of gypsum) is higher for dense soils. These observations are consistent with previous results reported by Huang (1994).

For the suction installation tests, the soils with 10% and 15% gypsum were chosen to simulate "weak" and "strong" cemented layers. Their densities were also similar to those of the dense samples here (both also similar to the density of the uncemented sand tested in the centrifuge). The corresponding unconfined compressive strengths, as seen in Figure 3.13, are 80 kPa and 120 kPa respectively.

3.7 Sample preparation techniques

Due to the differences in the properties of the various soils tested, different techniques were used to prepare the samples. These are described in the following sections of this chapter. The soil density in each sample was estimated from the total mass of soil used, and the volume occupied in the test chamber. The sample uniformity was checked by conducting cone penetration test (details shown later in this thesis).

3.7.1 Homogenous sand

It can be seen from above that the three different types of sands, namely the fine silica sand, the North Rankin calcareous sand, and the mixed soils, have very different particle size distributions. While most of the silica sand particles are larger than silt size, the latter two sands contain a significant amount of fines. Therefore, different techniques were needed to prepare the homogenous sand samples.

The saturated silica sand sample was prepared by first placing the test chamber on the vibrating table, then filling it with water. Dry sand was then pluviated into the chamber at

a slow rate. Continuous vibration was applied during the sand pluviation process. Additional vibration was also applied to the chamber sides by a pneumatic hammer. It was found that the technique created very dense samples. The soil density was calculated afterwards, and found to give a relative density D_r of around 91 %. From the D_r-k relationship shown before in Figure 3.2a, this corresponds to a soil permeability k_o of 1.0 $\times 10^{-4}$ m/s. Saturation was also checked by stirring a separate sample prepared using the same technique. No air bubbles were observed, hence it is likely that the technique produced a satisfactory saturated condition. Subsequent cone penetration tests (presented later in Chapter 5) also indicated that very uniform samples were created.

For North Rankin calcareous sand and mixed soils, the above technique could not be used. Initial trials indicated significant separation of the fines from the coarser particles during pluviation through water, especially for the mixed soils. Hence these soil samples were prepared using a different technique. Dry soil was first poured loosely into the test chamber. Two different techniques were then tried: (a) the dry loose soil was vibrated for 30 minutes, before flushing water from the bottom of the sample to saturate; (b) water was flushed through the loose soil deposit first, with vibration applied once the saturation was complete.

In both techniques, slight (and unavoidable) segregation was observed. For the first technique, it occurred during the dry vibration. For the second technique, it happened when the saturated samples was vibrated. In this case, a small amount of fines were transported upwards as the water in the loose sample escaped to the surface. Nonetheless, the created samples in all cases were dense and uniform, as indicated by subsequent cone test results (shown in Chapter 5). The North Rankin calcareous sand relative density was also found to be around 91% (or saturated unit weight of ~16 kN/m^3), corresponding to a permeability of 1.5 $\times 10^{-5}$ m/s (from Figure 3.2b). The mixed soil unit weight was estimated at around 20 kN/m^3, quite similar to that of silica sand.

During flushing, the water head difference was always kept less than 200 mm to prevent piping. The saturation process was achieved overnight for method (a), but only within a few hours for method (b). It is noted here that silica sand samples could also have been prepared by this flushing method. However, this is likely to result in a longer saturation process without creating much advantage.

3.7.2 Layered sand-silt soil

The bottom sand layer in a layered sand-silt sample was prepared following the same procedure for silica sand described above. The silt (silica flour) layer was then added on top of the vibrated dense sand, and was allowed enough time to settle before vibration was again applied to clear the remaining air bubbles trapped in the silt. The same process was repeated if there were more sand or silt layers on top. Additional vibration was also applied to the box sides using a pneumatic hammer. However, once a silt layer was present, a shorter vibration period (~5-10 minutes) was applied. This was because the silt at the sand-silt interface would tend to mix with silica sand if a long vibration period was applied. As a result, the top sand layer in some cases was not as dense as the lower ones, for example profile 4 in the centrifuge test shown in Figure 2.19.

The saturated unit weight γ_{sat} for silt (silica flour) was around 20 kN/m^3, also similar to γ_{sat} of silica sand. As mentioned in the previous section, the silt permeability for this density is about 1.3×10^{-6} m/s, roughly 2 orders of magnitude lower than the sand.

3.7.3 Layered uncemented-cemented soil

The bottom sand was prepared using the previously described technique, i.e. by first vibrating the loosely deposited dry sand. The dry sand-gypsum mixture was added on top of the vibrated dense sand, and the soil was levelled. Vibration was then again applied to densify the soil in this layer. The same process was repeated for the overlaying sand, or cemented layers.

As for the layered sand-silt, when a cemented layer was present, less vibration was applied due to concern that the soil at the interface would be mixed. As a result, the top sand was generally less dense, with relative density estimated at around 80%. Once the required profile was achieved, water was then flushed from the bottom of the sample, following the procedure in the UCS tests mentioned previously. Immediately after the saturation, the sample was put on the centrifuge, and left overnight (with the centrifuge stationary) for curing before the suction installation tests were performed. Examples of the cementation can be seen in Figure 3.14, where cemented layers can be observed from the oven-dried soil cores taken from the tested samples.

It is noted here that the above method was not applied to prepare the sand-silt soils because, unlike the calcareous sand-gypsum mixture, dry vibration of the silt (silica flour) was found ineffective. On the other hand, cemented layers were not created by pluviation through water as in the sand-silt case, mainly because of concerns that this would affect the uniformity of the mixture and the gypsum content in the soil, hence affect the cementation. The cemented soil layers are assumed to have the same permeability as that of the uncemented sand (although the addition of the fine gypsum particles and the subsequent cementation occurs may lower the soil permeability).

Chapter **4**

Installation Behaviour at Normal Gravity (1g)

4.1 Overview

Results of all installation tests at 1g are presented in this chapter. This chapter first investigates the plug formation mechanism by using a half-caisson model and particle image velocimetry (PIV) technique, which was described previously in Sections 2.5 and 2.8. It then presents results for the 1g suction installation tests, whose details can be seen in Sections 2.6 and 2.8. Results of the derived seepage flow, and the internal heave development during the test will also be shown. The latter is also discussed in relation to the previous PIV observations. The last part of this chapter investigates the caisson installation in sand-silt soils. The aim here is to provide more knowledge of the generic behaviour of suction caissons during installation in different conditions. This chapter concentrates only on examining the test observations and drawing general conclusions based on those results. Further discussions, including attempts to explain some of the key behaviour by numerical simulations are deliberately left until the caisson response at higher soil stress levels (similar to those in the field) has been addressed. Such discussions are presented in Chapters 5, 6 and 7.

4.2 Soil deformation investigation using PIV

4.2.1 Homogenous silica sand

Figure 4.1 shows a typical raw post-analysis PIV result for L/D of 0.3 (each pixel represents 1/16 mm for this case) superimposed on the photo taken from the test. Figures 4.2 to 4.4 present the displacement fields from tests with different penetration depths in mm. To assist with the interpretation, these displacements have been scaled up as indicated on the figures. The average measured suction pressure for each case is also shown.

The sand displacement field for shallow penetration depth L/D of 0.1 (i.e. L = 10 mm) is shown in Figure 4.2a. Note that the magnitudes (lengths) of the arrows divided by the scaling factor represents the measured (average) displacement of soil within that patch. It can be seen from the results that there are two distinct areas of sand movement: a large displacement zone in the two regions (a single semi-toroidal region) close to the inner caisson wall, and the remaining field with essentially no movement. The largest displacements are observed along the wall, but these reduce quite rapidly towards the plug centre, where no sand movement is recorded. This field of large movement forms a wedge shape adjacent to the inner wall.

More details of the displacements around the caisson's left hand side, shown in Figure 4.2a, are shown in Figure 4.2b. While there is a clear trend that the sand tends to flow around the tip into the caisson compartment, the level of inflow movement is very small compared to the vertical movement along the inner wall. The zone of influence, where movement is still recorded, extends to only a small depth below the caisson tip. At the same time, almost no movement is observed in regions adjacent to the outside caisson wall.

The results are interesting, as it is might be expected that a large amount of sand, especially from along the outer caisson wall, could flow into the caisson during suction installation, thus contributing to the internal heave. Observations here suggest that this is unlikely to be the case. Rather they suggest that the sand inflow is likely to be small, and the majority of the sand heave in the wedge formed along the inner caisson wall is the result of its own expansion in volume, not an extra supply of sand due to inflow.

Although unexpected, the results are, however, explainable. Under suction, sand adjacent to the inner caisson wall will experience the most extreme seepage flow conditions due to the location of the shortest hydraulic path along the caisson wall. As the sand in this region loses its equilibrium (under the influence of the seepage body force), it moves up and loosens, causing it to expand in volume. For dense sand, the expansion can be quite substantial. In addition, the material immediately adjacent to the inner caisson wall will undergo shearing at the same time. This action will lead to dilation of the dense sand, causing additional loosening and expansion of the sand inside the caisson in the vicinity of the walls.

Figures 4.3 and 4.4 show test results for deeper wall embedment depths of L/D of 0.2 and 0.3 respectively. Unlike previously, where no movement was observed for the central plug, considerable upward movement of the whole sand plug occurred at these deeper penetration levels. There are large displacements within wedge zones along the inner wall in both cases. It is noted that the displacement zone only extends to a relatively small distance below the caisson wall embedment, less than about 30% of the penetrated depth in these cases. Apart from zones next to the caisson wall, the displacement level appears to be quite uniform for the rest of the plug inside the caisson, but reduces quickly with further depth below the tip embedment level. Only modest sand displacement is recorded in the outer caisson wall areas and below the caisson tip, showing a similar trend to the previous observations at shallow penetration. It should be noted here that the tests were only conducted for wall embedment depth L/D of up to 0.3 due to leakage problems at greater depth. Nonetheless, the similarity in the results at L/D of 0.2 and 0.3 seen here suggests that the soil deformation mechanism at greater L/D is likely to be similar.

The results are interesting considering the high suction pressure recorded for each case. The normalised pressures $p/\gamma'D$, where p is the measured peak pressure, γ' is the soil submerged unit weight (= 10 kN/m^3), and D is the diameter of the full caisson, are 0.75, 4.1 and 5.1 for L/D = 0.1, 0.2 and 0.3 respectively. For comparison, at similar depths, the values of $p/\gamma'D$ during suction installation using similar pumping rates (which will be presented in the next sections of this chapter) are only around 0.5, 0.8 and 1.0 respectively. The results clearly indicate that, at least for the soil type and test conditions

here, no excessive sand inflow occurs even under very large suction pressures. Rather, the sand heave formed during the recording period, either in the form of the small wedges seen in the shallow penetration case, or the whole plug motion at greater caisson embedment depths, is primarily due to volumetric expansion of the sand. Only a very small amount of sand inflow contributes to the overall sand heave.

The philosophy of these restrained tests was to explore what happens in the most critical situations, and determine how the results can be safely interpreted during installation when the caisson is free to move. It is believed that the fixed caisson experiment represents the worst installation condition, where a very high suction pressure is suddenly applied (through fast pumping) while no movement is permitted. The restrained conditions create a very significant preferential flow region, because of the pronounced loosening in the wedge zones, and optimal conditions for triggering a piping failure. The initial expectation was that the sand outside would move into the caisson under the influence of this very high suction. However, the results obtained clearly show that this is not the case, and that the heave is mostly caused by plug expansion. This result, to some extent, can be applied to the moving cases. Although the expansion along the inner wall may be less extreme (due to lower suction) in the moving cases, the generic heave formation mechanism is likely to be the same. Indeed, considering effective heave (i.e. total heave minus the caisson wall volume embedded in the sand) as the result of sand inflow and expansion, if the heave in these extreme cases is mainly caused by plug expansion, not the sand inflow, then in the moving cases it is most likely that sand heave will be created in the same manner. This is because in the moving caisson installation, there is even more restriction to sand inflow due to much lower suction pressures and the continuous extension of the cut-off wall length.

4.2.2 Layered sand-silt soil

This section investigates the soil deformation where a layer of low permeability silt is present. Details of the tested soil profiles were described in Section 2.9. Figure 4.5 shows the results for the case where the caisson wall is above, but close to the silt layer. Figure 4.5a shows the raw displacement field relative to the experimental set-up, and Figure 4.5b shows the analysed displacements (in mm). It can be seen from Figure 4.5 that

within the caisson, there is a clear trend of upward soil movement under the influence of the suction pressure, similar to previous observations in homogenous sand. An interesting observation is that the silt layer "bends" slightly upward when pumping is applied. Note that the caisson wall tip has not penetrated into the silt, and is still above it in this case; this clearly indicates that the suction pressure is likely to have some effect on the underlying silt layer as the caisson wall approaches it. The silt deformation, however, only occurs in the section within the projection of the caisson wall. The sections outside that zone appear unaffected, having negligible deformation. This can be explained by the creation of a pressure difference across that section of the silt layer, which results in a net uplift force. This will be discussed in detail later in this section. Figure 4.5b also shows that as the silt layer "bends" up, the sand below it also moves upward, indicating that sand loosening occurs below the silt layer.

It is also observed that there is relatively uniform soil displacement inside the caisson above the silt. The sand movement along the inner wall appears to be larger than that towards the plug centre, a pattern which is similar to that observed previously in homogenous sand. However, unlike the homogenous sand case, the difference between the displacements along the wall and towards to plug centre is much smaller in this case. Sand movement in the regions adjacent to the outer caisson wall is also recorded, but is negligible. This once again indicates that the sand inflow (around the caisson wall) is insignificant. While this soil deformation pattern appears to be similar to that in homogenous sand, seen in the previous section, the heave formation mechanism is likely to be slightly different in this case due to the presence of the silt layer. Indeed, apart from the plug expansion caused by seepage as discussed before, the upward deformation of the silt layer also lifts the overburden sand with it, hence further contributes to the total displacement of the sand inside the caisson as seen. Since the expansion caused by the seepage is likely to be limited here due to the flow restriction caused by the silt layer, the uplift action may contribute significantly to the total recorded movement of the internal sand plug in this case.

The result where the caisson wall tip is inside the silt layer is shown in Figure 4.6. It is clear from the displacements that the silt layer section within the caisson wall projection moves upward when suction is applied. The movement appears uniform throughout the

whole section, which is slightly different from that in the previous case, where larger displacements are seen towards the middle of the plug. Outside the caisson, there is no significant displacement of the silt.

Figure 4.6 also shows that the sand above the silt layer inside the caisson moves upward very uniformly. It should be noted that the caisson tip is inside the low permeability silt layer in this case, which, as a result, reduces most of the seepage flow into the caisson interior. The observed sand displacement is quite significant, and therefore unlikely to be due to plug expansion as a result of the seepage alone, because this would require large seepage body force acting on the soil skeleton. Rather, the recorded displacement can also be attributed to the upward movement of the silt layer. Indeed, as the silt layer moves up uniformly, it "lifts" the overburden sand with it. Assuming insignificant expansion results from the seepage, the overburden sand above the silt should move in the same manner and in fact, by a similar amount as the silt, which appears to be the case here. Displacement is also seen in the sand below the silt layer, similar to that when the caisson tip was just above the silt layer. Displacement occurs in a conical zone, and extends to some depth below the wall tip, about 100% of the wall embedment depth in this case. Apart from this region, no significant displacement is recorded for other zones, including those adjacent to the outer caisson wall.

Figure 4.7 shows the result where the caisson tip is at a small depth below the silt layer. The recorded displacement field is essentially similar to that discussed in the above case (i.e. Figure 4.6). In particular, the silt layer within the caisson is seen to move up, and uniform movement is observed for the overburden sand. Movement is also seen in the sand below the silt as before, but the zone of movement appears to larger. In fact, in all three cases, whether the caisson tip is above, inside or below the silt layer, sand movement in a conical zone below the silt is consistently observed. Note that no significant sand movement is recorded in the adjacent regions. The conical zone is interpreted as a zone of sand expansion (loosening) occurring below silt. This loosening zone appears to be more significant than that in homogenous sand, where the displacement field only extended to a relatively small depth below the wall tip (see Figures 4.2 to 4.4). It is clearly larger in sand-silt soils, indicating that the loosening zone extends deeper in these cases. The displacement of sand below the silt layer also

indicates that the upward movement of the silt layer results in the transfer of suction to the underlying sand, and this is believed to be the main reason for it to loosen. This will be discussed further in Chapter 6.

It is seen consistently from the above results that the silt layer is lifted up when suction is applied. It was discussed before that this is likely to be due to the creation of a pressure difference across the silt layer, which is further explained here by the schematic diagrams in Figures 4.8a and b. As the caisson approaches and penetrates into the low permeability silt layer, a significant differential water pressure develops across the layer. While the pressure on the lower interface remains relatively constant, possibly close to the hydrostatic pressure, the pressure on the upper interface reduces due to the influence of the suction pressure inside the caisson (see Figure 4.8a). This, as a result, creates a net upward pressure, hence uplift force, that pushes the silt layer up (Figure 4.8b). Note that the pressure on the upper sand-silt interface is only affected in the region within the projection of the caisson wall; a differential pressure is hence only created in this zone. No differential pressure, hence uplift force, was created across the silt layer outside the caisson. This is indeed reflected in the recorded deformation of the silt layer, where no movement is recorded in the silt layer outside the caisson. It is also worth noting that, in these tests, very fast pumping was applied causing high suctions, thus large soil displacement. In smaller pumping tests, where the suction pressure is lower, the magnitude of the sand movement and silt deformation may be less. Nonetheless, the generic soil deformation behaviour and the plug formation mechanism in these smaller pumping cases are likely to be the same as those discussed above.

4.2.3 Summary

The soil deformation in both homogenous silica sand and sand-silt soil was investigated directly using a half caisson model. The soil movements were traced using the particle image velocimetry (PIV) technique. The following conclusions can be made:

In homogenous sand:

- The sand movement patterns were different for shallow (L/D of 0.1) and deeper caisson wall embedment. For the first case, no soil deformation was observed

towards the middle of the plug, while for the latter, fairly uniform movement was recorded for the whole soil plug.

- When pumping was applied, most of the instantaneous sand heave was created by volumetric expansion (loosening) of the sand. Negligible sand inflow was observed, even in regions adjacent to the outer caisson wall.
- Larger displacements were recorded along the inner caisson wall. This may be due to the higher hydraulic gradient (due to more critical flow path) along there, which results in large upward movement of the sand, accompanied by dilation as it shears against the inner wall, and loosening.
- The sand displacement extended to only a small depth below the caisson wall tip, less than about 30% of the penetrated wall depth for these cases.

In layered sand-silt soil:

- Upward deformation of the silt layer was recorded in all tests, where the caisson tip was above (but close to), inside and below the silt layer. The deformation however, only occurred in the section of the silt layer within the projection of the caisson wall.
- Quite uniform displacement was observed for the sand plug inside the caisson. This is thought to be due to both the sand expansion and slight upward movement of the silt in the case where the caisson tip is above the silt layer. However, where the wall tip is inside and below the silt, the seepage is greatly reduced, and the upward movement corresponds to a piston movement of the silt layer and the overlying sand.
- Upward sand movement was seen below the silt layer, indicating that the upward silt movement results in transfer of suction to the underlying sand. The movement is likely due to volumetric expansion, since no significant displacement was recorded in the surrounding regions, including those along the outer caisson wall.
- The zone of movement extended considerably further than in homogenous sand, up to 100% of the penetrated wall depth in these cases. This indicates that soil may loosen to a deeper depth below the wall tip in sand-silt soil.

4.3 Installation in homogenous silica sand

4.3.1 Effect of pumping rate

Figures 4.9a to h show the test results where the caissons were installed by very slow and very rapid pumping (or slow and fast installations). In this context, "slow" refers to the pumping corresponding to a penetration rate of around 0.5 mm/s (or 1.8 m/hr) and below, and "fast" for a rate of 6-7 mm/s (22 m/hr) and above. The slow pumping was created by a minimum opening of the "pump control" butterfly valve, and the fast one was achieved by fully opening the valve. In both cases, the pumping rate was relatively constant during installation. All installations proceeded well, with no piping occurring. The installation rate for each test can be seen in Table 2.4b. The marginal differences in the initial penetration depth (less than 3 millimetres), as observed in some cases in Figure 4.9, were caused by small disturbances created when manually closing the water evacuation valve on the caisson lid. This nonetheless does not affect the observed trends, which are consistent for various installations as seen in Figure 4.9. The results show that changes in pumping rate clearly have a very significant influence on the suction pressure. Fast pumping (which results in fast penetration, or fast installation) creates a sharp increase in differential pressure, which can be twice as high as for the slow pumping in these tests. This effect, however, requires a very significant increase in pumping rate, of almost 20 times higher. The differential pressures appear to vary quite linearly with wall penetration depth, but at a slightly higher gradient for the fast pumping installations.

This behaviour was further checked by varying the pumping rate during installation. The results obtained are presented in Figures 4.10a and b. Figure 4.10a shows the effect on the differential pressure of a rapid change in pumping rate. In the test, pumping was initially started at a rate similar to that of the slow installation shown in Figures 4.9a and b. As expected, the resulting suction pressure trends are very close to each other. At a skirt depth-to-diameter embedment ratio (L/D) of around 0.5, pumping was suddenly increased to a very high value. An immediate jump in differential pressure occurred, with the pressure subsequently following the trend in the previous fast pumping test. Figure 4.10b shows the response of the differential pressure where, instead of applying a sudden change, the pumping rate was increased gradually from slow to fast during installation. The suction pressure can be seen to change accordingly from the lower trend to the

higher one, closely resembling previous data. The results once again confirm the significance of pumping, or installation rate, on the resulting pressure difference across the caisson base. It is also observed that, although pumping was applied in very different manners (i.e. constant, sudden change or gradual change) and at different wall penetration depths, the resulting suction values still remained similar for a given value of pumping rate. In other words, the suction pressure reported here appears to be closely related to the magnitude of the pumping rate (hence installation rate), and independent of the sequence of changes in pumping rate.

Another interesting observation is that there seems to be a "lower bound" for the suction pressure, i.e. below a certain threshold, no matter how much slower the installation is, the suction pressure will not drop any further. Figure 4.11 compares the slow installation seen previously in Figure 4.9a with another one where the penetration rate varies, but remains below 0.5 mm/s. The results show that although the penetration rate is reduced to as low as 0.04 mm/s (0.14 m/hr), which is almost 10 times lower than the highest rate of 0.4 mm/s in Figure 4.11b, it does not create any recognisable changes or drop in the resulting suction pressures, suggesting that there seems indeed to be a lower bound value for the suction pressure required at any given penetration. The threshold for "lower bound suction pressure" mentioned before appears to be around 0.8 mm/s for this case. This is observed from the gradually increasing pumping installation, where the suction pressure only starts to increase above that in the slow pumping case once the rate is above 0.8 mm/s. Details can be seen in Figure 4.12. This threshold may, however, be different for other geometries.

On the "upper bound" side, although the fast installation in this test series represents the highest pumping that could be achieved with the current set-up, the test results, e.g. Figure 4.10b, suggest that any upper limit has yet to be reached. Further results including comparisons with different tests with a larger pumping range, and more discussion regarding this upper bound value, as well as the general rate effect, will be presented in sections 4.3.7 and 4.3.8.

4.3.2 Effect of surcharge

Figure 4.13 shows the installations where the 70 mm and 100 mm diameter caissons were

installed under self-weight p/γ'D of 0.33 (or 2.6 N at model scale) and at various surcharge levels (or increases in caisson weight above p/γ'D of 0.33). For the 100 mm caisson, the results are compared for both slow (i.e. "lower bound suction") and fast installations. It has been shown before that while the suction pressure in slow installation is not very much affected by the rate as long as it is below a certain threshold, it is closely related to the magnitude of pumping in fast installations. Hence, to enable comparisons between fast installations with different surcharge, the pumping rates, or penetration rates, were kept similar in these tests so that the effect caused by different pumping could be eliminated. It is seen from Figure 4.13 that, in all cases, the increase in the caisson effective weight by adding more surcharge reduces the required differential pressure for a given penetration depth. Apart from an unexpected increase in pressure towards the end of the caisson installation with surcharge Δp/γ'D of 0.25 (or 4.6 N caisson weight) in Figure 4.13b, the rest of the data show a consistent trend in suction reduction with increasing level of surcharge. These results are in good agreement with previous observations by Tjelta (1995), Erbrich and Tjelta (1999).

The suction pressures are observed to increase quite linearly with depth, and the response curves appear to be quite parallel to each other, i.e. the shape of the curves are quite similar for installations with different surcharge. This suggests that changes in the caisson effective weight, while resulting in variations in the magnitude of the required suction pressure, do not seem to alter the general suction pressure trend. Comparison of results in Figures 4.13b and c also shows that for a given surcharge (or 1.5 N at model scale in this case), the pressure reduction Δp/γ'D in the 70 mm caisson is higher than in the 100 mm case. This is consistent with the force-pressure conversion trend (e.g. 1 N converts to a Δp/γ'D of 0.26 in the 70 mm caisson, but only 0.13 for the 100 mm one). Back calculations of the force reduction due to the added surcharge yield mixed results. The average pressure drops in Figure 4.13b and c suggest an equal, or larger, force reduction compared with the added weight, while results in Figure 4.13a show otherwise, indicating that the reduction is lower. It is difficult to make a firm conclusion based on these results because only slight differences in the suction pressure drop could lead to an opposite conclusion. However, it is believed that the reduction in the required suction force should be lower than the added weight amount, especially under higher soil stress

condition. Further reasoning will be presented in Chapter 5. Nonetheless, it is clear that the increase in the caisson effective weight by adding surcharge lowers the required suction pressure.

4.3.3 Effect of caisson geometry

The effect of the caisson wall thickness and sizes is investigated in this section by comparing caissons of the same diameter but different wall thickness; then comparing caissons of the same thickness ratio, but different diameters (i.e. one caisson being a scaled copy of the other); and finally comparing all of them. The caissons were of the same self-weight (2.6 N), and were installed at a similar slow rate. This was intended to eliminate any effects caused by different caisson weights (which form part of the driving force) and rapid installations, allowing any changes in suction pressure to be evaluated solely as due to differences in geometry. Figure 4.14 shows the installation results of two caissons of the same 80 mm internal diameter, but different wall thicknesses. As shown, the caisson with larger t/D requires higher suction pressure for penetration. Note that as the rest of the geometry and installation conditions in the two cases are similar, this suction increase is believed to be required to overcome the increase in end bearing due to the larger wall tip area. However, this increase is only marginal. The required pressure for a caisson with thickness ratio (t/D) of 2% is on average only about 10-15 % more than that for the thinner-walled caisson, in spite of a 100% increase in t/D (i.e. twice the thickness).

The influence of absolute caisson size on the differential pressure can also be seen in Figure 4.15. Installation results of the 100 mm and 70 mm diameter caissons, both with the same thickness ratio t/D of 0.5 %, show that the required suction pressures for a given normalised penetration depth L/D are almost identical for the two cases. The similarity in their magnitudes seen here may, however, be just a coincidence for the tested caisson weight. If a different self weight is chosen, say, 3.6 N (i.e. 1 N surcharge is added), the suction pressure in the smaller diameter 70 mm caisson may drop below that of the 100 mm one due to the force-pressure conversion discussed before. To compare further the effect of both size and wall thickness, the suction pressures in Figure 4.14 and 4.15 are plotted together, and shown in Figure 4.16. The results once again indicate that for the

caisson diameter and wall thickness range tested here, variations of absolute caisson size, or the relative wall thickness, do not seem to have any significant effect on the general shape of the suction. In all cases, they appear to increase linearly with depth with a similar gradient.

4.3.4 Effect of movement obstruction

Installations where the caissons were restrained at some stage during penetration were conducted. Figure 4.17 shows a typical result of a restrained installation. It was observed that there is a significant jump in suction pressure when the caisson was restrained, and piping failure occurred, which resulted in the loss of hydraulic "seal" within the caisson (as seen from the rapid suction drop in Figure 4.17). However, if the obstruction is removed, the caisson could then penetrate further without notable problem. This behaviour is very similar to that reported by Tjelta (1995), Erbrich and Tjelta (1999). It is noted here that, although suction penetration could be proceeded after the removal of the restraining force, quite substantial heave and sand disturbance due to the formation of the piping channel were observed.

4.3.5 Seepage flow behaviour

It is not possible to measure seepage flow directly during the installation test. However, it can be derived easily from other measured parameters. In these tests, seepage was calculated by subtracting the displaced volume of water from the total flow according to:

$$Q_{seepage} = Q_{total\ pumped\ out} - Q_{compartment\ volume\ displaced\ by\ the\ caisson\ movement}$$
$$= Q_{total\ pumped\ out} - r(\pi D^2)/4 \qquad (4.1)$$

where r is the caisson penetration rate.

Equation (4.1) allows for seepage flow to be calculated as both the overall flow rate $Q_{pumped\ out}$ and penetration rate r can be measured continuously during each test by means of the electronic scale and the displacement transducer on the caisson top respectively.

Typical seepage flows for constant slow pumping installations of the 100 mm and 70 mm diameter caissons are shown in Figures 4.18a and b. It can be seen that seepage increases

initially with deeper penetration, indicating that the increase in cut-off wall length (and thus average length of flow path) does not fully compensate for the greater suction pressure that induces more seepage. After some stage, at L/D of about 0.5-0.6 in this case, seepage appears to reach a terminal value, and remains relatively constant, or with a very modest increase afterwards. The seepage behaviour during faster installation was also investigated. Figure 4.19 shows typical seepages for fast installations. It is seen that the trend is similar to that in the slow cases, but the values are much higher. Figure 4.20 presents results where the pumping rate was suddenly increased during penetration (the suction pressure response for this installation was shown previously in Figure 4.10a). The effect is an almost immediate response in the seepage, with the seepage flow jumping to a very high value. Figure 4.21 compares the ratios between seepage flow and total pumping for typical slow and fast installations. It can be seen that although the seepage during fast installation is higher in terms of absolute values (Figures 4.18a and 4.19a), it is lower when compared as a percentage of the total flow. Figure 4.21 shows that in fast installation, the seepage flow rate is only about 8-9% of the total pumping rate. However, in slow installation, the seepage can be up to 35-40% of the total pumping flow. The results indicate that, in fast installation, most of the pumping is to remove the water volume in the caisson compartment, while in slow installation, it includes both the displaced water volume, and a significant proportion of seepage.

Typical seepage results, normalised against suction head $H = p/\gamma_w$, caisson diameter D and permeability k, are shown in Figure 4.22. The data include the seepage flow derived from both slow and fast pumping tests. The same value of permeability $k = 1.0 \times 10^{-4}$ m/s (typical for sand with D_r of 91%) was used for all sets of results, i.e. ignoring any potential change due to loosening of the sand. As seen, there is quite good agreement between the normalised seepage values in the slow installations, including the two "lower bound" suction installations of the 100 mm diameter caisson with normalised weights $p/\gamma'D$ of 0.33 and 0.59 (or 2.6 N and 4.6 N respectively). The theoretical seepage response (details are given later in Chapter 7) shows a similar trend, but slightly lower values. In fast installations, the normalised seepage is, however, considerably higher than that for the slower ones, suggesting that assuming a constant permeability for both installation cases may not be suitable. Instead, a higher (average) permeability value may be inferred.

4.3.6 Internal heave

The formation of excessive sand heave inside the caisson compartment as a direct result of seepage flow through sand, including any localised piping, is one of the key indicators of the success or failure of the installation process. In this study, sand heave was monitored on video during installation, aiming to explore and understand the effect of changing installation conditions on the amount of sand heave. At any time, heave was taken as the difference in height between the inside and outside sand surfaces. It was observed that the sand plug formed quite uniformly during the tests, and there was no notable movement of the outside sand surface during installation. A typical heave observation taken from these videos during penetration can be seen in Figure 4.23.

Figure 4.24a shows the typical sand heave recorded from the slow and fast installation of the 100 mm diameter caisson. Figure 4.24b compares the resulting sand heave during slow and rapid installations for various caisson geometries. In all but the thickest walled case (t/D of 2 %), sand heave is significantly less for the quicker installation, suggesting that, in these tests, fast installation is in fact better than slow installation in preventing heave. It also appears from the results that increasing the caisson wall t/D ratio tends to reduce this beneficial effect, with almost no difference in the resulting sand heave from fast and slow installation of the caisson with t/D of 2 %.

The rate of sand heave also appears to vary with the caisson wall penetration depth. Figure 4.25 shows the results for various installations, plotting the average incremental sand heave as a ratio of the incremental wall penetration. The results, calculated for every 20 mm wall embedment depth, show that for caissons with t/D of 1% or less, sand heave formation increases with increasing penetration (although the trend slows down towards the end), indicating that higher proportion of the total resulting sand heave is likely to form during the later stages of installation. However, this appears not to be the case for the caisson with t/D of 2%, where very high incremental heave ratios were observed from the beginning, and remained relatively constant throughout installation. This shows that for thicker-walled caissons, sand heave appears to increase quite linearly with the wall penetration depth.

Surcharge also has an important impact on heave formation. Figure 4.26a shows test results of similarly fast installations using the 100 mm diameter caisson, where different levels of surcharge were used (the suction pressures for these installations were shown previously in Figure 4.13b). Figure 4.26a shows that the use of surcharge appears to improve the installation performance by reducing sand heave formation. At a penetration depth L/D of 0.8, while the recorded sand heave for a caisson with no surcharge was as high as 6 % of the skirt penetration, this was reduced by almost 3 times to as little as 2 % with $\Delta p/\gamma'D$ of 0.25 (2 N) surcharge. The difference, however, tends to reduce at greater penetrations (after L/D of 0.8 in this case). It also appears that the amount of reduction in sand heave is quite consistent with the increment in the level of surcharge used, with the heave observed in the test with $\Delta p/\gamma'D$ of 0.13 (1 N) surcharge lying about midway between the heave values from self-weight alone and with $\Delta p/\gamma'D$ of 0.25 (2 N) surcharge. A similar result is also found for the $\Delta p/\gamma'D$ of 0.19 (1.5 N) surcharge case. The general heave reduction trend here is consistent with the decreasing suction pressures, shown in Figure 4.13b, and the reduction in the absolute seepage amount shown in Figure 4.26b.

The effect of wall thickness on sand heave formation is investigated further with results shown in Figure 4.27. It is noted again that operating conditions such as the installation rate and self-weight were kept similar to minimise their influence on the results obtained. The installation rates here were 0.4 mm/s on average, and the self-weight was 2.6 N. The results show that for shallower L/D (up to about 1 here), the heave ratio (ratio of sand heave h to wall penetration L) increases quite rapidly with penetration. However, this ratio levels out and remains relatively constant for greater penetration depths. It is also seen that the caisson wall thickness has a significant effect on the resulting sand heave with much higher heave recorded for thicker-walled caissons. For similar installation conditions, sand heave resulting for a caisson with t/D of 2% is several times higher than for a caisson with t/D of 0.5 %, particularly for penetration depths L/D < 1. If it is assumed that all the sand displaced by the caisson wall moves into the caisson interior (i.e. moves in the seepage flow direction) and only effective heave values are compared, the heave differences are then significantly reduced as seen in Figure 4.27. As discussed above, the effective sand heave is calculated by subtracting the penetrated wall volume

from the total recorded heave volume. For the installations reported here, the effective heave ratios appear stable for L/D of over 1, with the h/L remaining within the range of 11-14 %.

As mentioned before, it was generally observed that there were insignificant displacements of the sand surface near the caisson outer wall, even in cases where there were large heaves inside the caisson, for example in the thick-walled t/D of 2% caisson installations. Only small conical depressions around the outside of the caissons were seen. These observations suggest that the amount of sand flowing into the caisson during installation is not significant (otherwise, large soil depressions around the caisson should have been observed, especially where there is large heave such as in the thicker-walled case). This is consistent with the results recorded in the PIV tests, which indicated that the majority of the effective heave (i.e. minus the wall volume) forming during installation was due to plug expansion, and not sand inflow. All recorded sand plugs were stable, i.e. the heave height did not reduce after the test. It was also observed that in the fast installations, no piping channel developed, demonstrating that for the test conditions and soil type, rapid pumping could be used. In fact, fast installation was also found possible in previous field trials, where installation rates of up to 5 mm/s (18 m/hr) was applied without any notable problems (Hogervorst, 1980).

4.3.7 Comparison with Oxford 1g test results

1g installation tests were also conducted by the author at the University of Oxford, and the results of these tests are presented in this section. The test set-up and the guide system were similar to that in this study (which was described previously in Section 2.6). The steel caisson used in the experiment was 150 mm in diameter, with a wall thickness of around 1.5 mm (t/D of 1%). The maximum wall length was also 150 mm. However, larger pumping rates could be achieved by connecting the pumping hose (10 mm internal diameter) to a vacuum chamber. By varying the vacuum level, and the degree of opening of the butterfly valve, a large range of pumping rates could be simulated. The suction pressure was measured using a pair of pressure transducers, one inside the caisson, the other attached outside on the lid. The installations were conducted in dense Redhill 110 sand, with d_{50} of 0.12 mm, γ_{sat} of around 18 kN/m^3, and k of 1.5×10^{-4} m/s. Other sand

properties were reported by Kelly et al. (2004). Figure 4.28a shows the results where the caisson was installed at a wide range of penetration rates, which are shown accordingly in Figure 4.28b. The highest pumping seen in Figure 4.28 represents the fastest pumping available with this set up, using full vacuum (-100 kPa) and full opening of the flow control valve. The irregularities in suction pressure for higher speed installations may be caused by the friction in the guide rod. Nonetheless, it is clear from the results that suction pressures are indeed dependant on the installation rate, which agrees with the results discussed earlier.

Figure 4.29 plots the average increase in suction pressure against the increase in penetration rate. The Ox-150-1 test (the lowest line in Figures 4.28a and b) was chosen as the "base" case. The results show a relatively linear relationship between them. The results also do not seem to show that an upper limit for suction pressure has been reached. However, a lower bound value for suction pressure was recorded. Figures 4.30a and b show the results where the caisson was installed at different rates under 0.3mm/s. In one case, the rate was varied between 0.04 mm/s and 0.13 mm/s during installation. Despite these variations, Figure 4.30a shows no recognisable changes in the suction pressures as a result, suggesting that differences in rates do not appear to affect the suction pressure in these installations. This is once again very consistent with previous results in Section 4.3.1, confirming that there is indeed a lower limit for suction pressure. The rate threshold for this to occur was however not investigated in this test series.

Figure 4.31 shows the comparison between the "lower bound" suction here with that in the UWA 1g test discussed previously. It can be seen from the results that although the Oxford result gives a slightly higher normalised suction, the suction pressure gradients are almost identical for the two cases. Since the pressure here is normalised against the soil unit weight γ', the similarity in the responses suggests that γ' may be an important parameter. This will be investigated in more detail in Chapters 5 and 7.

4.3.8 Discussion

It has been observed in this study that the suction pressure can vary with installation rate. Considering that the suction pressure is related to the soil resistance at each stage, the

results indicate the sand resistance at any wall embedment is not unique, but increases with faster installation rates. A possible explanation is that in faster pumping installations, the seepage is higher, thus increasing the soil effective stress on the external caisson wall. This increases the outside skin friction, and results in a higher resistance, hence higher suction pressure as seen. While this line of argument seems reasonable, especially from the test results that show seepage was indeed higher during faster pumping installations, it cannot explain what causes the high seepage that occurs immediately after pumping commences. Note that seepage is induced by the suction pressure, the higher seepage must be the direct result of the higher suction. In other words, higher suction pressure (hence higher soil resistance) must exist first. Hence, there is likely to be a different mechanism that causes higher sand resistance, at least immediately after pumping.

Although the true causes are not yet fully understood, a possible reason that may be important is the transient, time dependent effect on the generation of pore pressure and any subsequent sand loosening. It is known that the penetration resistance (both tip and skin) is a function of the effective stress, which is affected by the change in the pore pressure, and subsequent sand loosening (if any). Hence, different changes in pore pressure and sand loosening at a specific wall depth are likely to result in different levels of soil resistance obtained. Practically, it may take a certain amount of time, although this will be small in sand, for the seepage flow net to fully develop. Even so, the created seepage flow still requires time to mobilise the sand particles to reach a final stable loosening state (corresponding to that seepage value). This is similar to the observation that sand loosening propagates progressively up, rather than occurring by spontaneous expansion, when a saturated sand column is subjected to upward seepage (Vardoulakis, 2004). In other words, changes in pore pressure and subsequent loosening (that lead to changes in the soil resistance) as a result of the generated seepage are unlikely to reach their final states instantaneously. This time effect in turn influences the penetration resistance. The faster the installation is, the less time is available for the pore pressure generation and any subsequent sand loosening to occur. This, in turn, results in less reduction in soil effective stress, causes larger penetration resistance, and hence higher suction pressure at a certain wall depth.

The time effect on any subsequent loosening, which was observed by Vardoulakis (2004), is also consistent with the observation that no piping channel developed in fast installations despite very high suction pressure. The reason is possibly because at a specific wall depth, there is insufficient time for mobilising the sand particles, thus piping channels to form, while at the same time the caisson penetrated rapidly into new soil. This is also consistent with the PIV observations that no instantaneous sand movement was observed in regions along the outer caisson wall, where piping channels would form, despite the high suction pressures applied.

The observation that below a certain penetration rate threshold, suction pressure does not vary with rate suggests that in those cases, similar soil resistance has been obtained. For these cases, it may be argued that sufficient time was available for seepage to create a stable hydraulic set-up and loosening condition. Even if more time is allowed by slowing down the installation, the effect of seepage on the soil remains relatively unchanged because stable conditions are developed, which results in a single value of soil resistance for a specific wall depth. The above threshold is likely to be related to the time to create a stable seepage flow net in the soil, which will be a function of the sand consolidation coefficient c_v.

An interesting question is how the suction pressure would respond when the installation is extremely fast, and whether there is an upper limit for the suction increase. In this case, the upper limit for suction is probably similar to the pressure required to jack the caisson into soil (i.e. there is no influence of the ground water field). This, however, requires verification from further experiments.

The variation in sand heave observed in fast and slow installations is also puzzling. In faster installations, higher suction pressures and higher absolute seepage flows were obtained. It is therefore expected that the resulting sand heave would also be larger as this is directly influenced by the seepage body force. However, the test results show quite consistently the opposite, that heave is lower in faster installations (apart from the thick-walled caisson with t/D of 2%). This unexpected result leads to the suggestion that consideration of seepage alone may not be sufficient in determination of sand heave formation. Rather it may be a combination of a number of factors that affect the heave. In faster installations, although the overall calculated seepage is larger, it does not

necessarily mean that the flow is uniformly distributed throughout the whole plug, which of course if true would tend to suggest increased risk of piping, and greater resulting sand heave. Rather, a large proportion of the total seepage may flow along the wall-soil interface, because this is the shortest and most critical flow path, and as a result is likely to loosen sand more in this region (i.e. sand permeability here will be higher). This localised effect makes the remaining part of the flow, through the bulk of the soil plug, less significant, and hence minimises its effect on heave formation. The fast penetration of the wall may also help reduce heave by preventing sand inflow, and possibly forcing some of the displaced sand outwards. The time effect on subsequent sand loosening discussed before may also further contribute to the prevention of sand heave.

4.3.9 Summary

This 1g test series has revealed that the suction pressure is rate dependant when the installation rate is faster than a certain threshold. Below this rate, however, the suction pressure appears to be unique for a given geometry and surcharge. Although this behaviour is not yet fully understood, it is thought that it may be caused by the time necessary for the seepage flow net to be established and any subsequent sand loosening. Variations in the caisson diameter and wall thickness within the range used here do not seem to change the general shape and trend of the suction pressure. In all cases, the suction pressures increase quite linearly with depth, following a very similar gradient despite differences in the geometry. The use of surcharge lowers the required suction pressure at a given wall embedment depth, but does not appear to change the shape of the suction pressure response. Surcharge also tends to lower the amount of sand heave, a trend which was observed in all installations. In this study, fast pumping installation could be achieved without any negative effects. The tests also demonstrate that the installation of long caissons with L/D of up to 2 is possible in dense sand, but a large amount of heave may occur, especially at deeper wall embedment.

4.4 Installation in layered sand-silt soil

The following section investigates the influence of a silt layer on the suction installation. Note that all tests were conducted using the 100 mm caisson with 2.6 N self-weight. Physically, the saturated silica flour (silt) layer was considerably "harder" than the sand, possibly due to its greater dilational characteristics. This is also evident from the cone tip resistance in the centrifuge, which will be shown and discussed later in Chapter 6. The tested soil profiles were shown previously in Chapter 2 (Figure 2.17). It is also noted that the submerged unit weight γ' of the tested sand and silt were found to be quite similar, around 10 kN/m^3.

4.4.1 Layered soil with surface silt layer

Installations were conducted for the soil profile shown in Figure 2.17a, using both slow and fast pumping. For slow installation (around 0.1-0.4 mm/s), especially when the caisson wall was still within the silt layer, penetration could not be achieved, and piping failure occurred. The corresponding suction pressures are shown in Figure 4.32, where the slow installation was attempted 3 times. For each attempt, a large jump in suction pressure is observed, followed by a quick drop afterwards. This drop coincides with the occurrence of the piping failure, indicating the loss of pressure seal in the caisson compartment. The large jump in suction pressure, which created piping, shows that significant driving force is required to penetrate the caisson in this case.

Installation was, however, possible when fast pumping was applied (the possible reasons will be discussed later in this chapter). The suction pressure recorded during the fast installation test (~6-7mm/s) is shown in Figure 4.33. The soil profile is the same as before (Figure 2.17a). The required suction pressure for similar installation in homogenous sand is also included for comparison. The results show that the presence of the silt layer on top of sand clearly influences the installation behaviour. The suction pressure in this case is significantly higher than that for homogenous sand, consistent with the expectation that the hydraulic blockage created by the silt reduces the seepage gradient and hence the reduction of the soil effective stress in the underlying sand. As a result, the penetration resistance increases. During the initial penetration, the suction

pressure increases relatively linearly with depth, before dropping to a lower level at L/D between 0.4 and 0.5. This drop is likely to be created by a reduction in the hydraulic blockage caused by the silt. Indeed, it occurred at the same moment where silt scourings along the caisson wall were observed, followed by a significant flow of water emerging from below the silt layer. This, however, did not cause any penetration disruption. The pressure is then seen to increase slowly with penetration, before suddenly increasing to very high value at L/D of 0.7 and greater. Note that the internal plug did not touch the caisson lid until L/D of around 0.8, so the increase in suction pressure between L/D of 0.7 and 0.8 is not the result of contact between the plug and the caisson lid. Rather, it may indicate that the caisson installation could be close to a penetration refusal limit for this particular case. This, however, may require further test investigation.

It was also observed that there were some disturbances at the interface between the silt and sand during installation. This was also often seen at the base of the silt in other sand-silt installation tests (described later in Section 4.4.3). However, a large disruption of the silt layer, as occurred in the test shown in Figure 4.33, leading to significant upward water flow at the inner wall-soil interface was not common. It is possible that local weaknesses in the silt layer (where the disruption in the layer was observed) may have been caused by disturbance to the surface of the silt layer when manually closing the water evacuation valve on the caisson lid. Nonetheless, the results here have clearly illustrated the flow blockage effect of the silt layer during installation, which causes a significant increase in the required suction pressure to penetrate the caisson in the underlying sand.

4.4.2 Layered soil with silt layer below the surface

This section explores the installation behaviour when the silt layer is inter-bedded in the middle of sand. Figure 4.34 shows the slow installation result in soil profile 2 (Figure 2. 17b). The average penetration rate in this case is around 0.3-0.4 mm/s. A similar slow installation result in homogenous sand is also shown in the graph for comparison. It can be seen that the suction pressure during penetration in the upper sand layer is almost identical to that in the homogenous case. However, as the caisson approaches the silt layer, the suction pressure starts to increase at L/D from 0.2 to 0.25. There could be

several reasons for this observation. It could be caused by different head loss distributions and seepage restrictions due to the decreasing gap between the wall tip and the low permeability silt layer, or increased caisson penetration resistance due to the stiffer response of the silt layer, or a combination of both.

When the caisson reaches the silt layer at L/D of around 0.25, a large jump in suction pressure is observed, showing that a large driving force is required to penetrate the silt layer. It was seen from the test that during this stage, a localised piping channel started to form along the wall, and eventually led to piping failure. This is also clearly reflected by the sudden drop in suction pressure. Silt traces were seen in the caisson compartment during this piping failure, indicating that scouring in silt indeed occurred (note that the top soil was sand in this case). The pumping was then stopped, and attempts to re-start the installation by slow pumping were not successful and still created piping failure.

Figure 4.35 shows another installation in a similar soil profile. As shown, the results obtained are quite similar, where the suction pressure was initially close to slow installation in homogenous sand, and jumped to a high value when the caisson penetrated into silt, followed by localised piping failure. At this stage, the suction installation process was stopped and re-started by applying rapid pumping instead of slow as previously (the fast installation rate was about 4-5 mm/s). Unlike re-starting the installation by slow pumping, the caisson penetrated into the soil in this case. Figure 4.35 shows the suction pressure significantly higher than for similar fast installation in homogenous sand. This is consistent with the previous observations from installation where the silt layer was on the soil surface.

The suction pressure from an installation where fast pumping was applied from the beginning can be seen in Figure 4.36. The soil profile for this test is illustrated in Figure 2.17c (the depth of the silt layer for this case is a bit shallower than the cases in Figures 4.34 and 4.35 above). It was observed that there was no piping failure in this case, and the caisson could penetrate well into the soil. It can be seen from Figure 4.36 that the suction pressure increased quite linearly with depth, before rapidly jumping to a high value as the caisson penetrated through the silt. After reaching a peak at wall embedment depth L/D of around 0.2, it then declined sharply, and continued to increase linearly with depth afterwards. It is noted that the pressure peak and rapid decline occurred while the

caisson wall tip was still within the silt layer, indicating significant changes in the penetration resistance during that period. Discussion of possible reasons for this observation are presented later in Chapter 6.

The above results are plotted together with that for a surface silt layer and installations in homogenous sand in Figure 4.37. In general, the suction pressures are seen to increase quite linearly with depth, but at a higher gradient when silt layers are present. The results also show that the required suction pressures for penetration in sand below a silt layer are significantly higher than those in the homogenous sand, on average about 2 to 2.5 times more in this study.

4.4.3 Internal heave

In all installations with the silt layer, either on the surface or embedded within sand, large sand heaves were observed, on average about 12-20 % of the penetration wall depth at L/D of about 0.8. These are considerably higher than those in similar installations in homogenous sand, which ranged from 5-8 % at the same penetration. During the tests, as the internal plug moved upward, soil disturbance in the form of regions of mixed sand and silt, and small water pockets were observed at, and below, the sand-silt interface. However, complete separation of the silt layer from the underlying sand was not observed at any stage during the installation. Scouring of silt along the inner caisson wall was also seen.

At the end of the test, when pumping was terminated, a small amount of water from below the silt layer was seen to continue to flow up into the caisson compartment through the scoured channels in the silt along the caisson wall (for 4-5 seconds). This suggests that a pressure balancing process across the silt layer was occurring, which was indeed evident from the gradual reduction in suction pressure over 20 seconds shown in Figure 4.38. For comparison, the pressure balancing normally took less than 4 seconds in homogenous sand. The heave was observed to reduce during the period of suction reduction, creating a gap of 3-6 mm between the soil surface and the caisson lid. This suggests that soil in the region below the silt layer is very loose and unstable. As noted above, there were also some water pockets formed during the installation process.

4.4.4 Discussion

It was observed in these tests with silt layers that fast pumping helped penetrate the caisson through the silt layer, while slow pumping was ineffective and resulted in piping failure. The reason for the success of fast pumping installation is believed to be due to the time required for the development of piping channels, and the available driving force during that stage. As previously discussed, it takes a certain amount of time for a piping channel (leading to piping failure) to develop. In slow pumping, as the caisson penetrates into the hard silt layer, the large suction pressure required starts to induce soil scouring and a piping channel. Because of the slow motion of the caisson wall, the wall does not provide sufficient increase in effective wall cut-off to prevent piping from occurring. In other words, the piping channel is allowed enough time to develop, leading to subsequent piping failure. However, in rapid pumping, this is not the case. The large available driving "thrust" to quickly penetrate the caisson through the silt layer into new soil effectively cuts off the formation of piping channels when these start to form, or even does not allow enough time for them to occur altogether. As a result, the caisson penetrates into the soil without piping failure being observed. This is similar to the fast installations in homogenous sand seen before, where the suction pressure was very high but there was no piping failure.

It has been observed before that a small amount of water still flowed into the caisson interior from below the silt even after pumping was stopped. A question arising from this observation is where this water came from. There appear to be two possible sources: continuing seepage flow induced by the net suction pressure remaining in the caisson (Figure 4.38), or the extra water originating from the soil due to the changes in void ratio. Note that because pumping has already been stopped, water inflow due to continuing seepage from the outside is not the cause. Therefore, the upward water flow seen here must emerge from the soil below the silt layer. The observed water pockets below the silt are obvious sources, but a further contribution to the total upward flow may come from the sand below the silt layer itself as a result of the reduction in void ratio. This is consistent with the observation that sand heave was seen to reduce gradually with time, and once again suggests that the soil below the silt layer is indeed very loose and significantly disturbed. The hypothesis is consistent with the previous PIV results, where

significant sand loosening was observed below the silt layer (reflected in the zone with large sand displacement recorded).

4.4.5 Summary

It was found here that the hydraulic blockage created by the silt layer has a significant effect on the caisson response during installation. The required suction pressure to penetrate the caisson in sand below the silt layer is significantly higher than in the homogenous sand case, by almost a factor of two in this study. The possible reason for this is the effect of the hydraulic blockage of the silt on the underlying sand, and will be discussed in more details in Chapters 6 and 7 of this thesis. In penetration in sand above the silt layer, the pressure appears to increase slightly as the caisson wall tip approaches the layer. Some scouring of silt along the caisson wall was observed in the tests. Soil disturbances and small water pockets at the lower silt-sand interface were also seen. Slow installations (~ 0.3-0.4 mm/s) could not penetrate the caisson through the hard silt layer, and piping failure occurred. However, penetration was possible in faster installations (~ 4-5mm/s). This was thought to be because, in this case, insufficient time was available for the development of a piping channel in the silt (similar to that in fast installation in sand discussed previously). In addition, the penetration was further facilitated by the availability of higher "thrust" to penetrate the silt. In all cases, a large amount of heave, about 2-3 times higher than in homogenous sand, was observed. The soil plugs were unstable, with the heave heights observed to reduce after pumping was terminated.

4.5 Conclusions

The experimental study presented in this chapter has explored the caisson behaviour during installation in sand and layered sand-silt soil at normal gravity. In general, it was found that the model suction caissons with L_{max}/D of up to 2 could be installed in very dense sand by either slow or fast pumping. Above a certain installation rate threshold, the suction pressure will be rate dependent, where faster pumping resulted in higher suction. An upper limit for the suction increase with pumping rate was not observed in the tests. Below that threshold, a "lower bound" suction was, however, observed. During

installation in sand, significant sand heave, especially in longer and thicker-walled caissons, could result. The majority of the effective heave (i.e. minus the caisson wall volume) is likely due to sand plug expansion (loosening), not sand inflow. In soils where there was a layer of low permeability silt inter-bedded with sand, the installations were possible with sufficiently fast pumping. However, problems during installation were also recorded in the tests, including piping failure in slow installation, and the creation of large and extremely unstable sand heave.

So far, the tests presented in this chapter have revealed important caisson generic responses that can be expected in similar installations at larger scale. However, care should be taken in further interpretation of the 1g results here, such as extrapolation of the results to prototype scales. In these cases, as discussed previously in Chapter 2, such interpretations are often complicated by differences in soil-structure interaction response due to the stress dependant behaviour of the soil, as shown by Allersma et al. (1997). Nonetheless, the caisson behaviour in the 1g tests here can be compared with other test results at high soil stress levels to help draw more general conclusions. This is covered in the following chapters of this thesis.

Chapter **5**

Centrifuge Modelling: Installation Behaviour in Homogenous Sand

5.1 Overview

The expected caisson response during installation in homogenous dense sand was investigated previously through small scale models tested under low soil stress conditions, as described in Chapter 4. However, the low soil stress levels can affect the installation response due to the stress dependent behaviour of soil. This chapter presents results from investigations of the suction installation process through a series of tests at higher soil stress levels, similar to those in the field, by means of centrifuge model tests conducted at 100g. Initially, the installation in silica sand is examined, using the same type of sand that was used in the previous 1g tests. Direct comparisons with jacked installation, where no sand loosening due to seepage occurred, and comparisons with the 1g results are also made. The investigation is then extended to uncemented calcareous sand from the North Rankin site, and "artificially" mixed soils with 10%, 20% and 40% fines contents. The installation responses in all tested soils are then compared, and general trends for the suction pressures required for a given penetration are identified. The suction pressures predicted using a q_c-based method and an analytical method are compared with the experimental results. The installation results are presented here in a similar format to that for the 1g tests in Section 4.3. In cases where similar results are obtained, only typical ones will be shown. In the discussion of the results in this chapter and the next one, equivalent prototype dimensions will be used.

5.2 Installation in silica sand

5.2.1 Cone penetration tests

The sample uniformity and strength were evaluated by conducting cone penetration tests (CPTs) in the sand, using a 10 mm diameter cone penetrating at a rate of 0.2 mm/s. Figure 5.1 shows typical CPT results for a number of tests. It can be seen from the results that excellent consistency and repeatability of soil strength was achieved, and the very high tip resistance confirms that the sand is very dense. The relatively constant strength gradient, as shown in the CPT results, suggests that fairly uniform sand is achieved in each sample. The slight concavity is possibly due to the depth needed to achieve steady-state resistance, since the cone has an equivalent prototype diameter of 1 m. The depth required to achieve stable cone reading in silica sand could be up to 10 cone diameter (Bolton et al., 1999). Below a depth of about 120 mm (i.e. 12 m at equivalent prototype scale), the curvature increases slightly, probably due to interference with the base of the box (the sample thickness being 180 mm).

5.2.2 Jacked installation and suction installation

Figure 5.2 shows the soil resistance when the two 6 m diameter caissons were continuously jacked (pushed) into sand at the rate of 0.1 mm/s. This is equivalent to an extended self-weight installation phase, where the caisson penetrates under its own weight (the jacking force in this case). Figure 5.2a shows the jacking force and depth in prototype units, while Figure 5.2b shows the results in terms of normalised pressure $p/\gamma'D$ and normalised wall penetration L/D, where the pressure p equals the force divided by the caisson internal cross sectional area, γ' is the soil submerged weight (taken as 10 kN/m^3 here), and L is the wall embedment depth. Note that the jacking of the thicker-walled caisson, with t/D = 1.0 %, was stopped at a depth of $2/3L_{max}$ due to concerns of damaging the caisson. However, this does not affect the observed trends. Indeed, for the same caisson diameter of 6 m, the results show that the jacking force for the thicker-walled caisson is approximately double that for the thinner-walled case (t/D = 0.5 %). Given that the wall roughness was similar for the two caissons, this suggests that the resistance is dominated by the wall tip resistance. This result is expected due to the very

high cone resistance as seen previously in Figure 5.1. The jacking forces also show a non-linear behaviour, with increasing force gradient observed at greater penetration depths, as the component of resistance due to side friction increases.

The above jacked installation is compared with a typical result from suction installation in Figure 5.3. The suction test was conducted following the 2-phase installation described in Chapter 2. In the self-weight phase, it can be seen that the initial caisson penetration is in good agreement with that obtained from jacking, with an embedment ratio L/D of around 0.1 reached at an equivalent prototype force of 500 kN (or caisson mass of 50-tonnes). However, diverging responses are observed during the suction installation phase. A very significant reduction in force in the suction-installed case is seen in Figure 5.3, where the required force is several times smaller than that during jacking. This clearly illustrates the significant effect of seepage flow in degrading the tip bearing resistance. As mentioned in Chapters 2 and 4, while upward seepage inside the caisson reduces the effective stress and hence the friction along the inner wall, downward flow along the outside wall has the reverse effect. Although there may be some net difference in these relative effects, most of the force degradation observed here can be attributed to reduction in tip resistance, particularly given the dominance of tip resistance deduced from Figure 5.2.

5.2.3 Effect of initial penetration depth and surcharge

The effect of initial penetration depth on installation behaviour is shown in Figure 5.4. The slight increase in suction at the end of the installation was most likely caused by the increasing contact between the caisson lid and the internal plug. It is noted here that the installation set-up was kept similar in all installations so that similar total outflows (pumping) could be obtained. Therefore, effects due to different pumping rates as observed previously in Chapter 4 could be minimised, allowing the results to be directly compared. Furthermore, it was observed that, within the range of the pumping rates in this study, the installations in the centrifuge with water as pore fluid did not appear to be rate dependent, i.e. similar to the “lower bound” installations at 1g. This will be discussed in detail later in Section 5.5.

The results show comparisons between tests where (a) the caisson penetrated under its self-weight following the procedure described in Section 2.7.3, and (b) where it was arbitrarily pushed to different initial wall depths before applying pumping, but with the self-weight maintained at the equivalent prototype weight of 500 kN (or $\Delta p/\gamma'D$ of 0.29) during suction installation. It is clear that for a constant self-weight, pushing the caisson further into the soil does not appear to have any advantage, in terms of suction pressure or penetration capacity, over cases where the caisson was installed at a shallower initial depth. For the cases with artificially increased initial embedment, the pressures quickly rise to join the pressure level for the shallower embedment case. This illustrates that, as long as the caisson weight remains constant, a similar amount of extra suction force will be required to penetrate the caisson further. In other words, the soil resistance on the caisson does not change. It also implies that irrespective of the initial wall cut-off length, seepage still creates the same force degradation due to reduction in effective stress and sand loosening, providing the caisson has the same self-weight.

In other tests, instead of arbitrarily pushing the caisson to a greater initial embedment as before, the caisson was allowed to penetrate further by increasing its weight (i.e. adding surcharge), before pumping. The results of installations with different surcharges are summarised in Figure 5.5. In this case, it can be seen that the use of additional surcharge reduces the required suction pressure throughout installation. The pressure responses appear to be parallel. The average normalised pressure reduction $\Delta p/\gamma'D$ seen in Figure 5.5 is around 0.05, equivalent to a weight of 85 kN. Since the added surcharge was about 500 kN (at equivalent prototype scale), the suction reduction is therefore much smaller than the amount of extra weight added. Further discussion of the pressure reduction will be included in Section 5.5.

Figure 5.6 shows the results where the suction curves in Figure 5.5 are arbitrarily shifted to the same starting point, in this case the start of the $\Delta p/\gamma'D$ of 0.29 (500 kN) self-weight caisson installation by translating parallel to the embedment axis. The purpose is to compare and see how the shapes of the suction curves differ as a result of variations in the caisson weight. The result is interesting, with a virtually unique response curve obtained. This suggests that installation with higher surcharge does not appear to change the suction behaviour. Rather, the suction curve is just simply shifted along the wall

embedment depth axis to the new starting point, i.e. the new self-weight penetration position caused by the added surcharge. This result is very useful in predicting the required suction pressures for installations with different surcharge. In particular, if the above unique curve (details of which will be investigated in Chapter 7) for a caisson can be derived, the required suction for installation can be predicted easily for any self-weight and surcharge.

5.2.4 Effect of caisson geometry

Installations of caissons with different wall thicknesses are illustrated in Figure 5.7. The results show the installation behaviour of a 6 m (60mm model), t/D = 0.5 % caisson and the same size, same self-weight caisson but with a thicker wall with t/D = 1.0 %. Figure 5.27a shows the result for the caisson weight p/γ'D of 0.29 (500 kN), and Figure 5.7b shows the result for the caisson weight p/γ'D of 0.88 (1500 kN, or 1000 kN surcharge). It is seen in both cases that the thinner-walled caisson penetrates deeper under self-weight because of the reduced wall tip resistance, which is consistent with the jacking results shown in Figure 5.2. The behaviour during suction installation, where the suction curves appear to be quasi-parallel, is interesting when compared with the jacking results, and essentially mimics that seen for different self-weights shown in the previous section. For suction installation, there is only a small increase in force for the thicker-walled caisson, compared with the difference shown in Figure 5.2. The result again confirms the significant effect of seepage flow on reducing the resistance, particularly tip resistance. The observation of parallel suction curves for both cases shown in Figure 5.7 suggests that the difference in the wall thickness does not seem to have any noticeable effect on the subsequent force gap between the two cases (i.e. the gap remains relatively constant for deeper depth). This is markedly different from the rapidly diverging trend for jacked installation.

The larger pressures in the thicker-walled cases in Figure 5.7 indicate that the thicker caissons require larger driving forces than the thin-walled caissons, not only during self-weight penetration but also during suction installation. The higher suction pressures suggest that although most of the tip resistance is reduced as seen in Figure 5.3 and discussed above, it is not fully eliminated. Indeed, if there was no tip resistance during

suction installation, the wall thickness would become almost irrelevant and there would be no difference in suction required for a given installation depth for caissons of different wall thickness (providing all other geometry and load conditions were the same, which is the case here). However, the results here indicate otherwise, showing that thicker-walled caissons still require higher pressures to penetrate; this confirms the presence of tip resistance, even if small, during suction installation.

The effect of absolute caisson size on suction pressure behaviour was also investigated, by comparing the installations of caissons with identical wall thickness ratio t/D, but different diameters of 6 m and 10 m. Each installation of the 10 m diameter caisson was conducted twice to check the repeatability of the tests. As seen in Figure 5.8, excellent consistency between the installations was observed. It should be noted here that the caisson was installed only up to L/D of about 0.65-0.7 because of insufficient pumping capacity. Modifications to increase the pumping capacity, such as by increasing the water depth difference, were not feasible because of the physical limitations of the centrifuge. Nonetheless, this does not affect the observed seepage trend, as seen in the graphs. Typical results from the 10 m diameter caisson installation are compared with those of the 6 m diameter caisson on Figure 5.9a. It can be seen that despite a slight difference initially, the results show very similar pressure gradient for deeper wall embedment depth. It is also observed from Figure 5.9a that for the same surcharge increment of 1000 kN, the (normalised) pressure drop for the 10 m diameter caisson is smaller than that in the 6 m case. However, this is consistent with the force-pressure conversion, since a 1000 kN weight converts to a normalised pressure change $\Delta p/\gamma' D$ of 0.59 for the 6 m diameter caisson, but only 0.13 for the 10 m diameter case. This is similar to the 1g observations discussed in Chapter 4.

Figure 5.9b compares typical results for each caisson installation in absolute dimensions, of pressure and prototype penetration depth. It is seen that the trend in this comparison is almost the same, including the early stage. Hence the differences seen in Figure 5.9a are partly the result of normalisation. The suction curve for the 10 m caisson with larger surcharge has also been shifted as seen; the identical curves obtained once again confirm the previous observation for the smaller 6 m diameter caisson shown in Figure 5.6.

5.2.5 Seepage flow behaviour

A typical seepage result during installation of the 10 m diameter caisson is shown in Figure 5.10a. The seepage was calculated using Equation (4.1) in Chapter 4. In this case, the total flow was determined from the water collected in the four outflow containers. The seepage value shown is at model scale, i.e. as collected from the test. It can be seen from the results that seepage flow increases very rapidly during the initial stage of installation. However, the rate reduces rapidly with penetration and only very minor increases in seepage occur afterwards. For deeper caisson penetrations, seepage appears to reach a terminal value. This behaviour is very similar to that observed in the previous 1g tests, with a typical result (also for a 100 mm diameter caisson model) re-shown here in Figure 5.10b for comparison. It can be seen that the centrifuge seepage value is much higher than the 1g seepage. This is due to the much larger suction pressure obtained in the centrifuge, which in turn induces more seepage. The observation of large amounts of seepage obtained in the centrifuge (with water as pore fluid) is consistent with results reported by Allersma (2003). Note that the seepage resulting from the "lower bound pressure" 1g installation is chosen here because the centrifuge behaviour is similar to the 1g "lower bound" installations. Further details will be discussed later in Section 5.5. Figure 5.11 shows the typical seepage flow for the 6 m diameter caisson. It can be seen that although the data are very scattered, a general trend for the seepage flow to be relatively constant at deeper depth, averaged at ~40 cm^3/s, can be observed. The larger scatter range, compared with the 10 m caisson case, is believed to be due to more influence of the transducer noise on the (markedly) smaller absolute seepage, due to smaller caisson size.

Figure 5.12 shows the seepage results in normalised form (with $k_{plug} = k_o = 1.0 \times 10^{-4}$ m/s). The 1g seepage and a theoretical result (assuming a single permeability as k_o) are also included. It can be seen that although the data were a bit scattered during the initial stage and the seepage is slightly higher than the theoretical one (which is most likely due to the increase in sand permeability as a result of loosening during installation), the general trends of the normalised seepage are very similar: they gradually reduce to a terminal value for larger wall embedment depths.

5.2.6 Internal heave and plug loosening

In these tests, the sand heave could not be observed continuously during the installation as in the 1g case. Hence, the heave discussed here was the final sand heave measured at the end of the installation, when the internal sand plug was in contact with the caisson lid. It was taken as the difference between the maximum and the actual penetrated wall lengths. Note that the installations of the 10 m caisson were not complete (i.e. the internal plug did not reach the caisson lid); sand heave was hence not obtained for these cases. In the 6 m caissons, the final heave could be deduced because post-test inspection showed that the internal plug was in good contact with the bottom of the caisson lid.

Table 5.1 shows the final values of heave obtained from the tests. In general, it can be seen that, for the thinner-walled caisson (t/D of 0.5%), the total heave was around 7-9 % of the penetrated wall depth. In the thicker-walled case (t/D of 1%), total sand heave was marginally higher, at around 10-11 %. This appears to be consistent with the previous 1g result, where larger heaves were recorded in thicker-walled caissons. The heave measurements here are also similar to those recorded from centrifuge tests of similar caissons by Allersma et al. (1997). In their study, the reported heave ratio was around 9%. Compared with the average 3-4 % heave ratio reported by Erbrich and Tjelta (1999), the heave values in this study are higher. However, values of heave from Erbrich and Tjelta (1999) were measured at much shallower penetration, with L/D ~0.5.

There also seems to be a slight reduction in heave in installations with higher surcharge. However, it is difficult to make a firm conclusion here because the observations of small heave differences in these cases (normally less than 0.1 m, or 1 mm at true model scale) could be influenced by minor variations in experimental conditions (e.g. the soil surface not being absolutely flat). Nonetheless, it was observed quite consistently that final heave was in the range of 0.4-0.6 m, or 7-11 % of the wall embedment depth. The effective heave, i.e. minus the wall volume, was around 5-8 % for all cases.

As discussed before in Chapter 4, the heave is due partially to the caisson volume, and partially to plug expansion, which will result in a looser, and hence weaker, internal sand plug. To investigate this further, a number of cone penetration tests were conducted inside the suction-installed caissons. The results were then compared with those inside

jacked caissons, where no seepage-induced sand loosening occurred. In all cases, the cone penetration tests were conducted in the same manner, i.e. using the same cone, penetrating at the same rate and through the same opening on the caisson lid. This enabled relative comparison between results to be made. Indeed, since the cone test conditions were kept the same, any difference in the results was hence caused by the difference in soil condition in the plug. In these tests, the cone diameter was 10 mm (or 1 m prototype), and the tests were conducted at a penetration rate of 0.2 mm/s (i.e. 0.02 diameter per second). A typical test set-up can be seen in Figure 5.13.

Figure 5.14 shows the cone test results inside the 6 m, t/D = 0.5% caisson. If the sand inside the caisson had loosened, the cone tests would be expected to show a low resistance. However, initially very high tip resistances were obtained which later reached a peak value, before dropping down to a consistent increasing trend with depth. This unexpected behaviour is believed to be the result of the soil confinement inside the caisson (i.e. the internal sand plug was confined by the caisson wall). However, this confinement does not affect the test conclusions because as mentioned above, the results were compared relatively to each other.

It is observed that the cone resistance is much lower in soil inside the suction-installed caisson, compared with that in "non-loosened" soil inside the jacked caisson. This provides an additional indication of sand plug loosening inside the caisson compartment. The larger cone resistance for the caisson installed with a larger surcharge (Figure 5.14) also suggests that installation with a surcharge tends to reduce the extent of loosening in sand. This seems to be consistent with the apparent trend of lower suction and less heave with increasing surcharge, presumably partly as a result of less plug loosening. This was particularly clear in the previous 1g installations discussed in Chapter 4 (Figures 4.13b and 4.26a).

Cone penetration tests inside the thicker-walled 6 m caisson with t/D = 1% yielded very similar behaviour, as seen in Figure 5.15. Indeed, it is observed here again that the plug inside the suction-installed caisson is looser for the installation of a lighter caisson (i.e. the caisson effective weight is less). In other words, the use of higher surcharge (or increase in caisson dead weight) appears to reduce the loosening. It is noted here that the cone resistance inside the thicker-walled caisson is higher that that in the thinner-walled

installations, which is likely to be due to different confinement effects between the two cases (i.e. the stiffer thicker-walled caisson creates larger confinement). However, the overall trend and conclusions are not affected because the results are compared relatively for each case.

5.2.7 Comparison with previous 1g results

Figure 5.16 compares a typical normalised suction pressure response obtained from the centrifuge installation to that from a 1g test. It can be seen that although both appear to increase linearly with depth, the pressure gradient in the 1g case is slightly higher. This difference may be caused by the stress dependent behaviour of sand, which was also observed by Allersma et al. (1997). Nonetheless, it may be seen that there are similarities in the caisson generic behaviour between the centrifuge installations presented here and the 1g installations seen previously in Chapter 4. These are summarised as follows:

- For similar pumping rates, the use of surcharge reduces the required suction pressure. Surcharge also appeares to reduce the sand heave and plug loosening. For the same amount of surcharge, the reduction in the suction pressure was smaller for the larger caisson, consistent with the force-pressure conversion.
- Variations in caisson geometry including caisson size and wall thickness, although resulting in significant differences for jacked caissons, did not seem to alter the general suction pressure behaviour. In all cases, the suction pressure curves were observed to increase relatively linearly with depth with very similar gradient. The suction pressure value was, however, slightly higher for the same diameter, but thicker-walled caisson, indicating the presence of some small tip resistance.
- The seepage rate increased rapidly during initial penetration, but remained relatively constant afterwards, appearing to approach a terminal value.

5.3 Installation in calcareous sand (uncemented)

5.3.1 Cone penetration tests

Figure 5.17 shows the average cone penetration resistance in the North Rankin calcareous sand. For the upper 6 m soil, the resistance increases quite linearly with depth, suggesting quite uniform soil in this region. At the depth of around 6m, the tip resistance gradient reduces. This may be because the soil at that depth was slightly less dense. However, it may also be due to the cone having to penetrate to several cone diameters before a steady state cone reading is obtained. The result here suggests that steady state conditions are achieved at depth of ~6 m. It is also observed that the cone resistance in this case is significantly smaller than that in silica sand seen previously (see Figure 5.18), reflecting the greater compressibility of the sand. This will also reduce the tip resistance for caisson installation.

5.3.2 Jacked installation and suction installation

Figure 5.19a shows the normalised pressure for the two 6 m diameter caissons during jacking. The jacking of the 6 m diameter, t/D of 0.5% caisson was repeated, and the results show very good consistency. Figure 5.19b compares the force required to jack in the thinner-walled caisson in calcareous sand with that required in silica sand. The results are presented in prototype units. It can be seen that, for both caissons, the jacking force in the North Rankin calcareous sand increases quite linearly with depth, being very different from the non-linear behaviour in silica sand. This may be the result of less influence of the wall friction component due to lower frictional capacity in calcareous sand, caused by lower confining stress σ_n' at a given depth (due to smaller γ'). The jacking force is also significantly lower than that in the silica sand case, about 2-3 times less. This is consistent with the lower cone resistance obtained for the calcareous sand, although the ratio of the q_c values for silica and calcareous sand is higher, ranging from 5-10. The force difference between the thinner and thicker-walled caissons is also smaller for calcareous sand, indicating lower end bearing. This is again consistent with the lower cone resistance in calcareous sand.

Figure 5.20a shows the comparison between a typical suction installation result and the above jacking result. Figure 5.20b includes similar results in silica sand for comparison. As seen, it is clear that the required driving pressure in suction installation is lower than that in jacked installation. However, the level of reduction for calcareous sand is less than that in the silica sand case. At the end of the installation (L/D of around 0.9), the required pressure is about half of the jacking value, while it was only 1/5 in silica sand. Nonetheless, the observed reduction clearly illustrates that reduction in soil effective stress, which resulted in penetration force degradation, has actually occurred.

5.3.3 Effect of initial penetration depth and surcharge

The effect of initial penetration depth and surcharge can be seen in Figures 5.21 and 5.22. As seen in Figure 5.21, the suction pressure in the arbitrarily pushed caisson quickly rises and joins that of the shallower case (but same self-weight). This once again suggests that variation in the initial penetration depth does not appear to have any effect on the suction pressure trend, if the rest of the installation conditions are kept similar.

Figure 5.22 shows the effect of increasing caisson weight (or adding surcharge) on the suction pressure. It can be seen that the weight variations do result in changes in the suction pressure behaviour, with lower suction pressure being observed for higher self-weight. The average reduction in $p/\gamma'D$ is about 0.12, equivalent to 200 kN weight (at prototype scale). This is significantly lower than the added weight of 500 kN ($p/\gamma'D$ of 0.29), which is consistent with previous observations in silica sand. However, the $p/\gamma'D$ reduction of 0.12 here is more than that in silica sand, which was only around 0.05. Further discussion will be presented in Section 5.5. The results also show that in all cases, there is a pressure jump when starting pumping, indicating that large force is required to mobilise the caisson in this case.

Figure 5.23 shows the results where the response curves have been shifted horizontally towards a common starting point, in this case the $p/\gamma'D$ of 0.29 (500 kN) self-weight installation. Once again, as in the silica case, it is observed here that the suction pressure trend is almost identical, suggesting that the use of surcharge does not alter the general suction trend. Rather, it is just moved along the wall penetration axis.

5.3.4 Effect of caisson geometry

Figure 5.24 shows the comparison between the two 6 m diameter caissons, but with different wall thicknesses. Some irregularities seen in the thicker-walled caisson result may be due to small variations in the soil condition at that site. However, a general trend can still be observed for the suction pressure in the thicker-walled caisson installation to be higher than for the thinner-walled one, confirming the presence of some tip resistance during installation. When compared with the silica sand results, the pressure difference between the two installations seen here is higher. This indicates that the level of tip resistance degradation in this sand is lower, presumably due to a lesser reduction of the sand effective stress at the tip (although, overall, a net reduction in soil effective stress leading to force reduction has occurred, e.g. Figure 5.20). It is also observed from this result that the suction pressures increase with depth following a quite similar gradient, which is significantly different from the diverging trend seen in Figure 5.19a. This is very consistent with observations in silica sand.

The effect of caisson diameter was also explored. Figure 5.25 plots the results of the installations of 6 m diameter and 10 m diameter caissons, both with the same thickness ratio t/D of 0.5%. The suction pressure trends between these installations are similar, again showing good consistency with previous observations in silica sand.

5.3.5 Seepage flow, internal heave and plug loosening

The seepage flows during the 6 m diameter caisson installations were calculated, but the data obtained were very scattered. A typical result can be seen in Figure 5.26. Although the data seem to be scattered around a constant value close to zero, the large variability makes it difficult to draw a firm conclusion. However, a clearer seepage trend could be observed for the larger caisson, where the larger flow was less influenced by the noise in the measuring transducer. The calculated seepage flow during the installation of the larger 10 m diameter caisson is shown in Figure 5.27a. Figure 5.27b shows the comparison with the similar installation in silica sand. It can be seen that in calcareous sand, the seepage behaviour is very different. Although the seepage data are also quite scattered, the results, especially Figure 5.27b, clearly show that very small seepage flow (compared with silica sand) was obtained in this case. This observation is consistent with

previous permeability measurements in Chapter 3, where the North Rankin calcareous sand was found to be much less permeable (by nearly one order of magnitude for the densities tested). Reducing the seepage measured in the silica sand by a factor of 10 would result in a rate of ~8 cm^3/s, which is within the noise range for the tests on calcareous sand.

Examination of the final sand heave also reveals very different results compared with the installations in silica sand. Table 5.2 gives a summary of the final heave measured at the end of the suction installations. It can be seen that the amounts of heave were very small, generally around 0.1 m (1 mm at model scale) and less, or lower than 2% of the penetrated wall depth. Although small variations in test conditions (e.g. flatness of soil surface) are likely to affect these heave results, it is still consistently observed that the heave values are significantly smaller than those in silica sand. The negligible heave suggests that sand plug loosening during installation was less significant, which also appeared consistent with the small seepage result. Indeed, the effective heave, minus the wall volume, is close to zero, indicating again that almost no loosening occurred.

This was further checked by conducting cone tests inside the caisson. The cone tests were conducted in the same manner as in silica sand, which was discussed in the previous section. Figure 5.28 compares the cone resistance inside the suction-installed caisson and the jacked one. It can be seen that very similar cone resistances were obtained in both cases. This is markedly different from the results shown previously for silica sand. The cone resistance in the suction-installed caisson in this case is even slightly higher, but this could be due to small variations in the soil conditions. The insignificant difference in the plug strength in the suction-installed and jacked caisson observed here clearly indicates that negligible loosening, or even no loosening, occurred during the suction installation. This is consistent with the seepage and heave observations discussed before.

5.4 Installation in mixed sand-silt soil

5.4.1 Cone penetration tests

Figure 5.29 show the cone penetration test results in silica sand mixed with different

silica flour (silt) contents. The average cone resistance in clean silica sand (0% silt) is also included for comparison. Note that a 35 MPa cone were used in the mixed soils, hence the penetration was terminated when the reading reached this value. Nonetheless, a consistent trend can be clearly observed from the results. The cone resistance is higher for soils with larger silica flour content, suggesting larger caisson tip resistance would be found in these cases. The results here are consistent with the observations that, physically, the mixed soils were very stiff. This was also reflected by the triaxial compression test results in Chapter 3, which showed that the mixed soil had very low compressibility. The smooth cone resistance profiles and their relatively constant gradient with depth indicate that the soil samples were uniform.

5.4.2 Installation results

The installations were conducted using the 6 m diameter, t/D of 0.5% caisson. The caisson weight was 1500 kN at prototype, or scale p/γ'D of 0.88. Considering the very high cone resistance in these soils (Figure 5.29), jacked installations were not conducted because of concerns that the caissons could be damaged. The suction installation results in different mixed soils are shown in Figures 5.30a and b. Figure 5.30a shows the results in prototype units, while Figures 5.30b presents them in the normalised form. The result for silica sand with the same size, same weight caisson is also included in Figure 5.30b for comparison. It is noted that the installation in the soil with 40% silt content (the one with the highest cone penetration resistance in Figure 5.29) was terminated early because further penetration could not be achieved due to lack of pumping capacity. Post-test inspection also revealed that the caisson deformed (buckled) slightly in that case, which was not surprising considering the very high pressure at very shallow penetration depth. Nonetheless, a clear installation trend can be observed from these results. It can be seen that the required suction pressures are larger in soils with higher silt content, indicating that the soil resistance was higher in those cases. These appear consistent with the cone penetration results in Figure 5.29. Part of this increase in resistance force may be caused by the increase in wall friction, as the interface friction angle is likely to be higher in these soils (shown previously in Chapter 3). However, the other important increase is due to the higher tip resistance. Considering the very high cone resistance seen previously in

Figure 5.29, it is likely that the contribution of the tip resistance component to the observed suction pressure increase is significant.

The above argument is based on the assumption that the tip resistance does not reduce to zero during suction installation, which was indeed indicated by the results presented here. Figure 5.31 compares the installations of the thinner-walled and thicker-walled caissons. It can be seen that the suction pressure in the thicker-walled case is higher, indicating the presence of some tip resistance. The result is very similar to those recorded in previous installations in clean silica sand and calcareous sand.

The behaviour of suction pressure with depth is also interesting. In all cases, it is seen ultimately to reach a steady rate of increase with depth, following very similar gradients despite differences in the silt content. This pressure trend will be discussed further in the next section.

5.5 Discussion and comparison of the installation results

5.5.1 Discussion of the obtained results

It was seen in Chapter 4 that the suction pressure behaviour with depth was rate dependent if the pumping rate (or installation rate) was above a certain value. However, the suction pressure obtained in the centrifuge tests appeared to be unique, i.e. similar to the "lower bound suction pressure" discussed in Chapter 4. This was investigated by conducting another series of centrifuge installations, using a much smaller pumping rate. This was achieved by using smaller tubing with internal diameter of 4 mm compared to the 10 mm tubing used in all the other tests.

Figures 5.32a and b compare the suction pressure and the measured outflow in these low pumping rate centrifuge installations with the results from the tests discussed in the previous sections of this chapter (which used larger rates of pumping). The results are for the 6 m diameter caisson. Figures 5.33a and b show a similar comparison for the 10 m diameter caisson. In both cases, the installations with low pumping rates could not be completed because of insufficient pumping capacity. However, this does not affect the observed trend. It is clear from the results that despite large variations in total flow (the

difference could be up to one order of magnitude), the suction pressures in both cases remain very similar. The behaviour is the same as that observed in the "lower bound suction" installation at 1g, where variation in pumping rate (below a threshold) does not affect the suction. Figures 5.34a and b show the seepage flow calculated for these fast and slow pumping rate centrifuge tests. It can be seen that the seepage results in the two cases are very similar. This is again consistent with the seepage behaviour for 1g "lower bound" installations seen previously in Figure 4.22.

The rate-independent behaviour observed in the centrifuge tests, as observed here, is likely to be attributed to the rapid generation of a seepage flow net in the centrifuge. This is probably due to increased stiffness (as soil stiffness is proportional to the soil stress), and therefore value of soil consolidation c_v. The increase in c_v allows for a full seepage flow net to develop quickly. As a result, a stable soil effective stress condition at each wall embedment depth can be reached faster, which hence results in similar penetration resistance.

The above argument also appears consistent with the behaviour observed in installations starting from different initial penetration depths. It was seen that for installations with artificially large initial penetration depths (i.e. greater than achieved by self-weight), the suction pressure quickly rose to the same level and joined the previous pressure trend (e.g. Figure 5.4). This is similar to observations by Allersma et al. (1997), where the pressure also responded in the same way in step installations. These results imply that a similar effective soil stress condition (hence penetration resistance) was created very rapidly after pumping was initiated, which again is possibly due to the rapid creation of a full seepage flow net in the centrifuge.

It was seen quite consistently from the centrifuge results that for installations with higher surcharge, the equivalent pressure reduction is smaller than the added surcharge (expressed as equivalent pressure), but by different amounts in silica and calcareous sands. However, in some 1g installations, it appeared that the reduction was larger than the added weight. These variations in pressure reduction are further investigated using a schematic diagram (which mimics Figure 5.3) as shown in Figure 5.35. It shows typical suction installation forces, with total force paths AA' and BB' resulting from two different self-weights (and hence initial penetrations). Note that the jacking line OAB can

be straight, as observed in calcareous sand. The slope of the suction installation lines AA' and BB' also appears to be distinct for a certain type of sand. This slope will be discussed later in the next section, and investigated in greater detail in Chapter 7.

Strictly speaking, to allow for the inclusion of self-weights on the graph, the suction response should be plotted as OAA' or OBB'. However, the results plotted so far were not presented in this way. Rather, they were compared relatively on the same axis O'x'. This was done by shifting point B down to level with A (see the dashed curve starting from B"). It can be seen from the diagram that by plotting the results like this, it gives a force (pressure) reduction of A"B" in the larger surcharge installation. Depending on the proximity of the suction-installed line (e.g. AA') and the jacking line (OAB), the amount of reduction A"B" in comparison to the added weight ΔW (BB") may vary. If the suction installation line is closer to the jacking line (i.e. gradient BB' is closer to that for jacked installation, see Figure 5.36) such as the case in calcareous sand, the A"B"/BB" ratio is higher, i.e. the average reduction is closer to the added amount. Similarly, if they are further apart such as the silica sand case, the average reduction is less, which was indeed observed in the previous test results. Note that in both cases in Figures 5.35 and 5.36, if the total force (self-weight plus suction force) had been plotted in the previous results, represented by lines AA' and BB' in the diagram, then the separation given by A"B shows an increase in total penetration force resulting from a larger self-weight or surcharge, which is consistent with previous observations by Tjelta (1995).

It has been suggested from the installation results that although the tip resistance is likely to reduce significantly during suction installation, it does not appear to be fully eliminated (i.e. reduced to zero). It will be influenced by the seepage flow direction around the caisson tip. It is known that on the inner side of the caisson tip, the upward seepage gradient reduces the soil effective stress, and possibly creates some subsequent loosening, which reduces the tip resistance. However, on the outer corner of the wall tip, the seepage flows around the wall in the downward direction (see the illustrations in Figure 5.37), hence increasing the local soil stress. Therefore, although the upward seepage and part of the horizontal flow may reduce the tip resistance significantly, a small proportion of tip resistance is likely to be present at the outer corner of the caisson

wall during penetration. This was clearly observed in the installations with a thicker-walled caisson (e.g. Figure 5.7) and stiffer soils (Figure 5.30).

5.5.2 Comparison of the general suction pressure trends

It is observed from the tests that despite differences in installation conditions, geometry and soil type, the suction curves appear to follow a very similar trend, consisting of two stages. In the first stage, referred to here as the transitional stage, the pressures are seen to rise rapidly as pumping is initiated as in calcareous sand; or rapidly rise and then to increase quasi-linearly with depth as in silica sand and mixed soils. In the second stage, the pressure increases with depth at a virtually constant gradient for the rest of the installation. The described behaviour is illustrated in Figures 5.38 a,b and c, which show the results for silica sand, mixed soils and calcareous sand respectively. A significant observation is that while the installation pressures can increase in a highly non-linear manner for jacked installation, with significant differences for different caisson geometries, the corresponding responses during suction installation always follow a very distinct slope. The best example is for installation of caissons with different wall thickness t/D, as seen in Figure 5.2 and Figure 5.7.

Figures 5.39a and b plot typical suction installation pressures in different soils together for comparison. Figure 5.39a plots the data in engineering units (at prototype scale), and Figure 5.39b shows the results in normalised form. It can be seen from the results in Figure 5.39a that after the transitional stage, the pressures increase with depth following very similar slopes for silica sand and mixed silica sand-silica flour soils, but at a lower slope for calcareous sand. However, the normalised data are interesting, showing that all pressures appear to follow a similar slope. The identical results observed for the installations in silica sand and calcareous sand are coincidental for the particular case of The caisson weight was 1500 kN at prototype scale, or p/γ'D of 0.88 (indeed, comparing installations of say, p/γ'D of 0.29 (500 kN) self-weight does not give such close similarity). Note that in Figure 5.39b, the pressure is normalised against the soil submerged unit weight γ', which also determines the critical hydraulic gradient i_c for that soil (as $i_c = \gamma' / \gamma_w$). Hence, the obtained similarity in normalised pressure slopes suggests

that the critical hydraulic gradient is an important factor during suction installation. This will be investigated in greater detail in Chapter 7.

The above results were also compared with other published data. Figure 5.40 shows the suction pressure trend from the NGI model tests in similar sand, where different levels of surcharge were used (Erbrich and Tjelta, 1999). Note that the NGI installations were conducted in a pressurised chamber with a relatively large caisson model (0.55 m diameter). The results show a relatively clear trend of the installation, where the pressures are seen to increase following a distinct slope, similar to the behaviour discussed above. It can also be seen that the average pressure drop $\Delta p/\gamma'D$ due to the addition of $p/\gamma'D$ of 0.77 (1 kN) surcharge is around 0.12, significantly smaller than the added amount of 0.77. This is similar to centrifuge results observed here. The installation results with larger surcharges have been shifted to the same starting point in Figure 5.41. Although the data points are limited and the installation depth is small, the shifted results appear to show good agreement in the pressure response. This is consistent with previous centrifuge test results, where the pressure responses were very similar, but simply offset by different amounts according to the extra self-weight penetration depth. Figure 5.42 compares these with typical results from centrifuge installations in silica sand in this study. As seen, the pressure slope with depth appears to be very similar in these results.

The results from field installations are also compared. Figure 5.43a shows the results from the suction caisson installations for the Draupner E and Sleipner T platforms (Tjelja, 1995; Bye et al., 1995; Lacasse, 1999). The soil conditions for both sites also comprised very dense sand, similar to the silica sand tested in this study. It can be seen from these results that, in both cases, the pressures are seen to increase quite linearly with depth initially, but then the gradient reduces sharply at some point and remains constant for the rest of the installation, which mimics the previous centrifuge behaviour. When compared with the installations here, as seen in Figure 5.43b, the results again show that consistent pressure trends are obtained. In fact, the field results are relatively similar to the centrifuge case for mixed soil with 10% silt.

The similarity in the suction pressure behaviour suggests that there is a common mechanism developing during installation. This mechanism will be investigated in greater detail in Chapter 7.

5.5.3 Comparison with current suction pressure prediction methods

In this section, the suction pressure obtained from the centrifuge tests will be compared against the suction pressure predicted using both a q_c-based method (Feld, 2001), and an analytical method (Houlsby and Byrne, 2005[b]). Figure 5.44 shows the predicted suction pressures using the q_c-based method, assuming a maximum reduction of 90% in the tip resistance and skin friction (due to the application of suction). It can be seen that the predicted suction pressures do not match well with those from the experiment. The main reason may be because the cone resistance in the centrifuge has not reached a stable condition. Bolton et al. (1999) suggests that results only appeared to stabilise at depths around 10 cone diameters or more. Noting that the diameter of the cone used in the centrifuge tests in this study is 10 mm, the depth for stable cone reading in this case should be 100 mm or more. The cone results used in the prediction were for depths of 60mm and less.

Figure 5.45 shows the predicted suction using the analytical method proposed by Houlsby and Byrne (2005). K of 1.9 and k_f of 1 were assumed, and the sand friction angles and interface friction angle reported in Chapter 3 were used. It is noted that K is the ratio of vertical effective stress and horizontal effective stress, and can vary between K of soil "at rest" (K_o), and $K_{passive}$ during the installation, i.e. typically between 0.5 and 3 .The results show that the predicted suction is relatively close to the experimental suction for silica sand, but does not match well in other cases. Especially for the mixed sand-silt case, the experimental trend where the pressure slope changed rapidly at L = 1.5m could not be captured. It is also noted that the suction pressure predicted using the Houlsby and Byrne method is quite sensitive to the choice of K (or Ktanδ), which can vary in a relatively wide range during installation.

The results shown in Figures 4.44 and 4.45 indicate that the current methods did not predict well the suction pressures in the centrifuge installations reported here. Furthermore, the general suction pressure trend, where similar suction pressure slopes were observed for installations in different sands, were not reflected in any of the predicted suctions, either using a q_c-based method or an analytical method. This similarity in suction pressure trend will be investigated further in a series of numerical analyses in Chapter 7.

5.6 Summary and conclusion

Caisson installations at prototype effective stress conditions have been investigated in a geotechnical centrifuge. The installations were conducted in various types of sand: clean silica sand, calcareous sand and silty sand (mixed silica sand and silica flour). The results were also compared with other published data, including field installations. The following conclusions can be drawn from the results in this chapter:

- In both silica sand and calcareous sand, the suction pressure required to penetrate the caisson during suction installation was significantly smaller than that during jacking (the reduction being less for calcareous sand). This clearly illustrates that reduction in the soil effective stress due to the generated seepage gradient in the soil, which leads to penetration force degradation, has occurred during suction installation.
- Tip resistance was significantly reduced during suction installation, but was not reduced to zero, i.e. a fraction of the tip resistance still remained.
- Forced differences in initial penetration depth did not have any ultimate effect on the suction pressure response.
- The use of surcharge reduced the required suction pressure, but did not seem to affect the general pressure trend. For installation with higher surcharge, the suction pressure curve was simply shifted along the wall embedment depth axis to the new starting point, i.e. the new self-weight penetration position caused by the added surcharge.
- Variations in caisson geometry, including caisson size and wall thickness, did not affect the pressure behaviour. In all cases, similar pressure curves (shapes) were obtained.
- Internal plug loosening was observed in silica sand, but not in calcareous sand. Nonetheless, in both cases, a reduction in soil effective stress at the tip and along the inner caisson wall occurred, as inferred from the reduction in penetration resistance (compared with jacking).
- The general trend for the suction pressure was found to be very similar for different caisson geometries in all sands tested, and for installations reported in

other studies. It consisted of two different stages: a transitional stage, and a stable pressure slope stage. In the transitional stage, the pressure comprised a pressure jump (calcareous sand), or a jump and a quasi-linear increase with depth (clean and silty silica sands). In the second stage, the pressure increased with depth following a distinct slope.

- The suction pressure predicted using a q_c-based method and an analytical method could not match all the test results. Especially, the general suction pressure trend observed in the test was not reflected in the predicted suction.

Chapter **6**

Centrifuge Modelling: Installation Behaviour in Layered Soils

6.1 Overview

This chapter investigates the centrifuge installation of suction caissons in layered soils. In particular, it explores the influence of the silt and cemented layers on the installation process. The detailed soil profiles and test programme have been presented previously in Chapter 2. The first part of the chapter studies the installation in layered silica sand-silt soil, similar to the tests discussed previously in Chapter 4. The key difference between them is that the installations in this chapter were conducted at high soil stress levels similar to those in the field, whereas those in Chapter 4 were at low stress. The results are presented in a similar order to those in Section 4.4. In particular, the installation in soils with surficial silt layer is first discussed. Then the results in soils with silt layers below the surface are presented, followed by the observations of internal soil heave formation in the installations. The centrifuge results are then compared with those at 1g (previously shown in Section 4.4), and the caisson generic behaviour is discussed. The second part of this chapter investigates a different layered soil type, where uncemented calcareous sand is inter-bedded by weakly cemented layers. In both cases (sand-silt and uncemented-cemented layered soils), the results are also compared with those for homogenous sands.

6.2 Installation in layered sand-silt soil

6.2.1 Cone penetration tests

Figures 6.1 to 6.4 show cone penetration test results for different soil profiles. Figure 6.5 compares them with that in homogenous sand. Figure 6.1 shows the cone resistance in soil profiles where a surficial layer of silt overlies sand. Two curves are shown, one where the thickness of the silt layer is around 0.5 m, and a second with a thickness of 1.0 m. Figures 6.2 and 6.3 show the cone penetration test results for two different soil profiles containing a single silt layer: one with the silt layer at a depth of 0.8 m below the sand surface, and the other with the silt layer at the deeper depth of 2 m. The sand above the silt in the latter case was also less dense, having a relative density of around 60 %. In both cases, the thickness of the silt layer was the same, around 1 m. Figure 6.4 shows the cone penetration test result for a soil profile containing two silt layers. Inspection of all these figures shows that when the cone enters the silt layer the penetration resistance increases, as does the rate of increase of the resistance with depth. As the cone approaches the bottom of the silt layers the rate of increase of resistance drops and the penetration resistance reverts towards that for the homogeneous sand. The higher penetration resistance of the silt (silica flour) compared with the sand as seen here may be attributed to the greater dilational characteristics at low effective stresses. The smooth resistance profiles indicate that the soil is uniform, and the high values suggest that the sand is in a very dense state. Only for the case with the thin silt layer (0.5 m thick) on the surface was the greater resistance in the silt not observed, possibly because the soil layer was too thin to have much influence as the cone diameter (1 m) was twice the thickness of the silt layer.

6.2.2 Layered soil with surface silt layer

Figures 6.6a and b show the suction penetration responses during caisson installation into sand with a surficial layer of silt 1.0 m thick. Figure 6.6a shows the suction results for three different caisson submerged weights. Figure 6.6b compares these with the responses in homogenous sand discussed previously in Chapter 5 (for both suction and jacked installations, with 500 kN and 1500 kN self-weights). It can be seen in Figure 6.6a that very similar suction trends are observed in each case, and that the suction required

appears to increase relatively linearly with depth over the recorded range of wall embedment, i.e. up to L/D of about 0.8. Note that because of sand heave within the caisson, the maximum penetration was always less than the aspect ratio of the caisson $L_{max}/D = 1$. More discussion on the sand heave will be presented later.

Comparison with the suction response in homogeneous sand in Figure 6.6b shows that greater suctions, by 50-80 % on average, are required to penetrate the caisson when the silt layer is present. This can be explained by the low permeability of the silt layer which causes most of the loss of hydraulic head to occur across the silt layer, and hence restricts the development of the upward seepage gradient in the caisson interior. This reduces its effect on the sand adjacent to the inner wall and around the caisson tip, causing less reduction in the effective stress level, and thus leading to higher penetration resistance. However, the suctions are still much less than the pressures required to jack the caisson into the sand, suggesting that there is still significant reduction of the soil effective stress, especially in the region of the tip. The smaller suctions compared with jacked pressures indicate that the hydraulic blockage is less than would be expected with an intact layer of low permeability material. This incomplete blockage is believed to be the result of silt scouring in preferential flow zones that develop adjacent to the inner caisson wall. Such preferential flow zones were observed in homogeneous sand, as seen in the PIV test results in Chapter 4. The mechanism of silt scouring is reasonable as the non-plastic fines can be transported when flow rates are sufficient. Further evidence supporting this scouring mechanism was provided by the observation of silt particles in the pumping hose at the end of the tests. In this case, it could be argued that the silt particles observed in the hose could have come from the surficial silt itself, particularly when the caisson lid comes into contact with the soil plug (note that the filter used could not block silt particles). However, silt was also observed in the hose when the silt layer was not at the surface (as discussed in the next section), supporting the silt scouring argument. This force reduction compared with jacked installation may also be caused by the effect of the uplift of the silt layer, which will be discussed later in this paper.

It can also be seen from Figure 6.6 that the effective caisson weight apparently has little effect on the required suctions. This is in contrast to the behaviour in homogeneous sand where larger caisson weights led to smaller suctions being required for a given

penetration. The absence of any clear effect of caisson weight, within the range investigated here, may be attributed to the hydraulic blockage caused by the silt layer. Considering the very large difference in penetration resistance between jacked installation (complete blockage) and suction installation (no blockage) in Figure 6.6, it is likely that even small variations to the extent of hydraulic blockage may result in significant differences in soil resistance. In the non-plastic silt used here, the silt tendency to move upward and its scouring may both assist the generation of the upward seepage gradient in the sand. During a test, these effects are unlikely to develop identically, which as a result may cause variations in the soil resistance, and effectively mask any dependence on the required suction due to variations in the caisson weight. The hydraulic blockage variations could also explain the pressure 'humps' (at L/D of about 0.6) seen in Figure 6.6a, which were not expected from the cone resistance profiles (Figure 6.1) which indicated uniform and homogeneous sand layers. Despite these effects, the general linear increase of the suction with depth is still clear.

Figure 6.6 also shows that there is initially a rapid suction pressure increase for the 500 kN caisson. In this case the wall embedment at the end of self-weight penetration, i.e. just before suction was started, was less than 1 m, so that the caisson tip was still in the silt layer. A higher penetration force would be expected because of the higher penetration resistance in the silt indicated by the cone penetration tests. This was indeed reflected in the observed pressure jump. For the other installations in Figure 6.6, similar pressure jumps were not recorded because the caisson tip had probably penetrated through the silt layer under self-weight.

Figure 6.7 shows the suctions required for installation in the case where the surface silt layer is only 0.5 m thick. The installation was repeated, giving reasonably consistent results as seen. The suction required for a given penetration is very similar to that in the previous case with a 1 m thick silt layer. In both cases the suction increases linearly with penetration, and the suction gradient (the slopes of the responses) are almost the same. The results obtained here show that varying the thickness of the top silt layer from 0.5 m to 1.0 m does not have any discernible effect on the suction pressures, indicating that similar soil effective stress below the silt layer (along the inner wall and at caisson tip level) has been created in these cases.

6.2.3 Layered soil with silt layers below the surface

Figure 6.8 shows the suctions required for installation of caissons with equivalent prototype self-weights of 500 kN and 1500 kN (or 50 and 150 tonnes mass) in the soil profile with a 1 m thick silt layer, 0.8 m below the soil surface. The initial wall embedment level during self-weight penetration depends on the caisson weight. For the 500 kN caisson the wall tip is in the upper sand layer at the end of self-weight penetration, while in the heavier 1500 kN caisson case, the tip has penetrated some depth into the silt layer. This explains the difference in the initial suction pressure responses, where the pressure increases relatively linearly over a small depth before increasing rapidly in the 500 kN case, compared with an immediate pressure jump in the 1500 kN case. Despite these initial differences, the pressures required for penetration through the silt layer are much the same. Indeed, as the caisson starts to penetrate into the silt layer, a rapid and very significant increase in suction was observed. The pressure peaks while the caisson wall tip is still embedded within the silt layer, then drops rapidly until the tip reaches the silt-sand interface, after which it increases again with further penetration. The behaviour is very similar to that observed in the 1g tests discussed in Chapter 4.

The large jump in suction pressures indicates large soil resistances are mobilised as the caisson penetrates into the silt. This appears to be consistent with the higher cone resistance in the silt at lower effective stresses (as expected at the caisson tip during suction penetration). The sharp suction increase also suggests that initially, little force degradation occurred in the silt with the result that the penetration resistance is probably more similar to that in jacked installation. The rapid drop in pressure while the caisson tip is still within the silt is interesting, because the cone test results (Figure 6.2) do not show any drop in resistance within the silt layer. However, interpretation of the caisson wall penetration based on the cone resistance profile is complicated by the size of the cone (1 m in prototype diameter) compared to the 0.03 m equivalent prototype thickness of the caisson wall. However, it is believed that the rapid drop can be mostly explained by the uplift of the silt layer caused by the suction, which was observed and discussed previously in the PIV results in Chapter 4. As this uplift force builds up with the suction, it weakens and ultimately shears the silt layer along the path of the caisson tip movement, resulting in a loss of soil resistance, especially at the tip (see the illustration in Figure

6.9). The sudden drop in suction, as observed in the results, suggests that the reduction in the penetration resistance is quite substantial. This is consistent with the results in Chapter 5 that the tip resistance is a significant component, and a reduction in the tip resistance is likely to cause significant reduction in total penetration resistance. A very similar behaviour is observed when the caisson penetrates the silt for the soil with the silt layer at 2 m below the surface, as shown in Figure 6.10.

As the caisson tip penetrates through sand, the suctions in all cases appear to increase linearly with depth both above and below the silt layers. It is expected that above the silt layer, the installation would be similar to that in homogeneous sand. However, as the wall tip approaches the silt layer, a (small) rise in suction pressure can be seen. This is similar to the observations from the 1g results in Chapter 4. The possible reasons for this suction rise were mentioned before in Section 4.4.2. Below the silt, some increase in suction compared with the case of homogeneous sand can be seen, as expected due to the hydraulic blockage by the silt discussed before. It is also observed that the relatively linear relationship between suction and wall embedment depth recorded in these soil profiles is very similar to that observed before in installations through a surficial silt layer. Figure 6.11 shows a comparison of all these installation responses. They show that not only are the gradients of the required suction pressures during penetration in sand very similar, but also the actual values of suction lie within a narrow range for any given wall embedment. This clearly shows that for the tests reported here, the effect of the silt layer on the underlying trend of suction required for penetration through the sand is not significantly affected by the depth of the silt layer below the surface.

These trends are further confirmed by the penetration into the soil profile with two layers of silt shown in Figure 6.12. This shows that the suction pressures required for penetration in either the sand layer trapped between the silt layers, or in sand below the lower silt layer, are very similar to those observed previously. In particular, the suction pressures required for caisson installation before reaching the second silt layer is very similar to installations in soil profiles in Figure 6.11 discussed above. The presence of a second silt layer does not seem to have any significant effect on the installation results other than the increase in suction required to penetrate the layer itself (a behaviour consistently observed in this test series).

It was observed that silt particles were present in the pumping hose in these tests, where the silt layer had an overlaying layer of sand. This suggests that scouring of the silt layer was occurring. The inner caisson wall-soil interface is subjected to the most critical hydraulic flow conditions, and hence scouring of silt is most likely in this region. This hypothesis is consistent with the observations from the transparent caisson installations in Chapter 4, where silt scouring at the inner wall-soil interface was seen. The scoured silt particles can then be transported up along the inner wall by the seepage into the water in the caisson compartment (which was being gradually pumped out). It is also possible that not all of the silt collected in the pumping hose came from scoured areas along the inner caisson perimeter. Given the evidence from the large heave of the internal plug, and subsequent settling once suction was stopped (discussed in the next section), it is possible that the complete soil plug became fluidised and that the silt particles could have been drawn from the body of the internal plug.

6.2.4 Internal heave

The installation of suction caissons in these soil profiles could be achieved, but not without complications. One of the significant observations in these tests was that substantial heave occurred inside the caissons, which, as a result, can introduce scouring around the foundation, and hence adversely affects its performance. The heave discussed here is defined as in Chapter 5, i.e. the difference between the soil surface levels inside and outside the caisson. It was determined at the end of installation, when the caisson lid was considered to be in full contact with the internal soil plug. The contact could be inferred from both the cessation of caisson movement and a sudden, rapid increase in suction pressure. For most of the tests with silt layers reported here, the final internal heave was found to vary between 15% and 20% of the wall penetration. This heave was considerably higher than for installations in homogeneous sand, where typical final heave ratios were around 7-9 % at a similar wall depth. After the end of the tests once the centrifuge was stopped, a small gap, around 5% of the wall embedment (~2 to 3 mm at model scale) between the caisson lid and the internal soil surface was observed in the tests with the silt layers, whereas no gap was observed in homogeneous sand. This suggests that the heave in the sand-silt cases reduced after the termination of suction,

indicating that the plug was extremely unstable, and could contain water voids or extremely loose pockets of soil (which was indeed observed and discussed in Chapter 4).

The different post-installation heave observations between homogeneous sand and sand with silt layers suggest that suction across the silt layers is responsible. As discussed previously in Chapter 4, the presence of a low permeability silt layer creates a net uplift force. In other words, the suction pressure may suck the silt disc upward when the caisson penetrates into the sand below the silt layer. This upward movement would result in water being drawn into the region immediately below the silt, possibly accompanied by unstable loosening of the silt (and any overlying material) within the plug. Essentially, this will lead to a transfer of the suction down to the sand, causing reduction of the soil effective stress, which assists further penetration of the caisson. The transfer of suction to the underlying sand, causing it to loosen was indeed observed in the PIV results shown previously in Chapter 4. When pumping is stopped, the unstable soil, above where water has been drawn in at the silt-sand interface, will settle down as the excess pore pressure there dissipates, resulting in a reduction of the overall plug height. The soil disturbance below the silt, and the water dissipation after the test, were observed in the 1g experiments presented before in Chapter 4.

6.2.5 Comparison with 1g results

Figure 6.13 shows a comparison between some typical centrifuge and 1g caisson installation results. It can be seen that the normalised suction in the 1g case is considerably higher than that in the centrifuge installation, a trend similar to that observed in the comparison in homogeneous sand (shown previously in Chapter 5). The difference may again be attributed to the stress dependant behaviour of sand. In addition, interpretation from direct comparison as the one presented here is complicated by uncertainties in the differences between 1g and centrifuge test conditions, such as scaling of the caisson weights. However, in both cases, the average increase in suction pressure when compared with homogenous sand is observed to be quite similar, in the range of 50% to 100%. It is also noted that the installation in the centrifuge was fast, averaged at 40-60 mm/s, and no piping leading to installation failure (i.e. large amount of water flows into the caisson without significant penetration) was recorded. The result is consistent

with the 1g tests observation, where piping did not occur in fast installations (the possible reasons having been discussed before in Chapter 4).

Although being different quantitatively, in general, there are similarities in the caisson generic response between centrifuge installations and those at 1g, which may be summarised as follows:

- During penetration in silt, the suction pressure quickly increased to a peak value, then rapidly dropped until the wall tip reaches the silt-sand interface. A small rise in the pressure was also observed when the tip approaches near the silt layer.
- The effect of the silt layer is clear: the suction pressure required during penetration in sand below the silt layer was higher than that in homogenous sand, and appeared to increase quite linearly with depth.
- Excessive sand heave was recorded at the end of each test. The soil plug, unlike that in homogenous sand, was very unstable and the heave reduced after termination of the applied suction.
- Scouring (erosion) of the silt layer occurred, even in cases where the silt layer was below the surface.

6.2.6 Summary

This centrifuge test series has revealed typical caisson behaviour that can be expected at high soil stress levels (similar to prototype stress conditions) in installation of suction caisson in layered sand-silt soil, where the seepage flow is restricted by the silt layers. It was found that installation in those soils was possible if sufficient pumping was available. However, the formation of excessive heave (up to 20% of the penetrated wall depth), unstable internal soil plug, and silt scouring were also observed. The recorded suction pressures showed a clear influence of the silt layer. The required pressures in these cases were higher than for installations in homogenous sand, about 50-80 % higher on average, but still much less than the equivalent pressure for jacked installation, indicating that the seepage gradient has caused partial reduction of the soil effective stress at the caisson tip and along the inner wall. For the tested conditions, the suction pressures during penetration in sand appeared to increase quite linearly with depth

despite some differences in the thickness of the silt layer, and its depth below the surface. The presence of a second silt layer did not seem to affect this trend. The effect of the caisson self-weight on the suction pressure (within the tested range here) was not clearly observed in the tests. This may be due to the variations in the seepage blockage of the silt, which masks the influence of the caisson weight. Comparison with test results at 1g showed that the caisson generic responses were similar in the two cases.

6.3 Installation in layered uncemented-cemented calcareous sand

This section investigates the caisson installation in North Rankin calcareous sand inter-bedded by cemented layers. For referencing convenience, the cemented sand layers with 10% and 15% gypsum contents (UCS of 80 kPa and 120 kPa respectively) are referred as "weaker" and "stronger" cemented layers respectively in this section. Note that these "strong" and "weak" concepts are used in the context that the strengths of these two layers are compared relatively to each other. They should not be confused with the absolute strength of the cementation, which, from the unconfined compressive strength values, may be classified as weak cementation in both cases. The equivalent prototype weight of the caisson used (i.e. the 60 mm diameter, 0.3 mm wall thickness caisson) was 500 kN in all tests.

6.3.1 Cone penetration tests

Figures 6.14 to 6.16 show the cone penetration resistance results in the tested soil profiles (shown previously in Section 2.8). Figure 6.14 shows the cone penetration results in soil with a cemented layer below the surface. Two curves are shown, one for the soil with a weaker cemented layer, and the other for the soil with a stronger layer. The thickness of the cemented layer in both cases is similar. Figure 6.15 shows the cone resistance in the soil where the weaker (and thinner) cemented layer overlays a stronger one, and Figure 6.16 shows the cone profile in soil where these two layers are separated by a layer of homogenous sand. It can be observed that, unlike the case in silt, the cone resistance in these cases generally decreases as the cone penetrates into the cemented layer. The results are contrary to the expectation that higher resistance should be encountered in

cemented soils, where the soil becomes harder due to the cementation. This may be due to the cemented layer being fractured, ahead of the advancing cone, due to the stresses generated by the cone as it penetrates the overlying sand. However, it is noted here that further evaluation of the effects of cementation from the cone penetration tests is difficult here, because the thickness of the cemented layers is small compared with the diameter of the cone (1 m at prototype scale), and the layers are weakly cemented.

Nonetheless, it is observed in Figure 6.14 that the cone resistance is slightly higher for the soil with the stronger cemented layer. Although this is consistent with the expectation that the soil is harder, the results are not interpreted further here as the observed increase is not significant, and may be influenced by small variations in the soil strength. In Figure 6.16, the effect of the upper cemented layer was not clearly observed in the cone results. This is, as mentioned above, probably because the cemented layer is too thin to be detected by the cone. The observation is also similar to that in the layered sand-silt soil with a 0.5 m silt layer discussed in the previous section.

Figure 6.17 plots all cone penetration results together. The cone profile in homogenous sand is also included for comparison. It can be seen that the results show relatively similar trends, and the cone resistance values lie within a narrow range, indicating the consistency in the soil strength between samples. It also appears that during penetration in cemented layers, the cone resistance in soils with two cemented layers is higher than for a single layer. However, this may be again influenced by small variations in the soil strength, as seen from the range of cone values. Nonetheless, the smooth cone profiles in sand indicate that the sand in these cases is relatively uniform.

6.3.2 Results

The installation results in soils with a single layer of cemented sand can be seen in Figure 6.18. Figure 6.18a shows the suction pressure response in soils with both weak and strong cemented layer, and Figure 6.18b compares them with similar installations in homogenous calcareous sand (which was discussed previously in Chapter 5). As observed from the results, the effect of the cemented layer on the installation is clear. Initially, the suction pressures are seen to increase relatively linearly with depth. As the caisson wall tip reaches the cemented layer, the suction pressure increases to a peak

value, and then rapidly drops while the caisson tip is still within the cemented layer. When the wall tip enters the homogenous sand below the cemented layer, a rapid increase in the suction pressures is observed, followed by a linear trend with depth.

Figure 6.18b shows that the observed linear trend of the suction pressures during caisson penetration in sand is similar to that in installations in homogenous sand. The suction pressures in the sand above the cemented layer are, however, lower than that in the caisson installation with the same self-weight (500 kN equivalent prototype) in homogenous sand. This is due to the top sand in this case being less dense because of less vibration time applied during the sample preparation (mentioned before in Chapter 3). In the sand below the cemented layer, the suction pressures are similar in both gradient and values, indicating that installation in sand below the cemented layers is the same as that in homogenous sand. This is consistent with the expectation that since the cemented layer does not create a hydraulic blockage (as the silt case), its presence will not affect the seepage flow net in the soil, and hence the penetration resistance will not be affected.

The observed caisson response during penetrating the cemented layers is interesting. For the weak layer, the suction increase relative to the uncemented sand is not significant. The suction is, however, clearly larger for the installation through the stronger cemented layer, with a higher pressure peak recorded. This is consistent with the higher unconfined compressive strength obtained for the soil. The drop in suction afterwards indicates a reduction in penetration resistance. As this occurs while the caisson tip is still in the cemented layer, the results suggest that the reduction is due to the loss of soil resistance within this layer during the wall penetration. The pressure drop, after reaching a peak, is similar to the observation during caisson penetration through the silt layers discussed previously. It is worth noting here that core samples from the test sites, as shown in Figure 3.14, indicated that cementation occurred throughout the whole layer. Hence the reduction in suction observed during the penetration in the lower part of the layer is unlikely to be due to the possibility that cementation may not occur there.

While the general behaviour in caisson penetration through silt and cemented layers is similar (i.e. the suction pressure peaks and rapidly drops while the caisson wall tip is still within the layer), the mechanisms leading to the suction reduction in the two cases are likely to be very different. In the silt case, it has been suggested that the reduction occurs

because of the uplift of the silt layer, which shears and weakens the soil along the caisson tip path. However, no uplift occurred in the cemented layer because a hydraulic barrier was not created. This was evident from the penetration results below the cemented layer presented above, and the observation of insignificant heave, discussed later in this section.

Hence, it is likely that a different mechanism was involved. Further examination of the results in Figure 6.18b show that the suction pressure drops to a value lower than that in homogenous sand, indicating that the soil resistance in this part of the cemented layer is lower than that in sand. A possible explanation for this observation is the formation of cracks in the cemented layer. As the caisson tip penetrates into this "brittle" soil layer, the stresses exerted on this layer may create cracking in the soil (similar to those observed from UCS tests in Figure 3.12b) underneath the caisson wall tip. The cracks may result in very significant reduction of the soil resistance on the caisson rim, which is indeed reflected by the large suction drop in the results in Figure 6.18. The mechanism discussed is further illustrated in Figure 6.19.

Figure 6.20 shows the result in the soil where the weaker cemented layer overlays the stronger one (profile shown in Figure 6.15). Figure 6.21 shows the result in similar soil, but where the two layers are separated by a thin layer of sand (profile in Figure 6.16). Figure 6.22 compares all the installations through a single and two cemented layers. It can be seen from the results that, in all cases, very consistent behaviour is observed. The pressure peaks during penetrating the cemented soil, then rapidly drops to below that in homogenous sand before picking up and increasing with depth following the same trend in homogenous sand thereafter. No significant differences in the pressure peaks were observed in the installations through the two cemented layers. For the case in Figure 6.20, the caisson wall penetrated into the upper cemented layer under self-weight. No increase in suction pressure was observed, possibly because the layer was too thin and the cementation was weak.

The results show that the caisson could "punch through" the cemented layer with no significant adverse effects. In all cases, negligible sand heave was observed, only around 2% of the wall embedment. This is very similar to the result in homogenous sand. Post-test inspection revealed good contact between the caisson lid and the internal sand plug.

These observations further suggest that uplift of the cemented layers did not occur in the tests.

6.3.3 Summary

The study here shows that it is possible to install caissons in sand inter-bedded by weakly cemented soil layers. During the installation, no piping failure or excessive internal sand have were observed. When the caisson penetrated through the cemented layers, the suction pressure was observed to peak, and then dropped rapidly to a very low value, below that required in uncemented sand. This was consistently observed in all installations. A possible explanation is due to a crack forming through the cemented layer underneath the tip, leading to significantly reduced caisson tip resistance. In sand below and above the cemented layers, the suction pressure trend is very similar to that in homogeneous sand, consistent with the expectation that since the cemented layers do not create a hydraulic blockage, their presence will not affect the seepage flow net in the soil, hence the penetration resistance.

6.4 Conclusions

The centrifuge tests in this chapter have shown that installation of suction caissons is possible in layered sands-silt and layered cemented-uncemented soils. In both cases, the suction response during penetrating the layer was similar, where the pressures were seen to increase to a peak, then rapidly dropped while the caisson wall tip was still within the layer. This pressure reduction is, however, likely to be caused by very different mechanisms in the two cases. In the layered sand-silt case, the reduction (to the level for homogenous sand) is thought to be because of the uplift of the silt under the influence of the suction pressure. In the layered cemented-uncemented soil, the reduction (to well below the level for homogenous sand) was most likely caused by the formation of cracks in the cemented soil.

Penetration in sand below the silt layered required higher suction pressure compared with homogenous sand, while penetration below the cemented layer was found to be very

similar to that in sand. The difference is caused by the hydraulic blockage created by the silt layer. Although the installation in layered sand-silt was possible, excessive sand heave was observed in all cases. However, the height of the soil plug reduced after the suction was turned off, indicating that the soil plug was extremely unstable. The installation in cemented soil, on the other hand, proceeded well with no significant internal heave being recorded.

Chapter 7

Numerical Investigation of Suction Installation Behaviour

7.1 Overview

This chapter presents the numerical simulations of the installation responses observed previously in Chapters 4, 5 and 6. The numerical analysis is limited to considering the seepage flow nets and condition for critical hydraulic gradient, under various uniform and non-uniform permeability regimes corresponding to the model tests. No attempt has been made to simulate the penetration resistance directly, as this would require good understanding of the rate effect on the soil resistance, especially at the caisson tip. This will be discussed further in Chapter 8. In this chapter, the modelling approach is first described, and the simulated results are then validated against experimental and field data to check on the applicability of the model. Limitations of the proposed modelling approach are also discussed. The model is then applied to simulate the sand loosening observed in the PIV tests discussed in Chapter 4, and to predict the range of loosening in silica sand during suction installation. The suction pressure trend in the caisson installations in homogenous sand, including silica sand, calcareous sand and mixed soils, is then simulated, with the aim to establish the general principles underlying the suction

response for different combinations of self-weight and wall thickness. This simulation is also extended to other installations, including field ones. The last part of this chapter explores the influence of the hydraulic blockage created by the silt layer on the installation in layered sand-silt soil. For this case, different penetration stages during the installation, where the caisson wall tip is above, in and below the silt layer, are investigated, focusing on the groundwater head distribution in the soil.

7.2 Numerical simulation approach

7.2.1 Model description

The caisson penetration at any stage can be considered as a self-balancing process between the total driving force, which includes the caisson submerged dead weight and the suction force acting on the caisson lid, and the soil resistance. In other words, at any wall embedment level, the total driving force is in equilibrium with the soil resistance, and the caisson will not penetrate deeper until a higher driving force is applied (through suction in this case). Therefore, it is possible to assume that the continuous caisson penetration is a combination of a series of discrete movements. This allows the process to be modelled using the finite element (FE) method.

The numerical simulations in this study were conducted based on the above assumption. The FE package PLAXIS was used to simulate the test results. At any specific wall embedment, the seepage induced by the pressure difference (suction) at that stage is assumed to be at an instantaneous steady state. The validity of this assumption will be checked and discussed in the next section. The experimentally recorded wall penetration depth and differential pressure at that depth were used as inputs. Permeability k is another important input parameter, which varies depending on the density of the investigated sand. This will be investigated later in this chapter.

The model geometry and boundary conditions for each simulation were similar to those from the test. In particular, the side and bottom boundaries (i.e. the test chamber boundaries) were chosen as “no flow” boundaries. The boundary along the caisson centre line (note that only half caisson was modelled) was also chosen as “no flow” due to the

caisson symmetry. Fine mesh was used in all simulations, although it was found that using a coarser mesh did not result in significant differences in the seepage flow results.

7.2.2 Validation with measured data

To check the applicability of the proposed modelling approach, the FE results will be compared with test data. These are performed for both 1g tests and centrifuge tests. Comparison with the field data from the Draupner E platform installation will also be made.

Figures 7.1 compares the theoretical seepage calculated from the FE modelling with test results from both a 1g installation of a 100 mm diameter caisson, and a centrifuge installation of a same diameter caisson model (i.e. 100 mm diameter). The theoretical seepage was calculated using the suction pressures recorded from the tests, which resulted in an identical curve for both 1g and centrifuge installations as seen. The simulations were conducted assuming a single value of sand permeability $k_{plug} = k_o = 1.0 \times 10^{-4}$ m/s (typical permeability value for the tested density), where k_{plug} is the permeability of the internal sand plug, and k_o is that of the surrounding sand (see the illustration in Figure 7.2). The same value of k_{plug} was also used in the normalisation of the experimental data in Figure 7.1. It can be seen from these results that while the theoretical flow appears somewhat lower than the experimental one, it captures the behaviour of the measured seepage very well. This suggests that the method of breaking down the installation into a series of discrete self-balancing movements can satisfactorily simulate the process. The assumption that the seepage flow, which occurs as a result of the differential pressure at any instant, can be described as steady state flow at that instant also appears to work well. The higher measured seepage values can be explained by loosening of the sand plug inside the caisson, and the resulting increase of permeability in the plug. This is illustrated in the results in Figure 7.3a and b, where k_{plug}/k_o ratios were increased to 1.5 and 2.0 to account for sand loosening (a more thorough investigation of the likely loosening range of the internal sand plug during suction installation will be presented later in this chapter). It can be seen that better agreement was indeed obtained in these cases.

The modelling approach is further checked by comparing the theoretical hydraulic gradient developed along the inner caisson wall and that measured during the installation of the Draupner E platform installation. Figure 7.4 shows the results assuming a single value of permeability k_o, also taken as 1.0×10^{-4} m/s. It is worth noting here that assuming a different (absolute) value of the soil permeability does not affect groundwater head distribution, and hence the hydraulic gradient result. It can be observed that the theoretical hydraulic gradient captures the measured trend very well, once again illustrating that the modelling approach performs reasonably well. The higher theoretical hydraulic gradient is likely to be due to the assumption of a single permeability value $k_{plug} = k_o$. Figure 7.5 shows the results where k_{plug} is assumed to increase to 1.5 and $2.0k_o$. It can be seen that the results in these cases, especially in the latter case, indeed agree much better with the recorded one.

7.2.3 Limitations of the modelling approach

The above results have shown that the proposed FE modelling method can simulate the installation reasonably well. However, this approach has some limitations. Strictly speaking, the seepage flow during installation may never be in a true steady state because both the suction pressure (seepage creator) and embedded wall length (seepage cut-off) vary continuously during caisson penetration. Hence, the proposed model, which assumes steady seepage flow, only work in cases where either the installation is slow (such as the "lower bound" slow installation at 1g), or a full seepage flow net develops very rapidly (such as at the higher effective stress level in a centrifuge test, with water as the pore fluid). In other words, it may not be applicable to installations such as those involving fast pumping rates at 1g, where a steady state seepage flow net was thought not to have been achieved at each wall penetration depth.

The model capability is also limited by the difficulties in correctly simulating the plug loosening during installation. Practically, the sand in regions along the inner wall is likely to loosen more than those towards the centre of the plug. This was indeed observed in the PIV test results shown previously in Chapter 4, although the loosening in these PIV results is believed to be excessive due to the caisson being fixed. The exact extent to which these regions extend towards the plug, and the sand permeability in those regions

are not known (see the illustration in Figure 7.6), which, to some extent, may affect the model performance. In this study, a single value of average permeability was assumed for the whole plug to simplify the problem when predicting the average plug loosening (during a suction installation test), or in the calculations of the hydraulic gradient.

7.3 Modelling of sand loosening

7.3.1 Simulation of the PIV results

In this section, the silica sand deformation recorded in the PIV tests will be numerically simulated. It should be noted that the observed sand movement is created by seepage. Indeed, when seepage flows through sand, it tends to drag the sand particles with it (through the seepage body force), and eventually mobilises the particles once the drag force is large enough. Therefore, a study of seepage flow may help explain the recorded pattern of sand movement. Theoretically, the soil movement velocity should be less than the seepage flow velocity unless piping occurs. The test geometry and suction pressures measured in the experiment were used as the input parameters in the simulations. A uniform value of permeability $k_o = 1.0 \times 10^{-4}$ m/s was adopted.

Figures 7.7a, b and c show the contours of the experimentally recorded sand movement velocities (in mm/s). The theoretical seepage velocities, also in mm/s, on the right hand half of each wall embedment case from the FE simulations are shown in Figures 7.8a, b and c accordingly. The results clearly show a close relationship between the theoretical velocities of the seepage flow and the measured velocities of the sand in the caisson. The simulated results show that seepage velocities around the caisson tip are very high, with extreme flow conditions near tip level. Considering the direct influence of seepage velocity on the sand stability as indicated above, this leads to the impression that under the applied suction, significant sand mobilisation will occur not only in the region immediately inside the wall, but also in the region outside the caisson wall, possibly by flowing into the caisson. While this is indeed reflected by the high measured sand velocities inside the caisson in Figure 7.7, it is clearly not the case for the outside zone where no significant movements are recorded. This may be because, unlike the inside zone where upward flow lifts the soil up and creates volume expansion and piping

conditions, the outside downward flow increases the effective stress on the soil skeleton, hence restricting its movement.

It is also noted that the theoretical seepage flow distribution for the inside region in Figure 7.8 compares well with the recorded sand velocity pattern. However, the values of seepage velocity from the simulated results are smaller than the sand velocities in the high velocity zones (i.e. in the 'wedge' regions). This is unexpected as seepage flow velocity is expected to be higher or equal to the sand velocities because the soil is transported by seepage. These results may be due to adopting a uniform value of permeability in the simulations. In reality, sand expansion will increase the soil permeability in these high flow velocity zones, in turn leading to faster seepage flow. Indeed, PLAXIS simulations, shown in Figures 7.9a,b and c, where "wedges" with twice the initial permeability were modelled (i.e. $k_{wedge} = 2k_o = 2.0 \times 10^{-4}$ m/s) clearly show much higher seepage velocity in these zones, and hence agrees better with the measured sand velocity pattern.

7.3.2 Estimation of plug loosening in silica sand

This section discusses the estimation of the level of loosening observed in silica sand. Loosening of the internal sand plug inside the caisson in this case cannot easily be investigated directly, but can be achieved instead by examining the seepage flow field into the caisson. When the sand plug loosens, its permeability will also change, resulting in differences in the amount of seepage. As mentioned above, it is likely that sand loosens more adjacent to the caisson wall than towards the middle of the plug due to the shorter hydraulic path (hence higher hydraulic gradient) as seen in Figure 7.6. However, as discussed, different values of k along the wall and towards the plug centre will be represented by a single average permeability value, k_{plug}, for the whole plug as illustrated in Figure 7.3. To some extent, this assumption is not unreasonable as observations from previous 1g installation tests showed that the sand plug moved up quite uniformly. By varying k_{plug} until the theoretical seepage matches the measured one from the tests, the level of loosening at that stage can be predicted using the permeability - void ratio relationship shown previously in Figure 3.2. Figures 7.10a and b show a typical result where k_{plug} was unchanged (Figure 7.10a), and k_{plug} was varied (Figure 7.10b) to match

the experimentally recorded seepage (note: the seepage shown in the figure is as recorded from the test, and the k_{plug}/k_o ratio used to calculate the results in Figure 7.10b will be presented next).

The above process was conducted for various installation tests, and the predicted plug permeability change during installation is shown in Figure 7.11a. It shows the results as a function of permeability ratio, i.e. the ratio between the estimated k_{plug} (to match the measured seepage rate) and the initial permeability k_o (= 1.0×10^{-4} m/s) when the test was started. It is seen that, for the reported sand and test conditions, the ratio remains below 2, typically varying between 1 and 2 with an average of around 1.5. These values appears reasonable considering the sand k_{max} and k_{min} in Figure 3.2, where the maximum permeability ratio that can be achieved is only about 4, unless piping of the sand occurs. For the investigated sand, this is probably the highest value for the plug to remain practically stable. The relatively small permeability range predicted here suggests that assuming a larger k ratio for the tested sand, say 4 or 5, in a numerical analysis is unlikely to be true unless the sand in the plug is unstable (piping).

Based on the permeability change estimated above, the plug loosening can be predicted using the relative density-permeability relationship shown in Figure 3.2a. The results are shown in Figure 7.11b. The majority of the centrifuge tests show a similar trend of reducing relative density with increasing penetration, reaching an average relative density D_r of about 60%. This is consistent with previous 1g test observations that more heave is likely to form with deeper wall embedment. However, the 1g test included on Figure 7.11b shows a much more rapid loosening of the soil than in the centrifuge tests. This can be explained by the lower stress levels at 1g, allowing more sand dilation. In one test, the relative density dropped to as low as 42%, but on average the estimated final plug relative density is about 60-70 %, suggesting that the initially dense soil column is likely to loosen to a medium, medium-dense condition during installation.

The predicted plug loosening estimated above was also checked against the experimental measurements. This was achieved by comparing the theoretical heave resulted from the estimated sand loosening against the recorded final sand heave. The expansion associated with the k/k_o ratio of 1.5 gives an average heave of 5-6 % of the final embedded wall length. This may be compared with typical total heaves averaged at 8% measured in the

tests. In suction installation in sand, the total heave is caused by the volumetric expansion of the loosened sand, the sand displaced by the caisson wall and the sand inflow, if any, into the caisson. Hence heave caused by the sand expansion alone should be smaller than, or at most equal to, the total recorded heave. The estimated loosening thus appears to be in reasonable agreement with the experiments. The heave due to loosening (or sand expansion in volume) is only slightly lower than the total heave, consistent with the previous PIV observations that most of the heave is created by plug expansion.

7.4 Modelling of installation in homogenous sand

7.4.1 Review of the general suction pressure trend

Before the results from the numerical simulations on the variation of suction pressures in installation in homogenous sand are presented, the general suction trends are briefly summarised here. The trends being investigated here are those from the centrifuge tests, where the suction pressure was observed to be unique (i.e. similar to the "lower bound" suction in the 1g tests), and the soil stress condition was more similar to that in prototype cases. These centrifuge observations also represent a more general behaviour, because the results were taken from different installations for various conditions and soil types.

As discussed previously in chapter 5, the suction curves always appear to follow a very similar trend, consisting of two stages: a transitional stage (1st stage), where the pressures either rise almost instantaneously (calcareous sand), or rise rapidly to start with before increasing relatively quasi-linearly with depth (silica sand and mixed soils). In the second stage, the pressure increases with depth following a distinct pressure slope. The slopes of the suction pressure, when normalised against the soil submerged weight γ', are seen to be very similar for installation in different soils. This trend was illustrated before in Chapter 5 in Figures 5.38 and 5.39.

7.4.2 Development of hydraulic gradient along the caisson wall

A series of FE simulations of the suction installation were conducted to investigate the above suction pressure trend, using the recorded suction values as inputs. It has been

observed in Chapter 5 that in suction installation in sand, the generated seepage gradient (i.e. hydraulic gradient) significantly reduces the sand resistance, evident from the comparison of the suction installation and jacked installation results. Furthermore, it was also shown in Chapter 5, and above, that in various types of soils, including silica sand, calcareous sand and mixed soils, normalisation of suction pressures by the soil γ', which also determines the critical hydraulic gradient as $i_c = \gamma'/\gamma_w$ (i_c is the critical hydraulic gradient of the soil), gives a very similar suction penetration slope. This result suggests that the hydraulic gradient is a key parameter in installation in sand. Therefore, the FE simulations focused on the pore pressure field within the caisson, and in particular the hydraulic gradient i developed along the inner caisson wall during installation. The purpose of these analyses has been to investigate if there is a link between this gradient and the pressure response described above.

Figure 7.12a shows the hydraulic gradient results from the FE simulations for installation in silica sand, using the recorded suction seen in Figure 5.5 as inputs. The permeability ratio k_{plug}/k_o was assumed as 1.5 in all cases, which corresponds to the average plug loosening estimated before. The analyses reveal two different mechanisms for the development of hydraulic gradient i during suction installation: a rapid increase in i initially, and a relatively stable i during the remaining installation. It is found that there is good link between this hydraulic gradient pattern and the suction pressure response. A typical result is illustrated in Figure 7.12b. It is seen that the rapid increase in gradient i coincides with the initially higher slope in the recorded suction, while the stable i, of around 1 here, is observed for the rest of the installation, where the pressure increase with depth following the linear (distinct) trend. Note that the critical hydraulic gradient $i_c = \gamma'/\gamma_w$ is about 1 for the soil conditions tested, this suggests that the observed distinct pressure slope corresponds to a critical hydraulic gradient condition existing along the inner caisson wall.

This observation was checked in a second series of FE simulations, where the hydraulic gradient along the inner wall was forced to equal i_c (i.e. the critical condition) for installations in different soils. For silica sand which has soil unit weight $\gamma' = 10$ kN/ m^3, i_c was taken as 1, and k_{plug}/k_o of 1.5 was assumed in the simulations. For calcareous sand, i_c was taken as 0.6 as γ' is only 6 kN/m^3, and $k_{plug}/k_o = 1$ was assumed because no plug

loosening was observed for this soil. The resulting variations in pressure for silica sand and calcareous sand are shown in Figure 7.13 and 7.14. The results are for both 6 m and 10 m diameter caissons. It can be that these theoretical pressure responses agree very well with the recorded ones. The simulations also show that changes in caisson size do not appear to have much influence on the suction gradient. This is consistent with the previous experimental observations in Chapter 5, where the suction responses followed very similar slopes for the 6 m and 10 m caissons. It is also noted that the caisson wall thickness (within the range of those used here) has little effect on the suction slope in the simulations. This explains well the similar slopes obtained in the thin-walled and thicker-walled caisson installations in Figures 5.7, 5.24 and 5.31. For mixed soils, the value of γ' was similar to that for silica sand, thus i_c was also the same. The above result suggests that the critical pressure slope for these soils should be similar to that in silica sand. This was indeed observed from the installation results (e.g. Figure 5.39).

It is also found that normalising the suction pressure by the effective overburden stress at tip level, $p/\gamma'L$, is a good indicator of the hydraulic gradient along the caisson wall. Figure 7.15 shows similar behaviour for the hydraulic gradient i and normalised pressure $p/\gamma'L$, with the latter seen to increase when i increases, and peaking when i also reaches its terminal stable value. The similarity in behaviour is not surprising, as the term p/L in fact reflects the average hydraulic gradient along the inner wall (after allowing for some head loss occurring outside the caisson). As discussed above, the behaviour of the gradient i agrees well with the suction response, hence the pressure term $p/\gamma'L$ can also be used to check quickly which stage the installation has reached. An increasing $p/\gamma'L$ indicates that the installation is in the transitional stage, while a peak $p/\gamma'L$, or the point where $p/\gamma'L$ reduces to a stable value, signals the stage of installation where the suction response follows the slope corresponding to critical hydraulic gradient along the inner caisson wall. This, as seen in Figures 7.16a and b, also works well for mixed soil and calcareous sand. For mixed soils, since similar results are obtained, only a typical one is shown here (in this case, the installation soil with 10% fines content).

7.4.3 Comparison with other installations

This section considers test results from both field installations and model studies and

compares them with the above findings. Figure 7.17 shows the results from the suction caisson installations for the Draupner E and Sleipner T platforms (Tjelja, 1995; Bye et al., 1995; Lacasse, 1999). The soil conditions for both sites comprised very dense sand, similar to that tested in this study. It can be seen from these results that, in both cases, the pressures are seen to increase quite linearly with depth initially, but then the gradient reduces sharply at some point and remains constant for the rest of the installation. The hydraulic gradient measured along the caisson wall during installation in the Draupner E platform, shown in Figure 7.17a, agrees well with the observed changes in these suction slopes. It shows that the hydraulic gradient i increases rapidly initially, then remains relatively constant at a value of around 1. This confirms that the pressure slope during the later stage of installation corresponds to conditions for critical hydraulic gradient. These results are very consistent with the responses discussed in the previous section. Figure 7.17 also includes the hydraulic gradient obtained from FE simulations. It is seen in Figure 7.17 that in both cases, the point of reaching the critical hydraulic gradient i_c is also the point of slope change in the applied suction. The normalised pressures $p/\gamma'L$ are shown to also reflect well the hydraulic gradient responses. In both cases, $k_{plug}/k_o = 2$ was assumed because this provides the best match with the measured data (see Figure 7.5).

Figure 7.18 shows a typical model test result in dense sand, similar to the sand tested in the present study, conducted by the Norwegian Geotechnical Institute (NGI) (Erbrich and Tjelta, 1999). The installation tests were conducted in a pressurised chamber with various surcharge levels applied to the caisson. The results show a relatively clear trend of the installation, where the pressures are seen to increase following a distinct slope. This slope compares well with that corresponding to critical i from FE simulations (in the analyses, a $k_{plug}/k_o = 1.5$, i.e. similar to that predicted in this study, was assumed).

7.5 Modelling of installation in layered sand-silt soil

FE simulations were also conducted to investigate the installation behaviour in layered sand-silt soil discussed in Chapter 6. The simulations focused on the distribution of the groundwater head, as this is thought to be greatly influenced by the presence of a silt layer. The purpose is to see if the groundwater pattern can be used to explain the

installation behaviour observed in the tests. Soil permeability values documented in Chapter 3 were used, i.e. $k = 1.0 \times 10^{-4}$ m/s for silica sand, and $k = 1.3 \times 10^{-6}$ m/s for silt. Due to the caisson symmetry, only the results on the right half of the caisson are shown. Because the aim here is to explain the installation behaviour conceptually, the simulations will be conducted only for a typical soil profile.

Figure 7.19a shows the groundwater head distribution for a typical layered sand-silt profile (similar to the one in Figure 6.3), as the caisson wall tip approaches close to the silt layer. The groundwater head for homogeneous sand is shown in Figure 7.19b for comparison. The sand properties in the two cases were kept the same. It is clear from these simulations that the silt layer causes differences in the ground water head distribution. More head loss occurs outside the caisson in the sand-silt soil (Figure 7.19a), compared with the homogeneous sand (Figure 7.19b). This implies that with a silt layer, the downward seepage gradient outside the caisson is higher, which as a result increases the external wall friction. In addition, the upward seepage gradient inside the caisson is lower, hence its effect on the reduction of the soil resistance along the inner wall and especially at the tip is less. Both lead to an increase in the overall penetration resistance, which explains the observed (small) increase in suction as the wall tip approaches the silt layer in both 1g tests and centrifuge tests (see Figures 4.34 and 6.10).

Figures 7.20 and 7.21 show the groundwater head distributions when the caisson wall penetrates in the silt and below the silt layer respectively. As seen from the results, all of the head loss occurs in the silt layer for both cases. The groundwater heads along the outside wall and the inner wall (above the silt) are constant, implying that the seepage gradients are effectively zero along there, diminishing their influence on the penetration force. In other words, the penetration resistance, especially for the situation in Figure 7.21, would be very much the same as that with no seepage flow (equivalent to jacked installation). This is obviously not what was measured in the tests, mainly because the silt layer would not be able to withstand the differential hydraulic head across it, and would be sucked up. This was clearly observed from the PIV test results in Chapter 4. The instability can be confirmed by a simple back-calculation from the recorded results in Figure 6.10. Below the silt layer, at L/D of ~0.5, the recorded normalised suction was around 0.87 (or ~52 kPa), corresponding to a net uplift force of 147 N. The two force

components resisting this uplift are the overburden weight, which was around 90 N in this case, and the skin friction acting at the inner wall-soil interface. The latter is estimated using the conventional skin friction calculation method, assuming $K\tan\delta = 0.24$ (δ is the interface friction angle). This gives a skin friction of around 24 N, and hence a total uplift resistance of around 114 N, which is clearly smaller than the uplift force. Hence the silt disc seen in Figure 7.21 is not in equilibrium. Its upward movement allows the transfer of the suction to the underlying sand (the mechanism similar to that created by a moving piston), which reduces the soil effective stress and thus soil resistance. Changing the silt thickness to 0.5 m, as seen in the results Figure 7.22, does not create any difference. The groundwater head distribution is essentially the same. As a result, the uplift mechanism and its subsequent effects on underlying sand can be expected to be similar in this case.

The caisson penetration can also be assisted by the scouring of the silt along the inner caisson wall. Figure 7.23 shows the result where the same simulation as in Figure 7.21 was implemented, but allowing a small breakage in the silt layer (simulating the silt scouring). The results show that although most of the head loss still occurs within the silt layer, some losses are observed in regions above and below the silt (unlike previously, where the ground water head was constant in these regions). This leads to the creation of net seepage gradient in the soil along the caisson wall. Therefore, it is expected to create some (small) degradation effects on the penetration resistance, which further assists the installation. In addition, it is observed that since most of the head loss still occurs within the silt layer, a pressure difference is maintained across this layer. Hence the uplift movement of the silt, and the transfer of suction to the underlying sand (discussed previously) still occurs. This illustrates that during suction installation below the silt, it is likely that the reduction in the penetration resistance compared with jacked installation (seen in Chapter 6) is caused by both of the silt uplift and silt scouring mechanisms.

7.6 Summary and conclusions

In this chapter, numerical modelling was conducted to simulate the experimental data. It was shown that the sand deformation pattern recorded in the PIV tests could be well

simulated by the pattern of seepage velocities. The level of sand loosening observed in the caisson installations in silica sand was predicted, and found that the internal plug was likely to be in the medium, medium dense state. The average relative density was estimated in the range of 60-70 %, resulting in an increase in average permeability by a factor of 1.5 to 2. Modelling of the variation in suction pressure in homogenous sand was also conducted. The most significant observation is that the suction pressures will ultimately increase with wall embedment depth following a distinct pressure slope. This 'critical hydraulic gradient' slope corresponds to that where critical hydraulic conditions are developed along the inner caisson wall. Installation data from field and other model tests also show similar results. In layered-silt soil, the FE modelling has also illustrated conceptually some important installation mechanisms observed in the tests.

Chapter 8
Conclusions

8.1 Summary

This thesis has investigated different aspects of the installation of suction caissons. Extensive experimental programmes on model caissons at both normal gravity and at elevated levels in a geotechnical centrifuge have been conducted to explore the caisson response during installation. The study focused on installation in various types of dense sand, including silica sand, calcareous North Rankin sand, and mixed soils where silica sand was mixed with various contents of silica flour. The effect of pumping rate, caisson geometry and the use of surcharge on the suction response and internal sand heave formation was investigated. The thesis also explored the influence of silt and cemented layers on the installation response. In particular, tests were conducted in various profiles of layered sand-silt soils and layered uncemented-cemented soils. The formation mechanism of the sand heave, and the deformation of the silt layer under the influence of suction were also examined in a separate test programme using a half-caisson model and particle image velocimetry (PIV) technique. In addition, finite element modelling of flow patterns was performed to simulate key installation behaviour, including the plug loosening during suction installation, the principle underlying the suction pressure

variation, and the influence of the hydraulic blockage by the silt layer. The conclusions drawn from this research programme are presented in the following sections.

8.2 Installation in homogenous dense sand

The following conclusions are made for suction caisson installation in homogenous dense sand:

- The 1g tests showed that pumping rate had some effects on the suction pressure. When the rate was above a certain threshold, increase in the rate results in an increase in the suction pressure required at a given wall embedment depth. No upper limit for this increase in suction was observed in the tests. However, a lower bound value for the suction pressure was observed for installation rates below that threshold. In this case, no matter how slow the installation was, the suction pressure always followed the same response with penetration depth. The installations in the centrifuge, using water as pore fluid, did not show any rate dependant behaviour, i.e. the suction pressures obtained in the centrifuge tests did not vary with installation rate (similar to the "lower bound" suction in the 1g tests). Although the true cause is not fully understood, the rate dependant behaviour at 1g is thought to be due to transient effects delaying the development of seepage flow in the soil, as well as some effects of the downward seepage gradient on the external caisson wall friction.

- Test observations, especially in the centrifuge, showed that the suction pressure (i.e. the "lower bound" suction) required during caisson penetration followed very similar trends in all sands tested. It comprised two different stages: an initial transitional stage, and a stable pressure slope stage. In the transitional stage, the pressure response comprised a pressure jump (calcareous sand), or a jump and a quasi-linear increase with depth (clean and silty silica sands). In the latter stage, the pressure increased with depth following a distinct slope. Normalisation of this slope against the soil submerged weight γ' gave a unique response for all sands. Finite element (FE) simulations show that this unique slope corresponds to the generation of a critical hydraulic gradient along the inner caisson wall. The

numerical simulations also show that the transitional stage corresponds to the stage during which the hydraulic gradient along the caisson wall is increasing. Normalisation of suction pressure against penetrated wall depth L (i.e. p/γ'L) is a good indicator of this hydraulic gradient.

- Centrifuge test results showed that the overall penetration force required during suction installation was several times smaller than that in jacked installation, clearly indicating that force degradation has occurred as a result of the generated seepage gradient in the sand.

- Surcharge lowered the suction pressure required to penetrate the caisson to a given wall depth. However, it did not appear to change the shape of the suction pressure response. In cases where larger surcharge was applied (i.e. a heavier caisson was used), the resulting suction pressure curve was simply shifted along the wall penetration axis.

- Variations in the caisson absolute size did not appear to affect the suction pressure trend, which was observed to increase following a very similar pressure gradient to that for the smaller size caisson, i.e. the "critical hydraulic gradient" path. Subsequent numerical simulations showed consistent results, in which the "critical" pressure gradient did not vary significantly with larger absolute caisson size.

- At a given wall depth, caissons with a thicker wall required higher suction pressure to penetrate. The increase in the suction force was however very small compared with the force required during jacking. This suggested that the soil resistance on the caisson rim reduced significantly during suction installation, but was unlikely to reduce to zero. Rather, some fraction of the tip resistance was still present, most likely at the outer corner of the caisson wall due to the downward seepage gradient, which would increase the soil effective stress there. The suction pressure trend in the installation of thicker-walled caissons was very similar to that for the thinner-walled case, increasing with depth following the same pressure slope (the "critical hydraulic gradient" slope). This was unlike the jacked results, where a diverging trend was observed. The similar pressure slope

observation was further supported by the results from the FE simulations, which indicated that the caisson wall thickness (within the range in this study) had little effect on the "critical" suction pressure slope.

- As long as the caisson effective weight remains the same, variation in the initial penetration wall depth does not cause any ultimate affect on the suction pressure. In cases where the caisson was arbitrarily pushed to larger depth, the suction pressure was seen to quickly rise and join that of the installation with shallower initial wall embedment depth.

- Sand heave and plug loosening was observed in silica sand. Most of the effective heave (i.e. minus the caisson wall volume) formed during the caisson installation is likely to be due to the volumetric expansion of the sand plug (sand loosening). The sand inflow was deduced to be insignificant. Fast pumping surprisingly reduced the amount of sand heave in the 1g tests. This was probably because the majority of the seepage flowed along the caisson wall-soil interface, leaving a less significant portion flowing through the soil bulk. Larger heave was observed in the installation of thicker-walled caissons. The use of surcharge was found to reduce the amount of internal heave.

8.3 Installation in layered soils

8.3.1 Installation in layered sand-silt soil

- Installation in layered sand-silt soil was possible if adequate pumping was applied. In slow pumping installation, piping failure was encountered when the caisson first penetrated through the silt. However, in rapid pumping installation, the penetration proceeded well, with no sign of soil piping. This was considered due to the large thrust available to penetrate the caisson quickly through the silt, hence effectively cutting off the formation of potential piping channels.

- Scouring of the silt layer was observed in all cases, including in soil where the silt layer was below the soil surface. This occurred not only along the caisson wall-soil interface, but probably also from the body of the silt layer. Uplift of the silt

layers during caisson penetration is believed to have occurred, as indicated by the back-calculation from the test results, and the numerical simulations.

- The effect of the hydraulic blockage created by the silt layer on the caisson wall penetration resistance was clear. It was found that the suction pressure required to penetrate the caisson in sand below the silt layer was higher than that in homogenous sand, about 50-80 % higher in this study. The penetration force below the silt layer was, however, still much less than that during jacking, indicating that a mechanism leading to a reduction in the soil resistance was generated. This mechanism is thought to be due to a combination of silt scouring along the caisson wall-soil interface, reducing the hydraulic blockage, and uplift of the silt layer, allowing the transfer of the suction to the underlying sand.

- In all cases, the suction pressure increased quite linearly with depth, but at a higher gradient compared with homogenous sand. This trend was not significantly affected by the thickness of the silt layer, or its depth below the sand (within the range in this study). Installation in soils with 2 silt layers did not result in any noticeable change in the suction pressure trend when compared with that for a single silt layer.

- Excessive sand heave was observed during the suction installation, with large voids or extremely loose pockets of soil being observed below the silt layer. For most of the tests, the final internal heave was found to vary between 15% and 20% of the wall penetration depth, nearly twice that in homogenous sand at the same wall depth. The plug height was seen to reduce after the suction was turned off, and water dissipation from below the silt layer was observed. The results suggest that the resulting soil plug was extremely unstable.

8.3.2 Installation in layered uncemented-cemented soil

- Installation of suction caissons in sand inter-bedded by weakly cemented soil layers was found to be possible. No negative effects, such as piping or excessive internal sand heave, were observed. In all cases, the caisson penetration through the cemented layers proceeded well.

- When penetrating the cemented layers, the suction pressure was observed to rise initially, and then dropped rapidly to a very low value, below that required in uncemented sand. This observation was thought to be attributed to crack formation through the cemented layer, underneath the tip. This led to significant reduction in the caisson tip resistance, which is a major component of the soil resistance force component, hence reducing the required suction pressure.
- Higher suction pressure was required to penetrate the stronger cemented layer, compared to weaker layer, or uncemented soil.
- During penetration in sand below the cemented layers, the suction pressure trend was very similar to that in homogeneous sand. Similar behaviour is also observed in the sand above the cemented layers. This is consistent with the expectation that since the cemented layers do not create a hydraulic blockage such as in the silt case, their presence will not significantly affect the seepage flow net in the soil, hence the penetration resistance.

8.4 Recommendations and suggestions for further research

An interesting result from this study is the installation rate effect on the suction pressure, provided this rate is above a certain threshold. However, this was only observed in 1g tests, not in the centrifuge tests with water as the pore fluid. The mechanism of this behaviour is not fully understood. The generalised value for this rate threshold for different cases is also not known. However, this behaviour has potentially significant implications to offshore practice. It implies that the suction pressure at a certain wall penetration depth can be "manipulated" by varying the pumping rate (if this rate is above the "lower bound suction" threshold). The result, if true at prototype scale, will greatly affect the suction pressure prediction methodology. So far, the rate effect has not been addressed in any of the proposed methods to predict the suction pressure (e.g. Hogervorst, 1980; Feld, 2001; Houlsby and Byrne, 2005). Furthermore, it is likely to affect the structural design of a caisson because the resulting suction force on the structure may vary depending on the pumping rate. Hence further research into this issue is recommended, both experimentally and theoretically.

Experimentally, it would be preferable if the behaviour can be confirmed in field installations. Further research on small-scale models is also recommended. This includes more 1g tests in different installation conditions, focusing on the installation rate around the "threshold" region, and installation tests in the centrifuge with appropriate silicon oil as the pore fluid (to account for the effect of increased c_v in the centrifuge). On the theoretical side, it is envisaged that modelling involving the timing effect (i.e. probably involving the soil c_v value) is required to account for this rate effect.

Installations with different rates using fast and slow pumping have their own advantages and disadvantages. Slow installation can be more beneficial in terms of structural design of the caisson because the resulting suction force is lower. Furthermore, in cases where the installation is slow enough to achieve the "lower bound suction" condition, the suction pressure is more predictable as this is independent of the installation rate. However, in slow pumping, the installations may be unnecessarily long. In some cases, such as the sand-silt case in this study, it was not possible to install the caisson by slow pumping because of piping failure. Fast installations, on the other hand, could prevent piping in the sand-silt soil, and in other cases, have so far not been found to cause any negative effects on the installation. Sand heave in these cases even appeared to be smaller (although this requires further research to reach a firm conclusion). However, the very large resulting suction during fast installations is clearly not beneficial in terms of caisson structural design. In addition, if obstructions such as large boulders, or restraint from other structures, are encountered during fast pumping installations, sand piping failure could develop very quickly. As a result, less time is available for preventative and remedial action. These observations are suggested to be taken into account when choosing the pumping method.

The study here has shown that the "lower bound" suction pressure curve is unique. It is shifted along the wall embedment axis if a different caisson weight is applied. Hence if this pressure curve for, say, zero caisson weight is identified, the pressure required in installations with any other weight can be easily predicted. This study has found that the general trend of this curve can be predicted from the "critical hydraulic gradient". However, the exact position where this curve lies varies depending on the soil resistance, especially the remaining fraction of tip resistance (for example, the results in Figure

5.39b). It is possible that this can be predicted using a CPT-based method, similar to that proposed by Feld (2001). However, this was not attempted here because of uncertainties in the cone results in the centrifuge, especially at lower penetration depths. In this study, the maximum soil depth to which the caisson penetrated corresponded to only 6-7 cone diameters, whereas Bolton et al. (1999) suggested that the cone results only appeared to stabilise at depths around 10 cone diameters or more. Hence, more research is suggested in order to calibrate the caisson tip resistance against cone resistance q_c.

In the installation in layered soils, further studies on various issues are needed. These include the effect of stopping and re-starting pumping during installation on the silt uplift and subsequent penetration resistance below the silt layers; the effective of caisson size and pumping rate below the silt; the relationship between the cemented soil strength (UCS) and the tip resistance required to penetrate these layers.

So far, the installations in this study have been conducted under idealised conditions, where the lateral movement of the caisson was prevented. In practice, this is unlikely to be the case. In most installations, the caissons are free to move laterally or tilt. Although there have been some initial studies on this issue (e.g. Erbrich and Tjelta, 1999), the understanding is still limited. Therefore, research into installations where the caisson is allowed to tilt during penetration is also recommended.

References

Aas, P.M., Sparrevik, P. and Hylen, S. (2002). "SAL suction anchor in shallow water and layered soil – a competitive alternative", *12th International Offshore and Polar Engineering Conference*, Kitakyushu, Japan, presented-only paper.

Alhayari, S. (1998). "Innovative developments in suction pile technology", *Offshore Technology Conference*, Houston, USA. Paper: OTC 8836.

Allersma, H.G.B., Plenevaux, F.J.A. and Wintgens, J.F.P.C.M.E. (1997). "Simulation of suction pile installation in sand in a centrifuge", *Proc. 7th International Offshore and Polar Engineering Conference*, Honolulu, USA, 1, 761-766.

Allersma, H.G.B, Hogervorst, J.R. and Pimoulle, M. (2001)[a]. "Centrifuge modelling of suction pile installation in layered soil by percussion method", *Proc. 20th International Conference on Offshore Mechanics and Artic Engineering*, Rio de Janeiro, Brazil. Paper: OMAE2001/OFT-1036.

Allersma, H.G.B, Hogervorst, J.R. and Pimoulle, M. (2001)[b]. "Centrifuge modelling of suction pile installation using a percussion technique", *Proc. 11th International on Offshore and Polar Engineering Conference*, Stavanger, Norway, 2, 620-625.

Allersma, H.G.B. (2003). "Centrifuge research on suction piles: installation and bearing capacity", *Proc. BGA International Conference on Foundations*, Dundee, UK, 91-98.

Andersen, K.H. and Jostad, H.P. (1999). "Foundation design of skirted foundations and anchors in clay", *Offshore Technology Conference*, Houston, USA. Paper: OTC 10824.

Andersen, K.H., Andersen, L., Jostad, H.P. and Clukey, E.C. (2004). "Effect of skirt-tip geometry on set-up outside suction anchors in soft clay", *Proc. 23rd International Conference on Offshore Mechanics and Artic Engineering*, Vancouver, Canada. Paper number: OMAE2004-51564.

Andersen, K.H., Murff, J.D., Randolph, M.F., Clukey, E.C., Erbrich, C., Jostad, H.P., Hansen, B., Aubeny, C., Sharma, P. and Supachawarote, C. (2005)[a]. "Suction anchors for deepwater applications", *Proc. International Symposium on Frontiers in Offshore Geotechnics IS-FOG*, Perth, Australia, 3-30.

Andersen, K.H., Jeanjean, P., Luger, D. and Jostad, H.P. (2005)[b]. "Centrifuge tests on installation of suction anchors in soft clay", *Ocean Engineering*, 32, 845-863.

Audibert, J.M.E., Clukey, E. and Huang, J. (2003). "Suction caisson installation at Horn Mountain – A case study", *Proc. 13th International Offshore and Polar Engineering Conference*, Honolulu, USA, 2, 762-769.

Bang, S., Cho, Y., Preber, T. and Thomason, J. (1999). "Model testing and calibration of suction pile in sand", *Proc. 11th Asian Regional Conference of the International Society of Soil Mechanics and Geotechnical Engineering ISSMGE*, Seoul, Korea, 1, 253-256.

Barusco, P. (1999). "Mooring and anchoring systems developed in Marlim field", *Offshore Technology Conference*, Houston, USA. Paper: OTC 10720.

Bolton, M.D., Garnier, M.W., Corte, J., Bagge, J.F., Laue, G. and Renzi, R. (1999). "Centrifuge cone penetration tests in sand", *Géotechnique*, 49(4), 543-552.

Brown, G.A. and Nacci, V.A. (1971). "Performance of hydrostatic anchors in granular soil", *Offshore Technology Conference*, Houston, USA. Paper number: OTC 1472.

Bruno, D. (1999). "Dynamic and static load testing of driven piles in sand", *PhD thesis*, the University of Western Australia.

Bussemaker, H. (2005). Operations and Engineering Manager, *SPT Offshore B.V.*, the Netherlands. Private conversation.

Butterfield, R. (1999). "Dimensional analysis for geotechnical engineers", *Géotechnique*, 49(3), 357-366.

Bye, A., Erbrich, C., Rognlien, B. and Tjelta, T.I. (1995). "Geotechnical design of bucket foundations", *Offshore Technology Conference*, Houston, USA. Paper: OTC 7793.

Byrne, B.W. (2000). "Investigations of suction caissons in dense sand", *PhD thesis*, University of Oxford, UK.

Byrne, B.W. and Houlsby, G.T. (2002). "Experimental Investigations of the Response of Suction Caissons to Transient Vertical Loading", *Journal of Geotechnical and Geoenvironmental Engineering*, 128(11), 926-939.

Byrne, B.W. and Houlsby, G.T. (2004). Experimental investigations of the response of suction caissons to transient combined loading. *Journal of Geotechnical and Geoenvironmental Engineering,* 130 (3), 240-253.

Cao, J., Phillips, R., Popescu, R., Ausibert, J.M.E. and Al-Khafaji, Z. (2002). "Numerical analysis of the behavior of suction caissons in clay", *Proc. 12th International Offshore and Polar Engineering Conference*, Kitakyushu, Japan, 2, 795-799.

Chen, W. and Randolph, M. (2004). "Radial stress around caissons installed in clay by jacking and by suction", *Proc. 14th International Offshore and Polar Engineering Conference*, Toulon, France, 2, 493-499.

Cho, Y., Bang, S. and Preber, T. (2002). "Transition of soil friction during suction pile installation", *Canadian Geotechnical Journal*, 39, 1118-1125.

Christensen, N.H. and Haahr, F. (1992). "A computer program to analyse suction effects", *Offshore Technology Conference*, Houston, USA. Paper number: OTC 6845.

Clukey, E.C., Templeton, J.S., Randolph, M.F. and Phillips, R. (2004). "Suction caisson response under sustained loop current loads", *Offshore Technology Conference*, Houston, USA. Paper: OTC 16843.

Colliat, J-L., Boisard, P., Andersen, K. and Schoeder, K. (1995). "Caisson foundations as alternative anchors for permanent mooring of a process barge offshore Congo", *Offshore Technology Conference*, Houston, USA. Paper: OTC 7797.

Colliat, J-L., Boisard, P., Gramet, J-C. and Sparrevik, P. (1996). "Design and installation of suction anchor piles at a soft clay site in the Gulf of Guinea", *Offshore Technology Conference*, Houston, USA. Paper: OTC 8150.

Colliat, J-L. (2002). "Anchors for deepwater to ultradeepwater moorings", *Offshore Technology Conference*, Houston, USA. Paper: OTC 14306.

Colliat, J-L. and Dendani, H. (2002). "Girassol: geotechnical design analyses and installation of suction anchors", *Proc. SUT Offshore Site Investigation and Geotechnics*, 107-119.

Cubrinovski, M. and Ishihara, K. (2002). "Maximum and minimum void ratio characteristics of sands", *Soils and Foundations,* 42(6), 65-78.

Deng, W. and Carter, J.P. (2000). "Inclined uplift capacity of suction caissons in sand", *Offshore Technology Conference*, Houston, USA. Paper: OTC 12196.

Deng, W. and Carter, J.P. (2002). "A theoretical study of the vertical uplift capacity of suction caissons", *International Journal of Offshore and Polar Engineering*, 12(2), 89-97.

Dyvik, R., Andersen, K.H., Hansen, S.B. and Christophersen, H.P. (1993). "Field tests of anchors in clay I: Description", *ASCE Journal of Geotechnical Engineering*, 119(10), 1515-1531.

El-Gharbawy, S.L., Olson, R.E. and Scott, S.A. (1999). "Suction anchor installation for deep Gulf of Mexico applications", *Offshore Technology Conference*, Houston, USA. Paper: OTC 10992.

Erbrich, C.T. and Tjelta, T.I. (1999). "Installation of bucket foundations and suction caissons in sand - Geotechnical performance". *Offshore Technology Conference*, Houston, USA. Paper: OTC 10990.

Erbrich, C. and Hefer, P. (2002). "Installation of the Laminaria suction piles – A case history", *Offshore Technology Conference*, Houston, USA. Paper: OTC 14240.

Fakharian, K. and Rismanchian, A. (2004). "A new method for reduction of trial and error in design of suction piles and its application in the Caspian Sea", *Proc. 14th*

International Offshore and Polar Engineering Conference, Toulon, France, 2, 545-551.

Feld, T., Rasmussen, J.L. and Sorensen, P.H. (1999). "Structural and economic optimisation of offshore wind turbine support structure and foundation", *Proc. 18th International Conference on Offshore Mechanics and Artic Engineering*, St John's, Canada.

Feld, T. (2001). "Suction buckets, a new innovative foundation concept, applied to offshore wind turbines", *PhD thesis*, Aalborg University, Demark.

Fines, S., Stove, O.J. and Guldberg, F. (1991). "Snorre TLP tethers and foundation", *Offshore Technology Conference*, Houston, USA. Paper: OTC 6623.

Fuglsand, L.D. and Stensen-Bach, J.O. (1991). "Breakout resistance of suction piles in clay", *Proc. International Conference Centrifuge 91*, Colorado, USA, 153-159.

Goodman, L.J., Lee, C.N. and Walker, F.J. (1961). "Feasibility of vacuum anchorage in soil", Correspondence, *Géotechnique*, 11(4), 356-359.

Haland, G. (2002). "Pro's and con's of foundations used for the Aasgard field development", *Proc. SUT Offshore Site Investigation and Geotechnics*, 93-105.

Helfrich, S.C., Brazill, R.L. and Richards, A.F. (1976). "Pullout characteristics of a suction anchor in sand", *Offshore Technology Conference*, Houston, USA. Paper number: OTC 2469.

Hesar, M. (2003). "Geotechnical design of the Barracuda and Caratinga suction anchors", *Offshore Technology Conference*, Houston, USA. Paper: OTC 15137.

Hogervorst, J.R. (1980). "Field trials with large diameter suction piles", *Offshore Technology Conference*, Houston, USA. Paper: OTC 3817.

Houlsby, G.T. and Byrne, B.W. (2000). "Suction caisson foundations for offshore wind turbines and Anemometer masts". *Wind Engineering*, 24 (4), 249-255.

Houlsby, G.T. and Byrne, B.W. (2005)[a]. "Design procedures for installation of suction caissons in clay and other soils", *Proc. ICE - Geotechnical Engineering*, 158(2), 75-82.

Houlsby, G.T. and Byrne, B.W. (2005)[b]. "Design procedures for installation of suction caissons in sand", *Proc. ICE - Geotechnical Engineering*, 158(3), 135-144.

House, A.R., Randolph, M.F. and Borbas, M.E. (1999). "Limiting aspect ratio for suction caisson installation in clay", *Proc. 9th International Offshore and Polar Engineering Conference*, Brest, France, 676-683.

House, A.R. (2002). "Suction caisson foundations for buoyant offshore facilities", *PhD thesis*, University of Western Australia, Australia.

Huang, J.T. (1994). "The effects of density and cementation on cemented sands", *PhD thesis*, University of Sydney, Australia.

Iskander, M.G., Olson, R.E. and Pavlicek, R.W. (1993). "Behavior of suction piles in sand", *Proc. Design and Performance of Deep Foundations*, Dallas, USA, 157-171.

Iskander, M., El-Gharbawy, S. and Olson, R. (2002). "Performance of suction caisson in sand and clay", *Canadian Geotechnical Journal*, 39, 576-584.

Kelly, R.B., Byrne, B.W., Houlsby, G.T. and Martin, C.M. (2004). "Tensile loading of model caisson foundations for structures on sand", *Proc. 14th International Offshore and Polar Engineering Conference*, Toulon, France, 2, 638-641.

Kim, Y., Kim, S., Park, J., Kim, S., Kim, H. and Kim, K. (2001). "A centrifuge study of suction pile installation in sand", *Proc. 11th International Offshore and Polar Engineering Conference*, Stavanger, Norway, 2, 615-619.

Kishida, H. and Uesugi, M. (1987). "Tests of the interface between sand and steel in simple shear apparatus", *Géotechnique*, 37(1), 45-52.

Lacasse, S. (1999). "Ninth OTRC Honors Lecture: Geotechnical contributions to offshore development", *Offshore Technology Conference*, Houston, USA. Paper: OTC 10822.

Larsen, P. (1989). "Suction anchors as an anchoring system for floating offshore construction", *Offshore Technology Conference*, Houston, USA. Paper number: OTC 6029.

Mackereth, F.J.H. (1958). "A portable core sampler of lake deposits", *Limnology and Oceanography*, 3(2), 181-191.

Masui, N., Yoneda, H., Zenda, Y., Ito, M., Iida, Y. and Hermstad, J. (2001). "Installation of offshore concrete structure with skirt foundation", *Proc. 11th International Offshore and Polar Engineering Conference*, Stavanger, Norway, 2, 626-630.

Masui, N., Ito, M., Inoue, A., Shimada, Y. and Hermstad, J. (2004). "Recovery of wall friction after penetration in skirt suction foundation", *Proc. 14th International Offshore and Polar Engineering Conference*, Toulon, France, 2, 462-646.

Mello, J.R.C., Moretti, M.J., Sparrevik, P., Schoder, K. and Hansen, S.B. (1998). "P19 and P26 moorings at the Marlim field. The first permanent taut leg mooring with fibre rope and suction anchors", *Proc. FPS'98 Conference on Floating and Production Systems*, 1-11.

Newlin, J.A. (2003). "Suction anchor piles for the Na Kita FDS mooring system. Part 2: Installation performance", *Proc. International Symposium on Deep Mooring Systems*, Houston, USA, 55-75.

North Sea report (1972). "Submersible sounding tools to test North Sea floor", *The Oil and Gas Journal*, 74-77.

Randolph, M.F., Jewell, R.J., Stone, K.J.L., Brown, T.A. (1991). "Establishing a new centrifuge facility", *Proc. International Conference Centrifuge 1991*, Colorado, USA, 3-9.

Randolph, M.F., O'Neil, M.P. and Stewart, D.P. (1998). "Performance of suction anchors in fine-grained calcareous soils", *Offshore Technology Conference*, Houston, USA. Paper: OTC 8831.

Rauch, A.F., Olson, R.E., Luke, A.M. and Mecham, E.C. (2003). "Measured response during laboratory installation of suction caissons", *Proc. 13th International Offshore and Polar Engineering Conference*, Honolulu, USA, 2, 780-787.

Riemers, M. (2005). Managing Director, *SPT Offshore B.V.*, the Netherlands. Private conversation.

Rusaas, P., Giske, S.R., Barrett, G., Christiansen, P.E. and Baerheim, M. (1995). "Design, operations planning and experience from the marine operations for the Europipe jacket with bucket foundations", *Offshore Technology Conference*, Houston, USA. Paper: OTC 7794.

Salgado, R., Bandini, P. and Karim, A. (2000). "Shear strength and stiffness of silty sand", *Journal of Geotechnical and Geoenvironmental Engineering*, 126(5), 451-462.

Schofield, A.N. (1980). "Cambridge Geotechnical Centrifuge Operations", *Géotechnique*, 30(3), 227-268.

Senpere, D. and Auvergne, G.A. (1982). "Suction anchor piles – A proven alternative to driving or drilling", *Offshore Technology Conference*, Houston, USA. Paper: OTC 4206.

Sohota, B.S. and Wilson, Q. (1982). "The break-out behaviour of suction anchors embedded in submerged sands", *Offshore Technology Conference*, Houston, USA. Paper number: OTC 4175.

Solhjell, E., Sparrevik, P., Haldorsen, K. and Karlsen, V. (1998). "Comparison and back calculation of penetration resistance from suction anchor installation in soft to stiff clay at the Njord and Visund fields in the North Sea", *Proc. SUT Conference on Offshore Site Investigation and Foundation Behaviour '98*, 325-349.

Sparrevik, P. (1998). "Suction anchors – A versatile foundation concept finding its place in the offshore market", *Proc. 17th International Conference on Offshore Mechanics and Artic Engineering*, Lisbon, Portugal. Paper: OMAE98-3096.

Sparrevik, P. (2002). "Suction pile technology and installation in deep water", *Offshore Technology Conference*, Houston, USA. Paper: OTC 14241.

Steenseb-Bach, J.O. (1992). "Recent model tests with suction piles in clay and sand", *Offshore Technology Conference*, Houston, USA. Paper number: OTC 6844.

Stevenson, P.R. (2003). "Large scale instrumented offshore suction caisson tests to study set-up around suction caissons", *Suction caisson research report*, Fugro-McClelland Geosciences, Inc.

Stove, O.J., Bysveen, S. and Christophersen, H.P. (1992). "New Foundation Systems for the Snorre development", *Offshore Technology Conference*, Houston, USA. Paper: OTC 6882.

Supachawarote, C., Randolph, M. F. and Gourvenec, S. (2004). "Inclined pull-out capacity of suction caissons", *Proc. 14th International Offshore and Polar Engineering Conference*, Toulon, France, 2, 500-506.

Taylor, R.N. (ed.) (1995). Geotechnical centrifuge technology. 1st edition, Glasgow: Blackie Academic & Professional.

Tjelta, T.I., Guttormsen, T.R. and Hermstad, J. (1986). "Large-scale penetration test at a deepwater site", *Offshore Technology Conference*, Houston, USA. Paper: OTC 5103.

Tjelta, T.I., Aas, P.M., Hermstad, J. and Andenaes, E. (1990). "The skirted piled Gullfaks C platform installation", *Offshore Technology Conference*, Houston, USA. Paper: OTC 6473.

Tjelta, T.I (1995). "Geotechnical experience from the installation of the Europipe jacket with bucket foundations", *Offshore Technology Conference*, Houston, USA. Paper: OTC 7795.

Tjelta, T.I. (2001). "Suction piles: Their position and application today", *Proc. 11th International Conference on Offshore and Polar Engineering*, Stavanger, Norway, 2, 1-6.

Vardoulakis, I. (2004). "Fluidisation is artesian flow conditions: Hydromechanically stable granular media", *Géotechnique*, 54(2), 117-130.

Wang, M.C., Nacci, V.A. and Demars, K.R. (1975). "Behaviour of underwater suction anchor in soil", *Ocean Engineering*, 3, 47-62.

Wang, M.C., Demars, K.R. and Nacci, V.A. (1977). "Breakout capacity of model suction anchors in soil", *Canadian Geotechnical Journal*, 14, 246-257.

Watson, P.G. and Randolph, M.F. (1997). "Vertical capacity of caisson foundations in calcareous sediments", *Proc. 7th International Offshore and Polar Engineering Conference*, Honolulu, USA, 2, 784-790.

Watson, P.G. (1999). "Performance of skirted foundations for offshore structures", *PhD thesis*, University of Western Australia, Australia.

White, D.J. and Take, W.A. (2002). "GeoPIV: Particle Image Velocimetry (PIV) software for use in geotechnical testing". Software manual.

White, D.J., Take, W.A., Bolton, M.D. (2003). "Soil deformation measurement using particle image velocimetry (PIV) and photogrammetry", *Géotechnique*, 53(7), 619-631.

Wilson, Q. and Sohota, B.S. (1980). "Pull-out parameters for buried suction anchors", *Offshore Technology Conference*, Houston, USA. Paper number: OTC 3816.

Yang, S.L., Grande, L.O., Qi, J.F. and Feng, X.L. (2003). "Excessive soil plug and anti-failure mechanism of bucket foundation during penetration by suction". *Proc. 13rd International Offshore and Polar Engineering Conference*, Honolulu, USA, 2, 660-665.

Zdravkovic, L., Potts, D.M. and Jardine, R.J. (2001). "A parametric study of the pullout capacity of bucket foundations in soft clay", *Géotechnique*, 51(1), 55-67.

Table 1.1. Some significant field applications of suction caissons.

Year		Name	Size D × L	Purpose	Water depth	Soil			References
						Clay	Sand	Layered	
Before 1995	1958*	Sampler[1]	0.45×1.2m	Anchoring	20-80m	✓			Mackereth (1958)
	1972	Sounding tool[2]	~3m*	Anchoring	>20m*		✓*		North Sea Report (1972)
	1980	Gorm[2]	3.5×8.5-9m	Anchoring	40m			✓	Senpere and Auvergne (1982)
	1989	Gullfaks C[2]	28×22m	Foundation	218m			✓	Tjelta et al. (1990)
	1991	Snorre	17×12m	Anchoring	330m	✓			Fines et al. (1991); Stove et al. (1992); Dyvik et al. (1993)
	1994	Draupner E[2]	12×6m	Foundation	70m		✓		Bye et al. (1995); Rusaas et al. (1995); Tjelta (1995)
The last decade 1995 - cuurent	1995	Nkossa[3]	4.5-5×12m	Mooring	200m	✓			Colliat et al. (1995); Colliat et al. (1996);
	1995	Harding[2]	5×8-10m	Mooring	110m			✓	Sparrevik (1998)
	1995	YME[2]	5×7m	Mooring	100m			✓	Sparrevik (1998)
	1996	Norne[2]	5×10m	Mooring	350m	✓			Sparrevik (1998)
	1996	Sleipner T[2]	14×5m	Foundation	-		✓		Bye et al. (1995); Lacasse (1999)
	1997	Njord[2]	5×9-10m	Mooring	330m	✓			Solhjell et al. (1998)
	1997	Curlew[2]	5-7×10-13m	Mooring	90m			✓	Alhayari (1998)
	1997	Aquila[4]	4.5-5×16m	Mooring	850m	✓			Alhayari (1998)
	1997	Visund[2]	5×11m	Mooring	335m	✓			Solhjell et al. (1998)
	1997	Lufeng[5]	5×10m	Mooring	30m	✓			Sparrevik (1998), Andersen et al (2005)[a]
	1997	Marlim P19-P26[6]	4.8×13.5m	Mooring	720-1050m	✓			Mello et al. (1998)
	1998	Laminaria[7]	5.5×13m	Mooring	400m	✓**			Erbrich and Hefer (2002)
	1998	Marlim P33-P35[6]	4.7-17m	Mooring	780-850m	✓			Barusco (1999)
	1998	Aasgard A[2]	5×11m	Mooring	350m	✓			Haland (2002)
	1999	Kuito[3]	3.5×11-14m	Mooring	400m	✓			Tjelta (2001); Andersen et al. (2005)[a]
	1999	Aasgard B and C[2]	5×10-12m	Mooring	350m	✓			Haland (2002); Andersen et al. (2005)[a]
	2000	Misaki[8]	18×5m***	Foundation	25m			✓	Masui et al. (2001)
	2001	Hanze[2]	6.5×6.2m	Mooring	42m			✓	Aas et al. (2002); Sparrevik (2002)
	2001	Girassol[3]	4.5-8×10-20m	Mooring	1400m	✓			Colliat and Dendani (2002)
	2002	Calder[9]	9.5×5.75m	Foundation	33m		✓		Bussemaker (2005)
	2002	Horn Mountain[10]	6×30-32m	Anchoring	1800m	✓			Audibert et al. (2003)
	2002	Na Kita[10]	4.3×24m	Mooring	1920m	✓			Newlin (2003)
	2003	Barracuda & Caratinga[6]	5×16.5m	Mooring	825-1030m	✓			Hesar (2003); Andersen et al. (2005)[a]
	2003	Bonga[3]	5×16-17.5m	Mooring	980m	✓			Andersen et al. (2005)[a]
	2004	Thunder Horse[10]	5.5×27.5m	Mooring	1830m	✓			Andersen et al. (2005)[a]

* : not clearly stated. ** : calcareous soil, but behaviour very similar to clay

***: the suction compartments form a ring shape

1: UK lakes 2: North Sea 3: West Africa 4: Adriatic Sea 5: South China Sea
6: Brazil 7: Timor Sea 8: Japan 9: Irish Sea 10: Gulf of Mexico

Table 1.2. Studies on installation of suction caisson in sand.

Reference	Year	Research Group	Test			Pene. Predict.	Brief summary
			1g	Centrifuge	Field		
Hogervorst (1980)	Late 1970s	Shell			✓	✓	Field installation of large caissons. Observed force reduction. Proposed a CPT-based soil resistance prediction.
Tjelta et al. (1986)	1985	Statoil, NGI			✓		Field installation of instrumented concrete panel, penetrated by 2 large suction caissons
Larsen (1989)	1987	Danish Geo. Inst.	✓				Brief discussions on installation in sand, where heave and force reduction were observed.
Iskander et al. (1993); Iskander et al. (2002);	1993 2002	Univ. of Texas, Austin	✓				Suction installations in sand by min. and max. vacuum.
Tjelta (1995), Erbrich and Tjelta (1999)	1993-1994	NGI	✓				Installation tests of highly instrumented suction caisson, in preparation for Draupner E, Sleipner T installations
Allersma et al. (1997), Allersma et al. (2001)[b]; Allersma (2003)	1997-2003	Delft Univ.		✓			Suction installations in sand study. Include both continuous installation and installation in pulses.
Bang et al. (1999); Kim et al. (2001); Cho et al. (2002);	1999 2002	South Dakota School of Mines	✓	✓			1g and centrifuge studies of suction installation by min. vacuum. Proposed the "mobilised effective soil friction angle ratio" concept.
Feld (2001)	2001	Aalborg Univ.				✓	Proposed a CPT-based penetration prediction method.
Yang et al. (2003)	2003	Nor. Univ. of Sci.& Tech.	✓				Suction installation in silt.
Houlsby and Byrne (2005)[b]	2005	Oxford Univ.				✓	Analytical method to predict the suction pressure during installation in sand.

Table 2.1: 1g caisson models.

Caisson dimensions (D × L_{max} × t)* (mm)	**L_{max}/D**	**t/D**
100 × 100 × 0.5	1	0.5%
70 × 140 × 0.35	2	0.5%
80 × 140 × 0.8	1.75	1.0%
80 × 140 × 1.6	1.75	2.0%

*diameter × total wall length × wall thickness.

Table 2.2: Scaling factors in centrifuge tests.

	Prototype/Centrifuge
Gravity level	1/n
Length	n
Area	n^2
Volume	n^3
Force	n^2
Time (dynamic)	n
Time (diffusion)	n^2

Table 2.3: Centrifuge caisson models.

Caisson dimensions D × L_{max} × t * (mm)	**L_{max}/D**	**t/D**
60 × 60 × 0.3	1.0	0.5 %
60 × 60 × 0.6	1.0	1.0 %
100 × 100 × 0.5	1.0	0.5 %

*diameter × total wall length × wall thickness.

Table 2.4a: PIV tests conducted.

Test no.	Half-caisson model $D \times L_{max} \times t$ (mm)*	Soil type	Soil γ' (kN/m^3)	L/D	Remarks
PIV-S1	100 × 100 × 1.2	Silica sand	10	0.10	-
PIV-S2	100 × 100 × 1.2	Silica sand	10	0.20	-
PIV-S3	100 × 100 × 1.2	Silica sand	10	0.30	-
PIV-L1	100 × 100 × 1.2	Layered sand-silt	10	0.20	Wall tip above silt layer
PIV-L2	100 × 100 × 1.2	Layered sand-silt	10	0.25	Wall tip within silt layer
PIV-L3	100 × 100 × 1.2	Layered sand-silt	10	0.30	Wall tip below silt layer

*diameter × total wall length × wall thickness.

Table 2.4b: 1g installation tests conducted.

Test no.	Caisson $D \times L_{max} \times t$ (mm)*	Caisson mass (grams)	Soil type	Soil γ' (kN/m^3)	Average rate (mm/s)
S1g-70-260-S	70 × 140 × 0.35	260	Silica sand	10	0.5
S1g-70-260-F	70 × 140 × 0.35	260	Silica sand	10	11
S1g-70-410-F	70 × 140 × 0.35	410	Silica sand	10	12
S1g-80(1.0)-260-S	80 × 140 × 0.8	260	Silica sand	10	0.5
S1g-80(1.0)-260-F	80 × 140 × 0.8	260	Silica sand	10	8.0
S1g-80(2.0)-260-S	80 × 140 × 1.6	260	Silica sand	10	0.7
S1g-80(2.0)-260-F	80 × 140 × 1.6	260	Silica sand	10	8.0
S1g-100-260-S	100 × 100 × 0.5	260	Silica sand	10	0.3
S1g-100-260-SV	100 × 100 × 0.5	260	Silica sand	10	0.05-0.4 (varying)
S1g-100-260-F	100 × 100 × 0.5	260	Silica sand	10	6.5
S1g-100-260-SFS	100 × 100 × 0.5	260	Silica sand	10	0.4-6.0 (sudden)
S1g-100-260-SFG	100 × 100 × 0.5	260	Silica sand	10	0.4-6.0 (gradual)
S1g-100-460-S	100 × 100 × 0.5	460	Silica sand	10	0.4
S1g-100-360-F	100 × 100 × 0.5	360	Silica sand	10	6.5
S1g-100-410-F	100 × 100 × 0.5	410	Silica sand	10	6.5
S1g-100-460-F	100 × 100 × 0.5	460	Silica sand	10	6.5
S1g-100-260-restr.	100 × 100 × 0.5	260	Silica sand	10	Caisson restrained
Ox-150-1	150 × 150 × 1.5	2500	Redhill silica sand	8	0.2
Ox-150-2	150 × 150 × 1.5	2500	Redhill silica sand	8	2.5
Ox-150-3	150 × 150 × 1.5	2500	Redhill silica sand	8	3.0
Ox-150-4	150 × 150 × 1.5	2500	Redhill silica sand	8	3.7
Ox-150-5	150 × 150 × 1.5	2500	Redhill silica sand	8	6.0
Ox-150-6	150 × 150 × 1.5	2500	Redhill silica sand	8	7.5
Ox-150-7	150 × 150 × 1.5	2500	Redhill silica sand	8	9.5
Ox-150-8	150 × 150 × 1.5	2500	Redhill silica sand	8	9.7
Ox-150-9	150 × 150 × 1.5	2500	Redhill silica sand	8	0.05-0.1 (varying)
Top silt-100-S	100 × 100 × 0.5	260	Sand-silt (profile 1)	10	0.3
Top silt-100-F	100 × 100 × 0.5	260	Sand-silt (profile 1)	10	6.5
Mid silt 1-100-S	100 × 100 × 0.5	260	Sand-silt (profile 2)	10	0.4
Mid silt 1-100-SF	100 × 100 × 0.5	260	Sand-silt (profile 2)	10	0.3-4.0 (sudden)
Mid silt 2-100-F	100 × 100 × 0.5	260	Sand-silt (profile 3)	10	6.0

* diameter × total wall length × wall thickness.

Table 2.4c: Centrifuge installation tests conducted.

Test no.	Caisson $D \times L_{max} \times t$ (mm)*	Caisson mass (grams)	Soil type	Soil γ' (kN/m^3)	g-level
S-60(0.5)-jacked	60 × 60 × 0.3	-	Silica sand	10	100
S-60(1.0)-jacked	60 × 60 × 0.6	-	Silica sand	10	100
S-60(0.5)-29-120g	60 × 60 × 0.3	29	Silica sand	10	120
S-60(0.5)-50	60 × 60 × 0.3	50	Silica sand	10	100
S-60(0.5)-50-deeper	60 × 60 × 0.3	50	Silica sand	10	100
S-60(0.5)-50-deepest	60 × 60 × 0.3	50	Silica sand	10	100
S-60(0.5)-100	60 × 60 × 0.3	100	Silica sand	10	100
S-60(0.5)-100-low Q	60 × 60 × 0.3	100	Silica sand	10	100
S-60(0.5)-150	60 × 60 × 0.3	150	Silica sand	10	100
S-60(1.0)-50	60 × 60 × 0.6	50	Silica sand	10	100
S-60(1.0)-150	60 × 60 × 0.6	150	Silica sand	10	100
S-100-150	100 × 100 × 0.5	150	Silica sand	10	100
S-100-150-repeat	100 × 100 × 0.5	150	Silica sand	10	100
S-100-250	100 × 100 × 0.5	250	Silica sand	10	100
S-100-250-repeat	100 × 100 × 0.5	250	Silica sand	10	100
S-100-250-low Q	100 × 100 × 0.5	250	Silica sand	10	100
S-100-230-60g	100 × 100 × 0.5	230	Silica sand	10	60
S-100-133-72g	100 × 100 × 0.5	133	Silica sand	10	72
C-60(0.5)-jacked	60 × 60 × 0.3	-	Calcareous sand	6	100
C-60(0.5)-jacked-repeat	60 × 60 × 0.3	-	Calcareous sand	6	100
C-60(1.0)-jacked	60 × 60 × 0.6	-	Calcareous sand	6	100
C-60(0.5)-50	60 × 60 × 0.3	50	Calcareous sand	6	100
C-60(0.5)-100	60 × 60 × 0.3	100	Calcareous sand	6	100
C-60(0.5)-100-deeper	60 × 60 × 0.3	100	Calcareous sand	6	100
C-60(0.5)-150	60 × 60 × 0.3	150	Calcareous sand	6	100
C-60(1.0)-150	60 × 60 × 0.6	150	Calcareous sand	6	100
C-100-150	100 × 100 × 0.5	150	Calcareous sand	6	100
M-60(0.5)-10%	60 × 60 × 0.3	150	Mixed (10% silt)	10	100
M-60(0.5)-20%	60 × 60 × 0.3	150	Mixed (20% silt)	10	100
M-60(0.5)-40%	60 × 60 × 0.3	150	Mixed (40% silt)	10	100
M-60(1.0)-10%	60 × 60 × 0.6	150	Mixed (10% silt)	10	100
1 m top silt-50	60 × 60 × 0.3	50	Sand-silt (profile 1)	10	100
1 m top silt-100	60 × 60 × 0.3	100	Sand-silt (profile 1)	10	100
1 m top silt-150	60 × 60 × 0.3	150	Sand-silt (profile 1)	10	100
0.5 m top silt-150	60 × 60 × 0.3	150	Sand-silt (profile 2)	10	100
0.5 m top silt-150-repeat	60 × 60 × 0.3	150	Sand-silt (profile 2)	10	100
0.8 m deep silt-50	60 × 60 × 0.3	50	Sand-silt (profile 3)	10	100
0.8 m deep silt-150	60 × 60 × 0.3	150	Sand-silt (profile 3)	10	100
2.0 m deep silt-150	60 × 60 × 0.3	150	Sand-silt (profile 4)	10	100
2 silt layers-50	60 × 60 × 0.3	50	Sand-silt (profile 5)	10	100
Weak layer-single	60 × 60 × 0.3	50	Cemented (profile 1)	6	100
Strong layer-single	60 × 60 × 0.3	50	Cemented (profile 2)	6	100
Weak strong-continuous	60 × 60 × 0.3	50	Cemented (profile 3)	6	100
Weak strong-separated	60 × 60 × 0.3	50	Cemented (profile 4)	6	100

* diameter × total wall length × wall thickness.

Notes: (for all tests in tables 2.4a,b and c)

- All sands were in very dense state (Dr ≈ 91%) except:
  - + The top sand layer in the centrifuge sand-silt profile 4 (i.e. in test 2.0m deep silt-150), which had $D_r \approx 60\%$, and
  - + The top sand layer in layered uncemented-cemented soil, which had $D_r \approx 80\%$.
- In the layered soils, the listed soil γ' applies to all materials, i.e.:
  - + $\gamma'_{silt} \approx \gamma'_{sand}$ =10 kN in layered sand-silt, and
  - + $\gamma'_{cemented\ sand} \approx \gamma'_{uncemented\ sand}$ = 6 kN in layered cemented-uncemented soil).
    (Details on soil properties are shown in Chapter 3).
- Permeability of the soils:
  - + Silica sand: $k = 1.0 \times 10^{-4}$ m/s
  - + Calcareous sand: $k = 1.5 \times 10^{-5}$ m/s (cemented and uncemented)
  - + Silica flour: $k = 1.3 \times 10^{-6}$ m/s
  - + Mixed soils: $k = 8 \times 10^{-5}$ m/s, 2×10^{-5} m/s and 0.6×10^{-5} m/s for soils with 10%, 20% and 40% fines content respectively.

Table 3.1: Summary of sand properties

Properties	**Silica sand**	**North Rankin sand**
Specific gravity $\mathbf{G_s}$	2.67	2.73
Dry weight $\boldsymbol{\gamma_d}$ (kN/m^3)	14.7 - 17.5	7.5 - 10.1
Saturated weight $\boldsymbol{\gamma_s}$ (kN/m^3)	19.0 - 20.6	14.0 - 16.2
Permeability **k** (m/s)	$1.0 - 3.0 \times 10^{-4}$	$0.15 - 1.5 \times 10^{-4}$
Void ratio **e**	0.49 - 0.78	1.65 - 2.59
Peak friction angle $\boldsymbol{\phi_p}$	43^0	40^0
Residual friction angle $\boldsymbol{\phi_r}$	38^0	40^0
Peak interface friction angle $\boldsymbol{\delta_p}$	22^0	19^0
Peak interface friction angle $\boldsymbol{\delta_r}$	19^0	15^0

Table 5.1: Recorded final heaves in silica sand (all in equivalent prototype units).

Test No.	**Remarks**	**Heave h**[(1)] (m)	**h/L**[(2)]
S-60(0.5)-50	500 kN self-weight	0.51	9 %
S-60(0.5)-100	500 kN surcharge	0.42	7 %
S-60(0.5)-150	1000 kN surcharge	0.47	9 %
S-60(0.5)-50-deeper	Arbitrarily pushed	0.46	8 %
S-60(0.5)-50-deepest	Arbitrarily pushed deeper	0.44	8 %
S-60(0.5)-29-120g	Tested at 120g	0.60	9 %
S-60(1.0)-50	Thicker-walled caisson	0.60	11 %
S-60(1.0)-150	Thicker-walled, 500 kN sur.	0.57	10 %

(1) Total sand heave measured at the end of the test (i.e. at final penetration depth)
(2) Heave ratio, i.e. ratio between the total heave and the final wall penetrated depth.

Table 5.2: Recorded final heaves in calcareous sand (all in equivalent prototype units).

Test No.	**Remarks**	**Heave h**[(1)] (m)	**h/L**[(2)]
C-60(0.5)-50	500 kN self-weight	0.10	1.7 %
C-60(0.5)-100	500 kN surcharge	0.04	0.7 %
C-60(0.5)-150	1000 kN surcharge	0.10	1.7 %
C-60(0.5)-100-deeper	Arbitrarily pushed deeper	0.05	0.8 %
C-60(1.0)-50	Thicker-walled caisson	0.12	2.0 %
C-100-150	100mm diameter caisson	0.11	1.1 %

(1) Total sand heave measured at the end of the test (i.e. at final penetration depth)
(2) Heave ratio, i.e. ratio between the total heave and the final wall penetrated depth.

(a) (b)

Figure 1.1: (a) Caisson in fabrication yard.
(b) Caisson with mooring chain and pad-eye (*Source: SPT Offshore B.V.*).

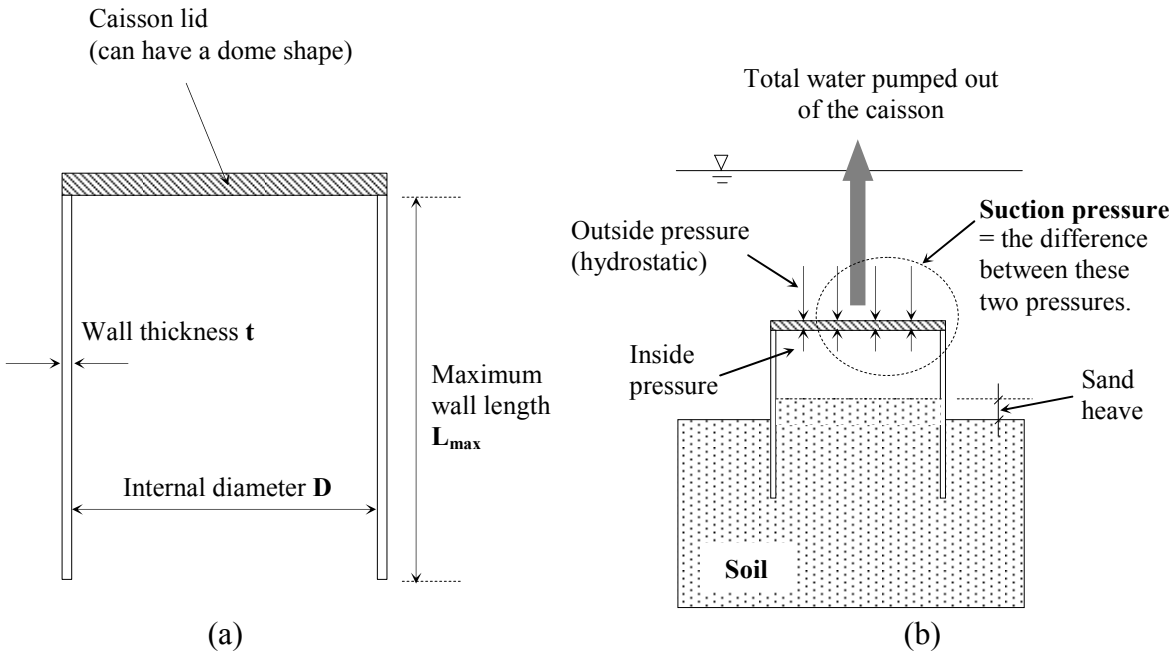

(a) (b)

Figure 1.2: (a) Definition of suction caisson components.
(b) Suction pressure definition.

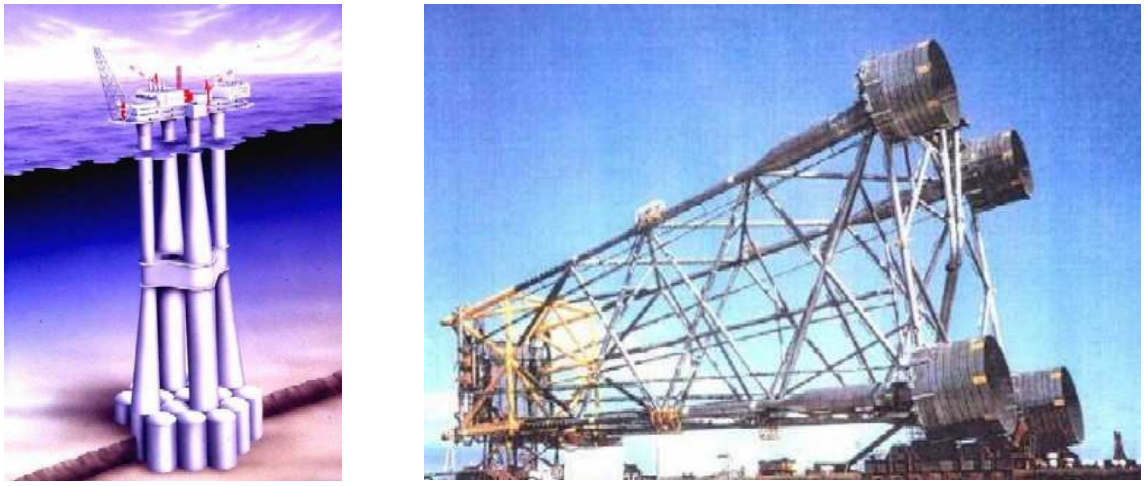

(a) (b)

Figure 1.3: (a) Gravity based platform using suction concrete cells.
(the Troll platform, similar to the Gullfaks C).
(b) Draupner E platform with suction caisson as foundation.
(*Source: NGI*).

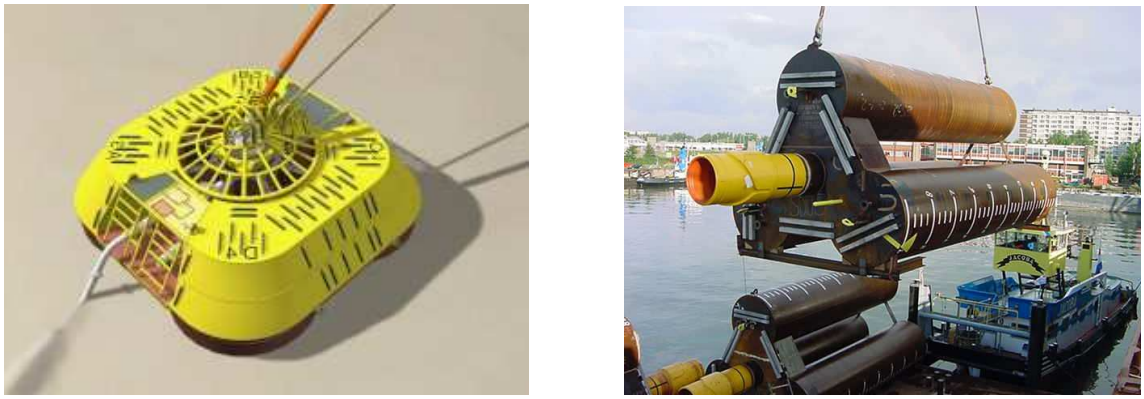

(a) Hanze 4-caisson cluster unit. (b) 3-caisson cluster.

Figure 1.4: Cluster caisson unit.
(*Source: (a) Sparrevik, 2002 (b) SPT Offshore B.V.*).

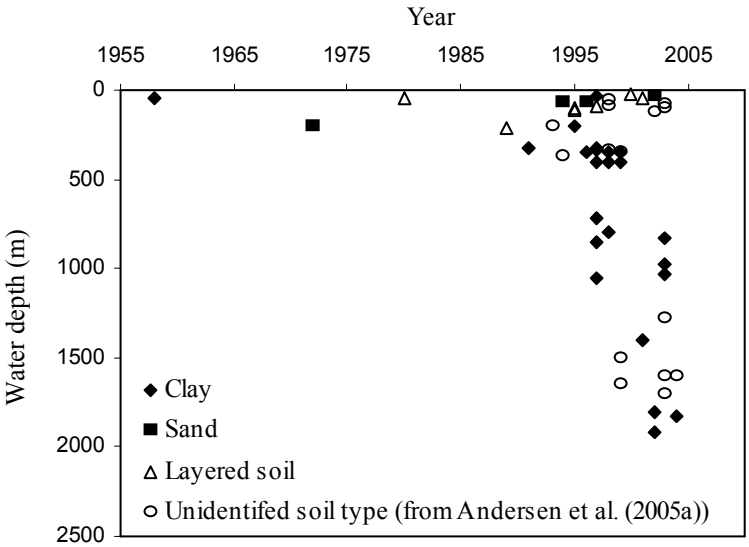

Figure 1.5: Field applications of suction caissons in a wide range of water depth. (from projects listed in Table 1.1 and Andersen et al, (2005)[a]).

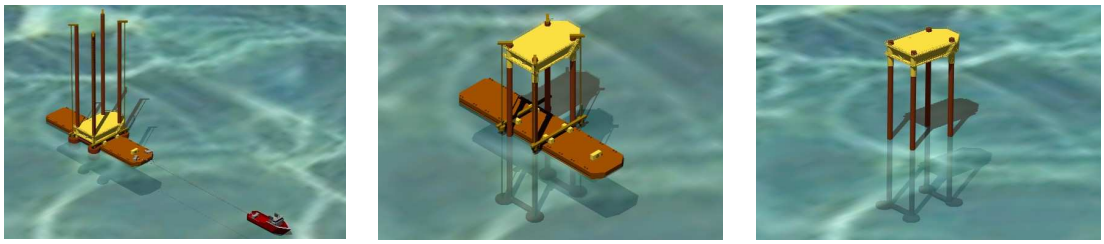

(a) Transported to site. (b) Lower legs and suction install. (c) Remove barge.

Figure 1.6: Self installation concept (*Source: SPT Offshore B.V.*).

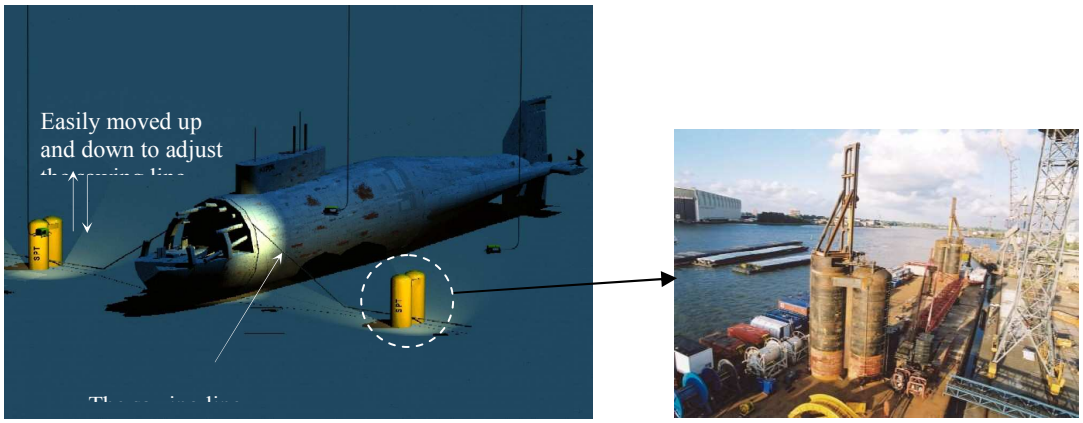

Figure 1.7: Suction caissons in the Kursk submarine salvage.

(*Source: SPT Offshore B.V.*).

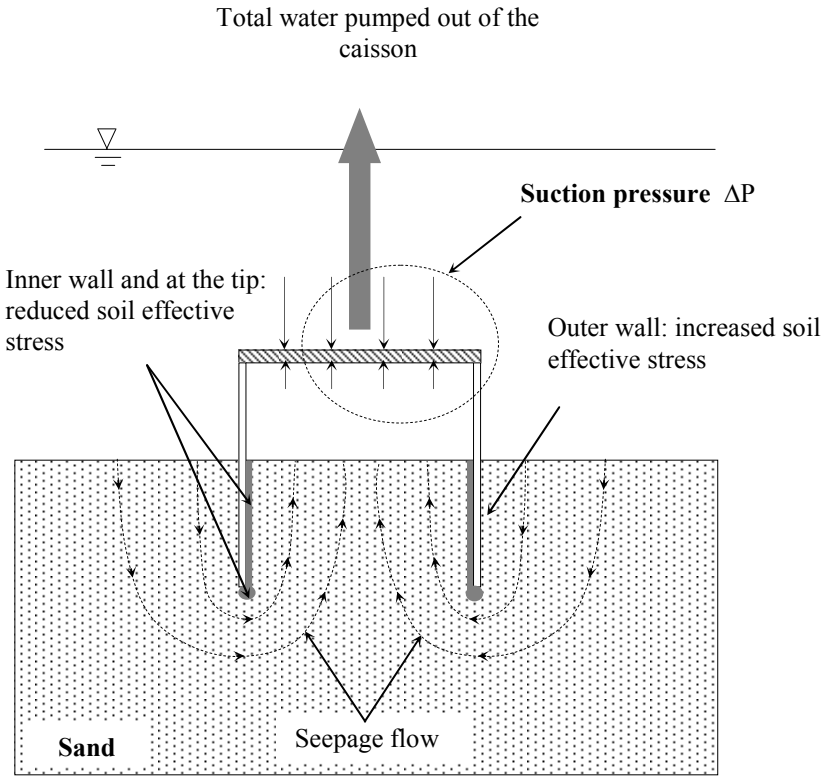

Figure 1.8: Effect of seepage gradient on soil effective stress.

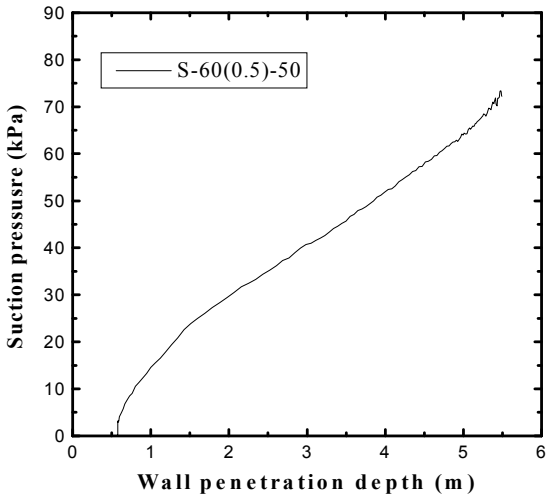

(a) Data in engineering units.

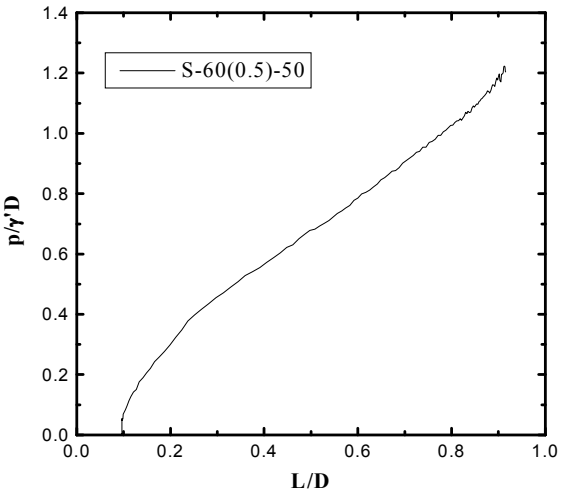

(b) Pressure normalised against D.

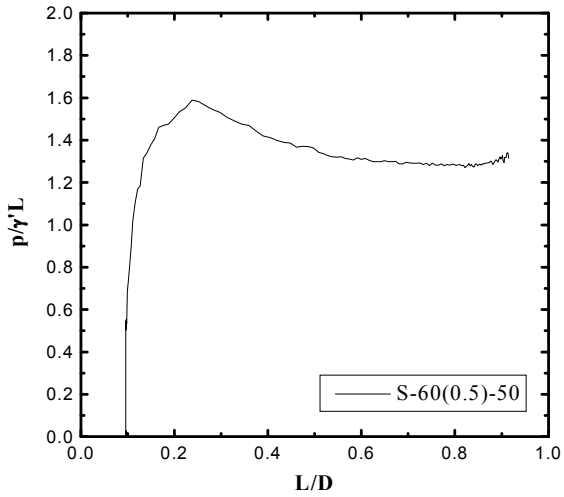

(c) Pressure normalised against L.

Figure 2.1: Normalisation of suction pressure data.

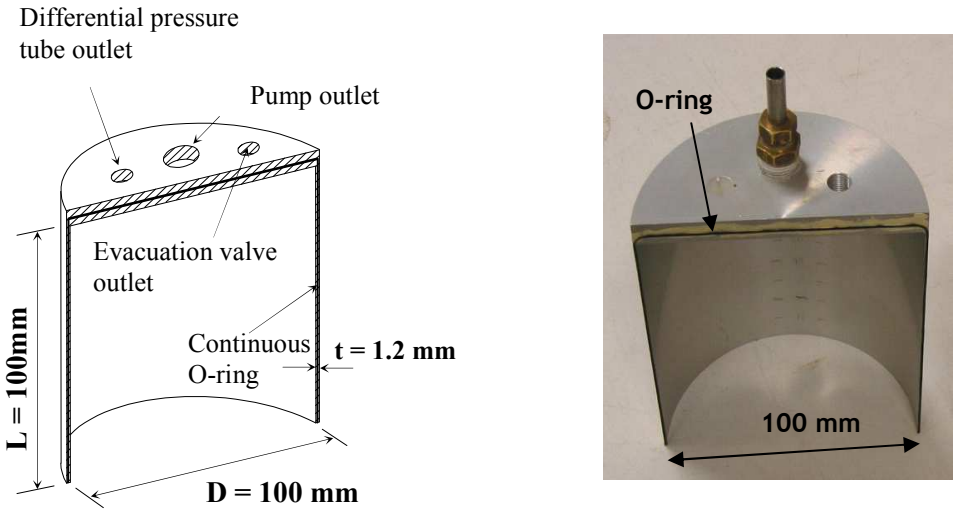

Figure 2.2: Half caisson model.

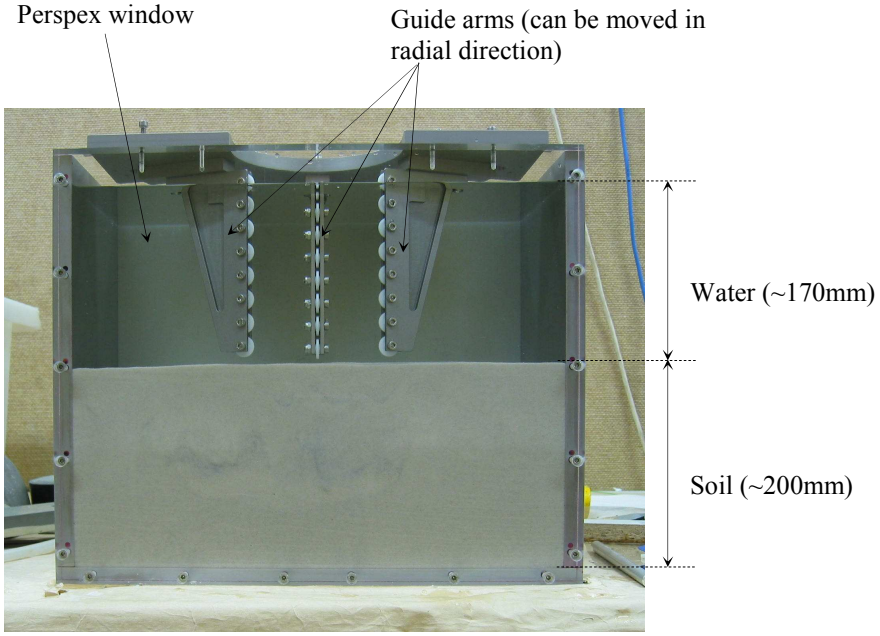

Figure 2.3: The test chamber and caisson guide for PIV tests.

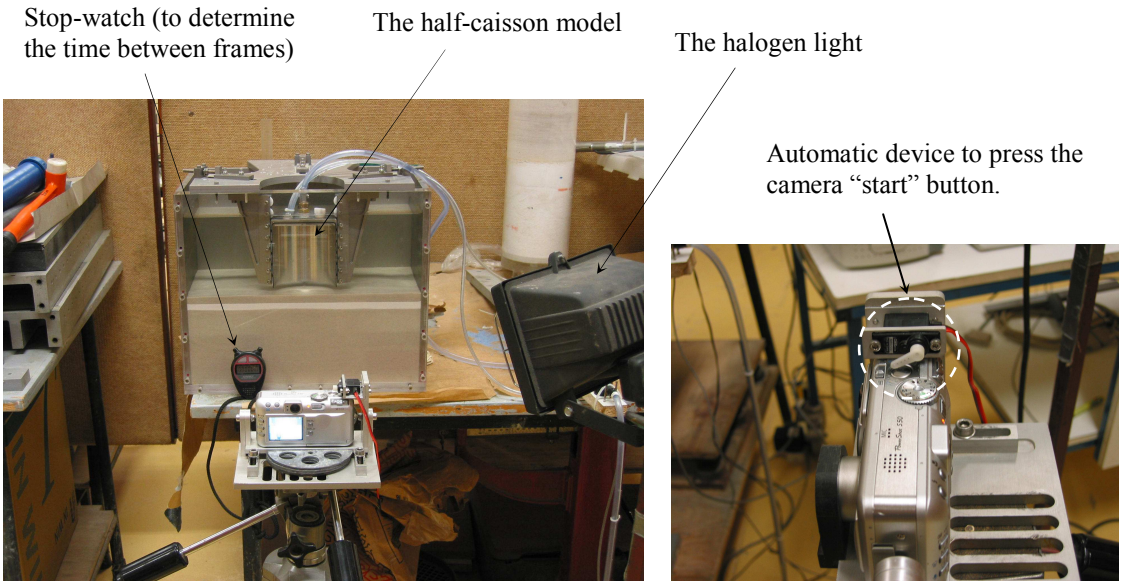

Figure 2.4: PIV test set-up and the automatic device for start the camera.

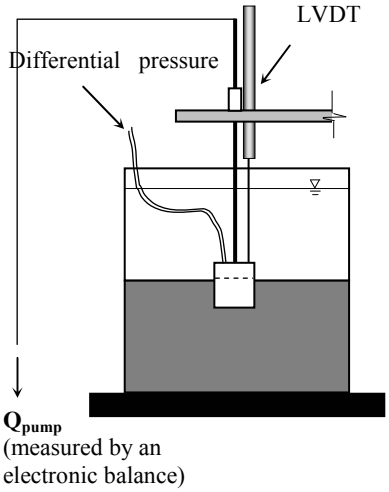

Figure 2.5: 1g test set-up.

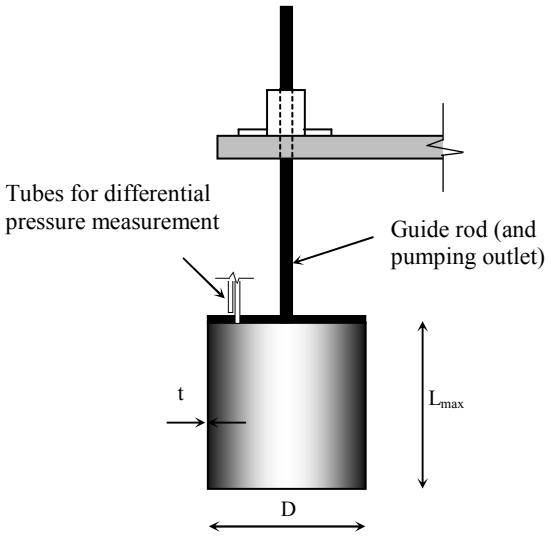

Figure 2.6: The 1g caisson model.

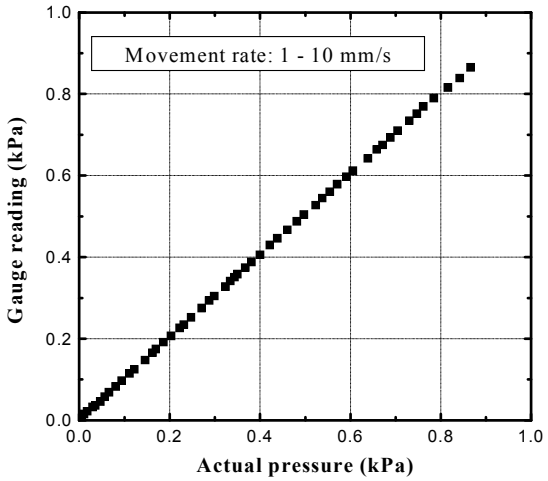

Figure 2.7: Effect of movement on the differential pressure gauge.

Figure 2.8: The geotechnical centrifuge at University of Western Australia (UWA).

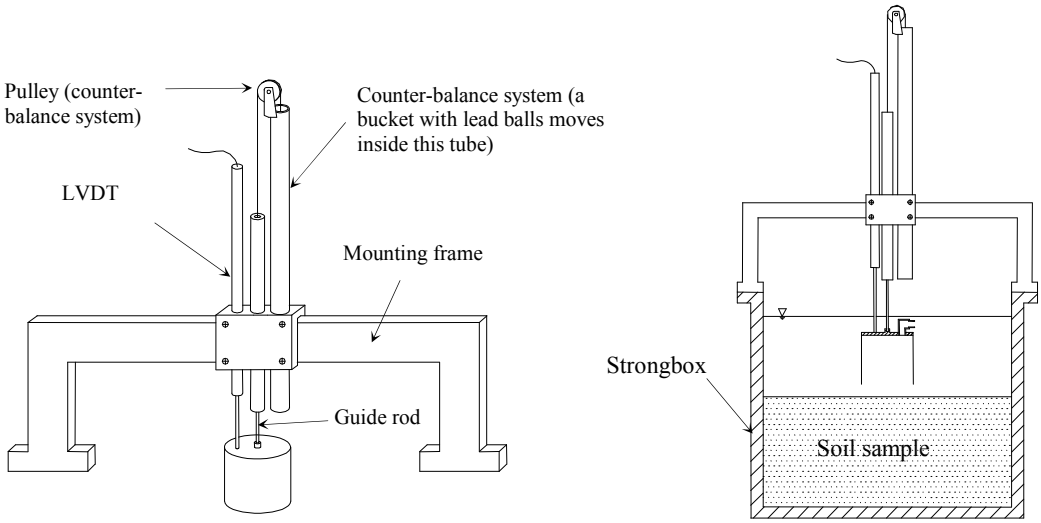

Figure 2.9: Centrifuge test apparatus.

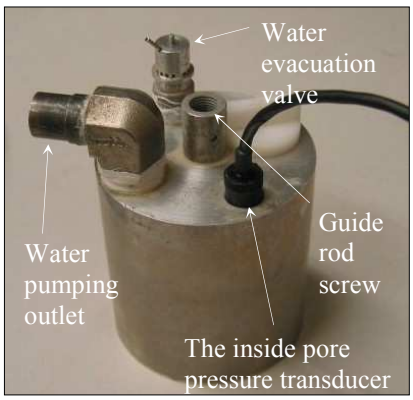

Figure 2.10: A typical centrifuge caisson model (60 mm diameter in this case).

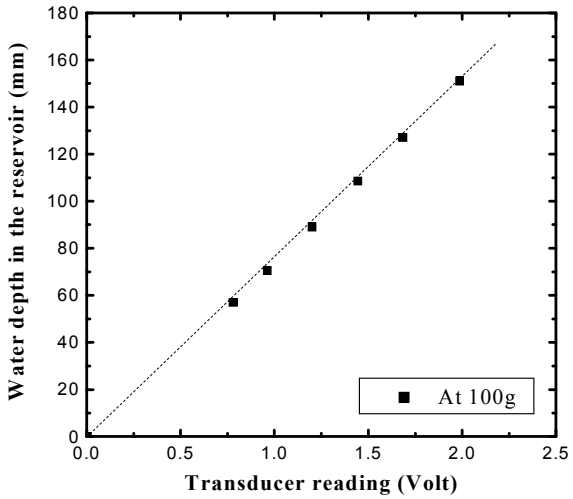

Figure 2.11: In-flight calibration of pressure transducer in the outflow reservoir.

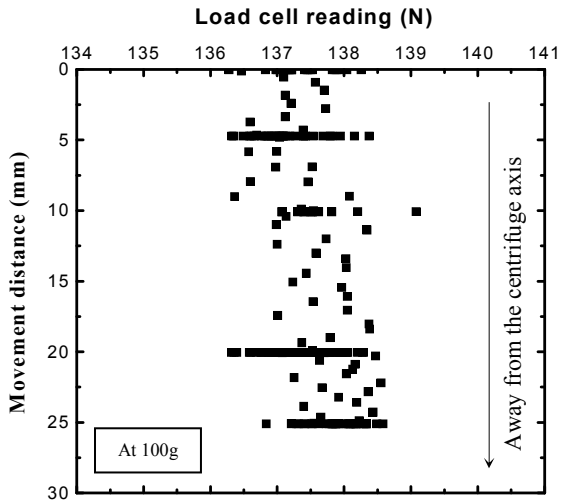

Figure 2.12: Effect of variations in radial length in the centrifuge.

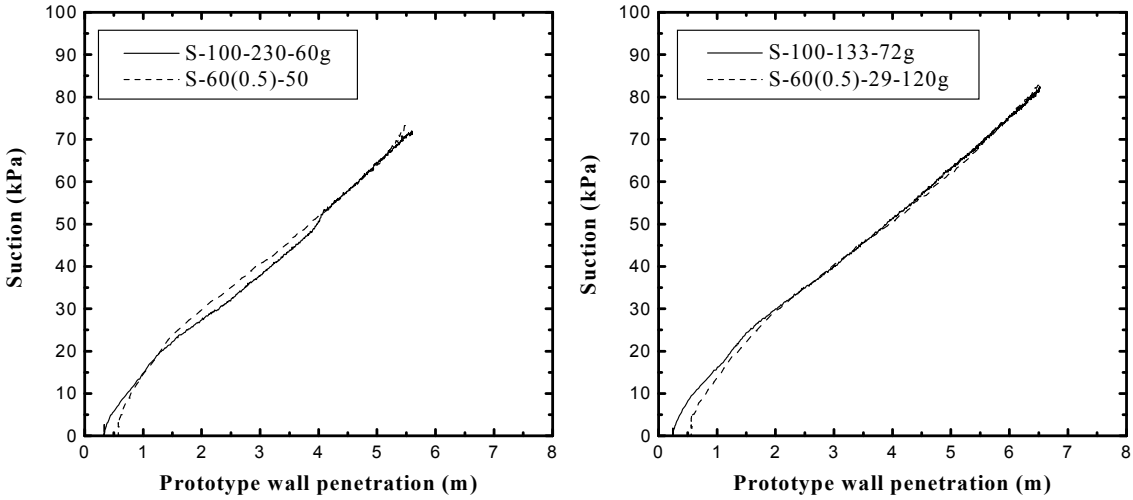

Figure 2.13: Absolute caisson wall thickness-soil particle size effect.

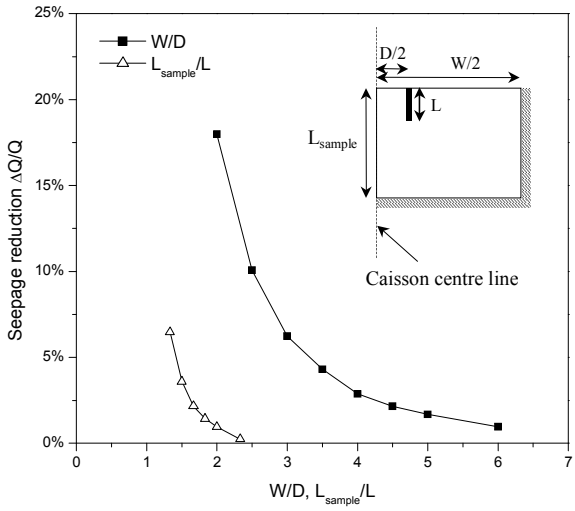

Figure 2.14: Flow restriction due to the test chamber.

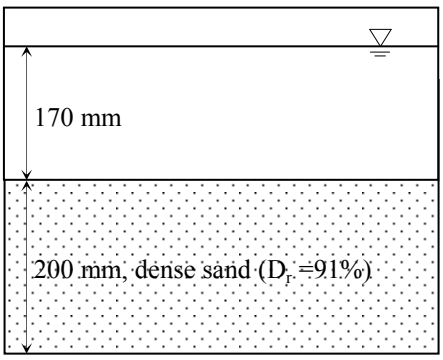

(a) Homogenous sand

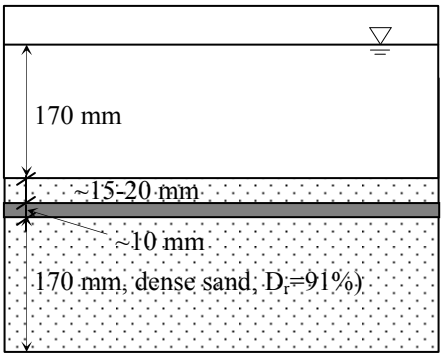

(b) Layered sand-silt

Figure 2.15: Soil profiles in PIV tests.

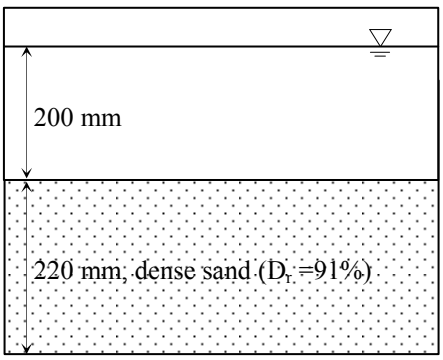

Figure 2.16: Soil profile for 1g suction installation tests.

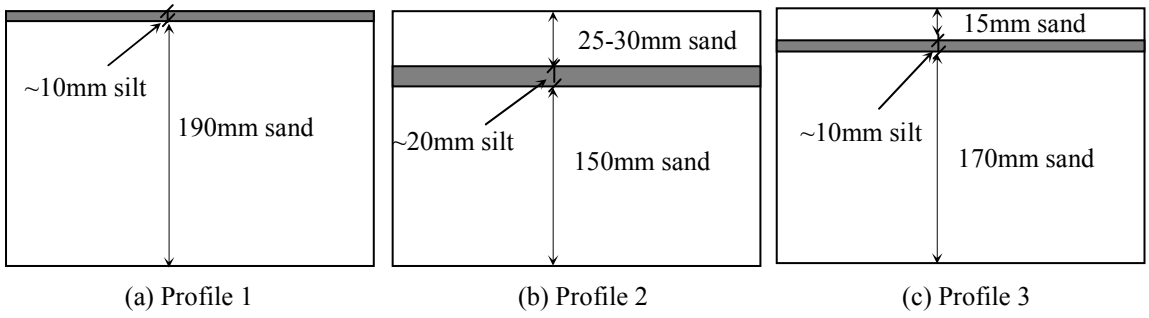

Figure 2.17: All layered sand-silt soil profiles for 1g tests.

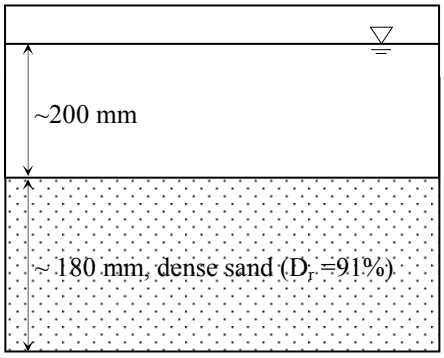

Figure 2.20: Homogeneous sand profile for centrifuge tests.

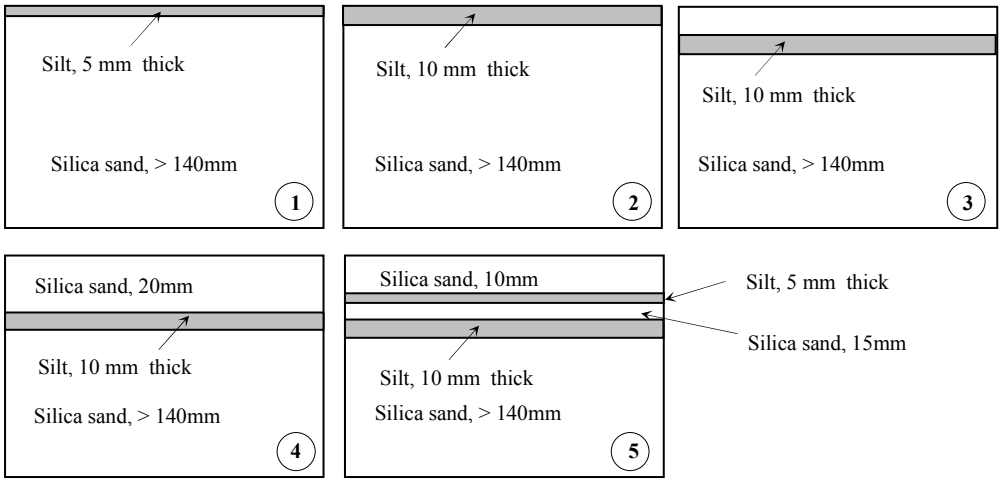

Figure 2.19: Sand-silt soil profiles for installation tests in the centrifuge.

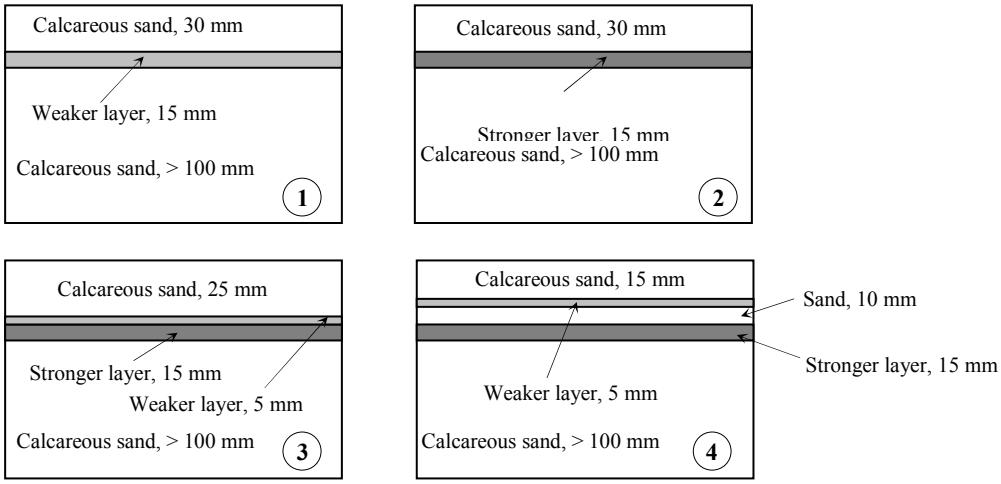

Figure 2.20: Cemented soil profiles for installation tests in the centrifuge.

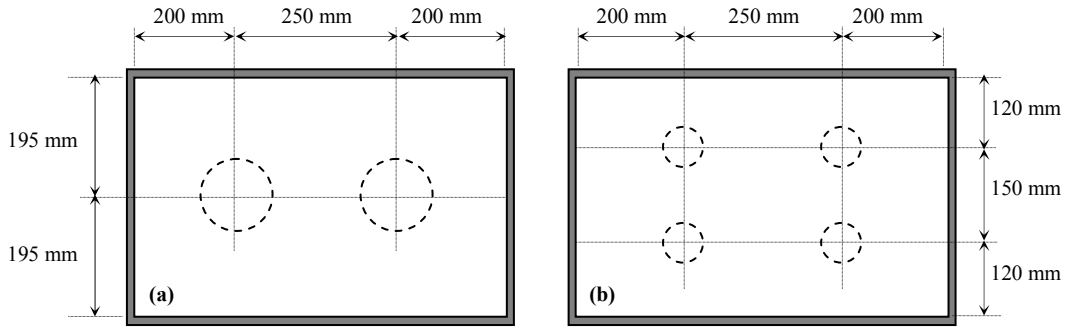

Figure 2.21: Test sites (plan view) in the centrifuge strong box.

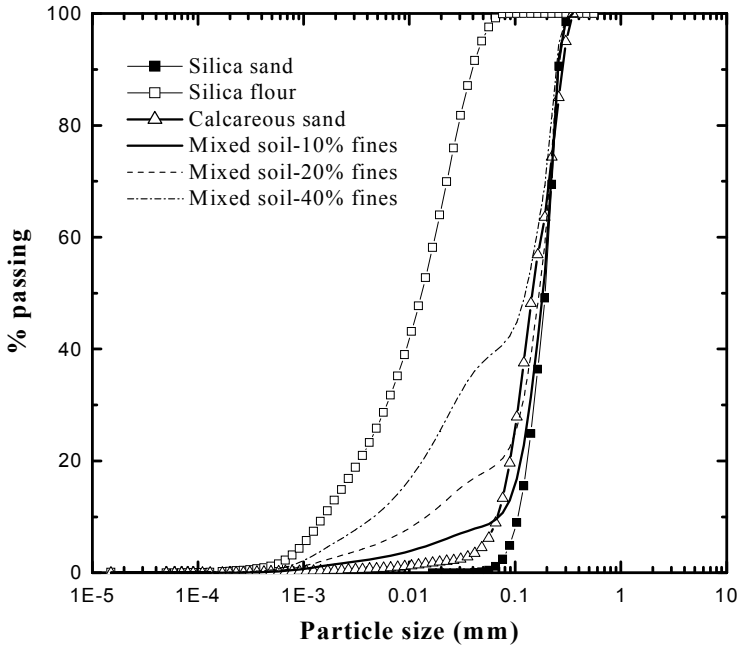

Figure 3.1: Particle size distribution of all the tested soils.

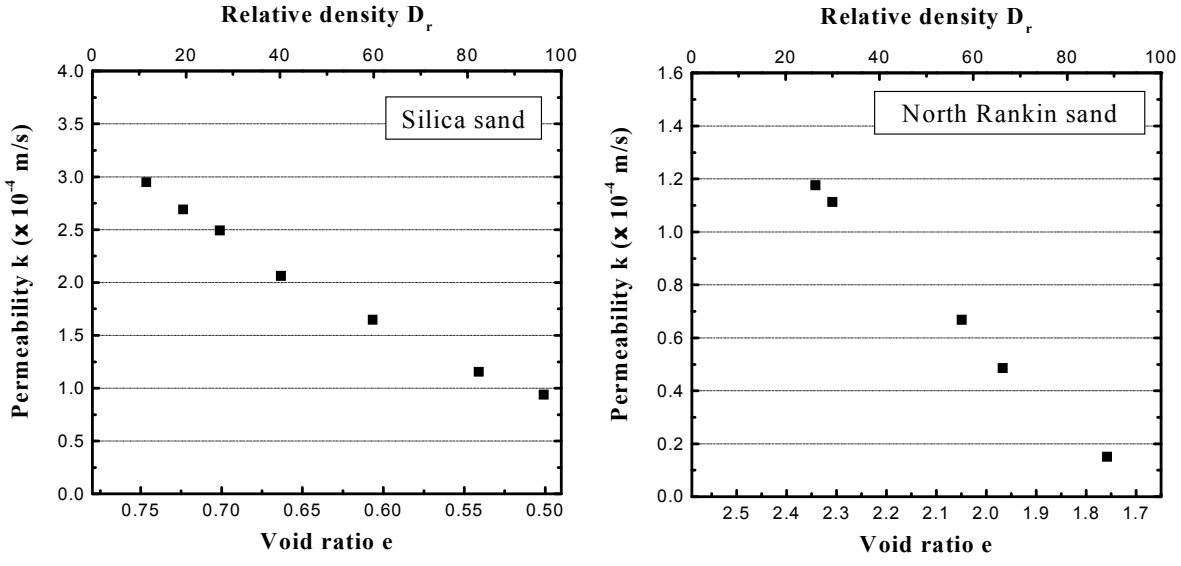

(a) (b)

Figure 3.2: Permeability for silica sand and North Rankin sand.

(a) (b)

Figure 3.3: Direct shear test apparatus and direct shear test box.

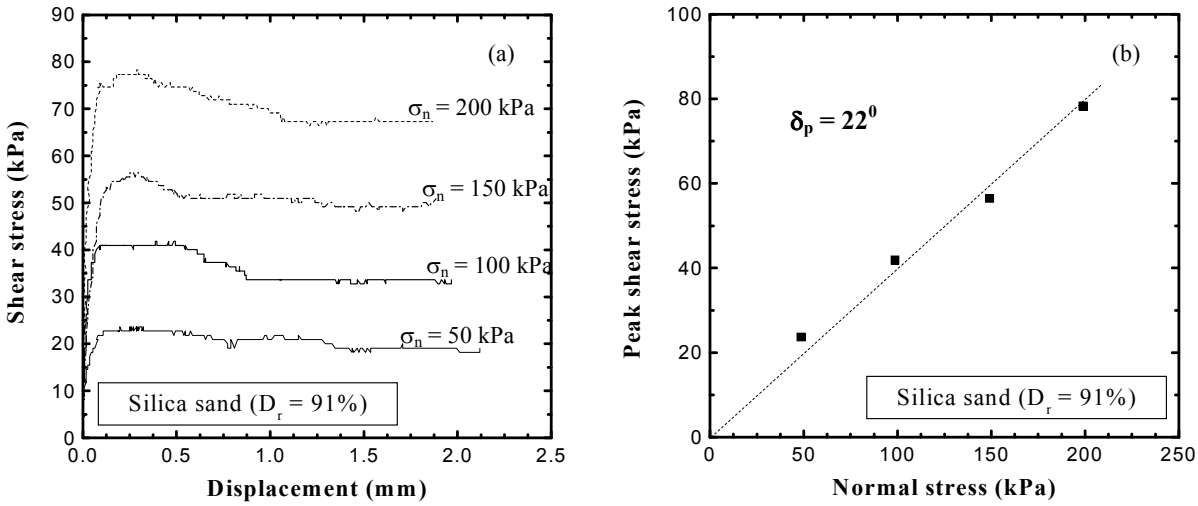

Figure 3.4: Shear test result for dense silica sand.

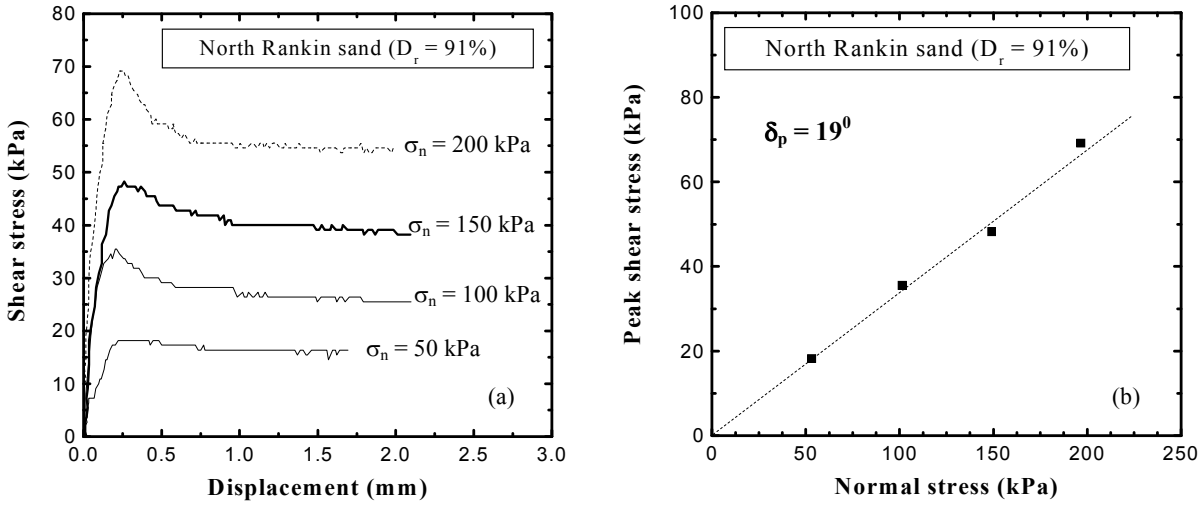

Figure 3.5: Shear test results for North Rankin calcareous sand.

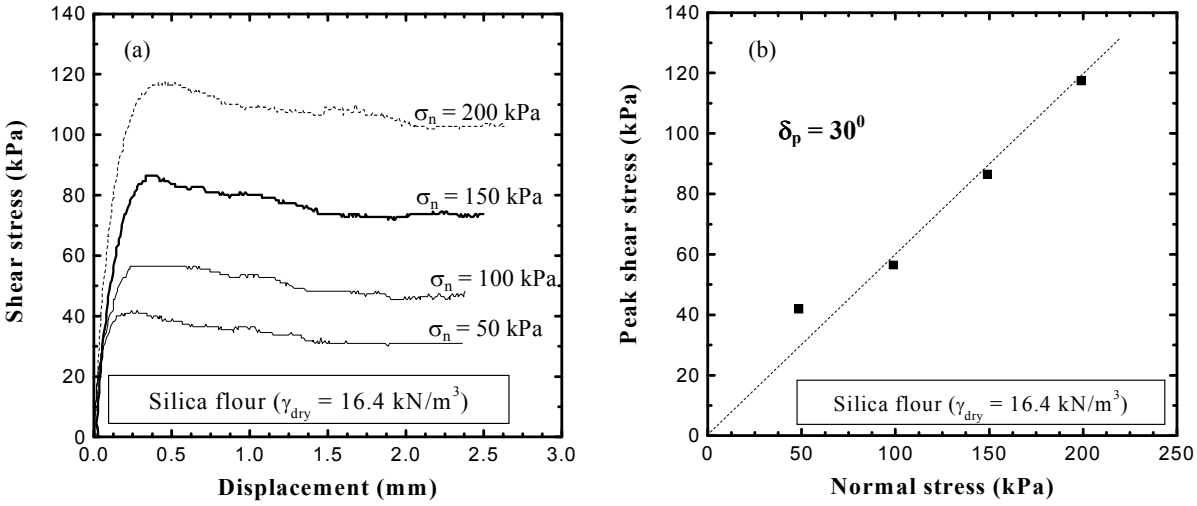

Figure 3.6: Shear test result for silica flour.

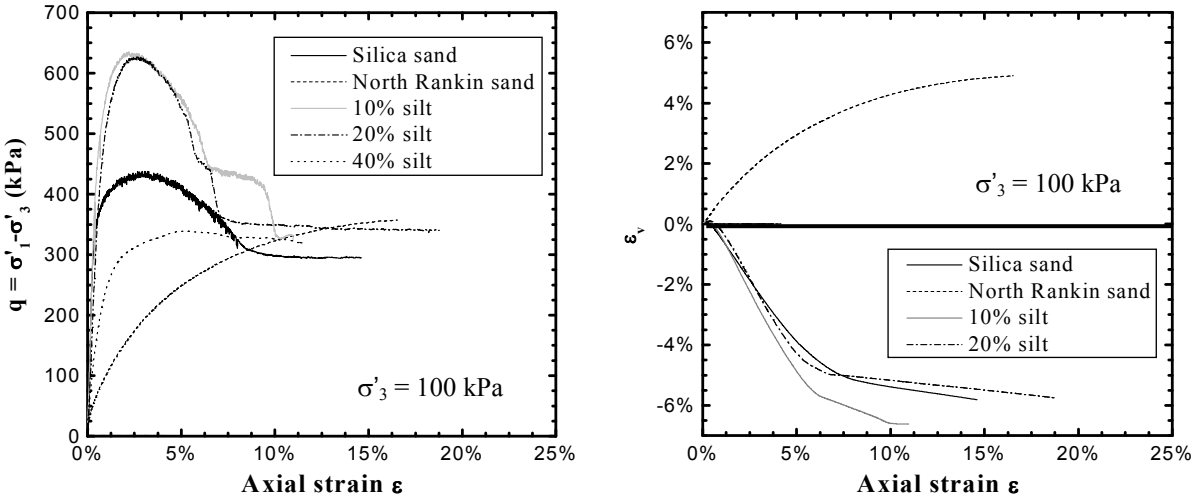

Figure 3.7: Triaxial compression test results for different soils.

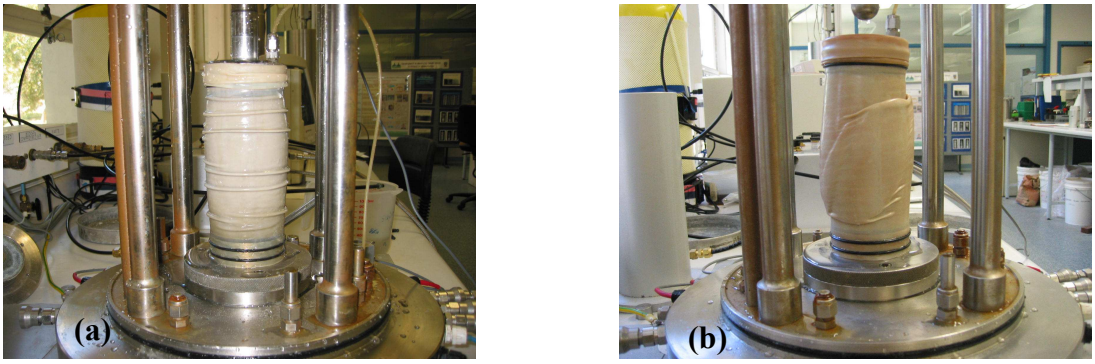

Figure 3.8: Post-test triaxial samples (a) North Rankin sand (b) Silica sand.

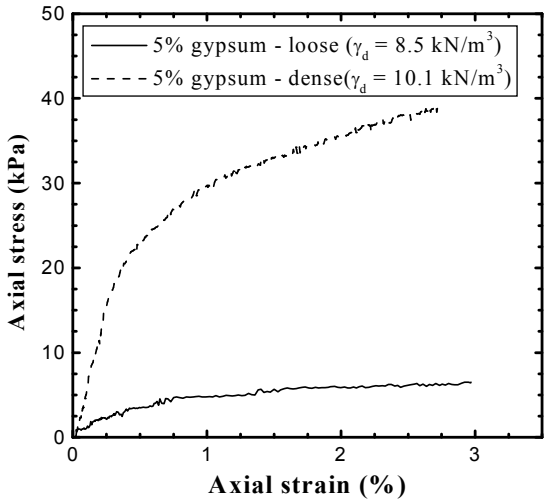

Figure 3.9: Soil with 5% gypsum.

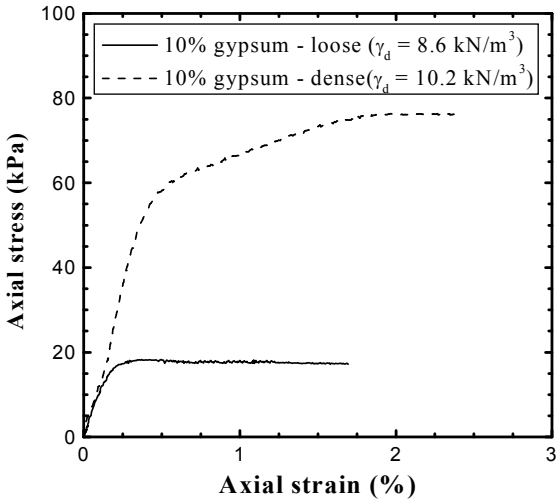

Figure 3.10: Soil with 10% gypsum.

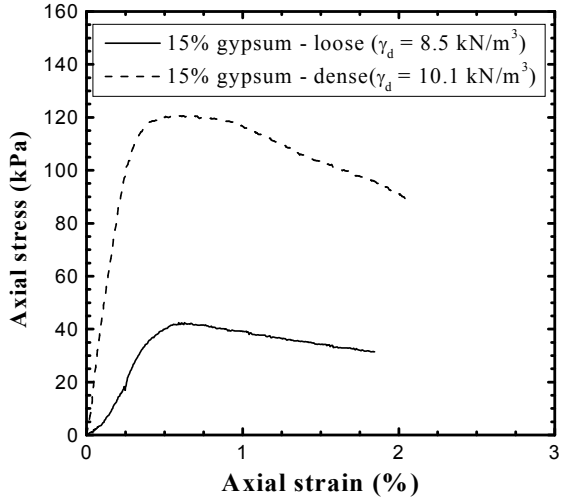

Figure 3.11: UCS result for soil with 15% gypsum content.

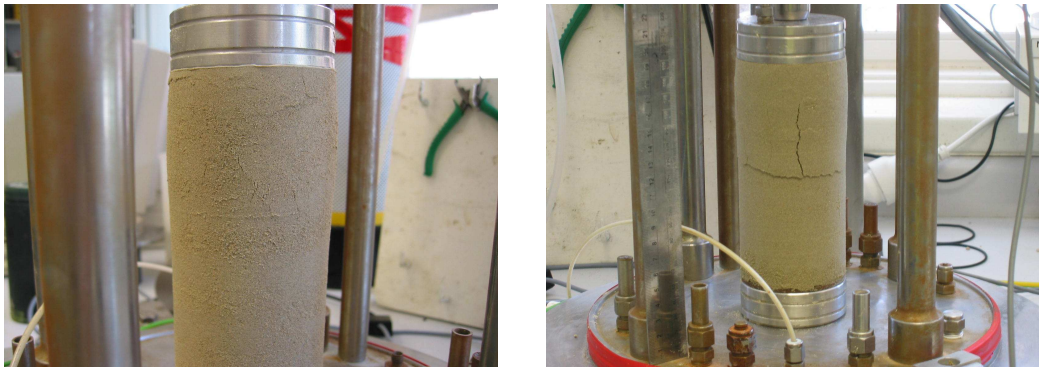

(a) 5% gypsum (dense). (b) 15% gypsum (dense).

Figure 3.12: Failure mode of cemented soil with different gypsum contents.

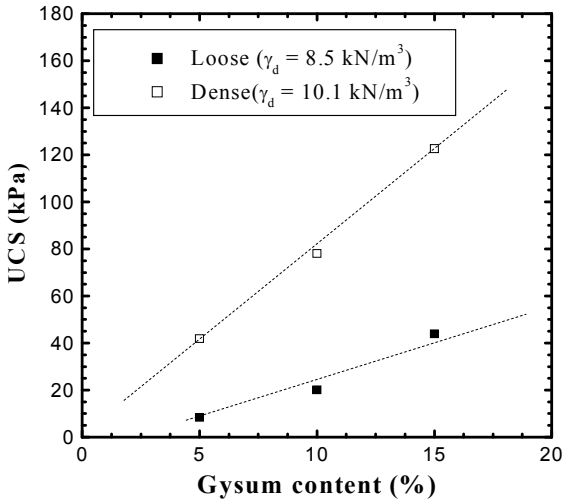

Figure 3.13: UCS as a function of gypsum content and density.

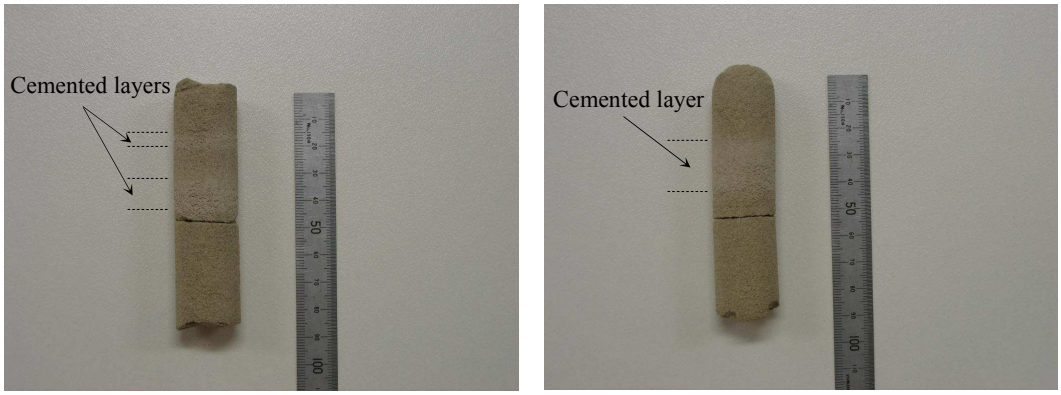

Figure 3.14: Oven-dried samples cored from the layered cemented test sites.

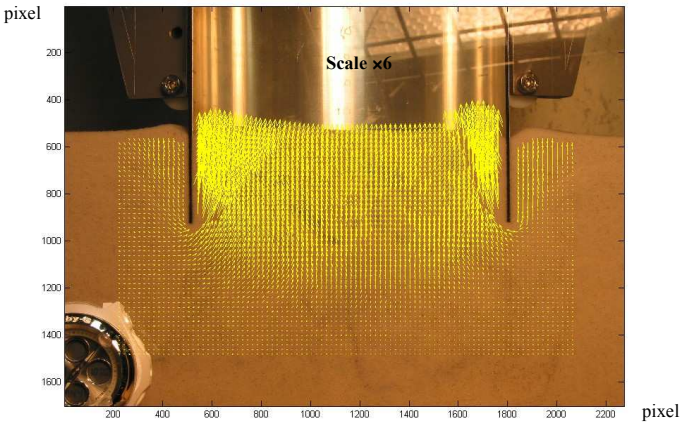

Figure 4.1: Soil deformation result using PIV technique.

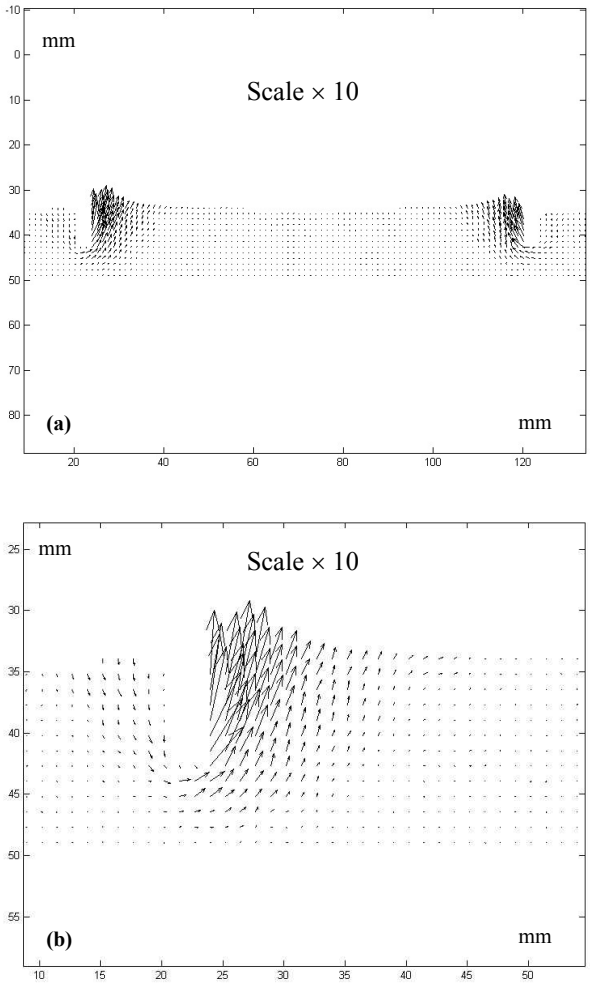

Figure 4.2: Soil deformation for L/D = 0.1 (p/γ'D = 0.75).

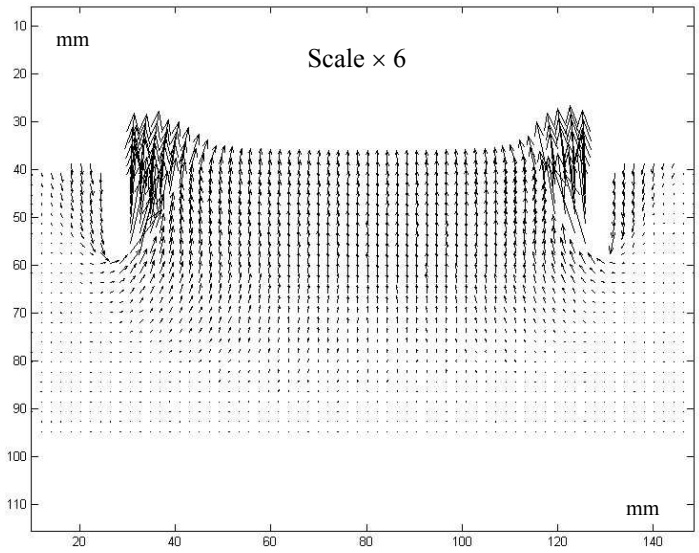

Figure 4.3: Soil deformation for L/D = 0.2 (p/γ'D = 4.1).

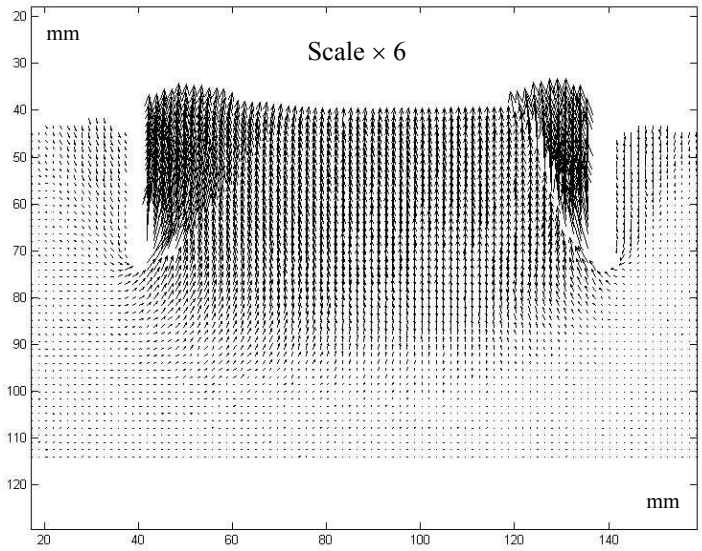

Figure 4.4: Soil deformation for L/D = 0.3 (p/γ'D = 5.1).

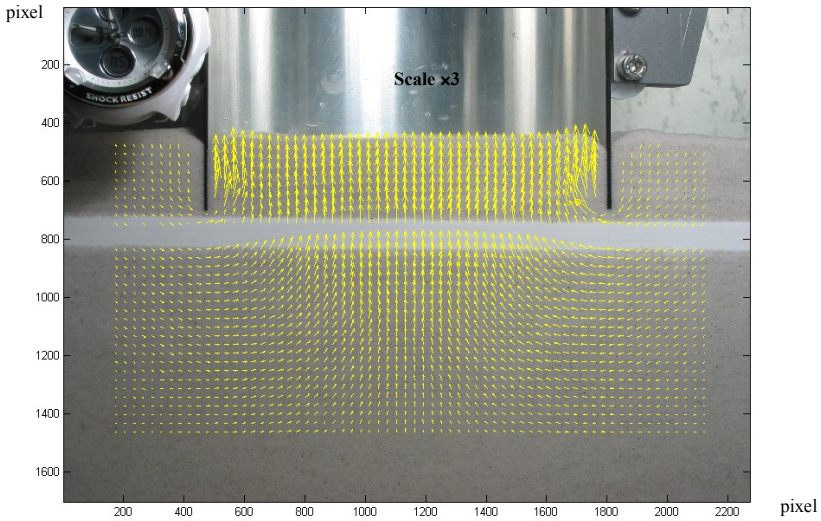

(a)

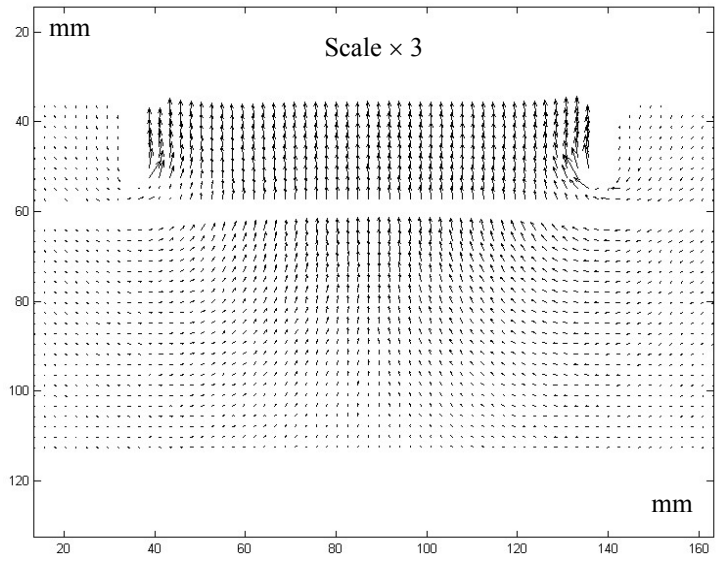

(b)

Figure 4.5: Soil deformation when caisson wall tip is above, but near the silt layer ($p/\gamma'D = 5.77$).

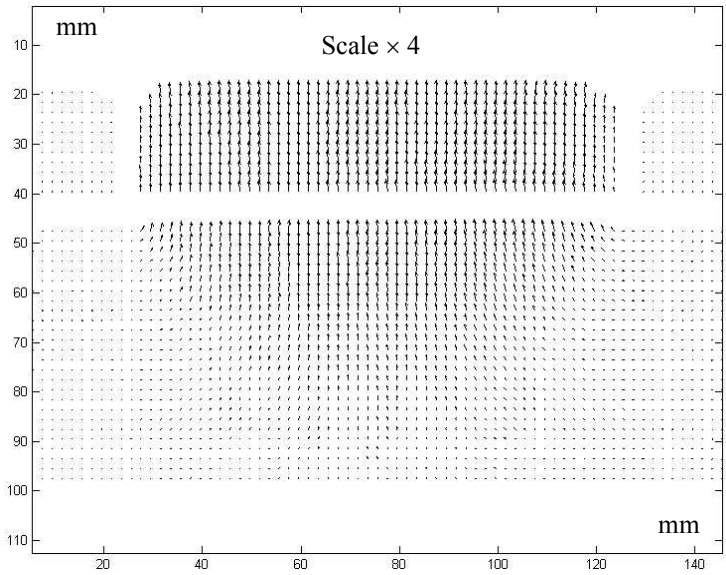

Figure 4.6: Soil deformation when caisson wall tip is in the silt layer (p/γ'D = 12.3).

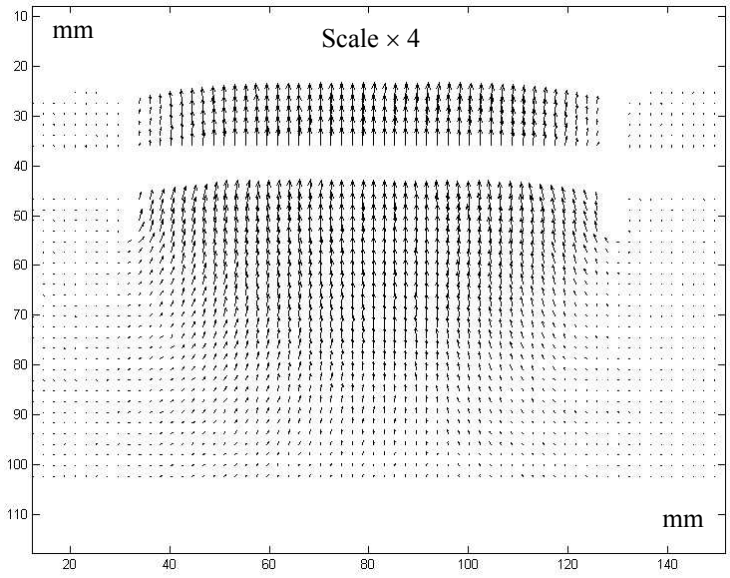

(b)

Figure 4.7: Soil deformation when caisson wall tip is below the silt layer (p/γ'D = 10.9).

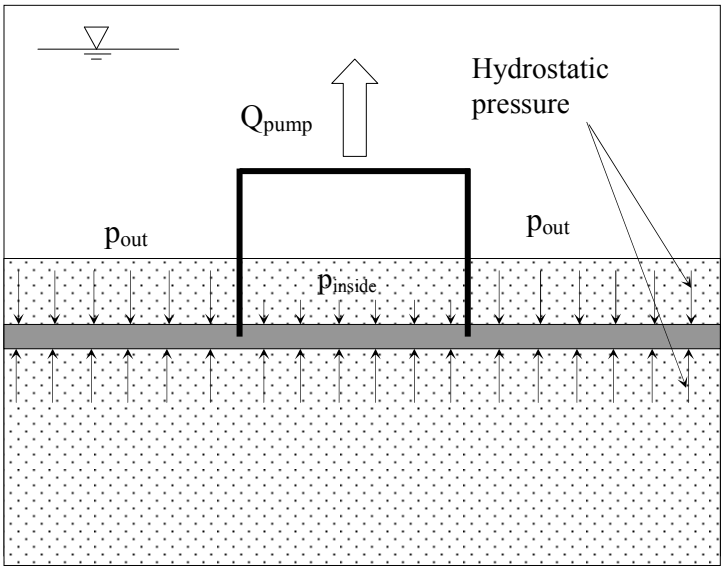

(a)

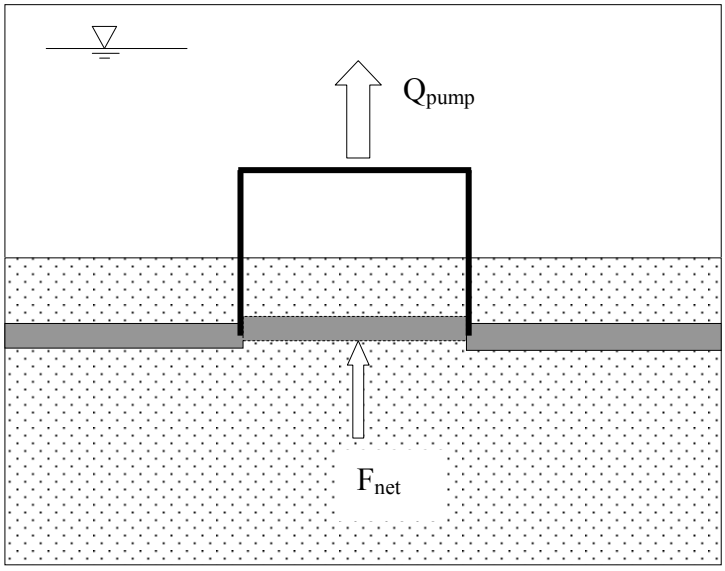

(b)

Figure 4.8: Uplift mechanism of the silt layer under the influence of suction.

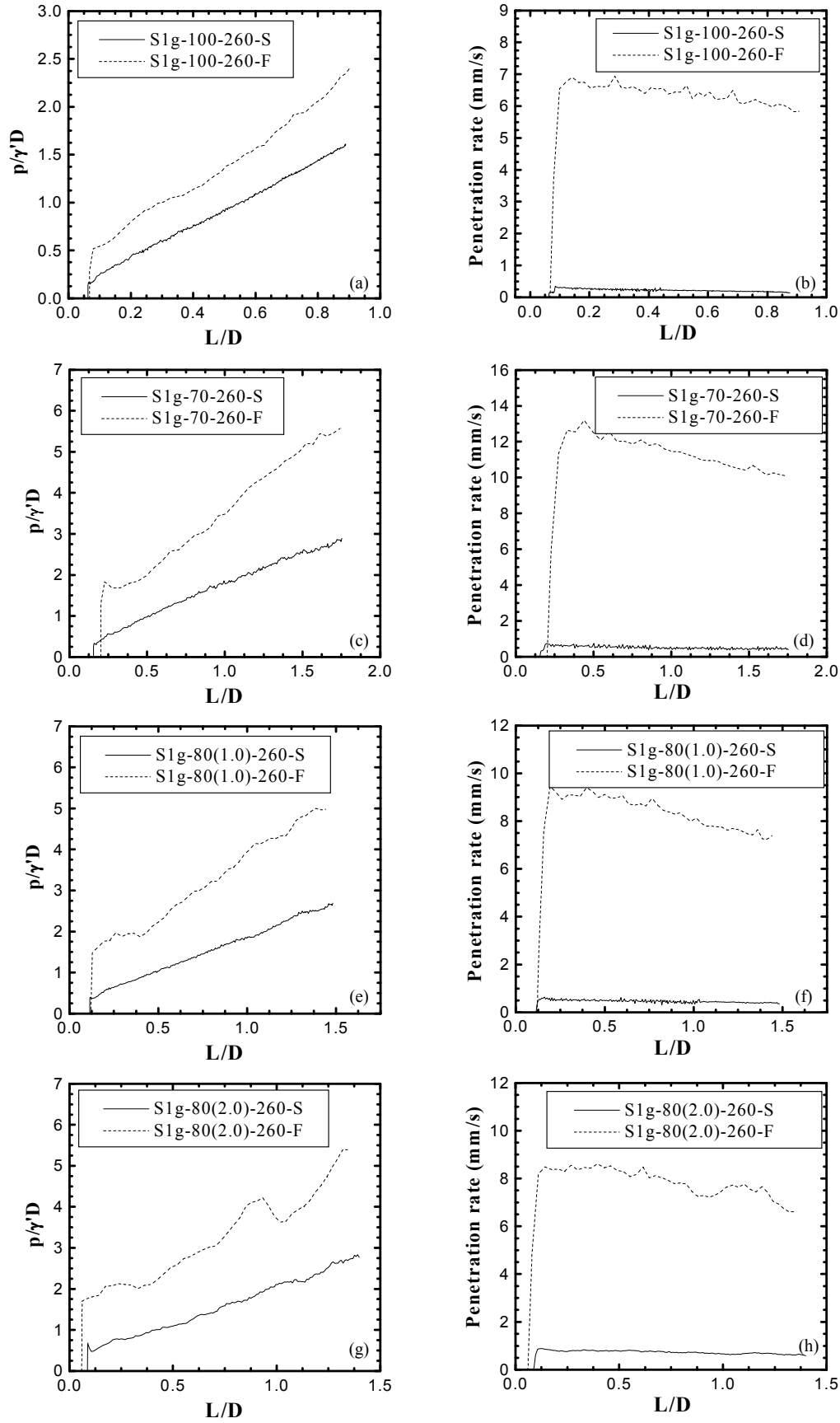

Figure 4.9: Suction pressure in slow and fast installations for different caissons.

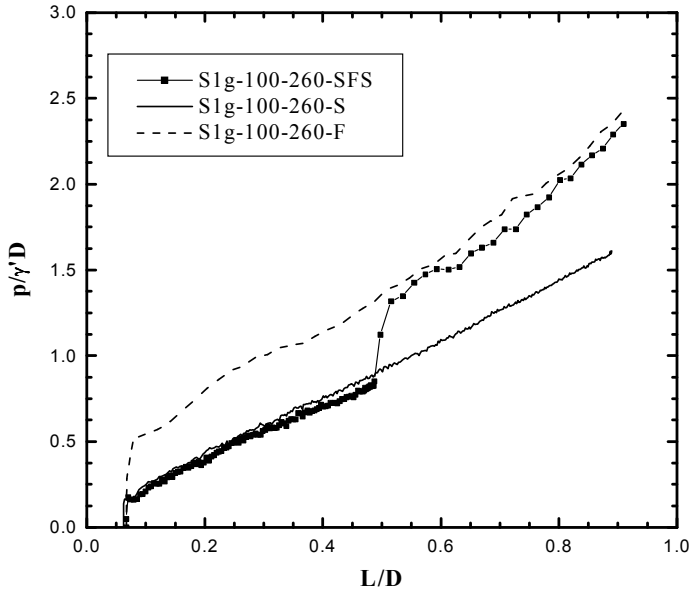

(a)

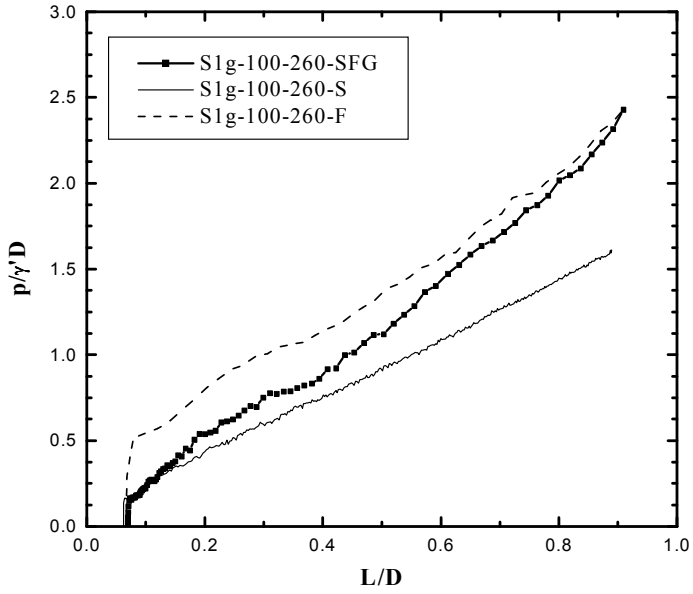

(b)

Figure 4.10: Effect of variation of installation rate on suction pressure.

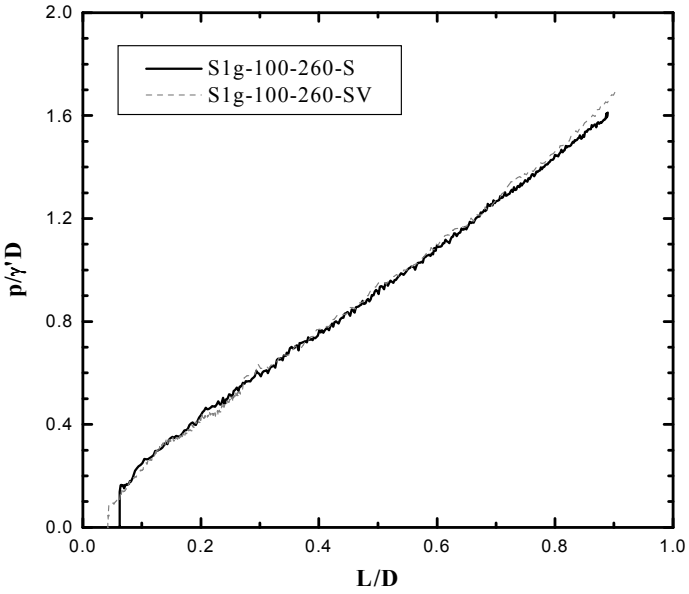

(a)

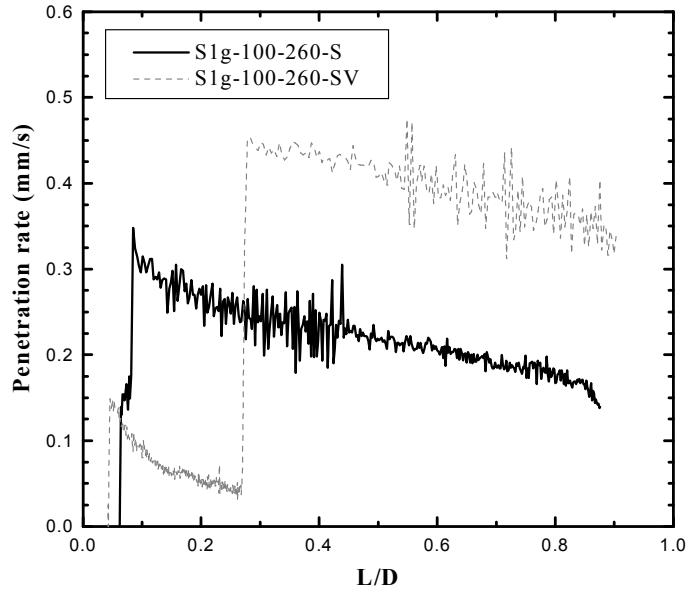

(b)

Figure 4.11: "Lower bound" suction pressure.

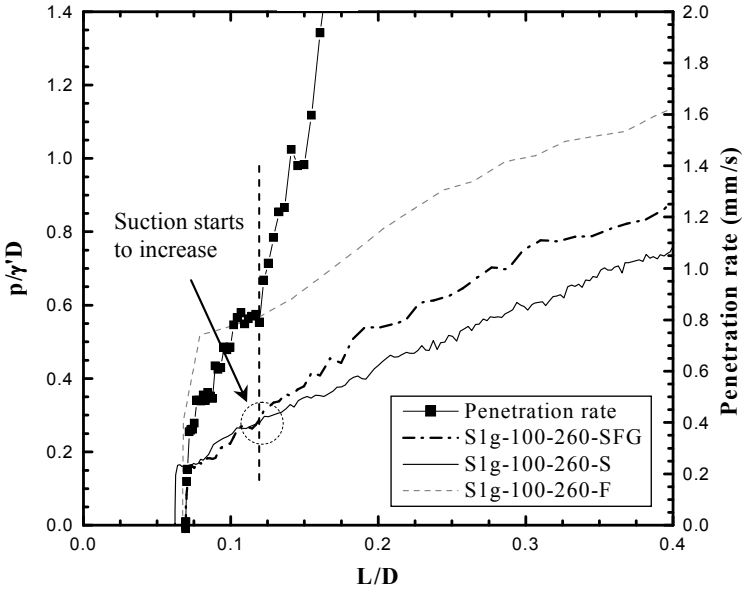

Figure 4.12: Effect of pumping rate on suction response.

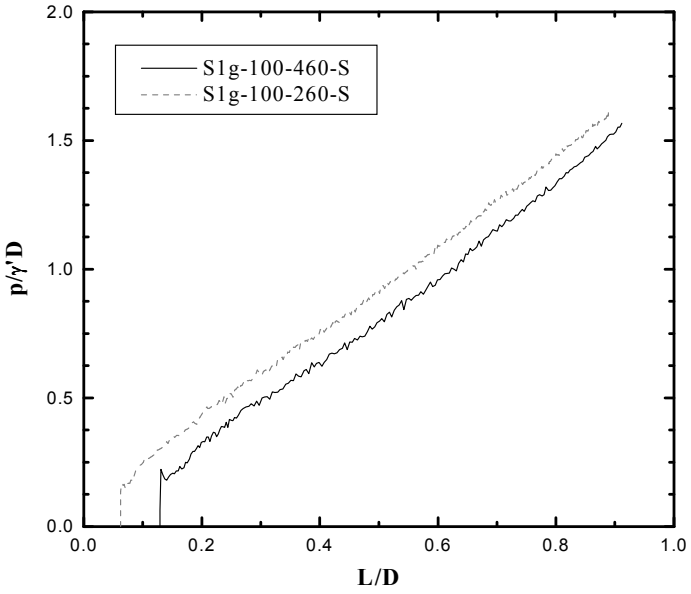

Figure 4.13a: Surcharge effect on suction in slow installation using 100 mm caisson.

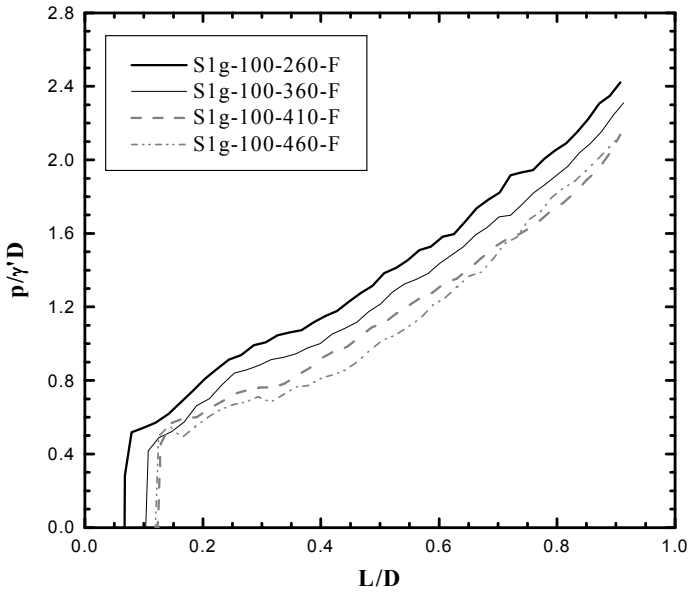

Figure 4.13b: Surcharge effect on suction in fast installation using 100 mm caisson.

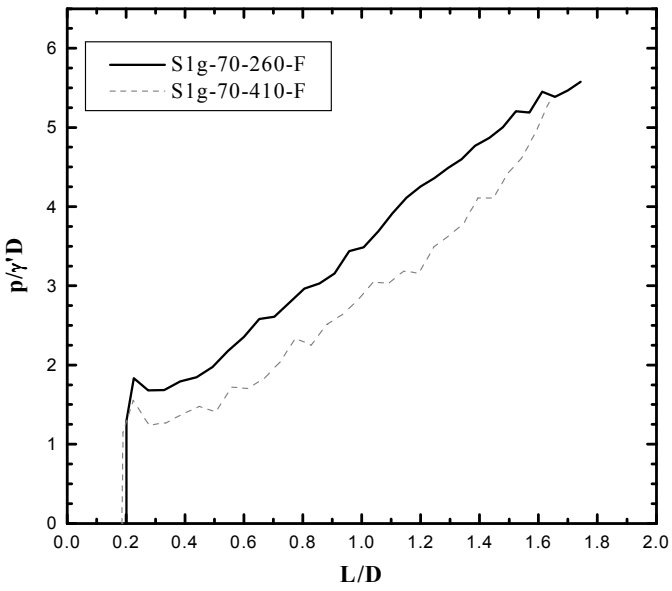

Figure 4.13c: Surcharge effect on suction in fast installation using 70 mm caisson.

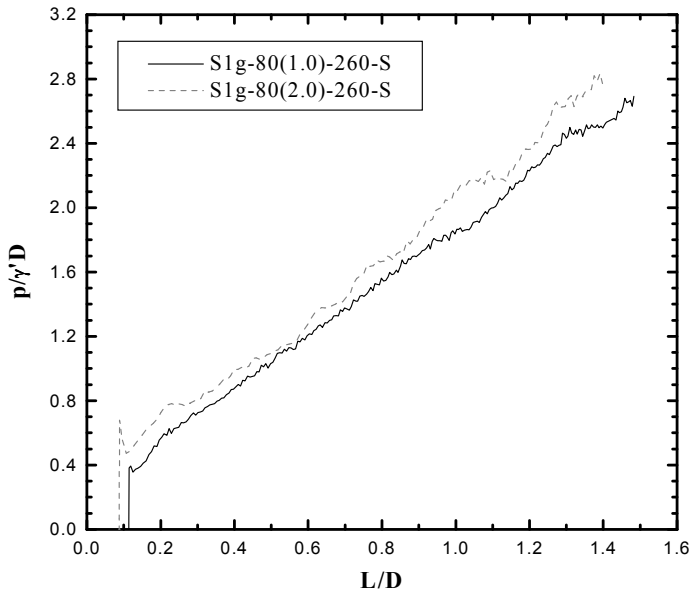

Figure 4.14: Effect of wall thickness on suction pressure during installation.

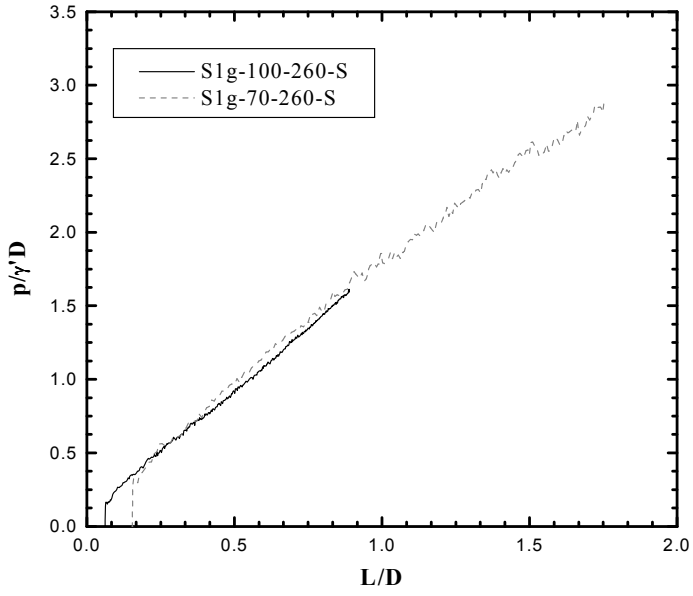

Figure 4.15: Effect of absolute caisson size on suction pressure.

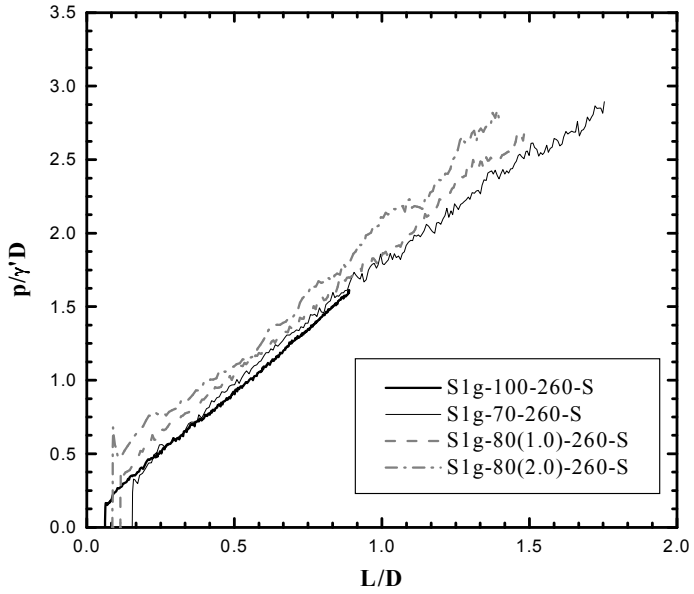

Figure 4.16: Effect of wall thickness and caisson diameter on suction pressure.

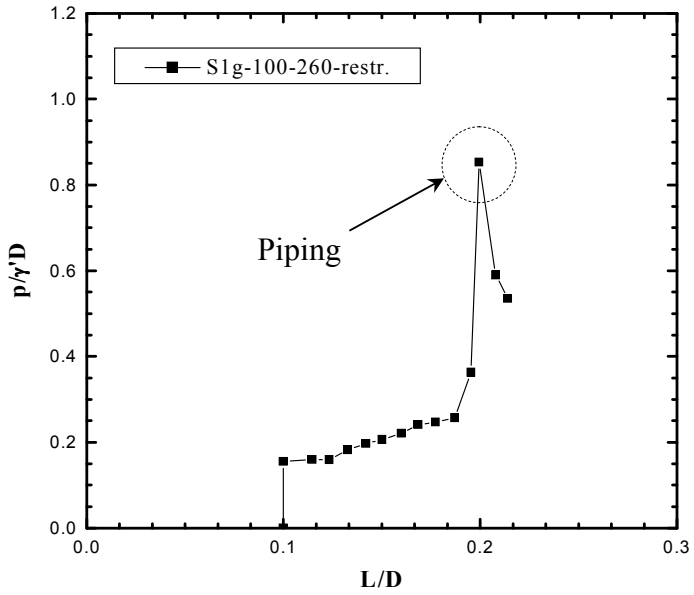

Figure 4.17: Piping failure when the caisson was restrained from movement.

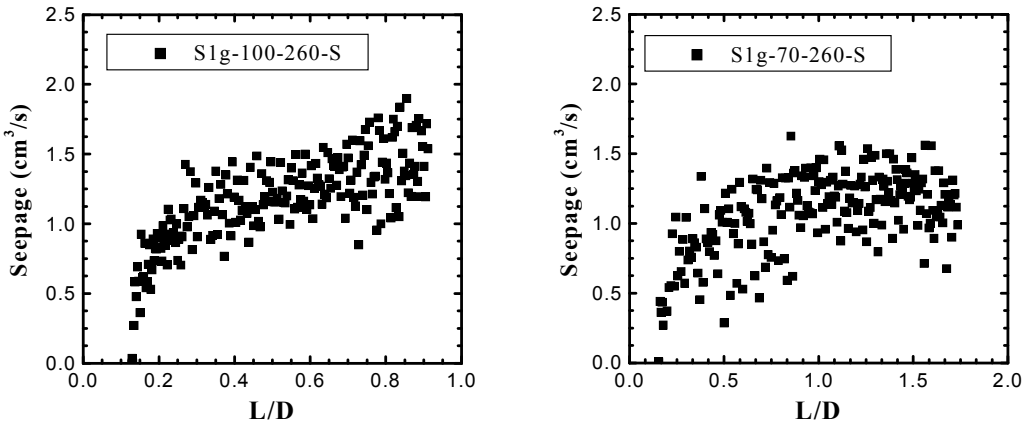

(a) (b)

Figure 4.18: Seepage behaviour in slow installations.

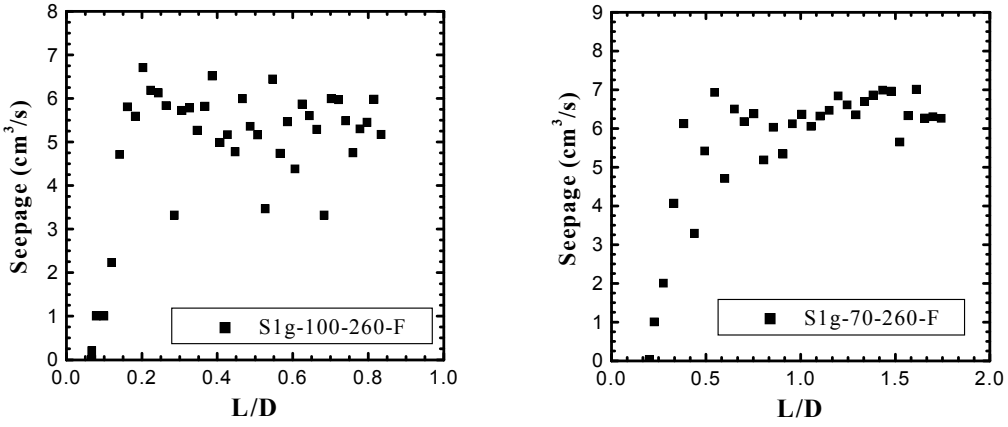

(a) (b)

Figure 4.19: Seepage behaviour in fast installations.

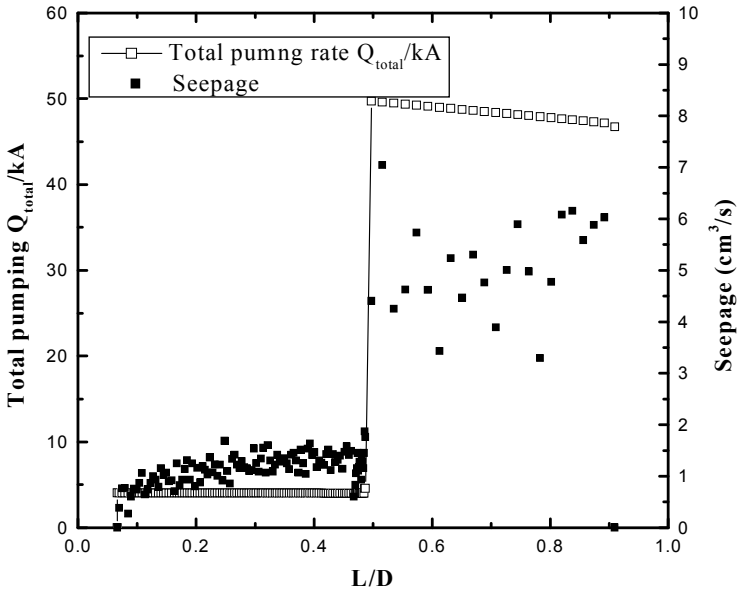

Figure 4.20: Effect of variation in total pumping flow on seepage.

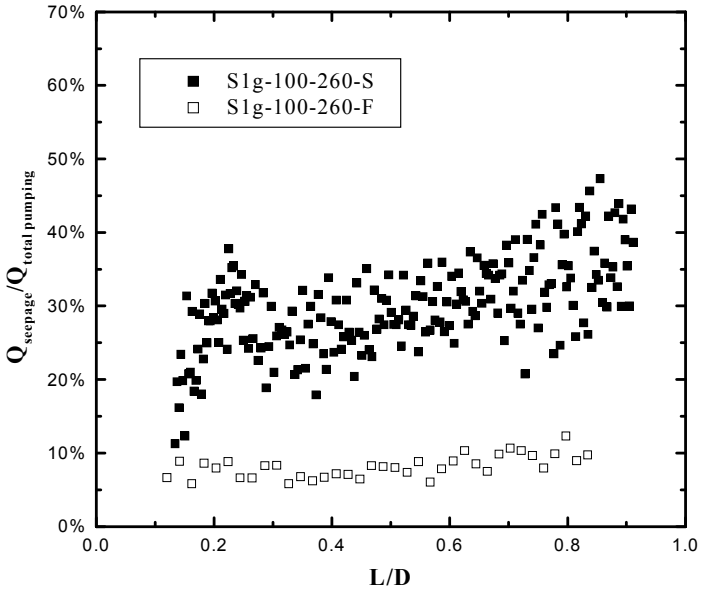

Figure 4.21: Ratio of seepage flow to total pumping in slow and fast installations.

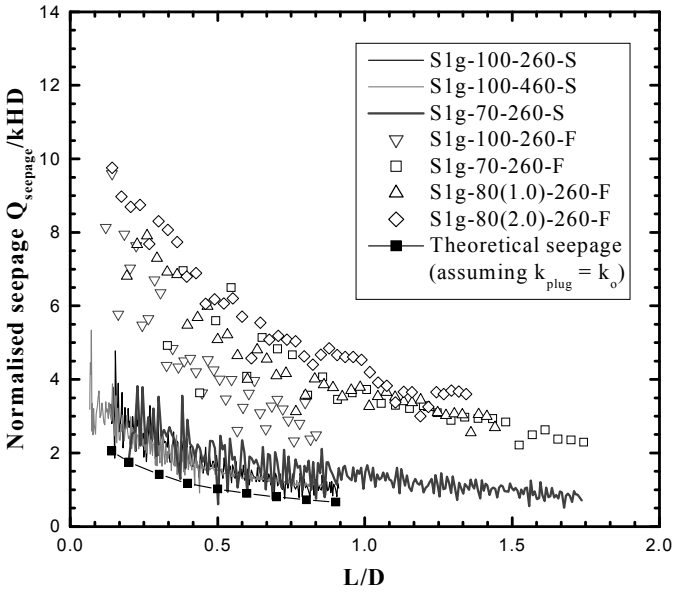

Figure 4.22: Comparison of normalised seepage flow for slow and fast installations.

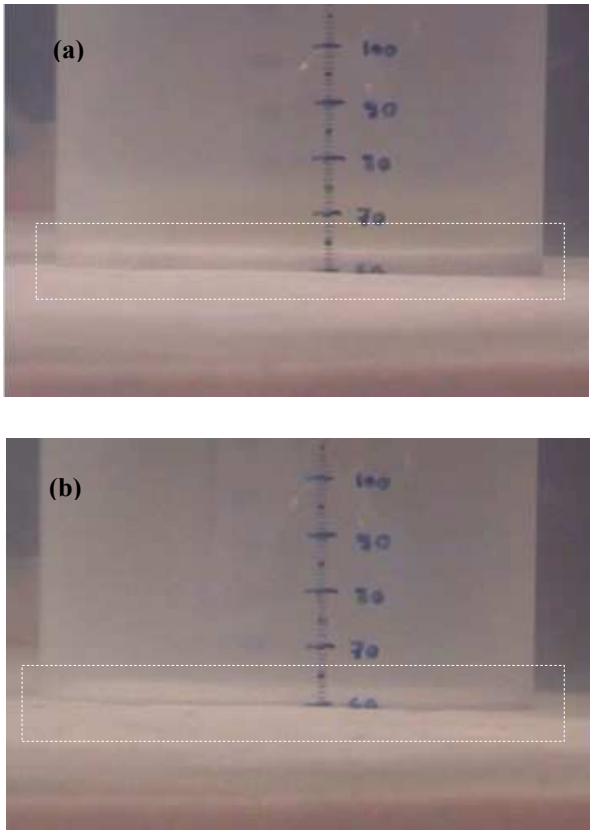

Figure 4.23: Examples of sand heave during suction installation.

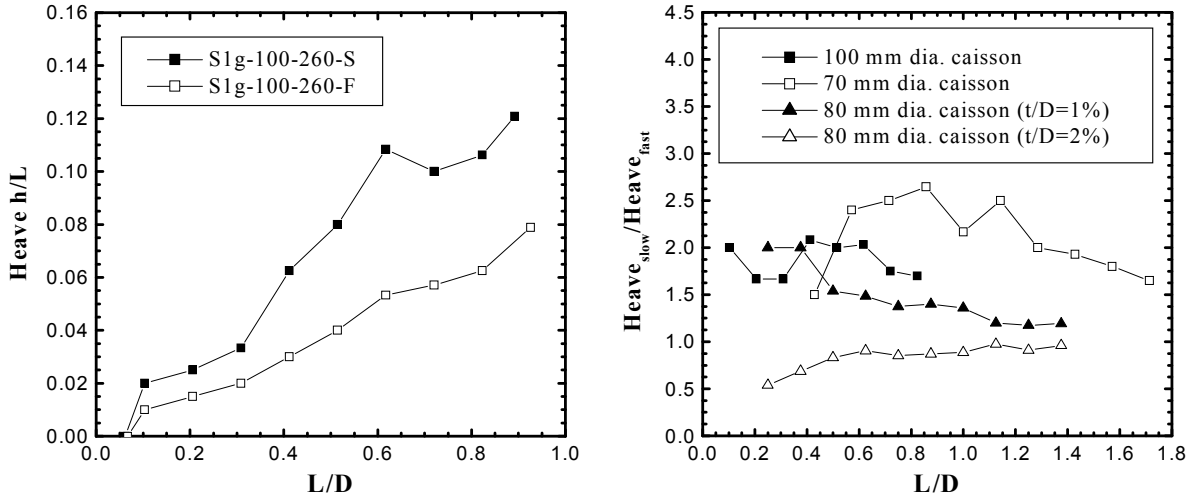

Figure 4.24: Effect of pumping rate on sand heave during installation.

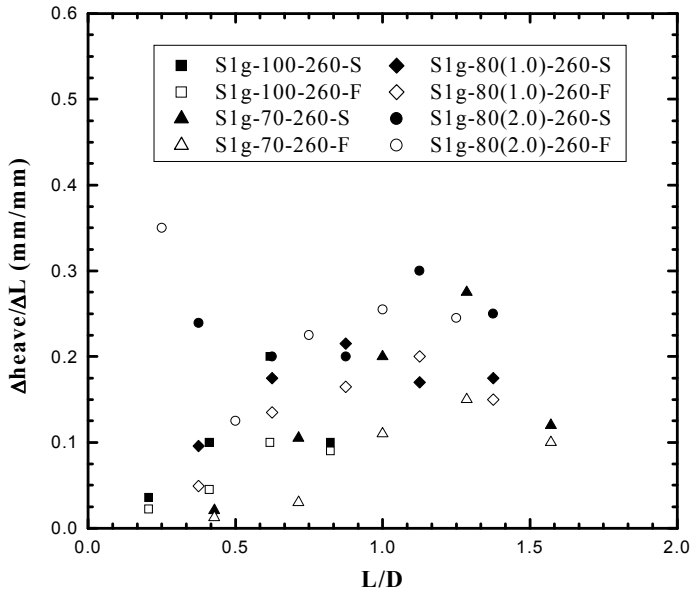

Figure 4.25: Variation of sand heave formation rate during installation.

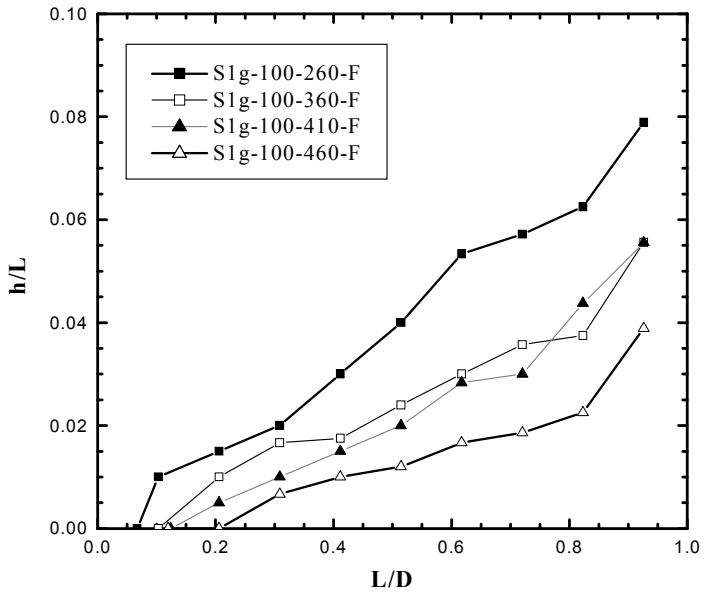

(a)

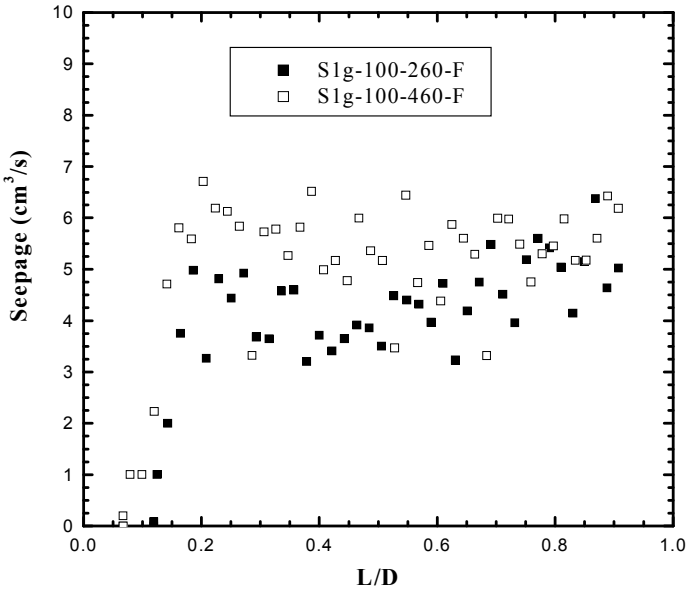

(b)

Figure 4.26: Effect of surcharge on sand heave.

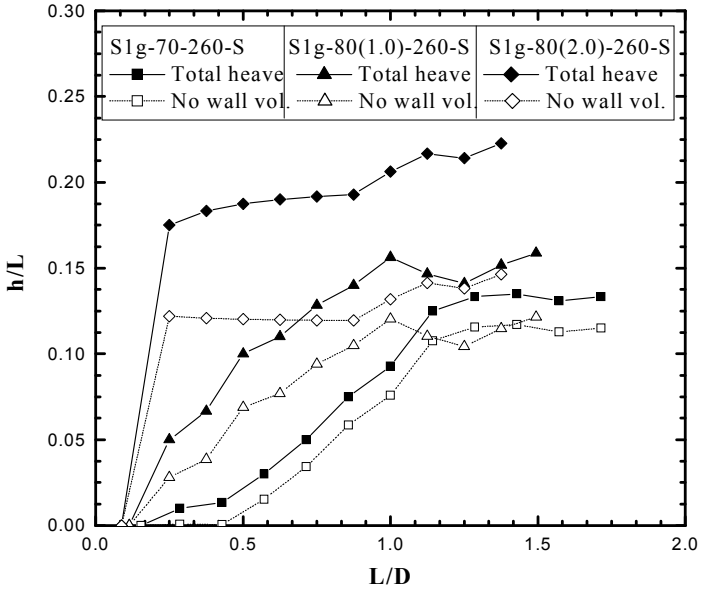

Figure 4.27: Effect of caisson wall thickness on sand heave.

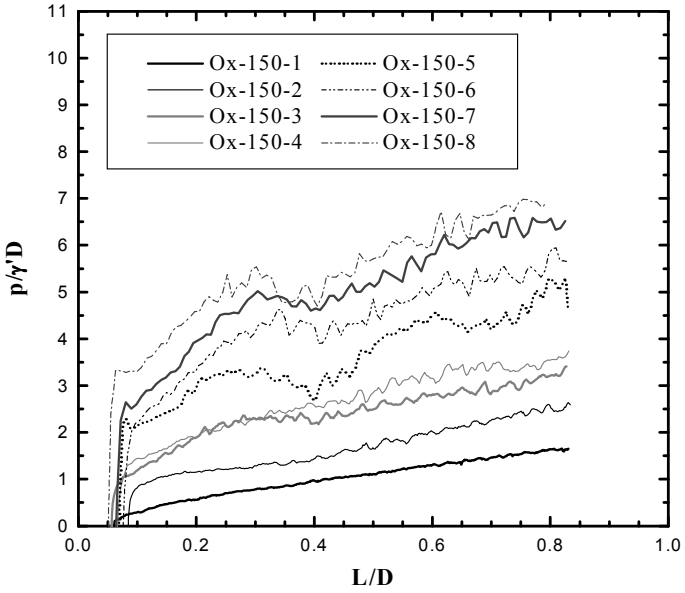

Figure 4.28a: Suction pressures in the Oxford tests.

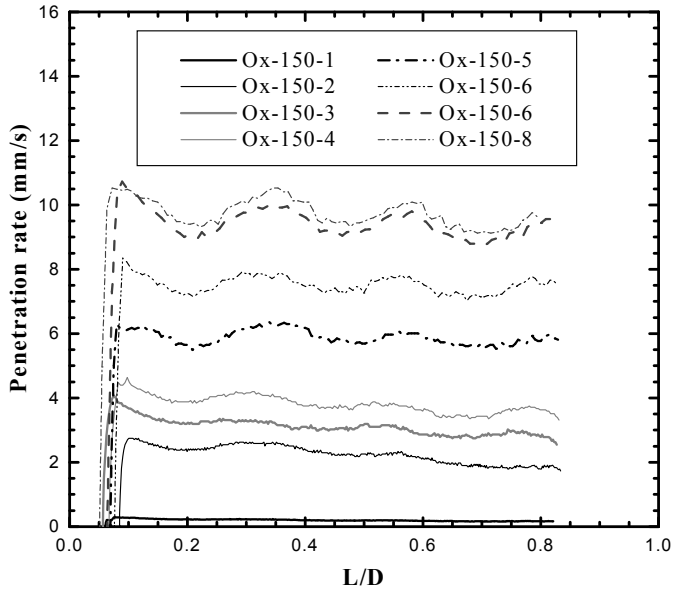

Figure 4.28b: Installation rate in the Oxford tests.

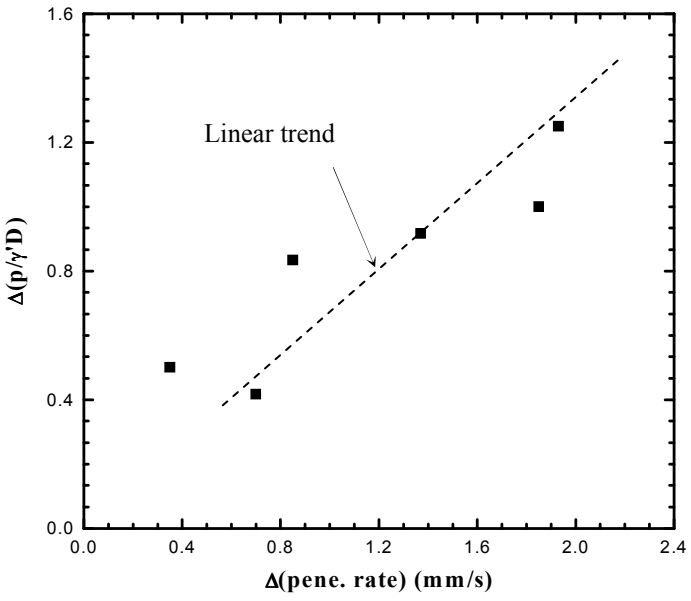

Figure 4.29: Increase of suction above the lower bound value with installation rate.

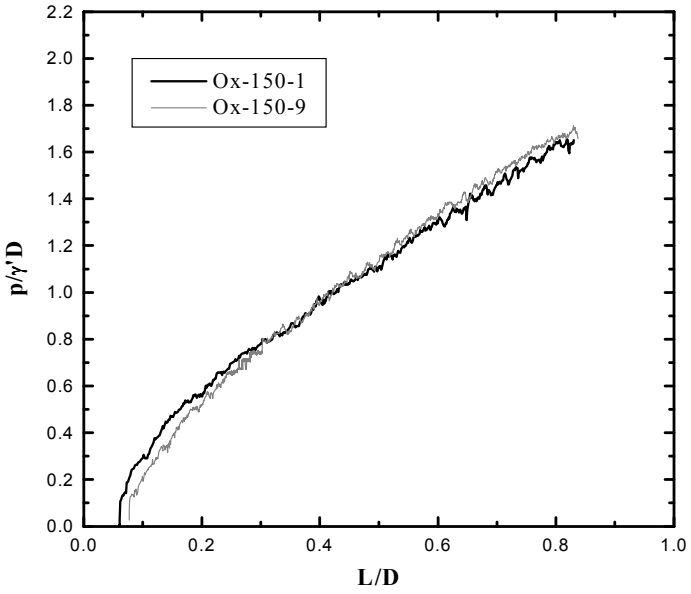

(a)

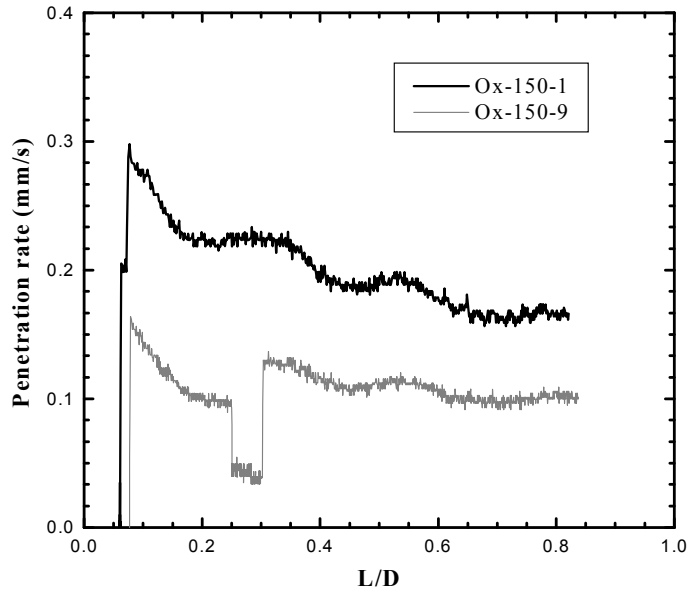

(b)

Figure 4.30: (a) Suction pressure (b) Installation rate in "lower bound" suction test.

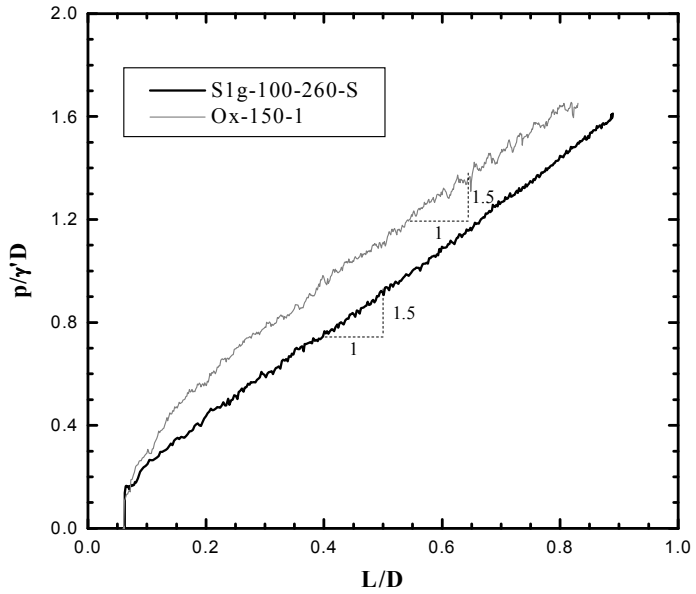

Figure 4.31: Comparison of Oxford and UWA results.

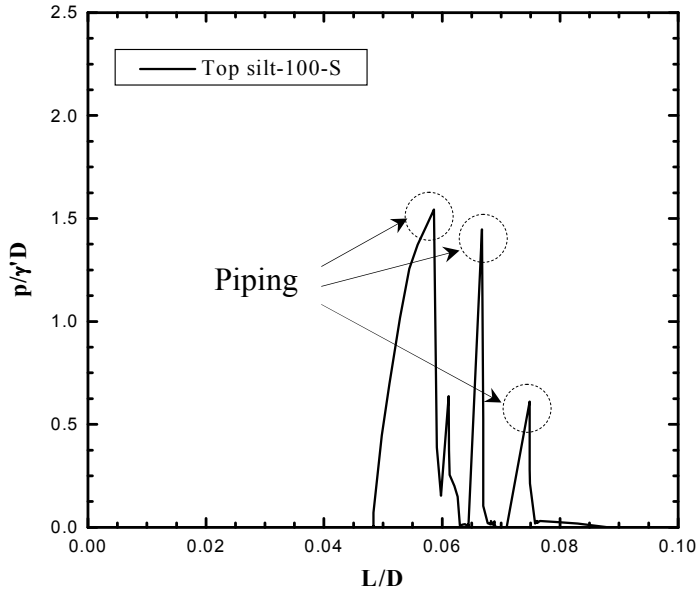

Figure 4.32: Piping failure in slow installation in soil with 10 mm thick surface silt layer.

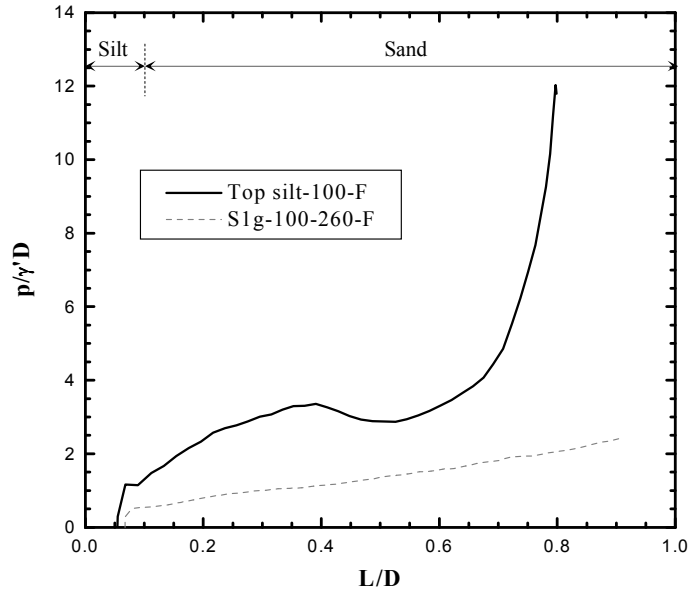

Figure 4.33: Installation in soil with a 10 mm thick surface silt layer.

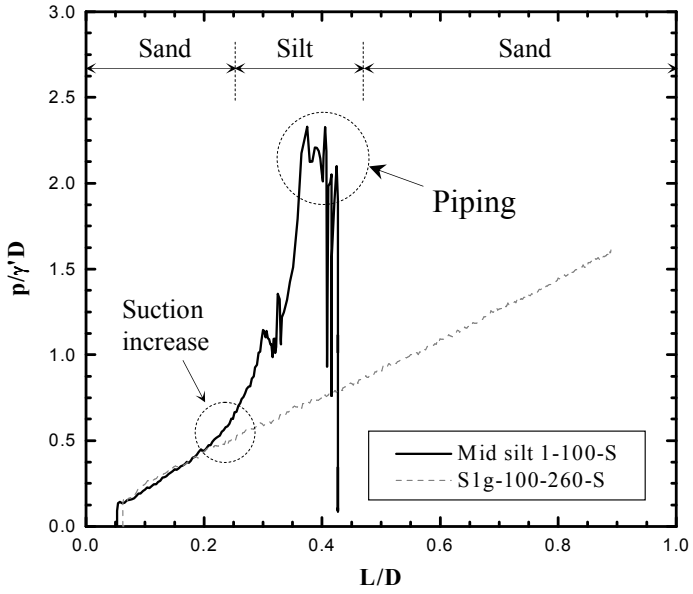

Figure 4.34: Piping failure during penetration of the silt layer in slow installation.

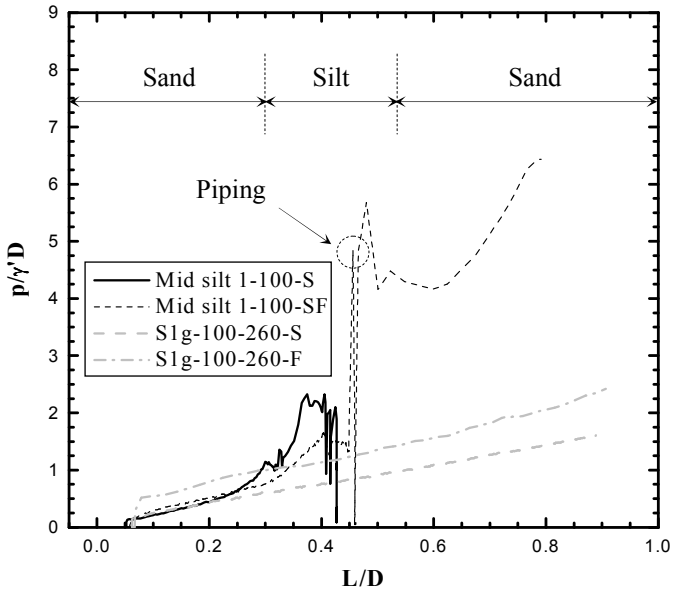

Figure 4.35: Installation in soil with 20 mm thick silt layer below the surface.

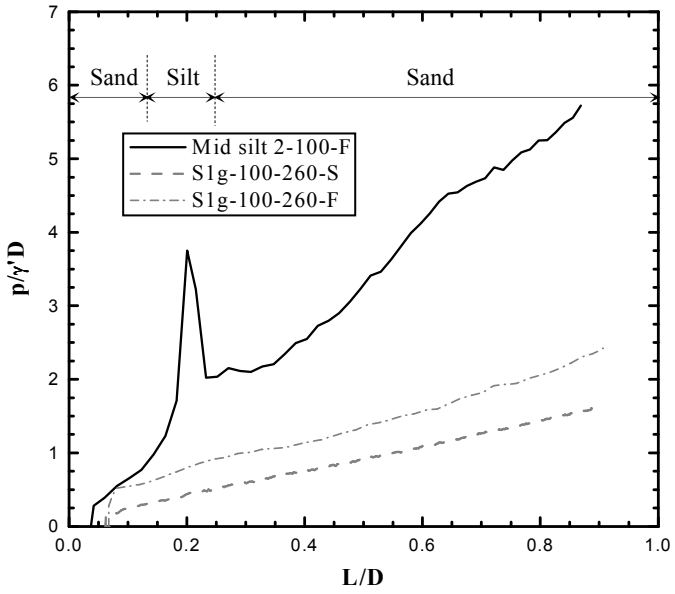

Figure 4.36: Installation in soil with 10 mm thick silt layer below the surface.

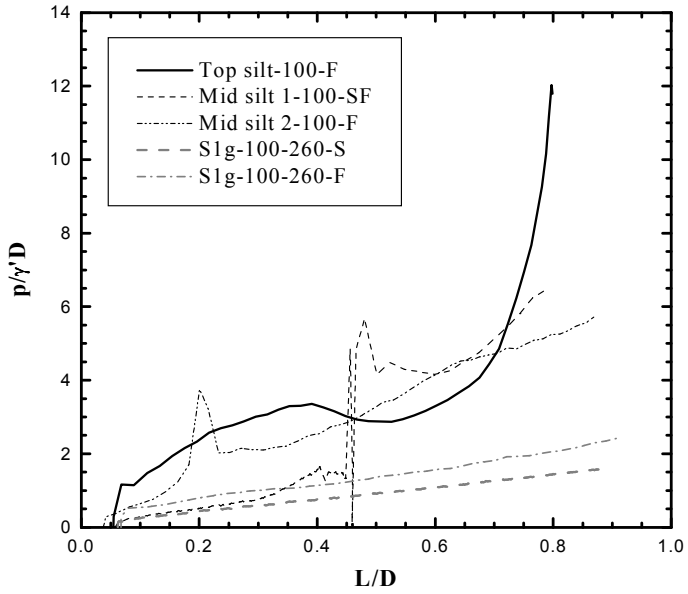

Figure 4.37: Comparisons of different installations in layered sand-silt soils.

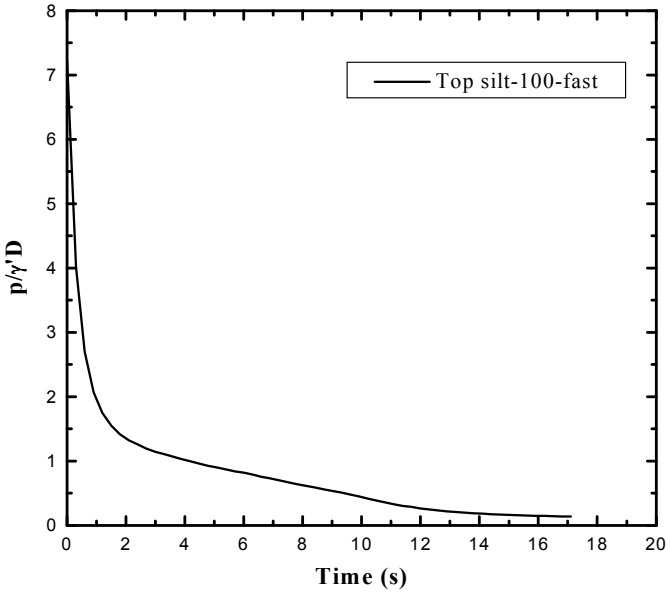

Figure 4.38: Pressure balancing across the silt layer after termination of pumping.

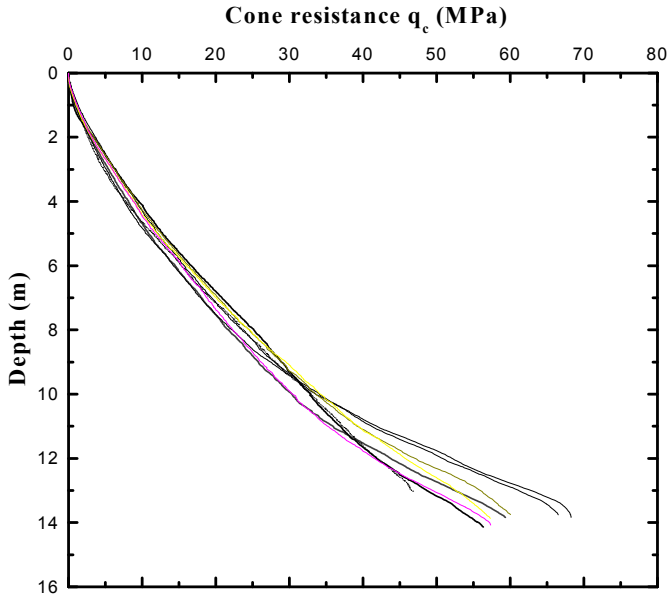

Figure 5.1: Cone penetration test result in silica sand.

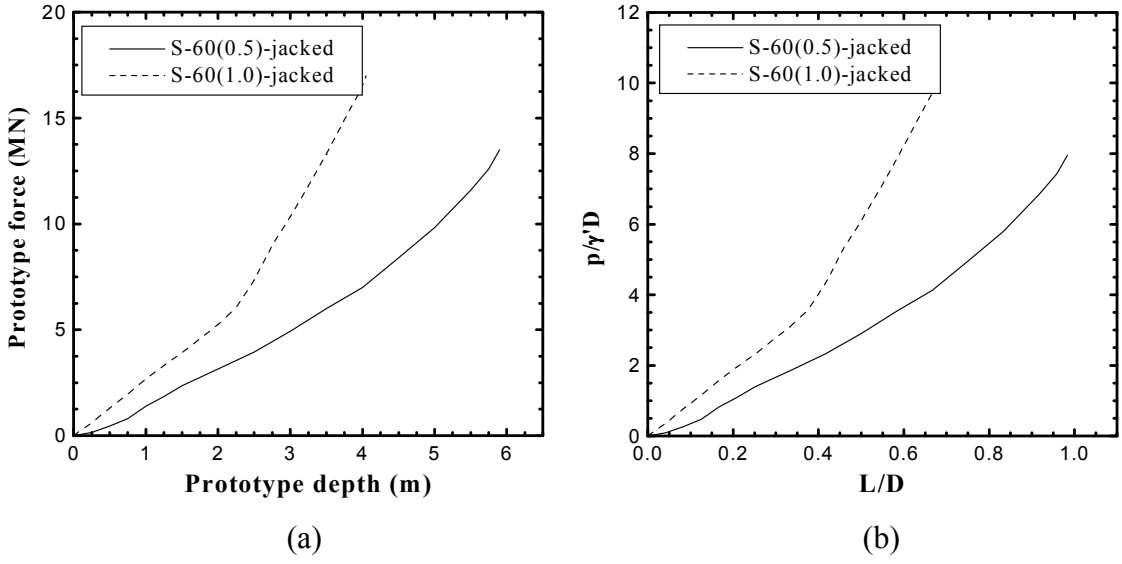

Figure 5.2: Jacked installation results in caisson with different wall thickness.

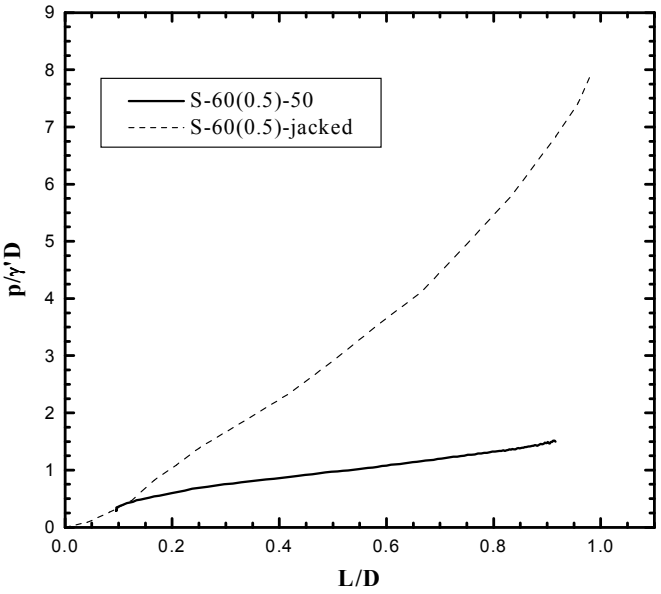

Figure 5.3: Comparison of suction and jacked installation results.

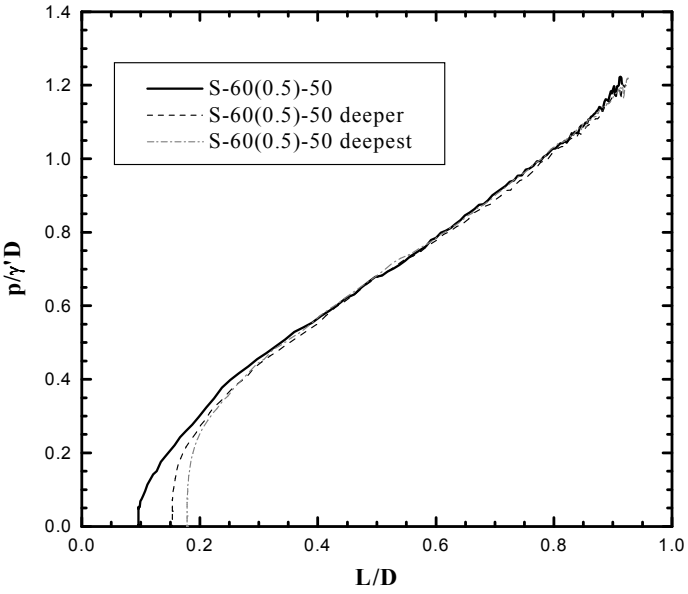

Figure 5.4: Effect on initial penetration depth on suction pressure.

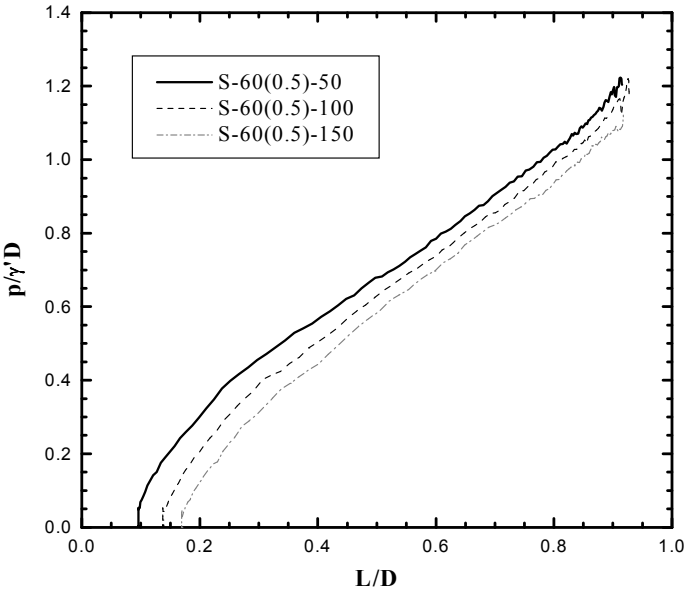

Figure 5.5: Effect of caisson weight in suction pressure.

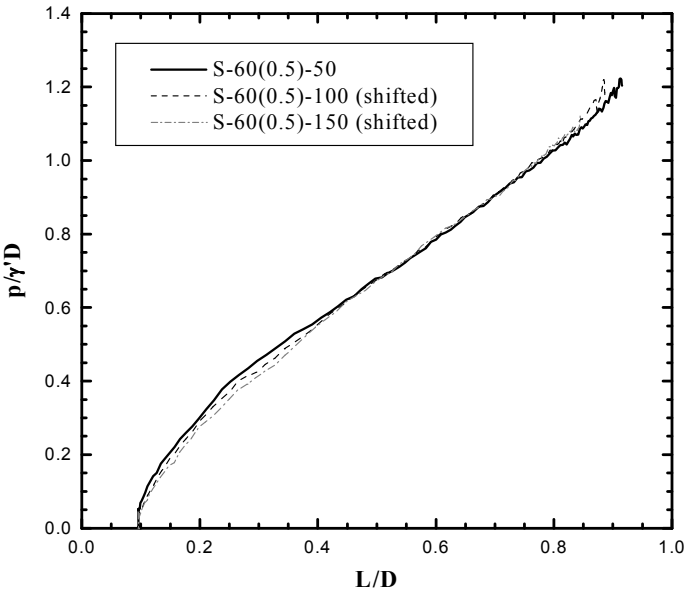

Figure 5.6: Shifted suction pressure in installation with different caisson weight.

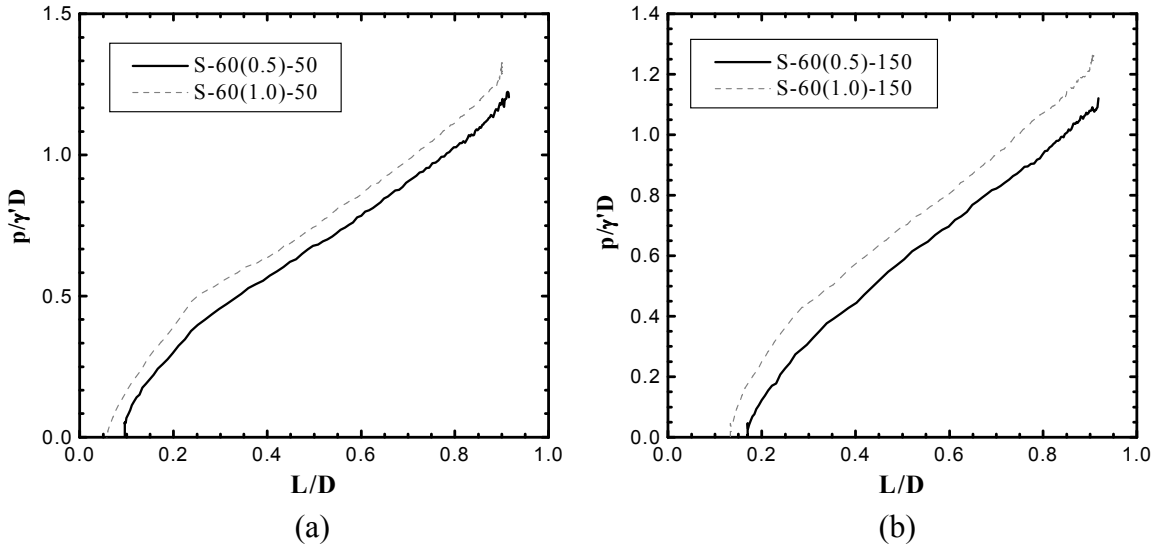

Figure 5.7: Effect of caisson wall thickness on the resulting suction pressure.

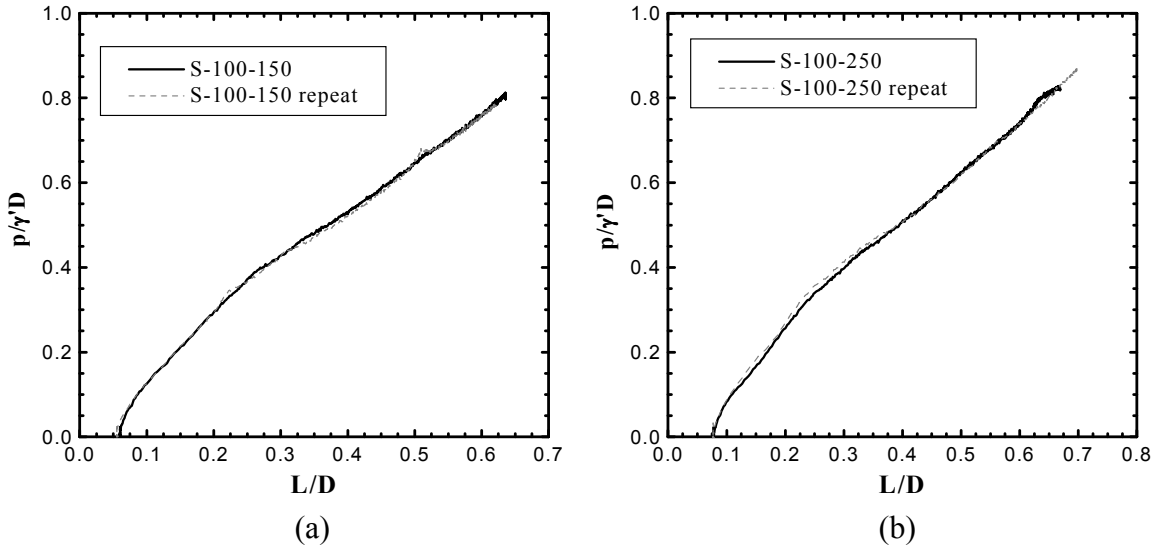

Figure 5.8: Repeatability of the suction installation tests.

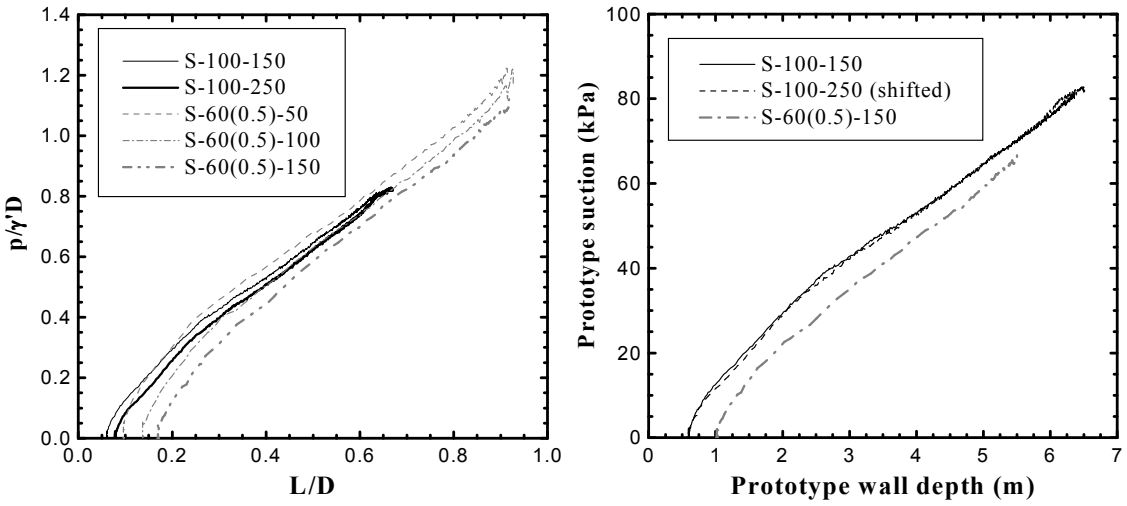

(a) (b)

Figure 5.9: Effect of absolute caisson size on suction pressure.

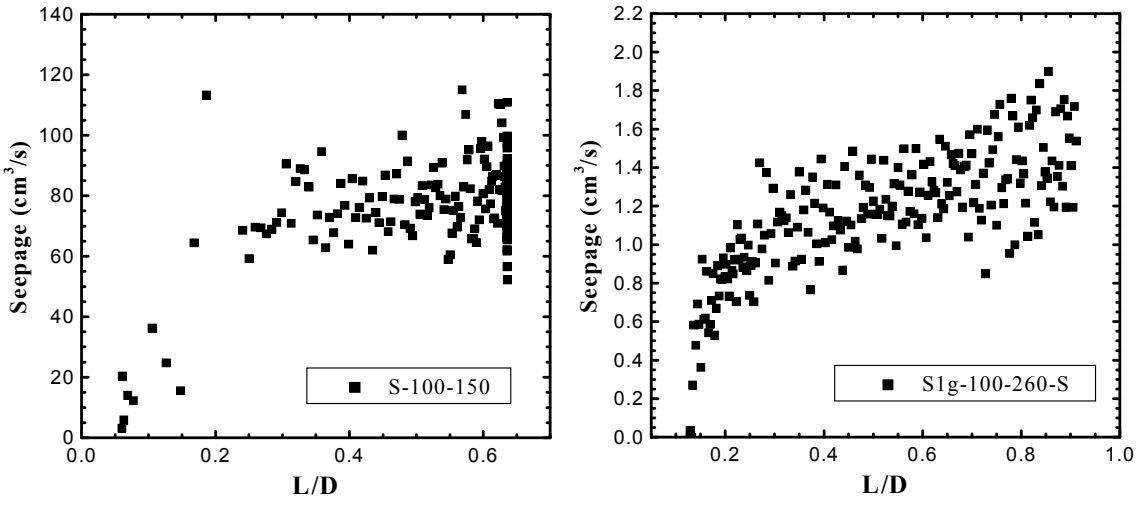

(a) (b)

Figure 5.10: Typical centrifuge and 1g seepage for the 100 mm model caissons.

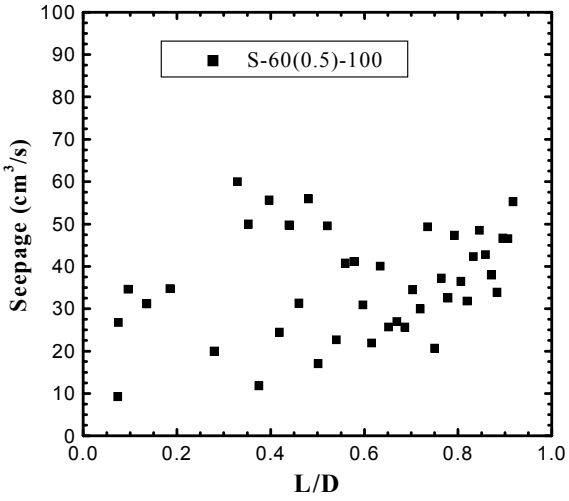

Figure 5.11: Typical seepage for a 6 m diameter caisson.

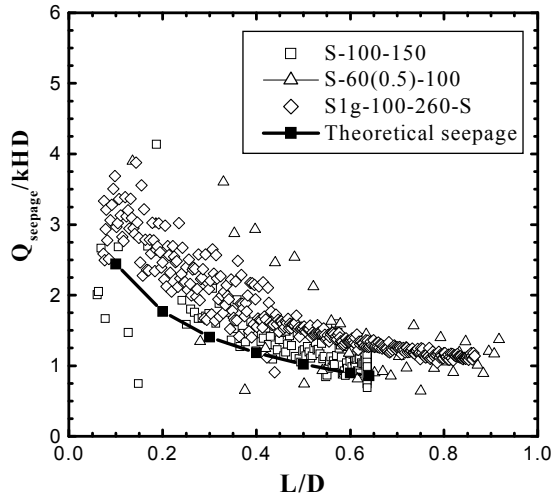

Figure 5.12: Comparison of normalised seepage data.

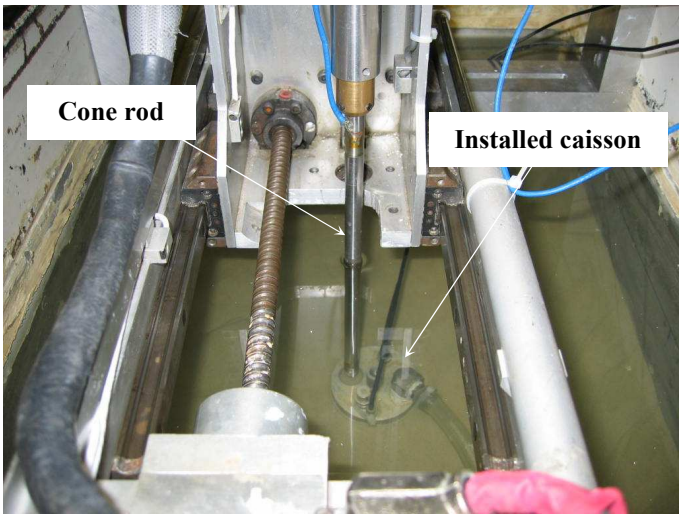

Figure 5.13: Set-up of the cone test inside the suction caisson.

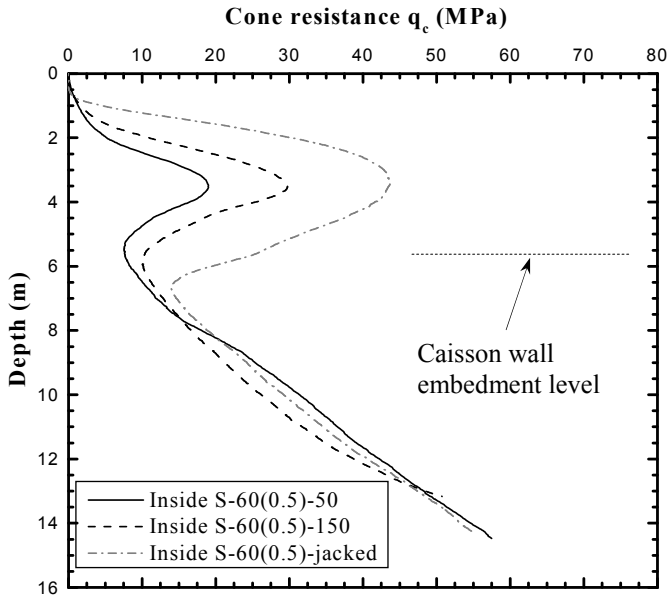

Figure 5.14: Cone test inside a 6 m diameter, t/D = 0.5% wall thickness caisson.

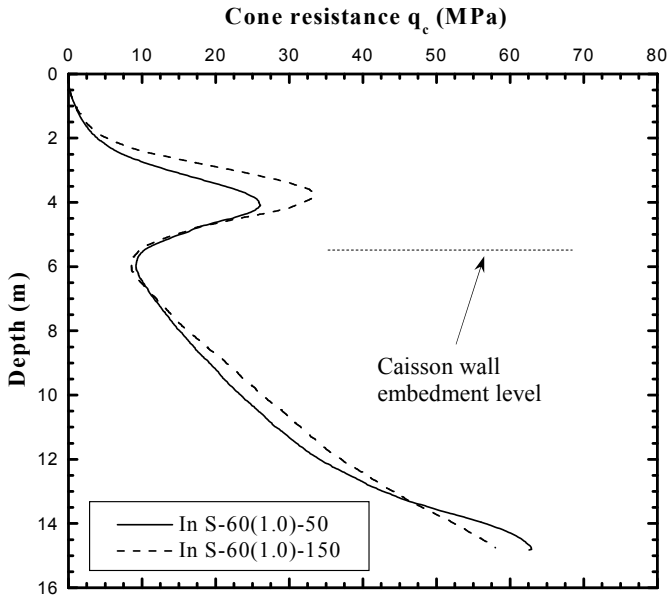

Figure 5.15: Cone test inside a 6 m diameter, t/D = 1% mm wall thickness caisson.

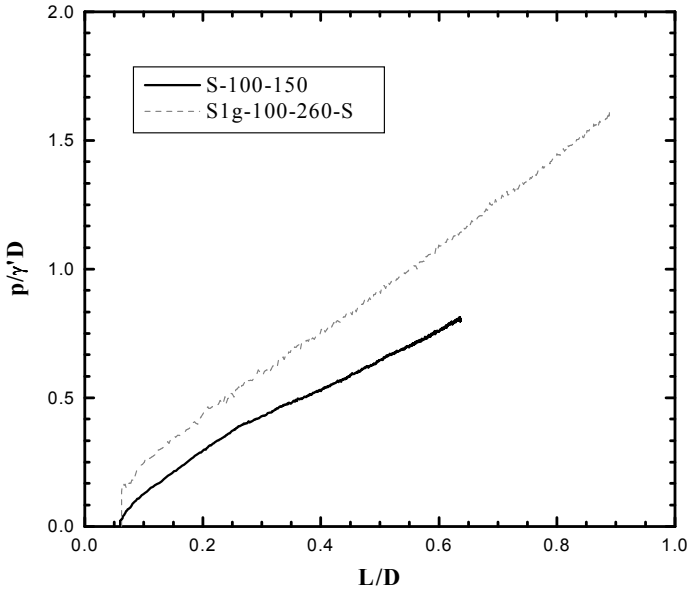

Figure 5.16: Comparison with 1g test results.

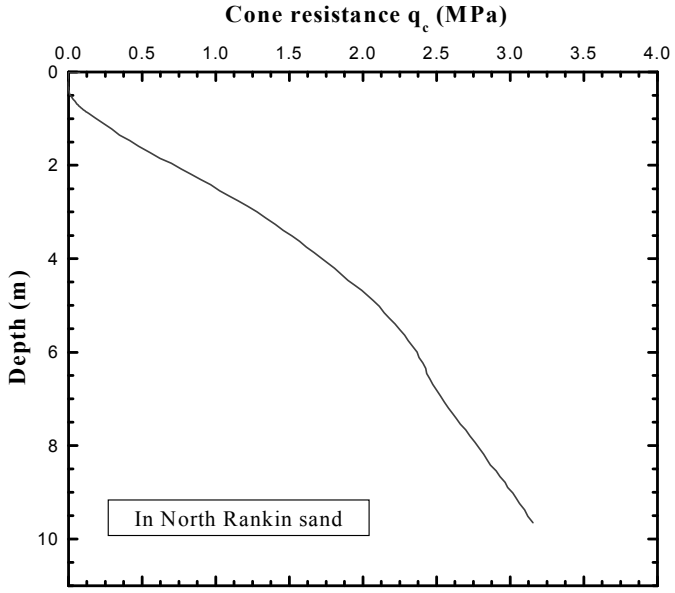

Figure 5.17: Cone penetration test in North Rankin calcareous sand.

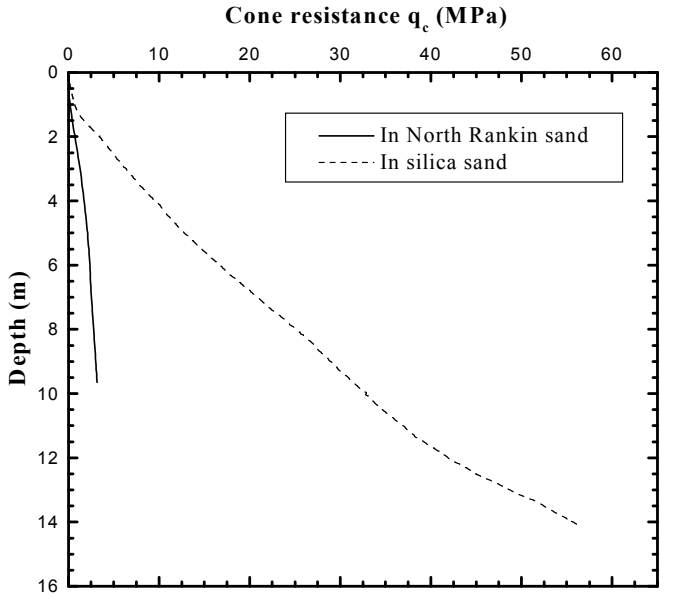

Figure 5.18: Comparison with cone test result in silica sand.

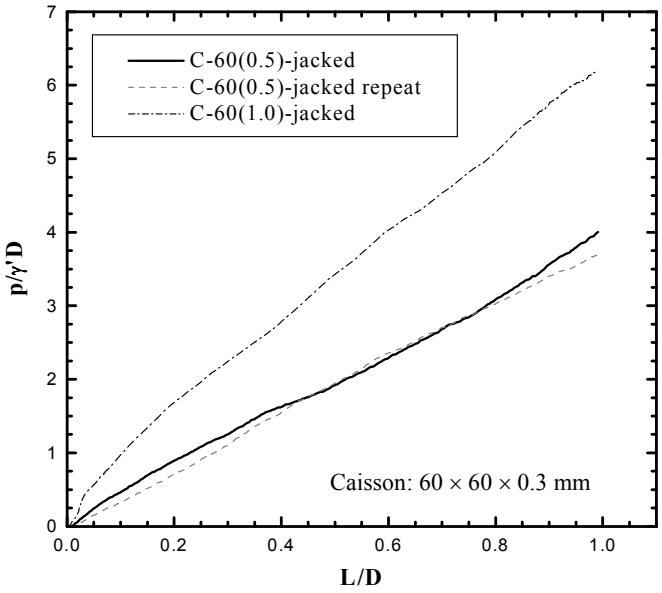

(a)

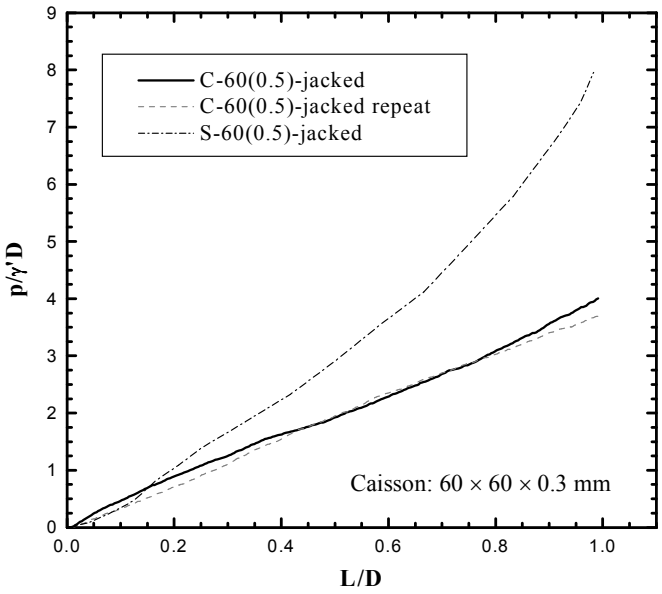

(b)

Figure 5.19: Results of caisson jacking in sand.

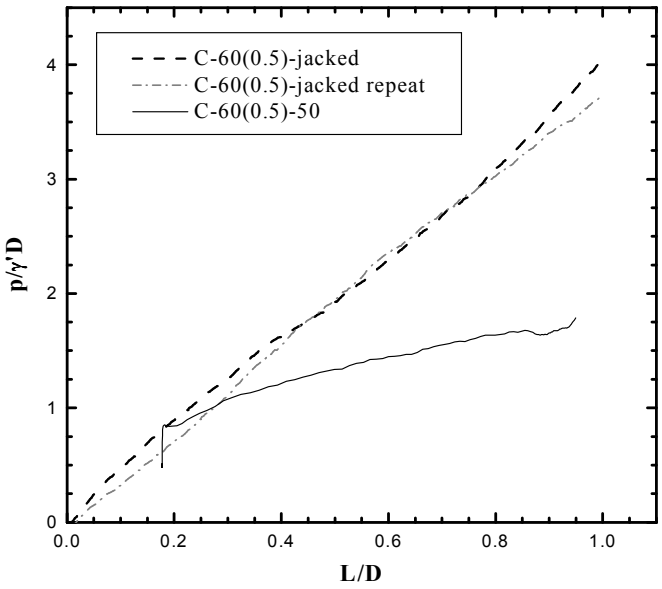

(a)

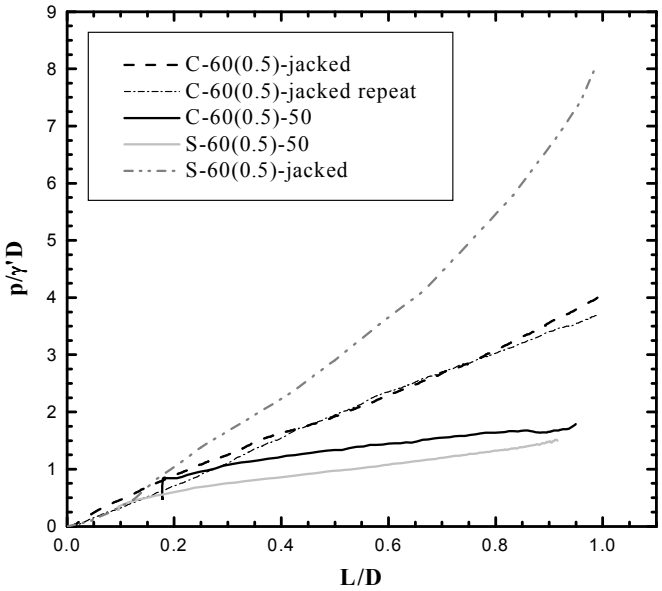

(b)

Figure 5.20: Comparison between jacked installation and suction installation in sand.

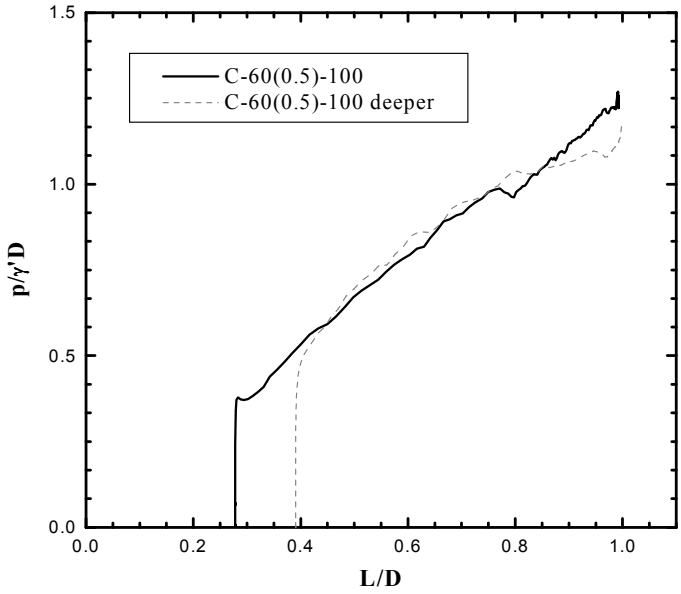

Figure 5.21: Effect of initial wall penetration depth on suction pressure.

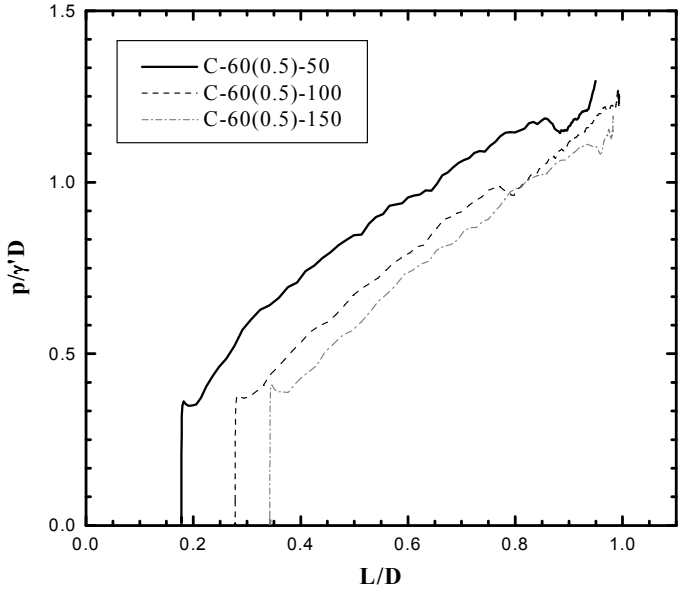

Figure 5.22: Effect of surcharge on the resulting suction pressure.

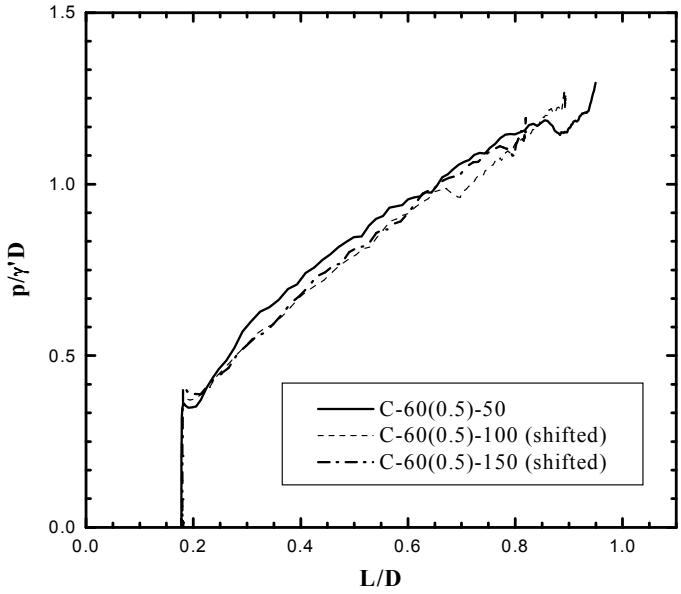

Figure 5.23: Common suction pressure trend for installations with different self-weights.

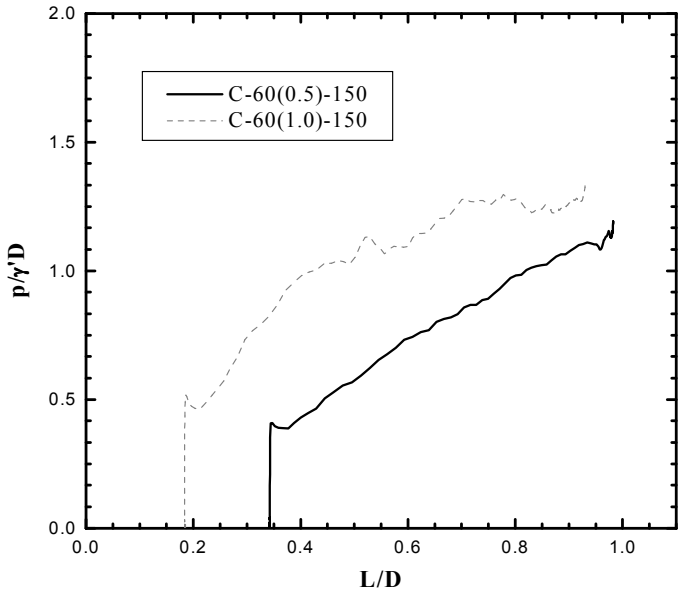

Figure 5.24: Effect of wall thickness on suction pressure.

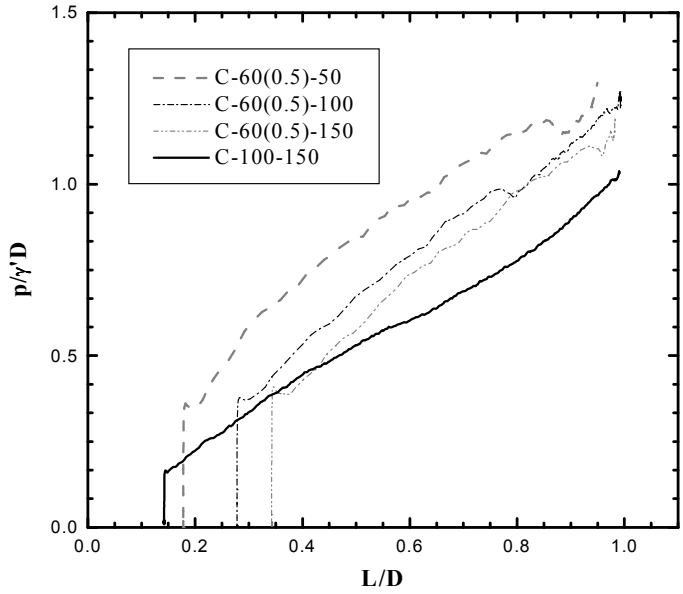

Figure 5.25: Effect of absolute caisson size on suction pressure.

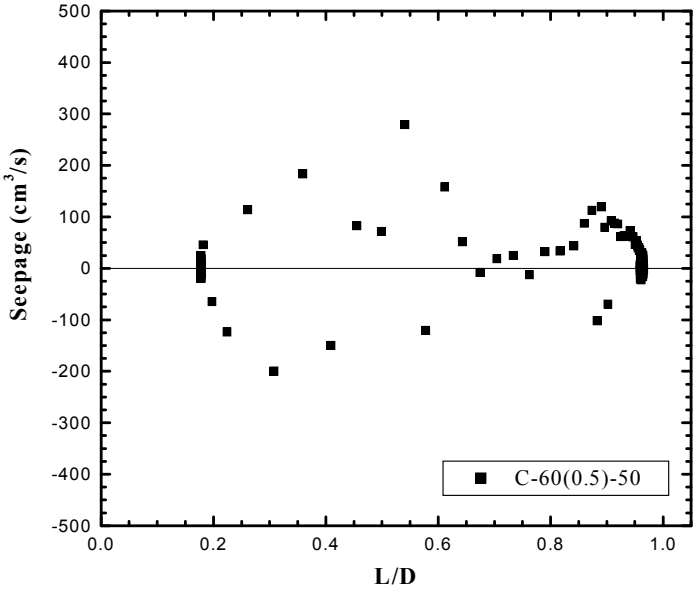

Figure 5.26: Seepage flow during the installation of 6 m caisson in calcareous sand.

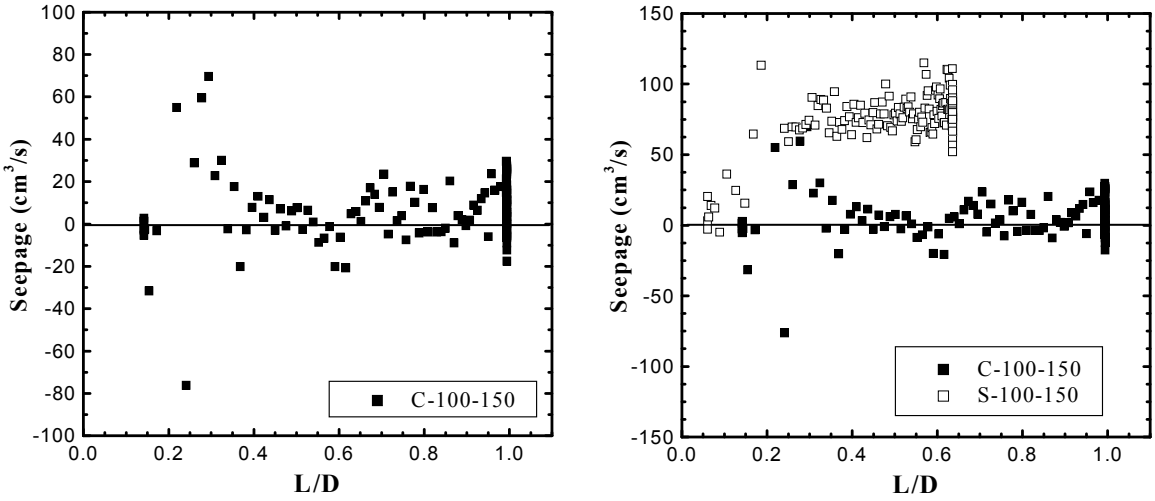

Figure 5.27: Seepage flow during the installation of 10 m caisson in calcareous sand.

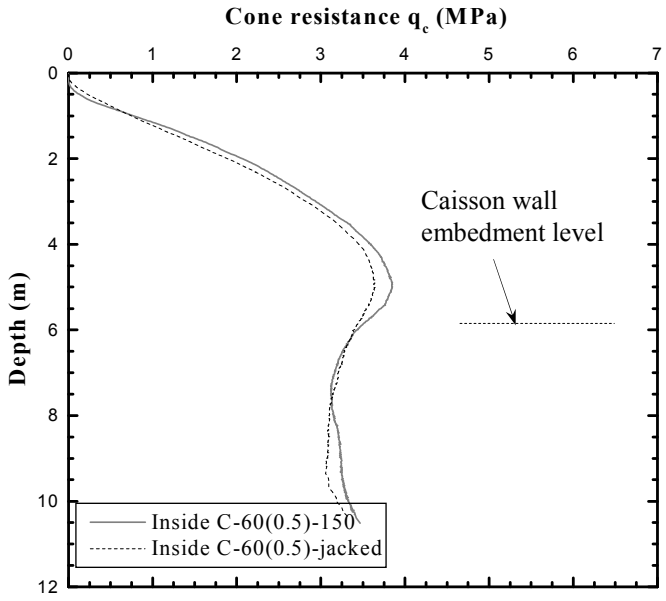

Figure 5.28: Cone tests inside the caisson installed by suction and by jacking.

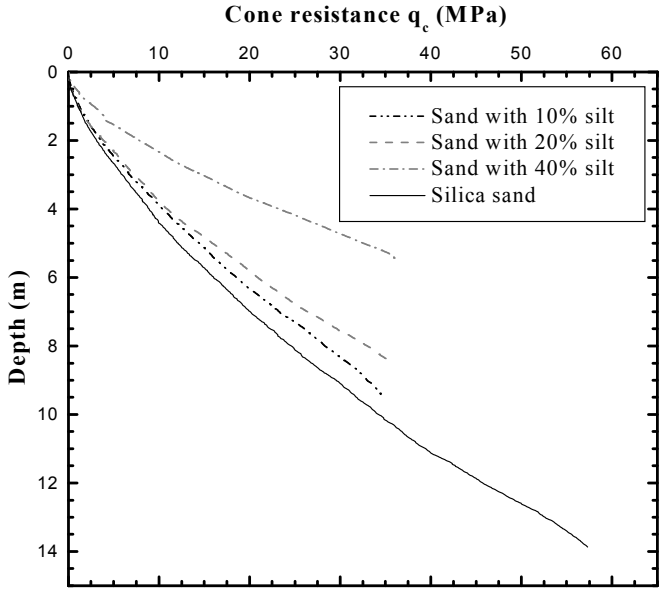

Figure 5.29: Cone resistance results in mixed soils.

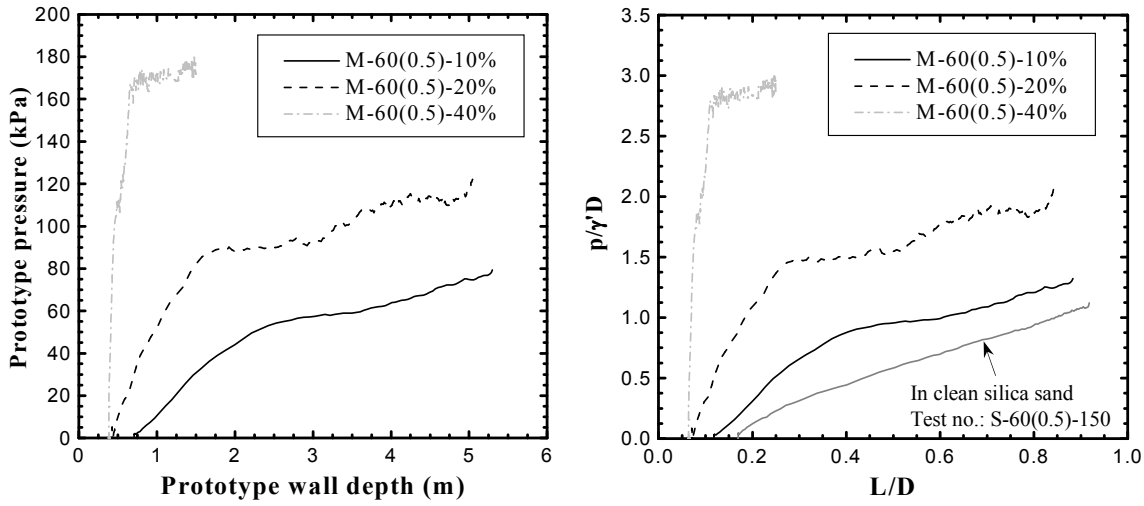

(a) (b)

Figure 5.30: Installation results in mixed soils.

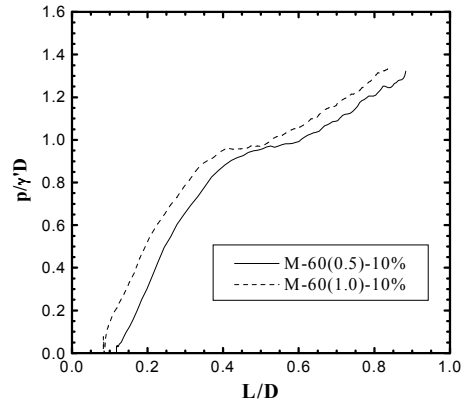

Figure 5.31: Effect of wall thickness on suction pressure.

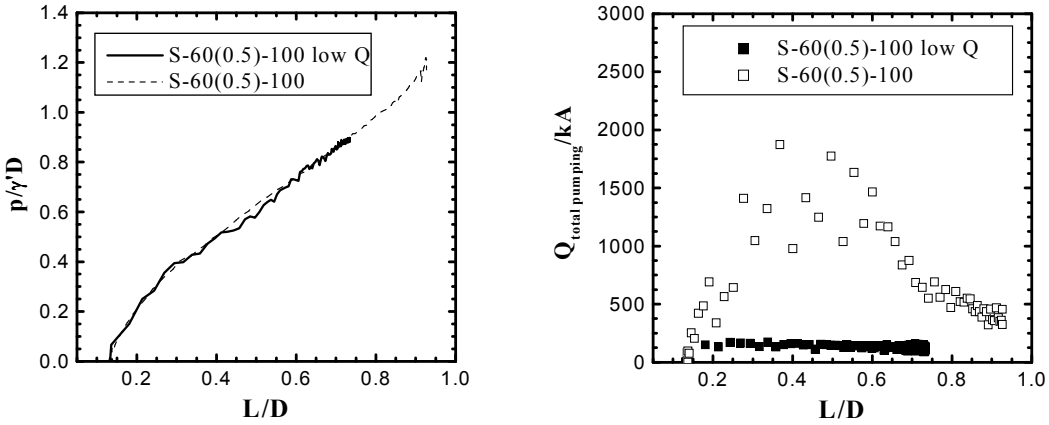

(a) (b)

Figure 5.32: Comparison of slow and fast pumping installation for 6 m caisson.

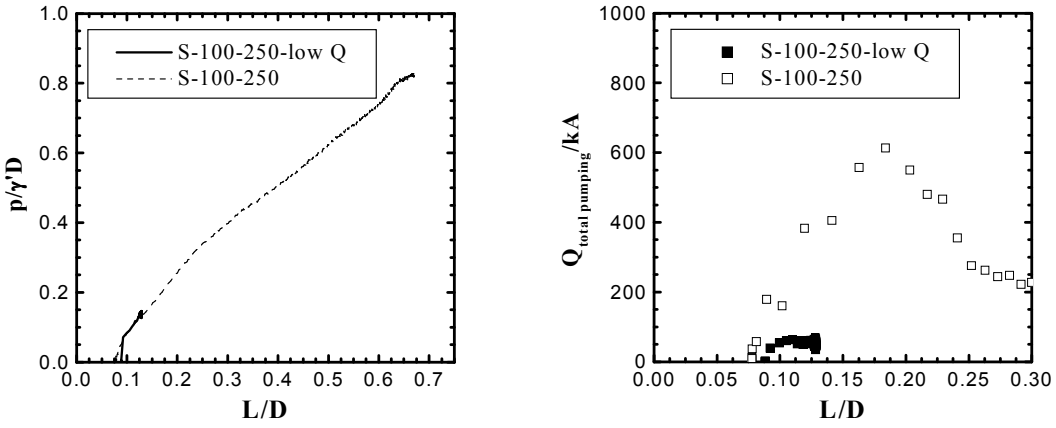

(a) (b)

Figure 5.33: Comparison of slow and fast pumping installation for 10 m caisson.

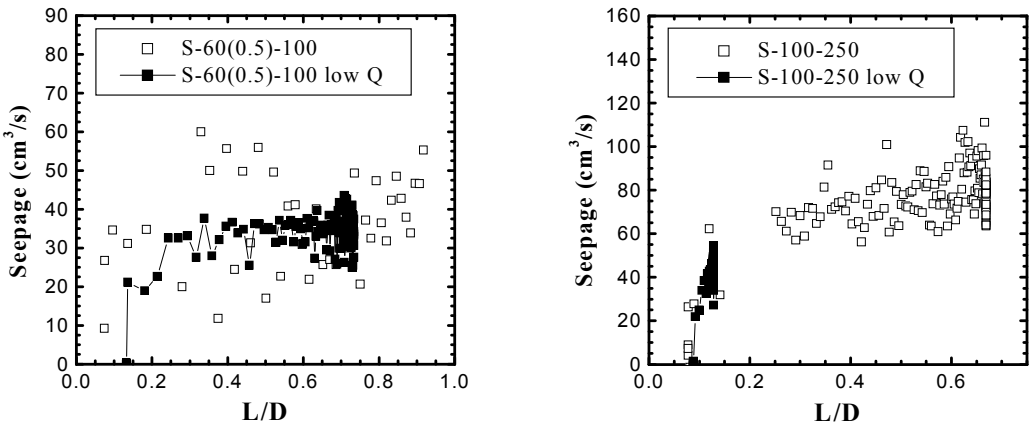

(a) (b)

Figure 5.34: Comparison of centrifuge seepage in slower and faster pumping.

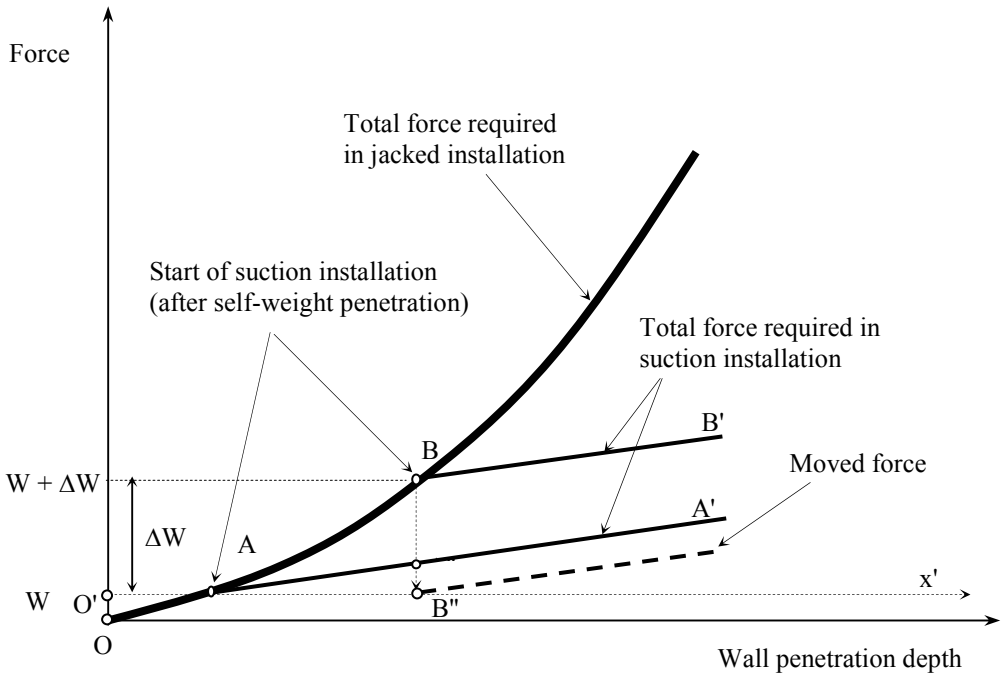

Figure 5.35: Plotting of suction pressure in comparison with total penetration force.

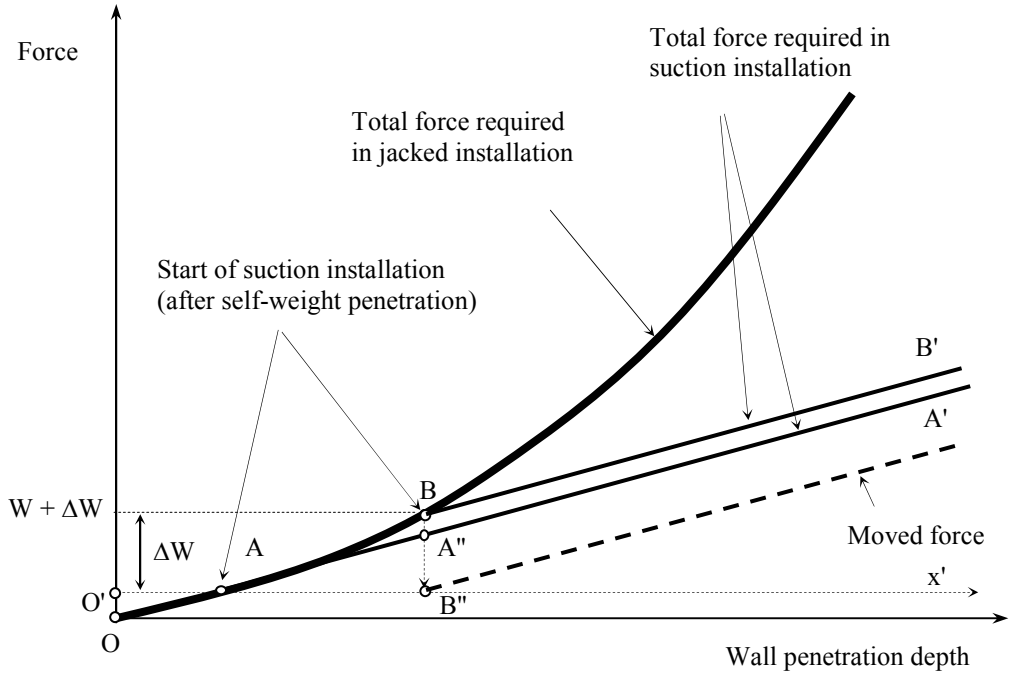

Figure 5.36: Plotting of suction pressure in comparison with total penetration force.

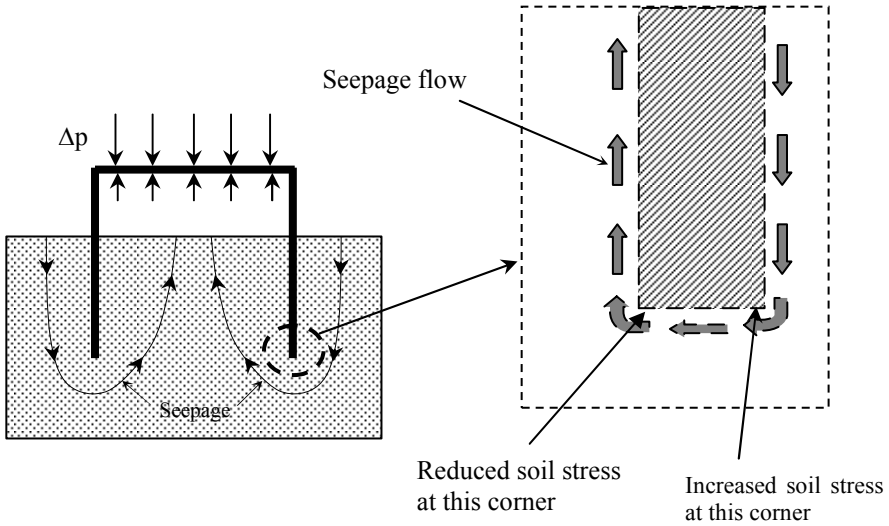

Figure 5.37: Seepage flow condition around the caisson wall tip during installation.

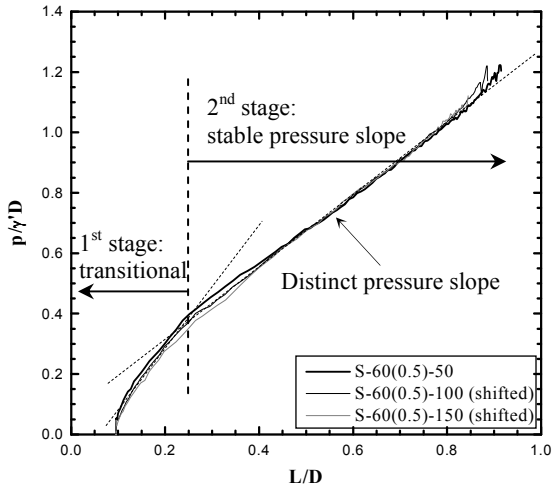

(a)

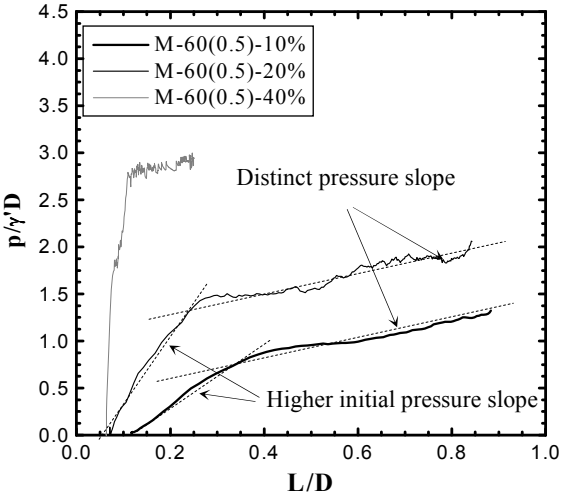

(b)

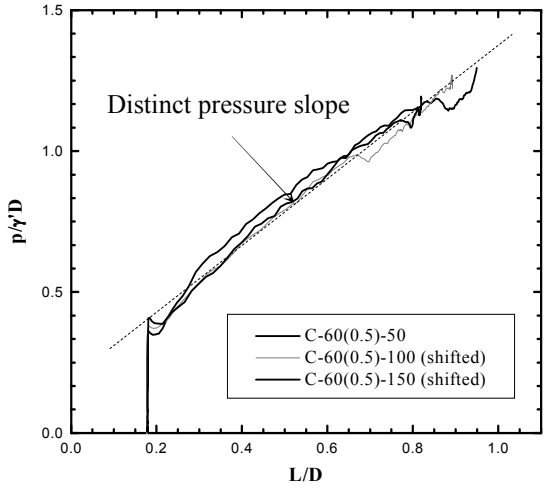

(c)

Figure 5.38: Observed distinct pressure slope in different installation results.

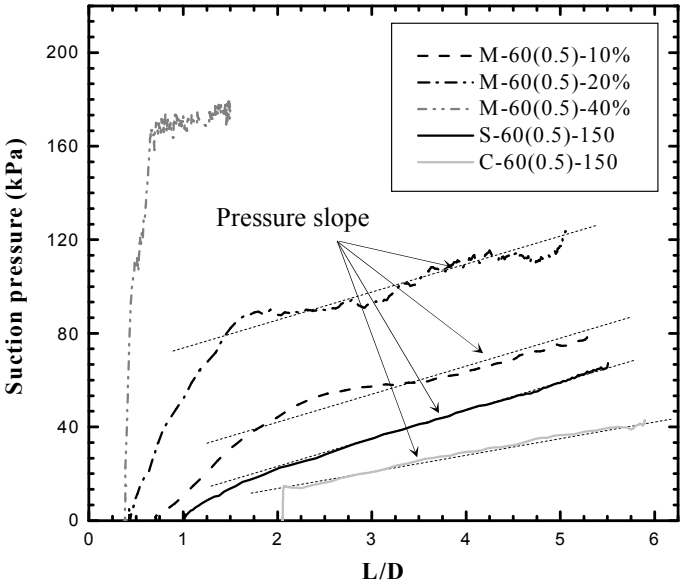

(a)

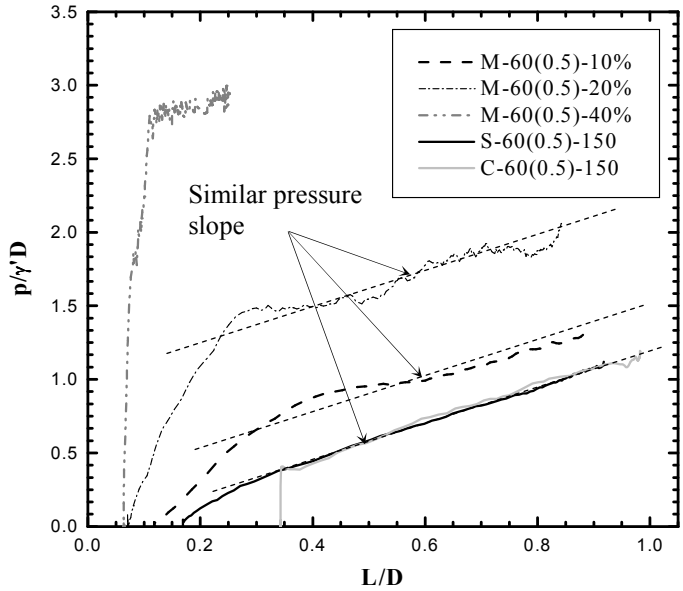

(b)

Figure 5.39: Comparison of suction pressure trends in various soil types.

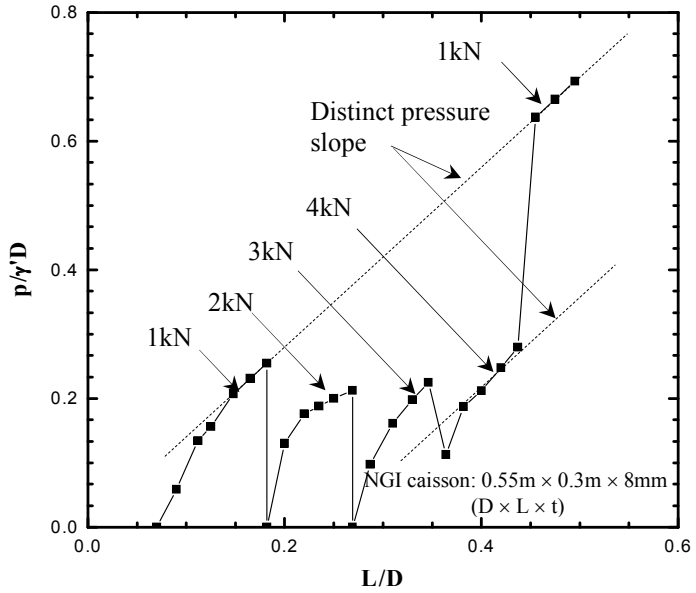

Figure 5.40: NGI results for caisson installation with different surcharge levels.

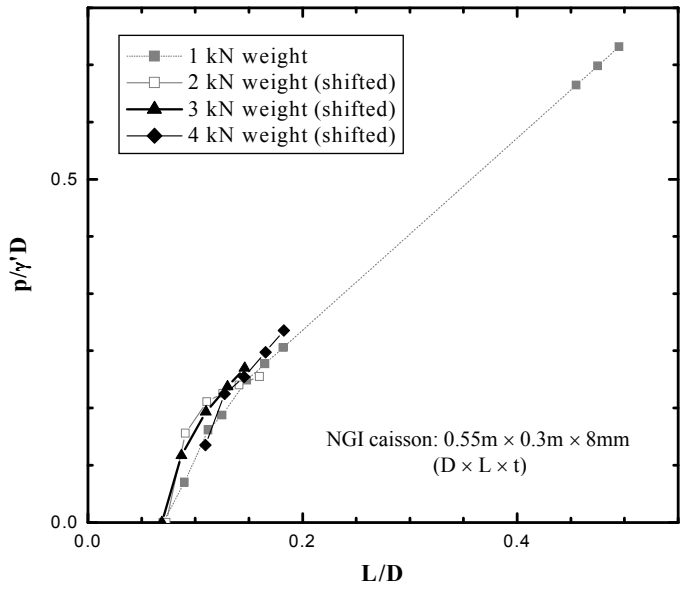

Figure 5.41: Shifted suction pressure for different caisson self-weights.

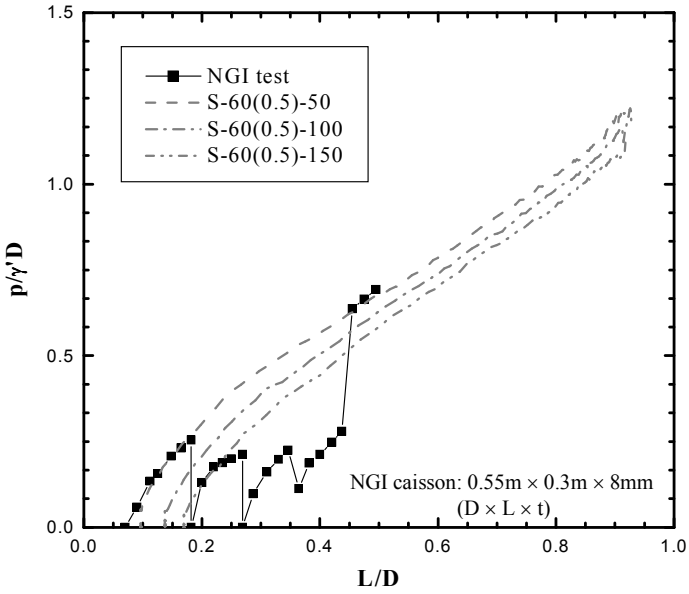

Figure 5.42: Comparison of NGI and UWA results.

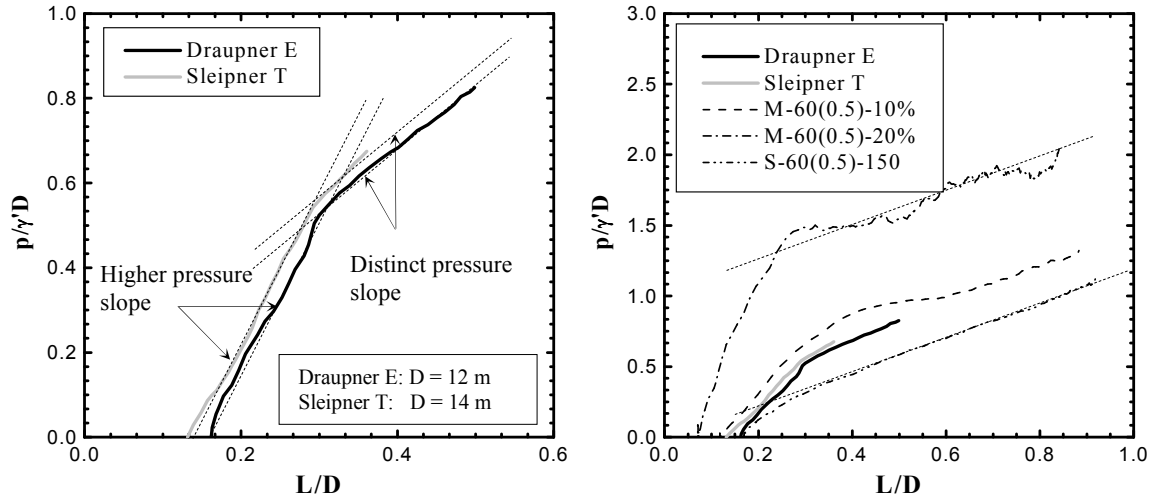

Figure 5.43: Draupner E and Sleipner T installations.

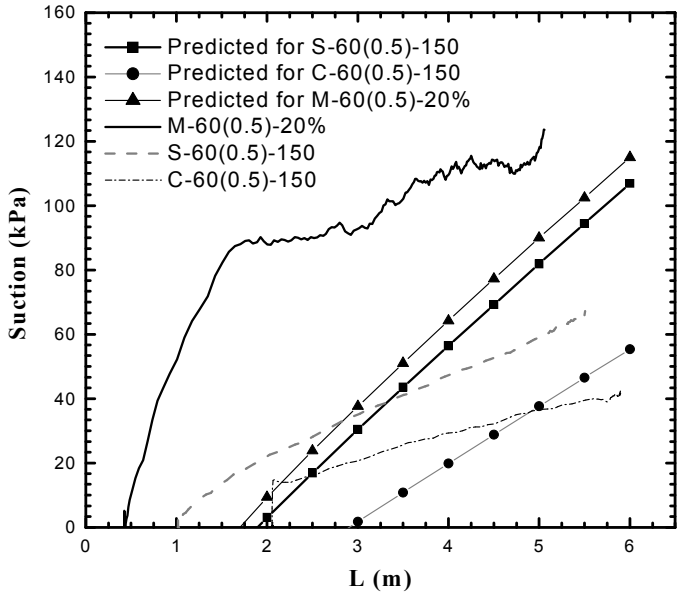

Figure 5.44: Comparison with suction pressure prediction proposed by Feld (2001).

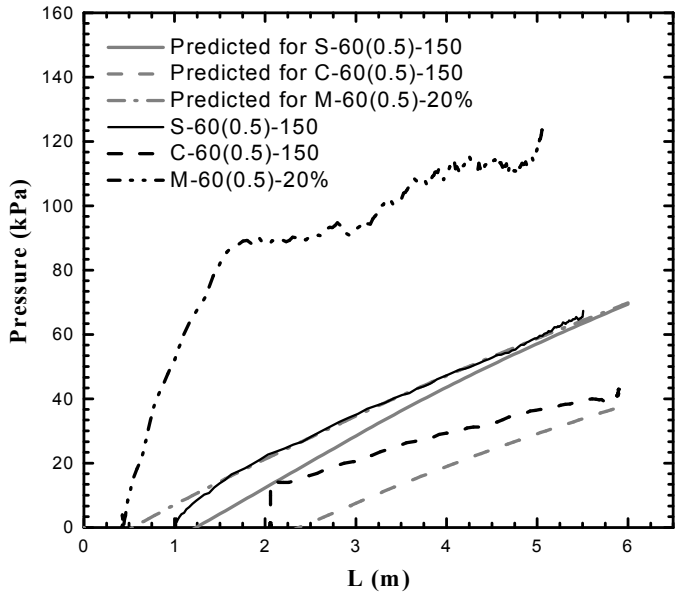

Figure 5.45: Comparison with suction pressure prediction proposed by Houlsby and Byrne (2005).

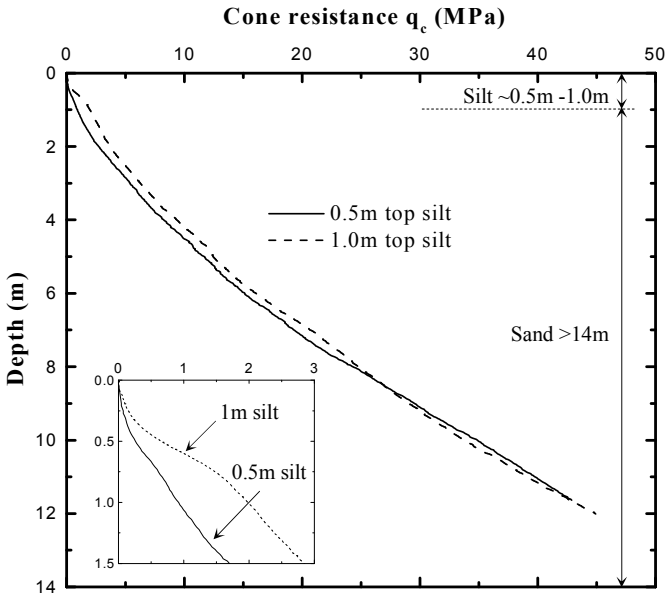

Figure 6.1: Cone tests in soil with surface silt layer.

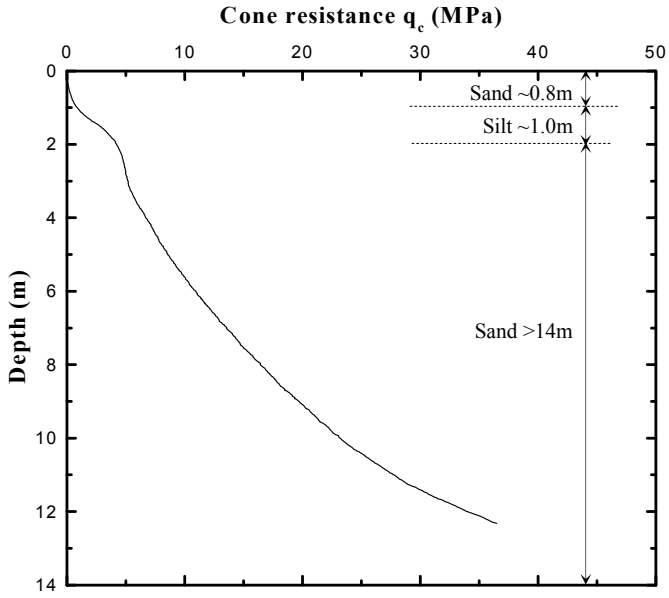

Figure 6.2: Cone test in soil with a silt layer 0.8 m below the surface.

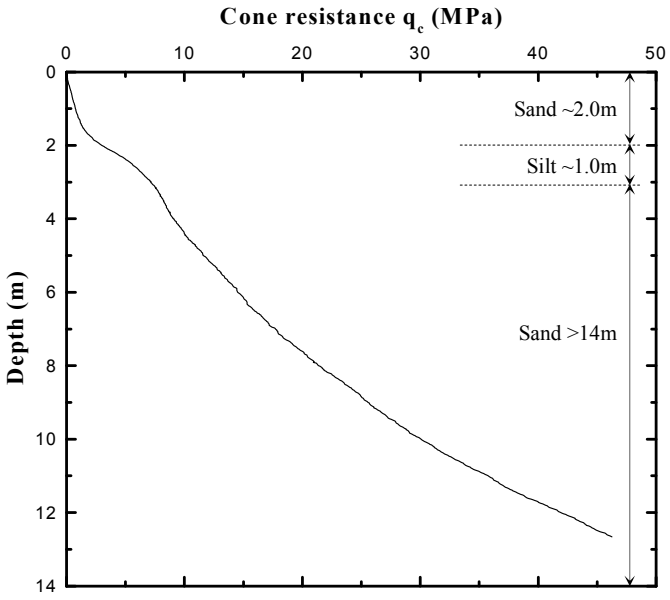

Figure 6.3: Cone test in soil with a silt layer 2.0 m below the surface.

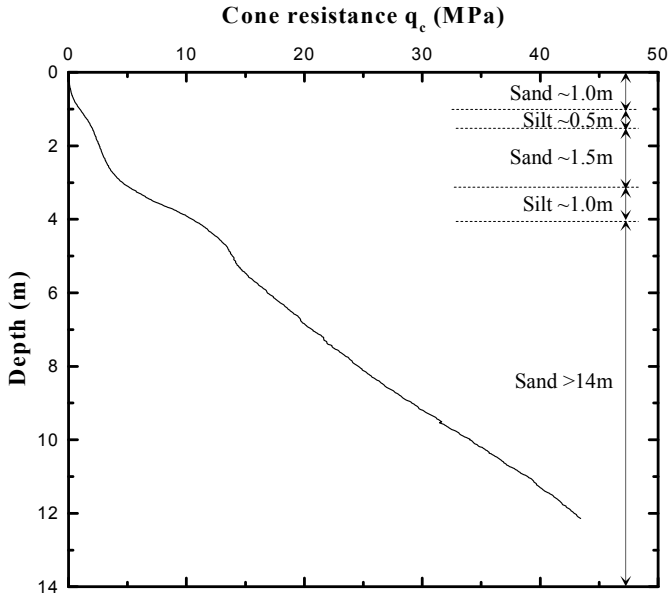

Figure 6.4: Cone test in soil with 2 silts layers.

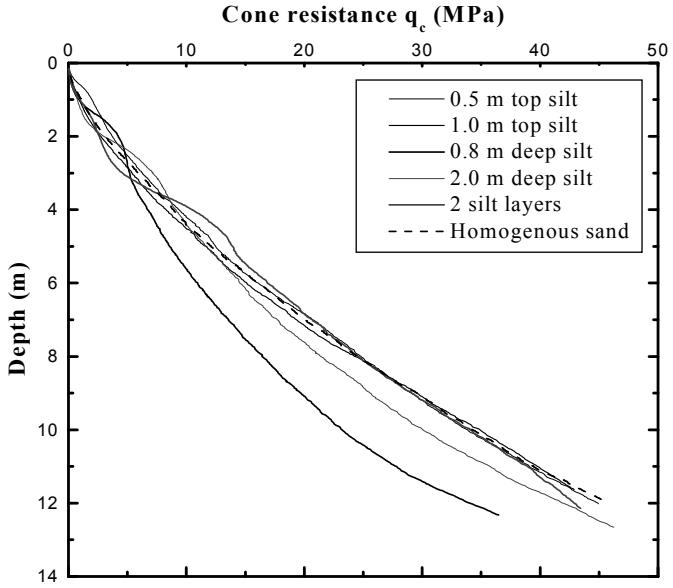

Figure 6.5: Comparison with cone test in homogenous sand.

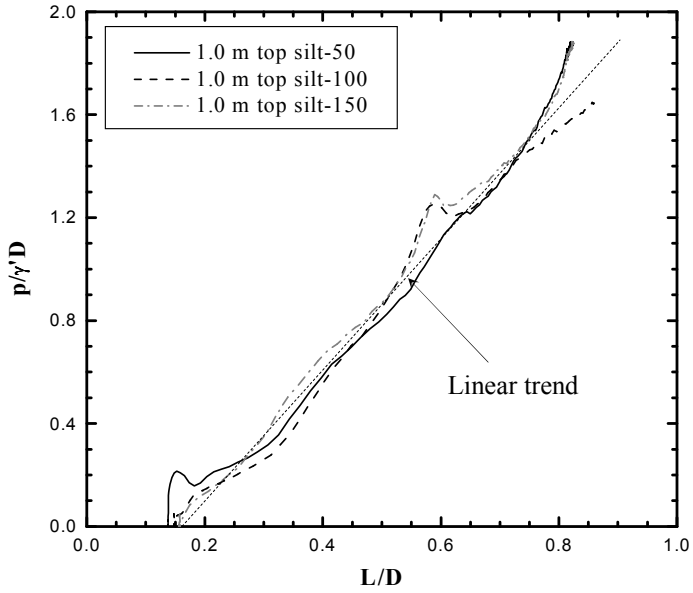

Figure 6.6: (a) Suction pressure in soil 1.0 m thick surface silt layer.

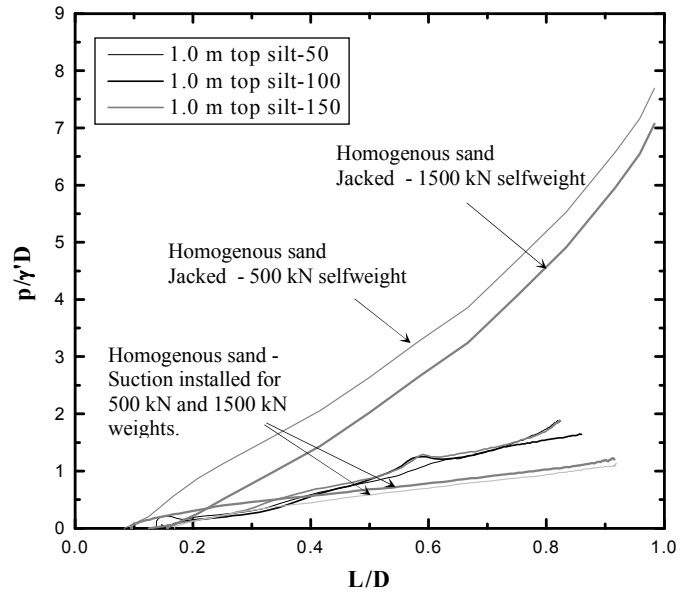

Figure 6.6: (b) Comparison with jacked and suction installation in homogenous sand.

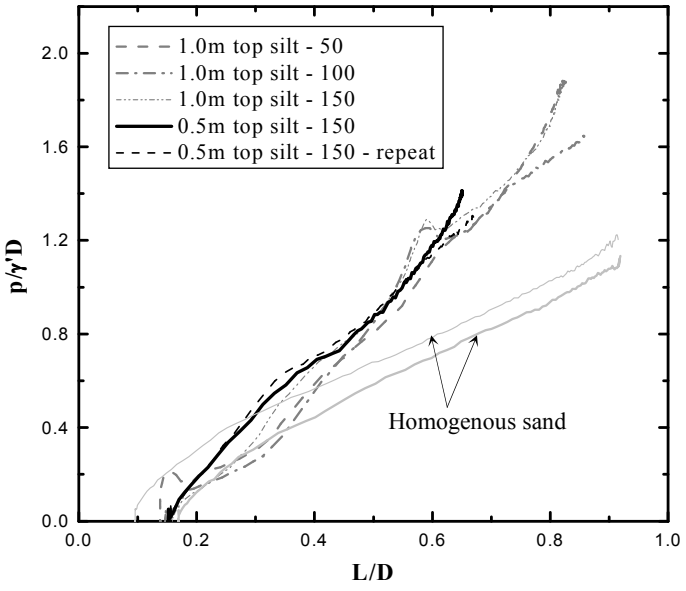

Figure 6.7: Suction pressure in soil 0.5 m thick surface silt layer.

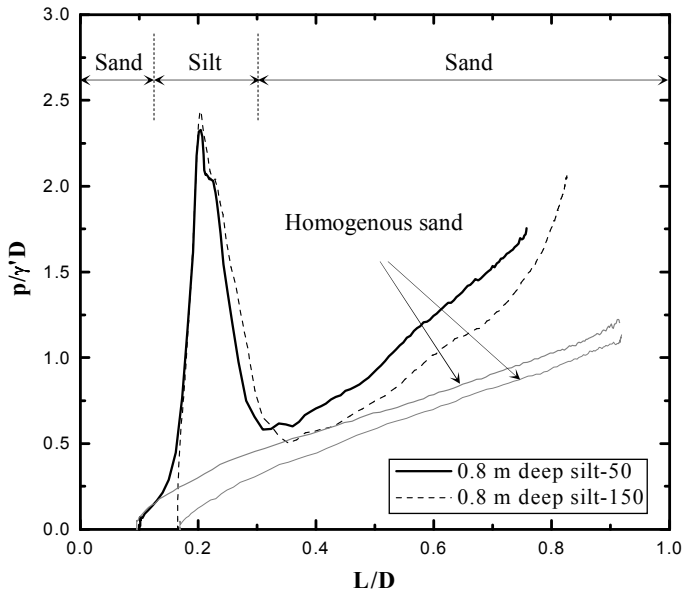

Figure 6.8: Suction pressure in soil 1.0 m thick silt layer, 0.8 m below the surface.

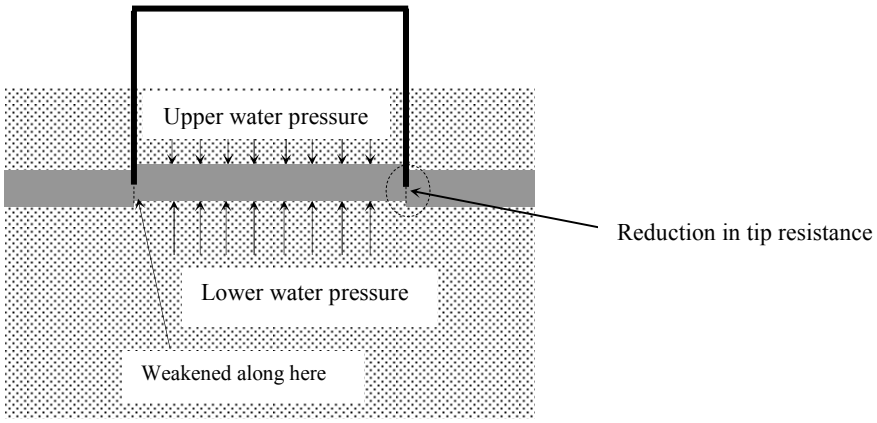

Figure 6.9: Uplift of silt layer during suction installation.

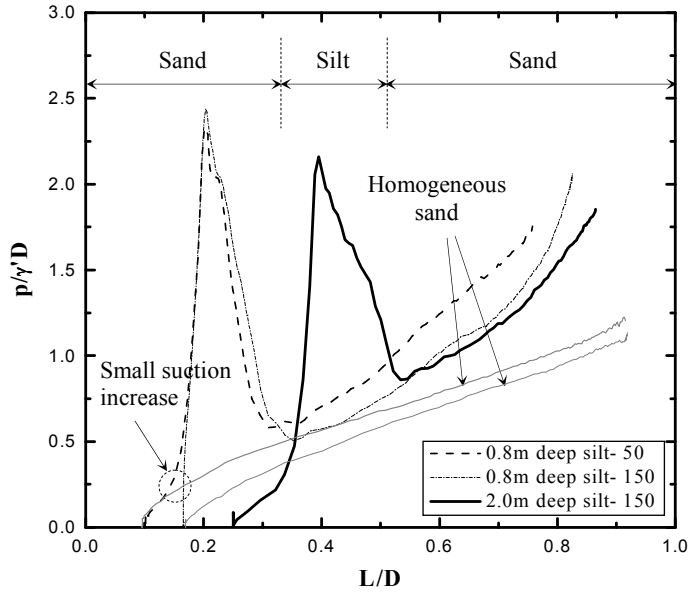

Figure 6.10: Suction pressure in soil 1.0 m thick silt layer, 2.0 m below the surface.

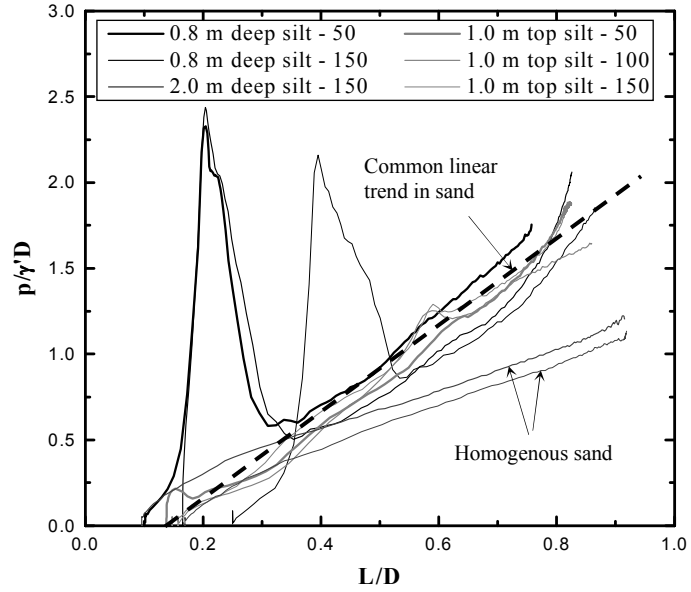

Figure 6.11: Suction pressure trend in sand below the silt layer.

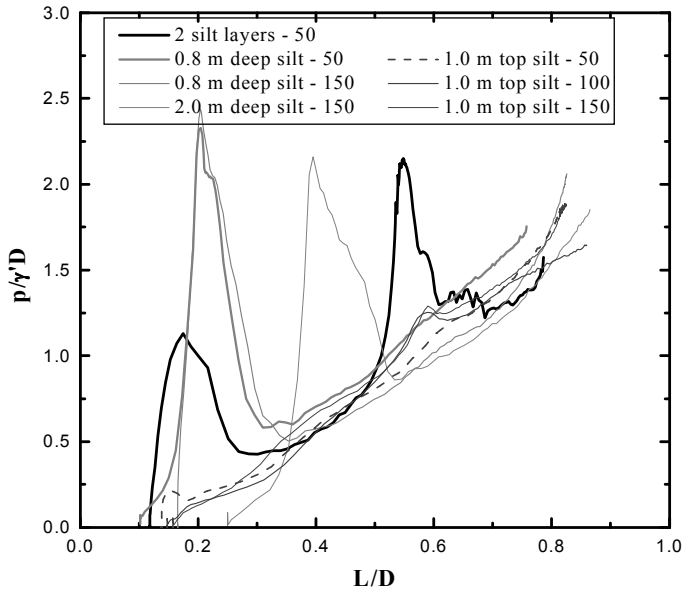

Figure 6.12: Suction pressure in soil with 2 silt layers.

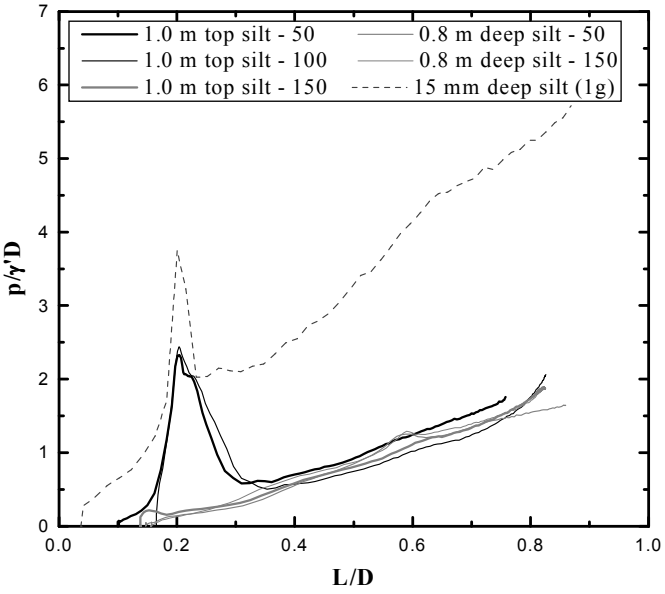

Figure 6.13: Comparison with 1g result.

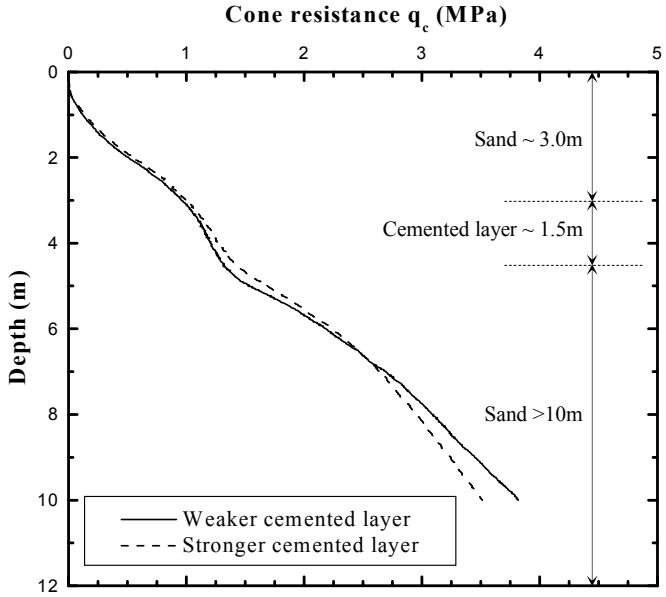

Figure 6.14: Cone tests in soil with a single cemented layer.

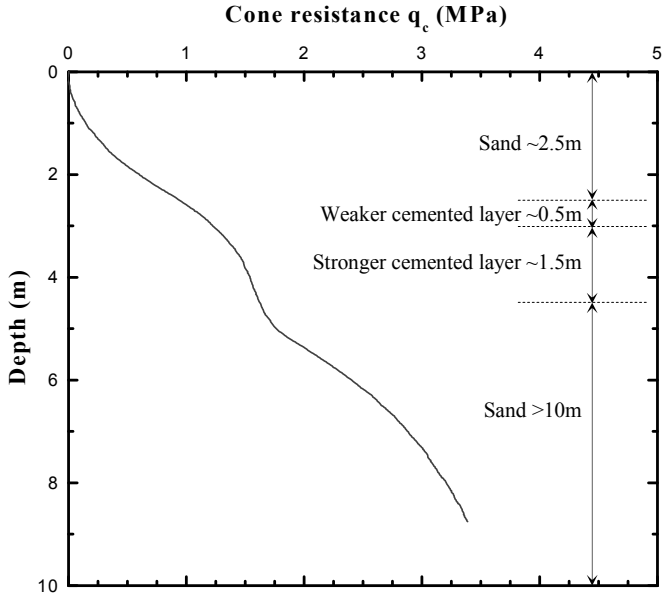

Figure 6.15: Cone tests in soil with a weak cemented layer overlying a stronger one.

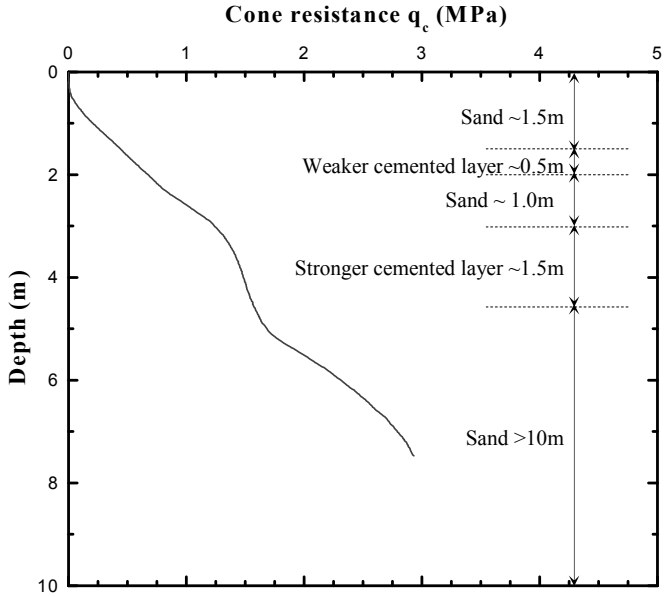

Figure 6.16: Cone tests in soil with 2 cemented layers, separated by a sand layer.

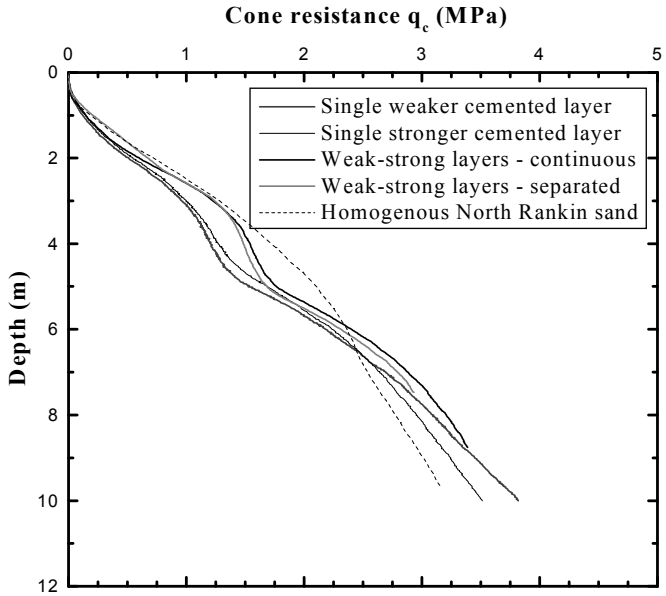

Figure 6.17: Comparison with cone tests in homogenous sand.

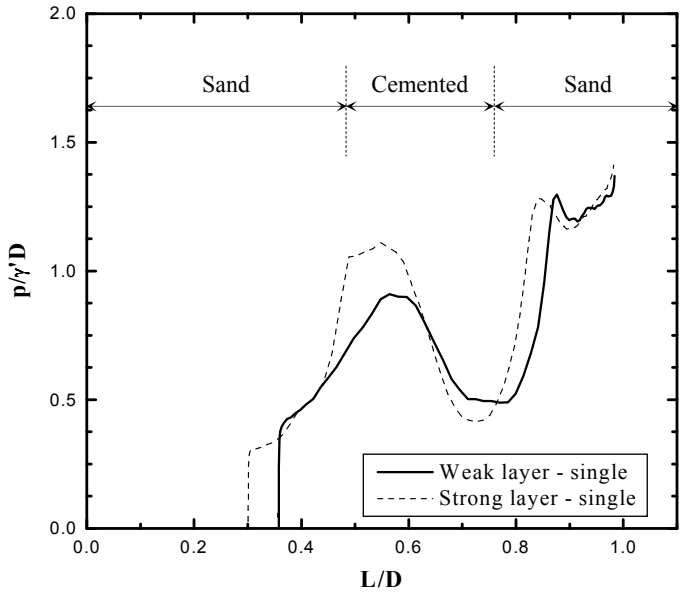

Figure 6.18: (a) Suction pressure in soil with a single cemented layer.

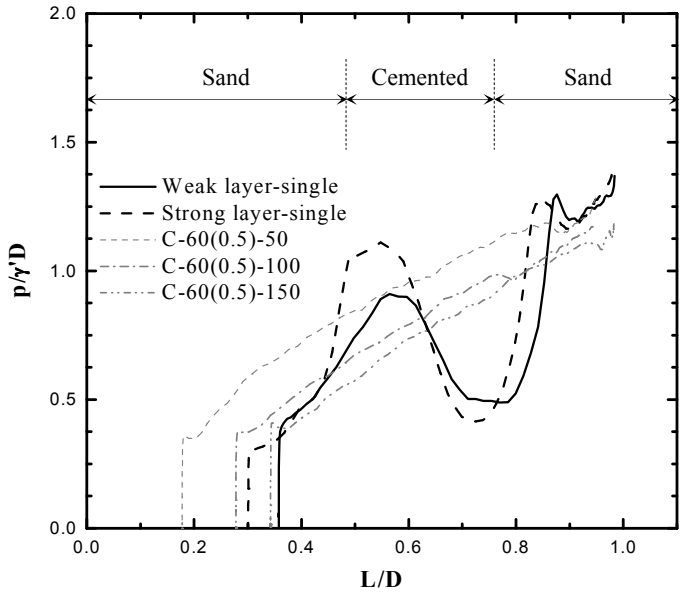

Figure 6.18: (b) Comparison with results in homogenous sand.

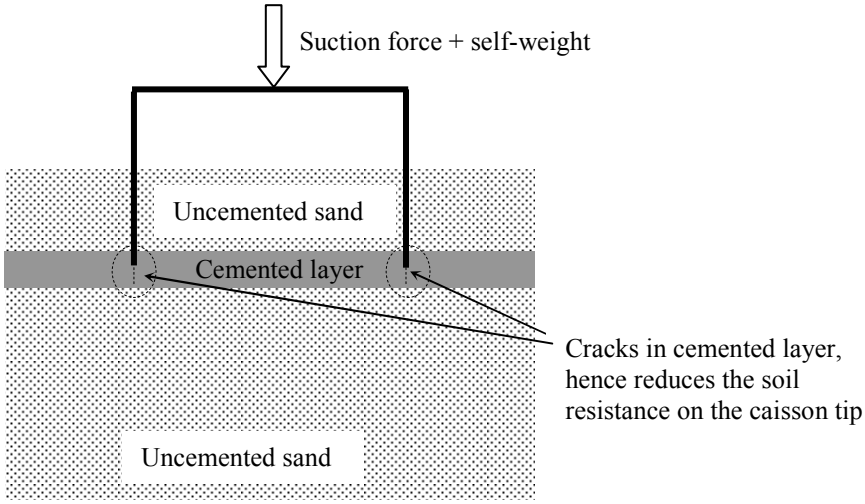

Figure 6.19: Crack formation mechanism during penetration.

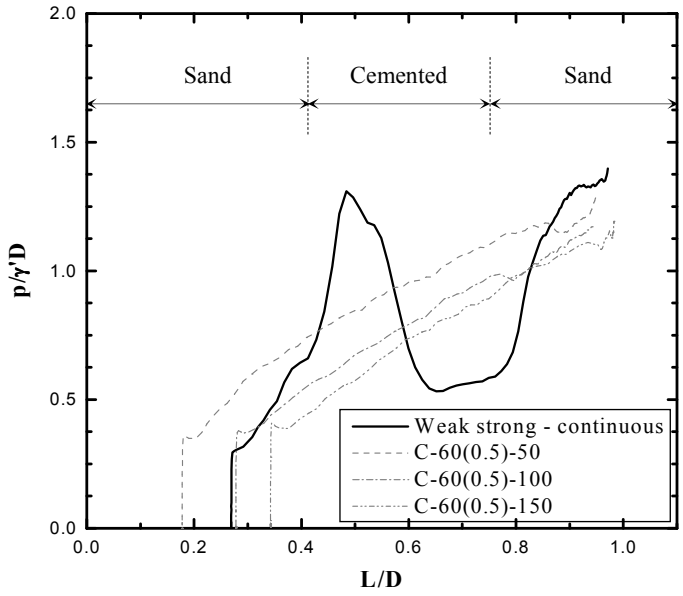

Figure 6.20: Suction in soil with a weak cemented layer overlaying the stronger one.

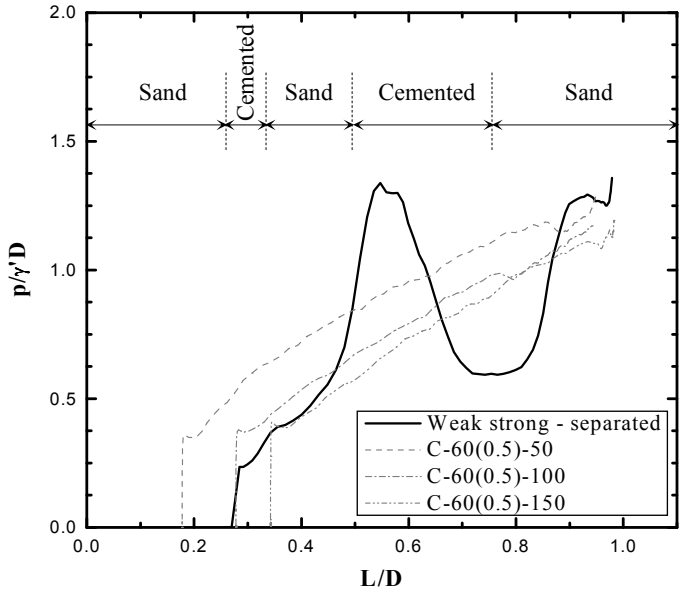

Figure 6.21: Suction pressure in soil with 2 cemented layers, separated by a sand layer.

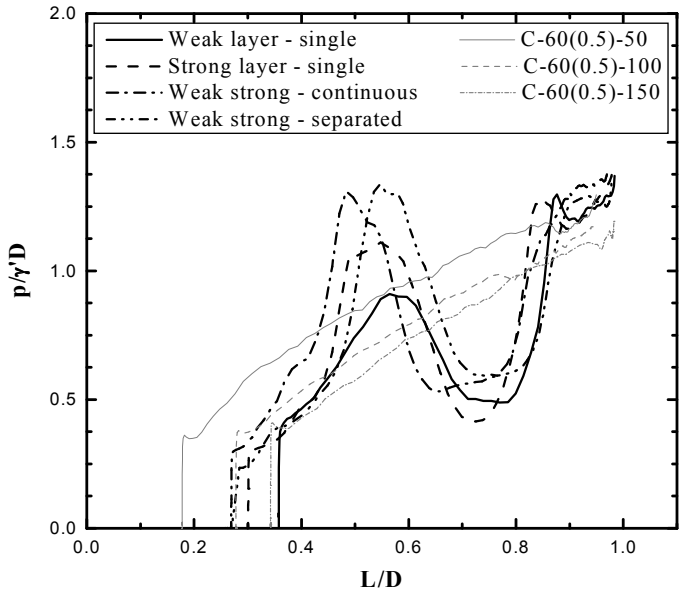

Figure 6.22: Comparison of all suction pressure results in cemented soils.

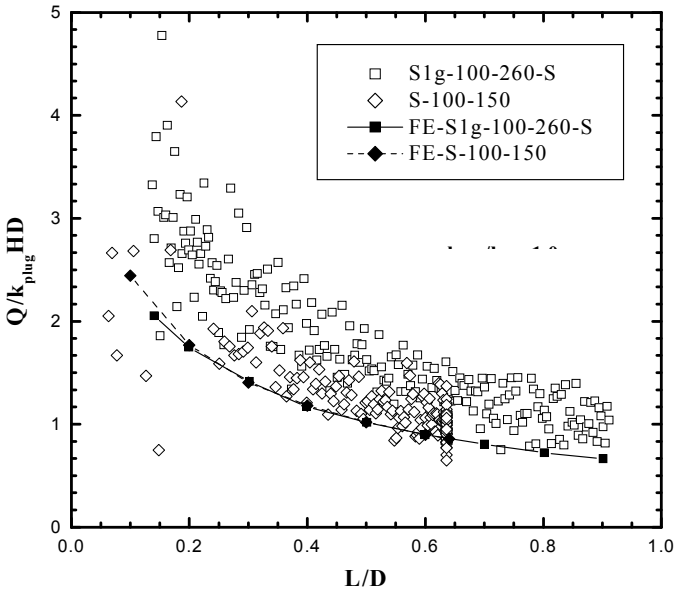

Figure 7.1: Check against experimental seepage.

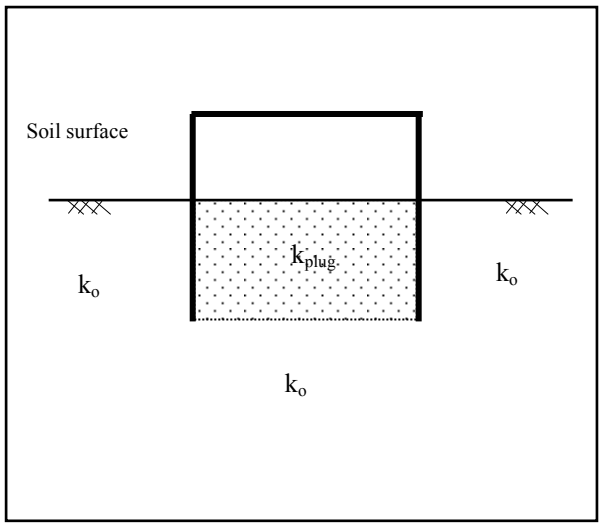

Figure 7.2: Internal plug permeability k_{plug}.

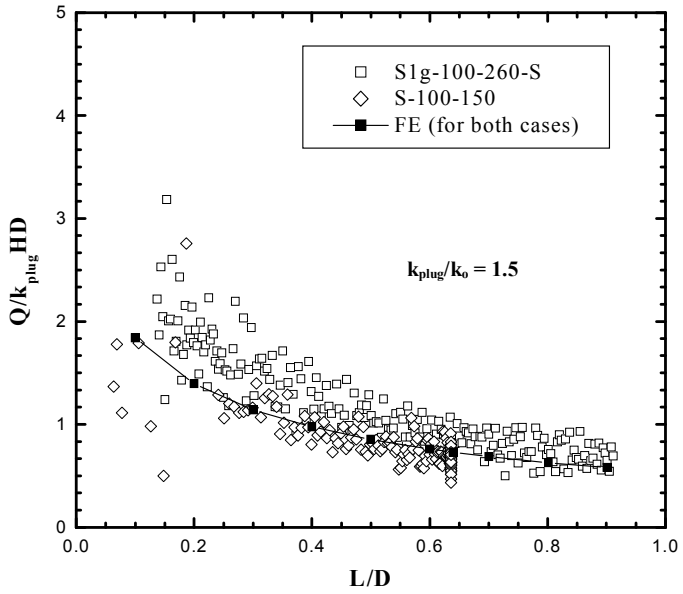

(a)

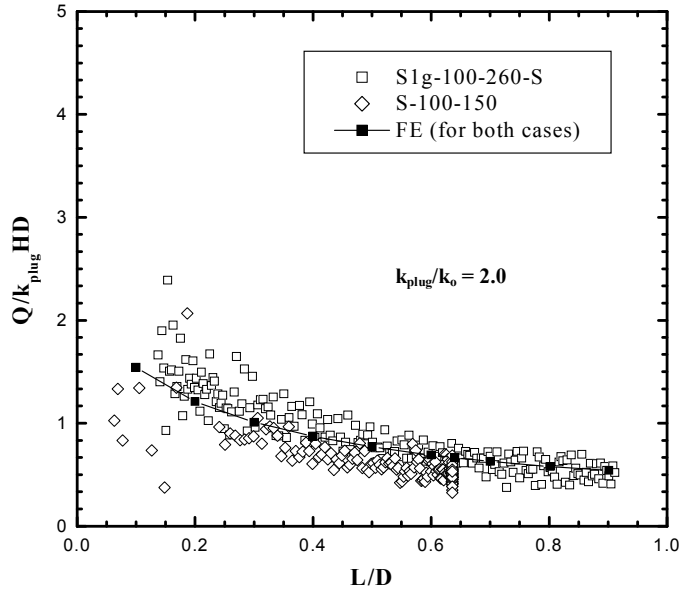

(b)

Figure 7.3: Normalised seepage flow for increased k_{plug}/k_o ratios.

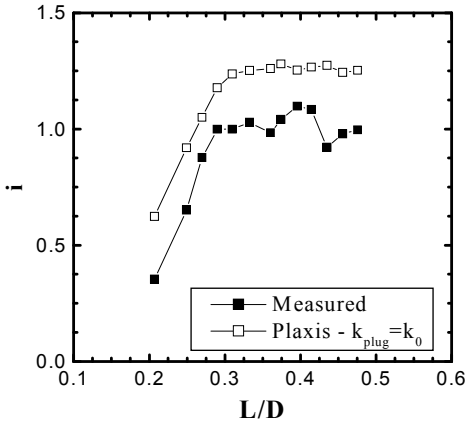

Figure 7.4: Result for no changes in k_{plug}.

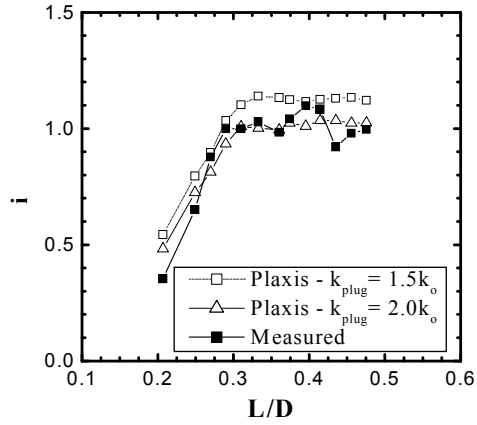

Figure 7.5: results for varying k_{plug}.

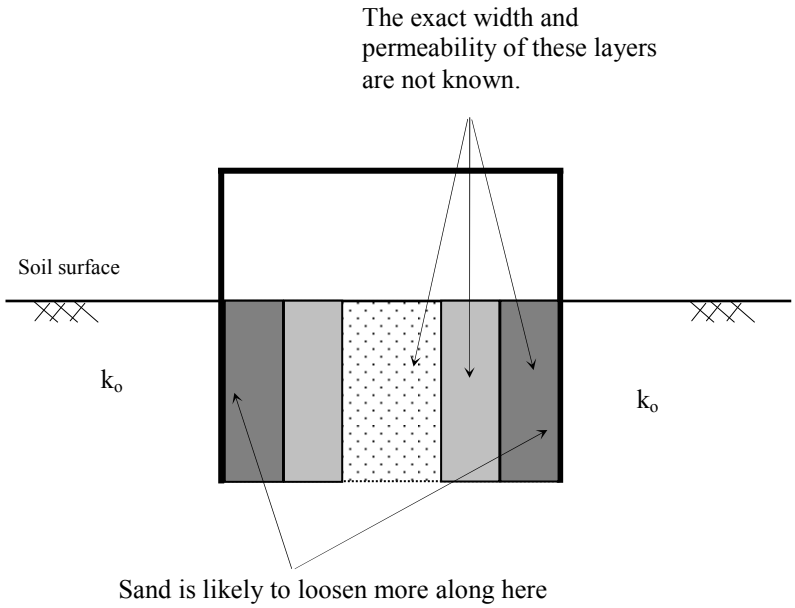

Figure 7.6: Variation of soil permeability within the soil plug.

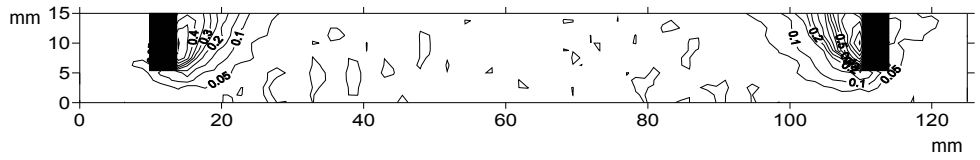

(a) L/D = 0.1, $Q_{seepage}$ / $A_{half\text{-}caisson}$ = 0.44 mm/s.

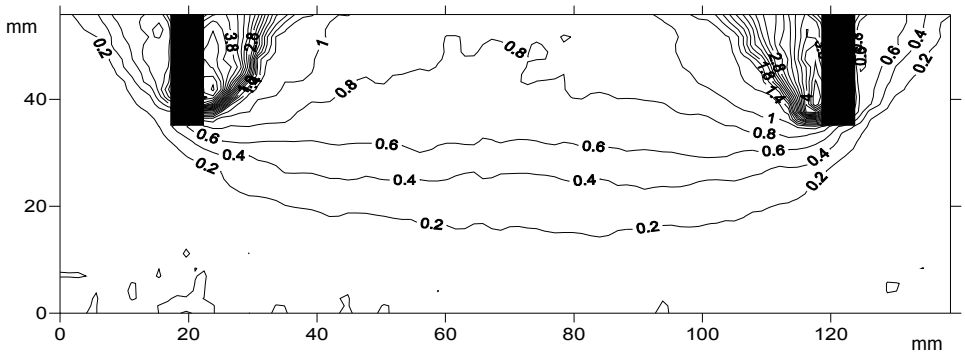

(b) L/D = 0.2, $Q_{seepage}$ / $A_{half\text{-}caisson}$ = 1.80 mm/s.

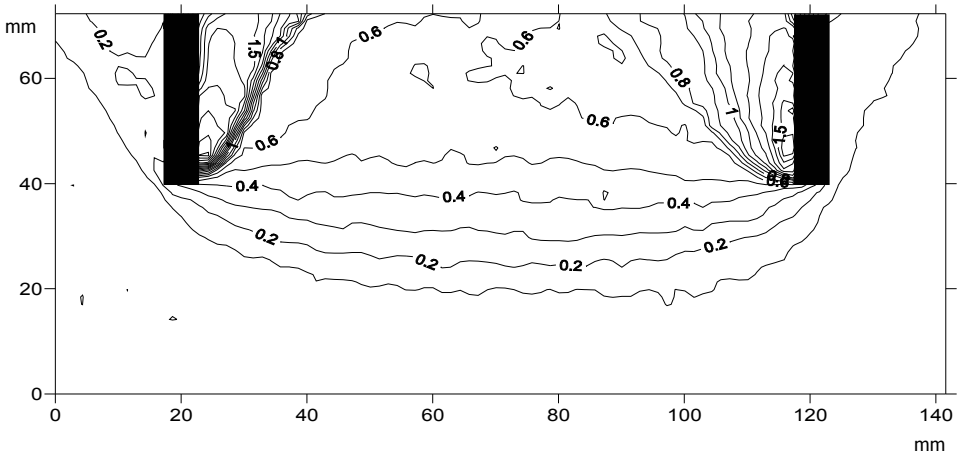

(c) L/D = 0.3, $Q_{seepage}$ / $A_{half\text{-}caisson}$ = 1.78 mm/s.

Figure 7.7: Measured sand movement velocity.

(velocity values shown on the contours are in mm/s).

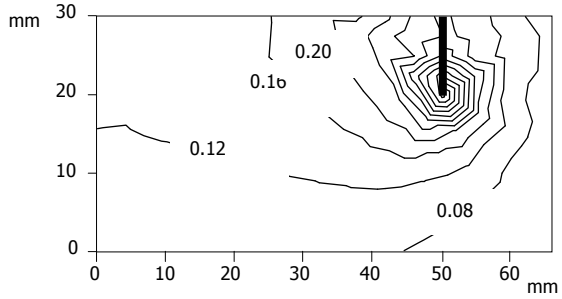

(a) L/D = 0.1, p/γ'D = 0.75

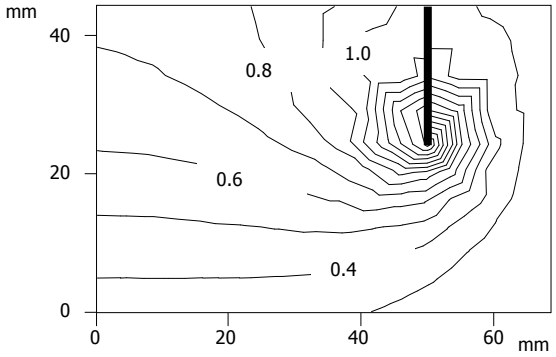

(b) L/D = 0.2, p/γ'D = 4.1.

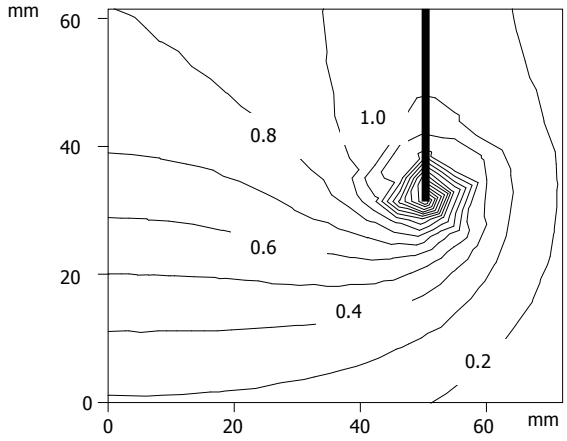

(c) L/D = 0.3, p/γ'D = 5.1.

Figure 7.8: Seepage velocity from FE simulations.
(velocity values shown on the contours are in mm/s).

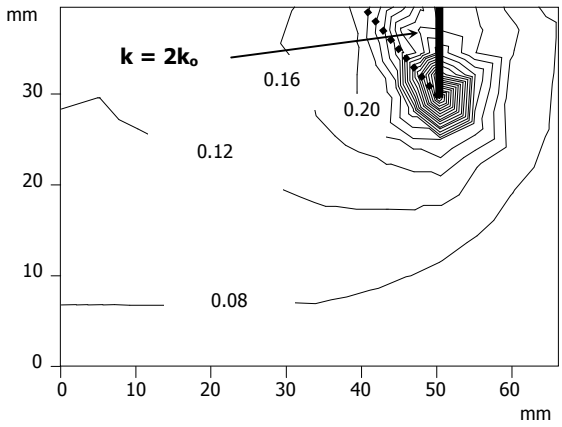

(a) L/D = 0.1, p/γ'D = 0.75.

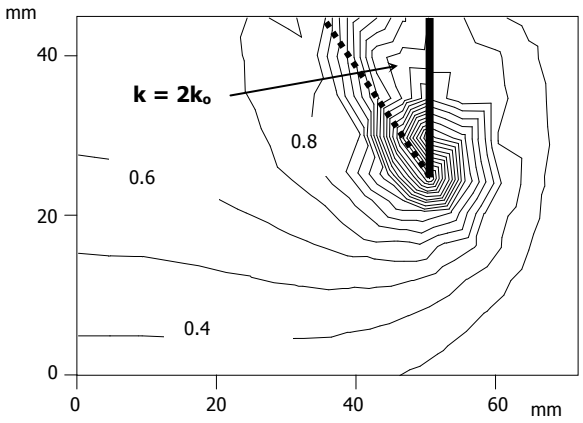

(b) L/D = 0.2, p/γ'D = 4.1.

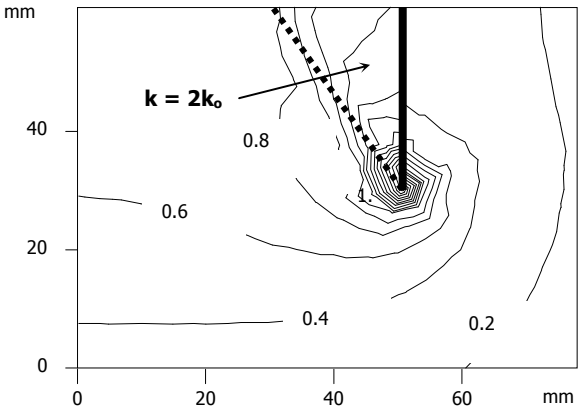

(c) L/D = 0.3, p/γ'D = 5.1.

Figure 7.9: Results from FE simulations with looser soil in the "wedge" zones. (velocity values shown on the contours are in mm/s).

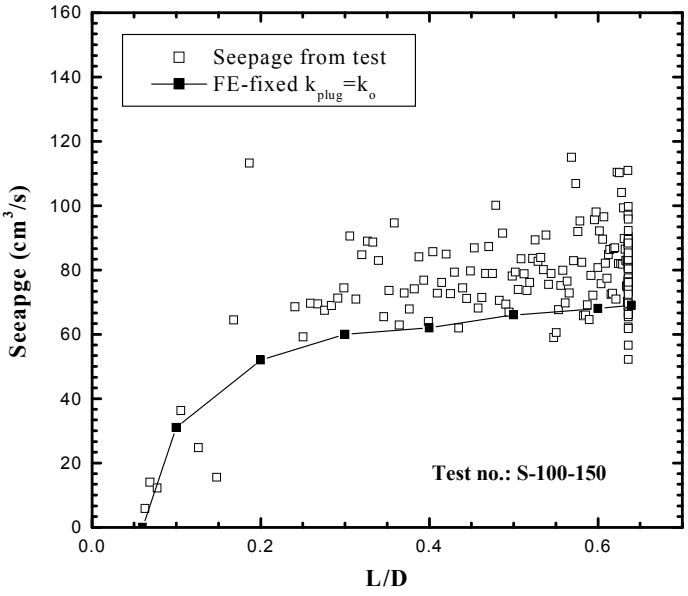

(a)

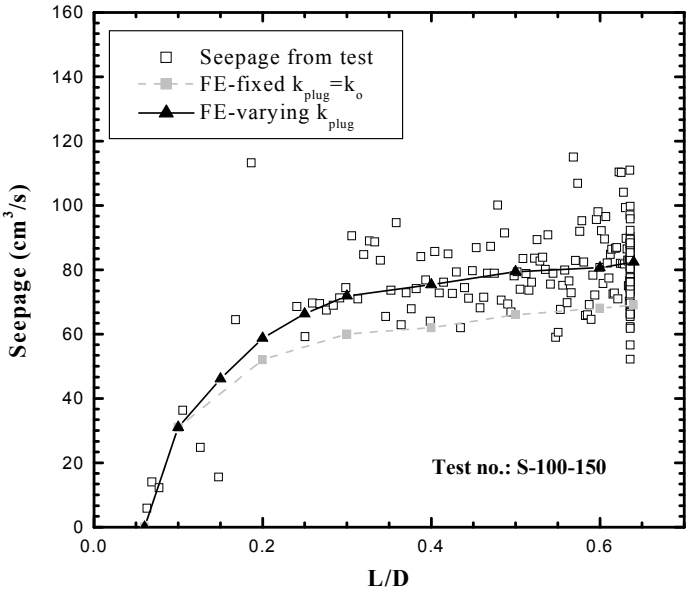

(b)

Figure 7.10: (a) Fixed $k_{plug} = k_o$ (b) varying k_{plug} to match with recorded seepage.

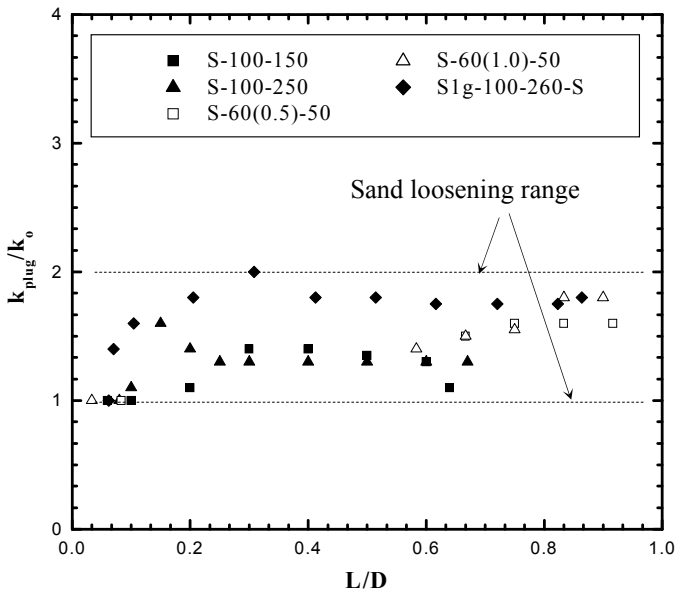

Figure 7.11a: Variation of plug permeability during installation.

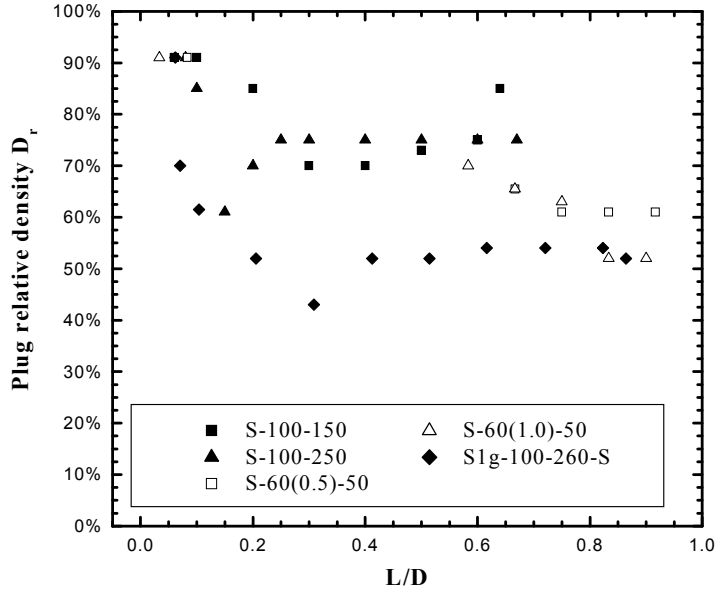

Figure 7.11b: Variation of plug permeability during installation.

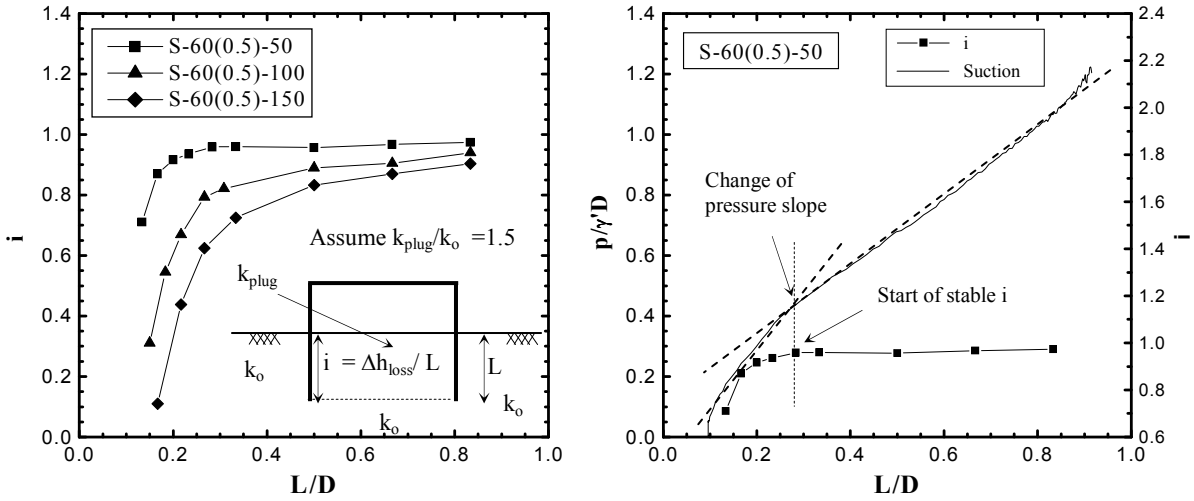

Figure 7.12: Development of hydraulic gradient i along the inner caisson wall.

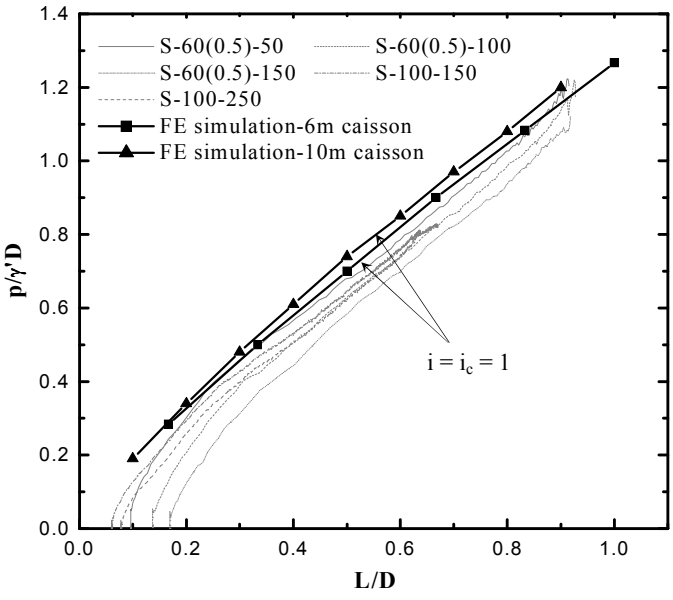

Figure 7.13: FE simulations of critical suction for silica sand.

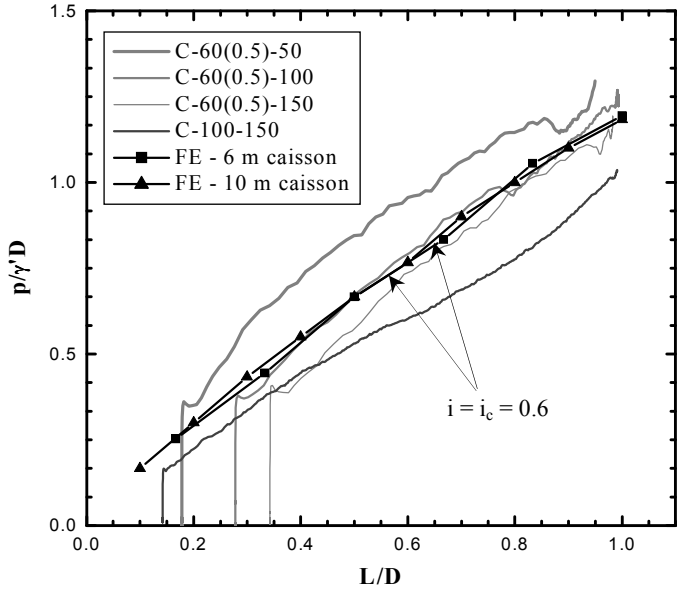

Figure 7.14: FE simulations of critical suction for calcareous sand.

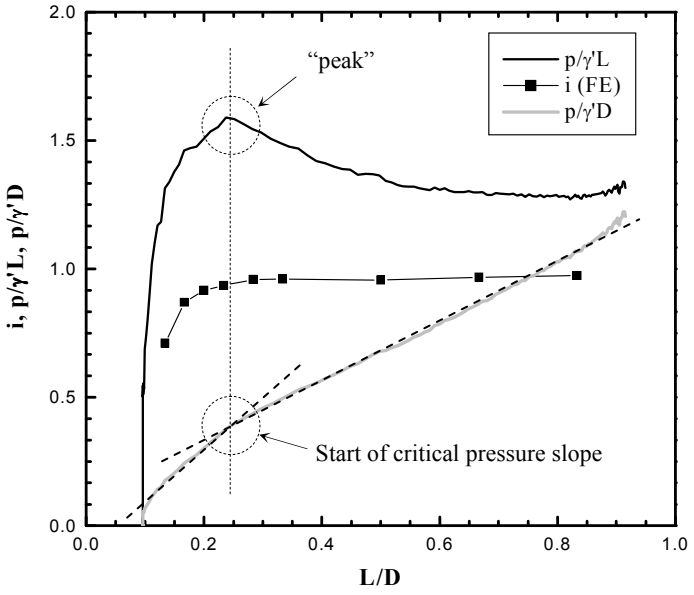

Figure 7.15: FE simulations of critical suction for calcareous sand.

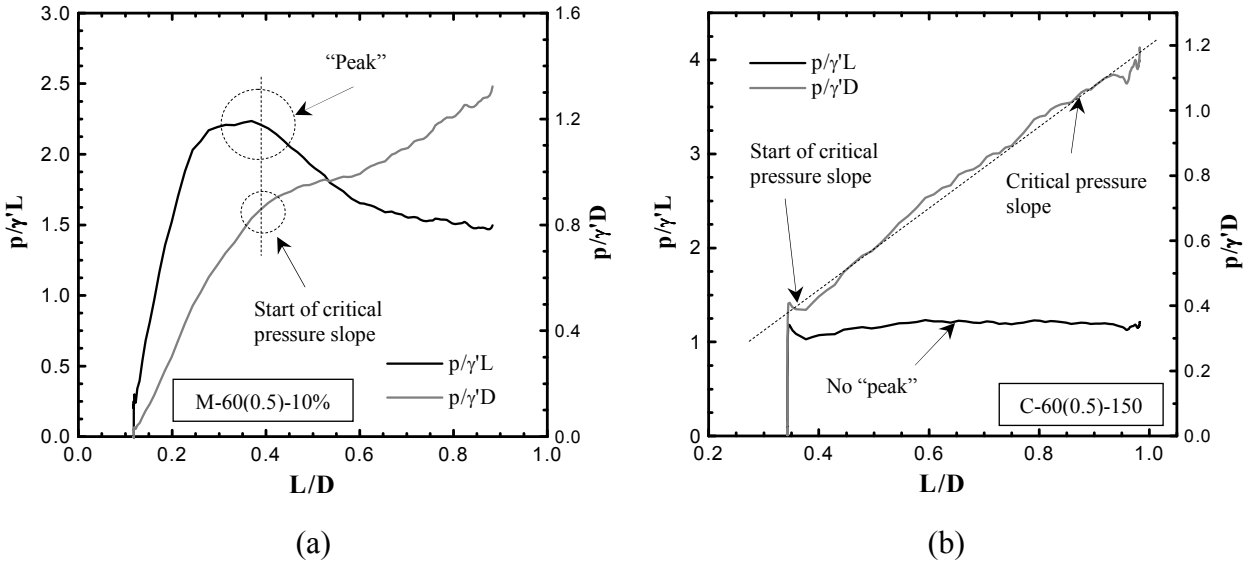

Figure 7.16: Normalisation against L for mixed soil and calcareous sand.

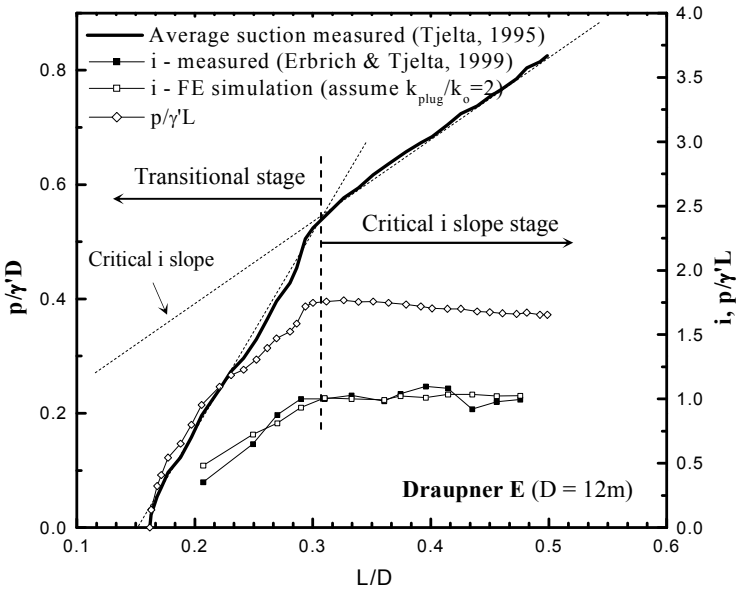

Figure 7.17a: Draupner E installation result.

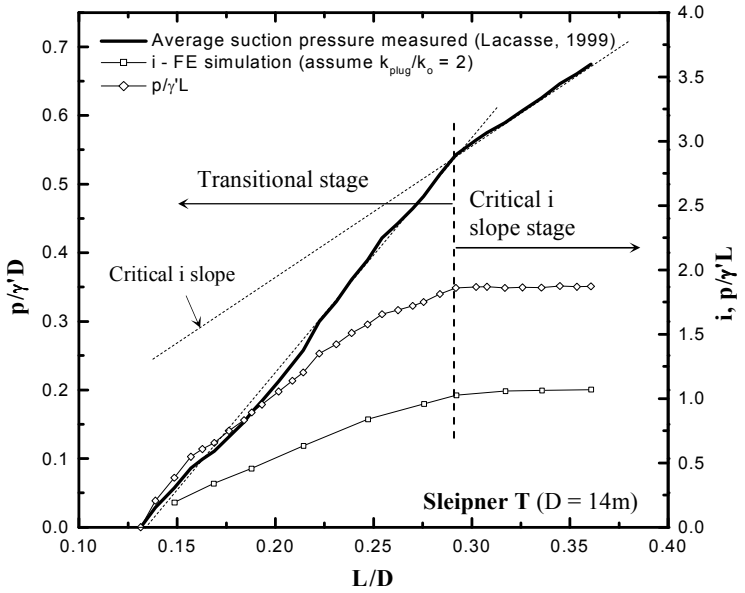

Figure 7.17b: Sleipner T installation result.

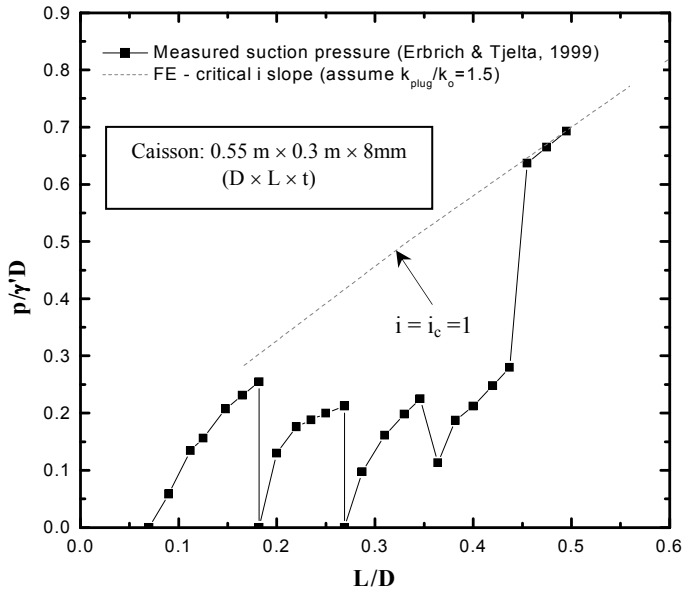

Figure 7.18: Comparison with NGI installation result.

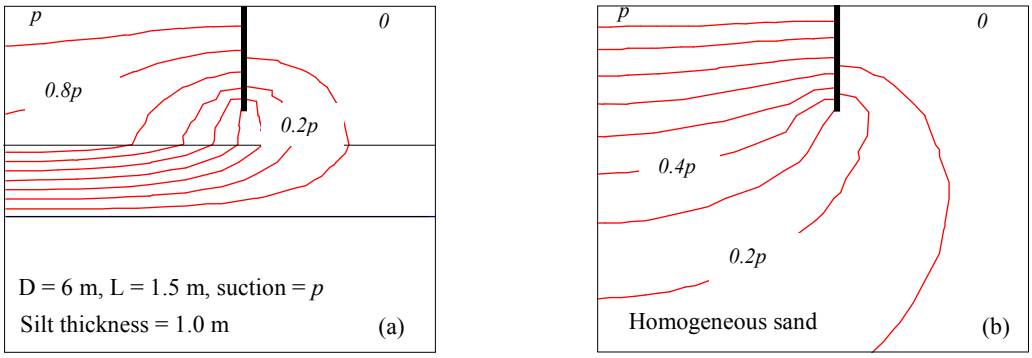

Figure 7.19: Wall tip above the silt layer, and comparison with homogeneous sand.

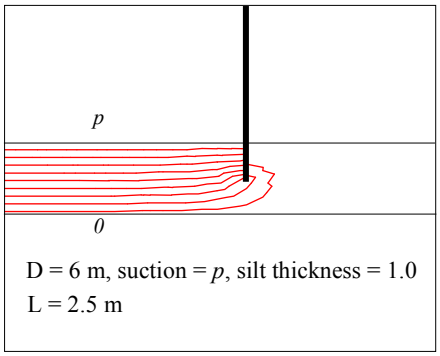

Figure 7.20: Wall tip in the silt layer.

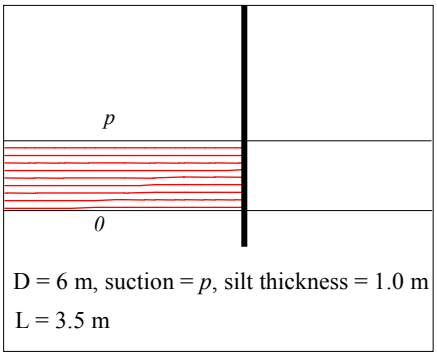

Figure 7.21: Wall tip below the silt layer.

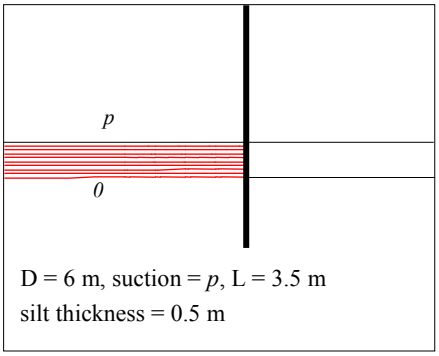

Figure 7.22: Thinner silt layer.

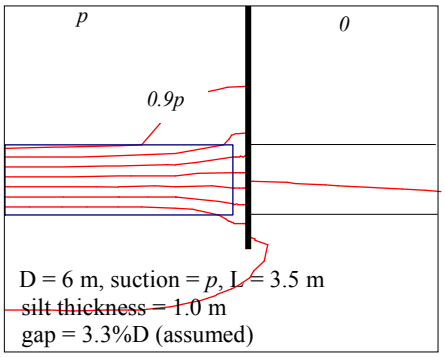

Figure 7.23: Gap in the silt layer.